SYNTHESIS, CHARACTERIZATION AND EVALUATION OF BIOLOGICAL ACTIVITIES OF PIPERAZINE RING BASED LIGANDS AND THEIR TRANSITION METAL COMPLEXES

A Thesis

Submitted in the partial fulfilment of the requirement for the award of the degree of

DOCTOR OF PHILOSOPHY

in

Chemistry

By

Rishi Kant

11719499

Supervised By

Dr. Suman Maji

LOVELY PROFESSIONAL UNIVERSITY

PUNJAB

2021

Declaration

I declare that the thesis entitled "SYNTHESIS, CHARACTERIZATION AND EVALUATION OF BIOLOGICAL ACTIVITIES OF PIPERAZINE RING BASED LIGANDS AND THEIR TRANSITION METAL COMPLEXES" has been prepared by me under the guidance of DR. SUMAN MAJI, Associate Professor, Department of Chemistry, School of Chemical Engineering and Physical Sciences, Lovely Professional University, Punjab. It is further certified that the results incorporated in this thesis have not been submitted, in part or full, to any other university or institution for the award of any degree or diploma.

RISHI KANT

Department of Chemistry,

School of Chemical Engineering and Physical sciences,

Faculty of Technology and Sciences,

Lovely Professional University,

Phagwara, (Punjab), India

DATE: 21 June, 2021

Certificate

It is hereby certified that thesis entitled, "SYNTHESIS, CHARACTERIZATION AND EVALUATION OF BIOLOGICAL ACTIVITIES OF PIPERAZINE RING BASED LIGANDS AND THEIR TRANSITION METAL COMPLEXES" being submitted by RISHI KANT, indepartment of Chemistry, School of Chemical Engineering and PhysicalSciences, Lovely Professional University, Punjab, for the award degree of Doctorof Philosophy in chemistry is a record of bonafied research work carried out by him. RISHI KANT has worked under my supervision and guidance and has fulfilled allthe requirements for the submission of the thesis. It is further certified that the resultsincorporated in this thesis have not been submitted, in part or full, to any otheruniversity or institution for the award of any degree or diploma.

DR. SUMAN MAJI

Associate Professor, Department of Chemistry,

School of Chemical Engineering and Physical Sciences,

Lovely Professional University

Phagwara, (Punjab), India

DATE: 21 June, 2021

Abstract

Piperazine based molecules have gained remarkable interest owing to their excellent bioactivity. In medicinal chemistry many marketed drugs are available which contains piperazine moiety. Piperazine based molecules with suitable donor atoms are potential ligands for metal complexes and are able to enhance their applications. Thrust area of this thesis represents the controlled study of piperazine based ligands and their complexes toward their interaction with various biological receptor. Thus, a total of fourteen ligands have been prepared with systematic variation in the ligand skelton with symmetric and asymmetric substitution in order to study their metal complexing behavior. Ligands werecharacterized using physical and spectroscopic methods viz. FTIR, UV-vis, ^{1}H NMR and Mass spectrometry.

Metal complexes of these ligands were prepared and characterized. Structure of these complexes were proposed on the basis of UV-vis, FTIR, Mass, isotopic distribution, TGA, molar conductance measurements. In the UV-vis spectra significant variations from the ligand absorptions were observed and further supported by M-N and M-O vibrational frequencies which were in the 400-600 cm^{-1} range in FTIR. Mass spectra and their fragmentation pattern matched well with proposed pathway(s). Isotopic distribution corresponding to the proposed formula of complexes measured experimentally and compared theoretically were similar for most of the cases. TGA analysis was assisted by the loss of coordinated solvent molecules before the actual loss of ligands and percentage ash content analysis in accordant with number of metal ion converting to metal oxide. Molar conductance data suggested nonionic nature of complexes which were in agreement to the proposed structure of complexes.

Biological applications of these ligands and complexes were conducted to check their interactions with different receptors. Antibacterial activity of ligands and complexes were tested against *E. Coli* and *S. Aureus*. While most of the ligands were inactive or very less active, all the metal complexes were found more active and even in some cases more active than standard amikacin. Structural activity relationship for these variation in activity were also suggested. Antioxidant activity of complexes using DPPH scavenging assay and results indicated some complexes were active and showed greater percentage inhibition. Protein binding studies were performed with

BSA using UV-vis absorption spectroscopy and binding constant were calculated which were in range of 10^2 M^{-1}. Moderate binding constant of these complexes suggested potential role of serum protein as carrier molecules in drug delivery. Cytotoxicity studies of selected complexes were performed against breast cancer cell line (MCF-7) and IC_{50}value were found in the range of 5-9. DNA binding studies for selected complexes were also performed with CT-DNA and calculated binding constant were in the range of 10^2 M^{-1}. Thus, complexes have been shown to be biologically active with respected to individual biological receptor.

Computational studies were performed to aid experimentally obtained results theoretically. Geometry optimization of ligands were performed to find stable equilibrium structure and to know about orientation of donor atoms. Hybrid functional B3LYP/6-31G method was used to optimize the structures. TDDFT studies were performed to corroborate experimentally obtained UV-vis spectra of ligands and selected complexes. All the compared results were in favour of experimental findings and theoretical transitions were also assigned to the metal complexes. Selected metal complexes were optimized using DFT calculations with LAN2DZ basis set. Molecular docking studies with BSA and DNA were performed to know binding interaction of the complexes with theses biomolecules. BSA docking studies reveled the complexes which lack aromatic system interact with hydrophilic interaction while the complexes with benzene ring show both hydrophilic and hydrophobic interactions with amino acid residues in protein chain. DNA docking studies revealed the selected complexes interact with DNA through nitrogenous base, pentose sugar and phosphate and are groove binder in nature.

Specially dedicated to my brother and his wife

SHRI KANT SHEETAL TRIPATHI

Acknowledgement

First and foremost, praises and thanks to the God, the Almighty, for Hisshowers of blessings throughout my research work to complete the research successfully.

I would like to express my deep and sincere gratitude to my research supervisor, **Dr. Suman Maji**, Associate Professor, Department of Chemistry, Lovely Professional University, Punjab, for giving me the opportunity to do research and providing invaluable guidance throughout this research. His dynamism, vision, sincerity and motivation have deeply inspired me. He has taught me the methodology to carry out the research and to present the research works as clearly as possible. It was a great privilege and honor to work and study under his guidance. I am extremely grateful for what he has offered me. I would also like to thank him for his friendship, empathy, and great sense of humor. I am extending my heartfelt thanks to his wife, family for their acceptance and patience during the discussion I had with him on research work and thesis preparation.

I am extremely grateful to my father **Mr. Kailash Prakash** and mother **Mrs. Kamala** for their love, prayers, caring and sacrifices for educating and preparing me for my future. Also, I express my thanks to my sister and brothers, for their support and valuable prayers. I would like to say thanks to my friends and research colleagues, **Dharmendra Sharma**, **Pavas** and **Mankomal** for their constant encouragement. I express my special thanks Dr. Vijay M. Kumbar, Manpreet Kaur, ZainibHilal, Tanjot Kaur and Ankita for their genuine support throughout this research work. I also thank to the non-teaching staff Manoj Kumar, Mamta and Sandeep for their kindness. Finally, my thanks go to all the people who have supported me to complete the research work directly or indirectly.

Rishi Kant

Table of Contents

List of Tables

List of Figures

List of Annexures

List of Abbreviations

Short Name	Abbreviation
FTIR	Fourier transform infra-red
UV-vis	Ultra violet-visible
^{1}H NMR	Proton nuclear magnetic resonance
TMS	Tetra methyl silane
ESI-MS	Electron Spray Ionization Mass Spectrum
TGA	Thermogravimetric Analysis
HIV	Human immunodeficiency virus
CML	Chronic myelogenous leukemia
Aq.	Aqueous
KOH	Potassium hydroxide
BPMP	Bis pyridyl methyl piperazine
DMF	Dimethyl formamide
DCM	Dichloromethane
MeCN	Acetonitrile
DMSO	Dimethyl sulfoxide
EtOH	Ethanol
MeOH	Methanol
AcOH	Acetic acid
THF	Tetrahydrofuran
Me	Methyl
BnOH	Benzyl alcohol
Et	Ethyl
^{i}Pr	Isopropyl
^{t}Bu	Tert-butyl
i.e.	That is (Latin *id est*)
OAc	Acetate
Py	Pyridine
ROP	Ring opening polymerization
MOFs	Metal organic frameworks
TLC	Thin layer chromatography
nm	Nanometer
mmol	Millimole
ml	Milliliter
m/z	Mass/charge
Str.	Stretching
Vib.	Vibrational
s	Singlet

d	Doublet
t	Triplet
m	Multiplate
m. pt.	Melting point
RBF	Round bottom flask
M	Molar
µM	Micromolar
MHA	Mueller-Hinton agar
DPPH	Diphenyl-picryl-hydrazyl
min	Minutes
Abs	Absorbance of sample
BSA	Bovine serum albumin
A	Absorbance of sample at given wavelength
A_o	Absorbance of blank at given wavelength
FBS	Fetal bovine serum
DMEM	Dulbecco`s Modified Eagle Media
IC_{50}	50% Inhibitory concentration
CT-DNA	Calf-thymus DNA
2D	Two dimensional
3D	Three dimensional
HOMO	Highest occupied molecular orbital
LUMO	Lowest unoccupied molecular orbital
DFT	Density functional theory
TDDFT	Time dependent density functional theory
Osc	Oscillator
Cal.	Calculated
Exp.	Experimental
Conc.	Concentration
Cond.	Conductance

CHAPTER 1

INTRODUCTION AND LITERATURE REVIEW

1.1 Introduction

Heterocycles containing nitrogen owing to their high therapeutic properties have gained remarkable interest of scientist in the recentyears.[1]Weather it be natural or synthetic compounds containing piperazine ring, biological activities of these compounds owe to this piperazine ring and play a key role in biochemical processes, irrespective of naturally occurring or of synthetic origin.[2] Phytochemical drugs such as papaverine, theophylline,ellipticine, procaine,quinine,emetine, morphine, containing nitrogen based heterocycles have established important mark.[3] New schemes are developed for the conversionand transform small building block into the nitrogen-containing heterocycles with desired applications.[4–6]

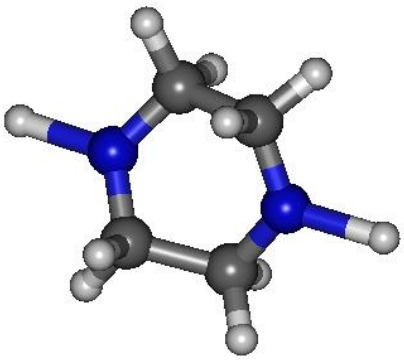

Figure 1.1: 3D structure of piperazine

Piperazine is a heterocyclic six membered ring compound two nitrogensin opposite side of the ring (Figure 1.1).[7]Piperazine is a weak base ($_p$Ka 5.35 and 9.73 at room temperature)[8,9]and is soluble in organic and aqueous solvent. It is considered a privileged structure because of its versatile binding properties and act as the backbone skelton of the moleculesin biological targets.[10]A library of molecules can be potentially designed by modifying the ring through nitrogen with the concept of without modifying the basicity of compounds for wide variety of applications.[11] This idealize to build molecules with an active core of piperazine ring[12] and screen it against various receptors for different therapeutics[13]such as antibacterial[14–18], antifungal[19,20], anticancer[21–26], antihistaminic[27], antipsycholytic[28,29] and neurobiology.[30]

Piperazine itself with nitrogen as donor as well as its different derivatives with suitable donor atom or groups act as potential ligands for metal complexes formation. Owing to the symmetry of piperazine ring further substitution on nitrogen can result

in the formation of unsymmetrically disubstituted and monosubstituted derivatives as well as symmetrically disubstituted compounds.[31,32] This implies that piperazine ring based ligands are unique for easy modificationproviding desired applications (Figure 1.2).

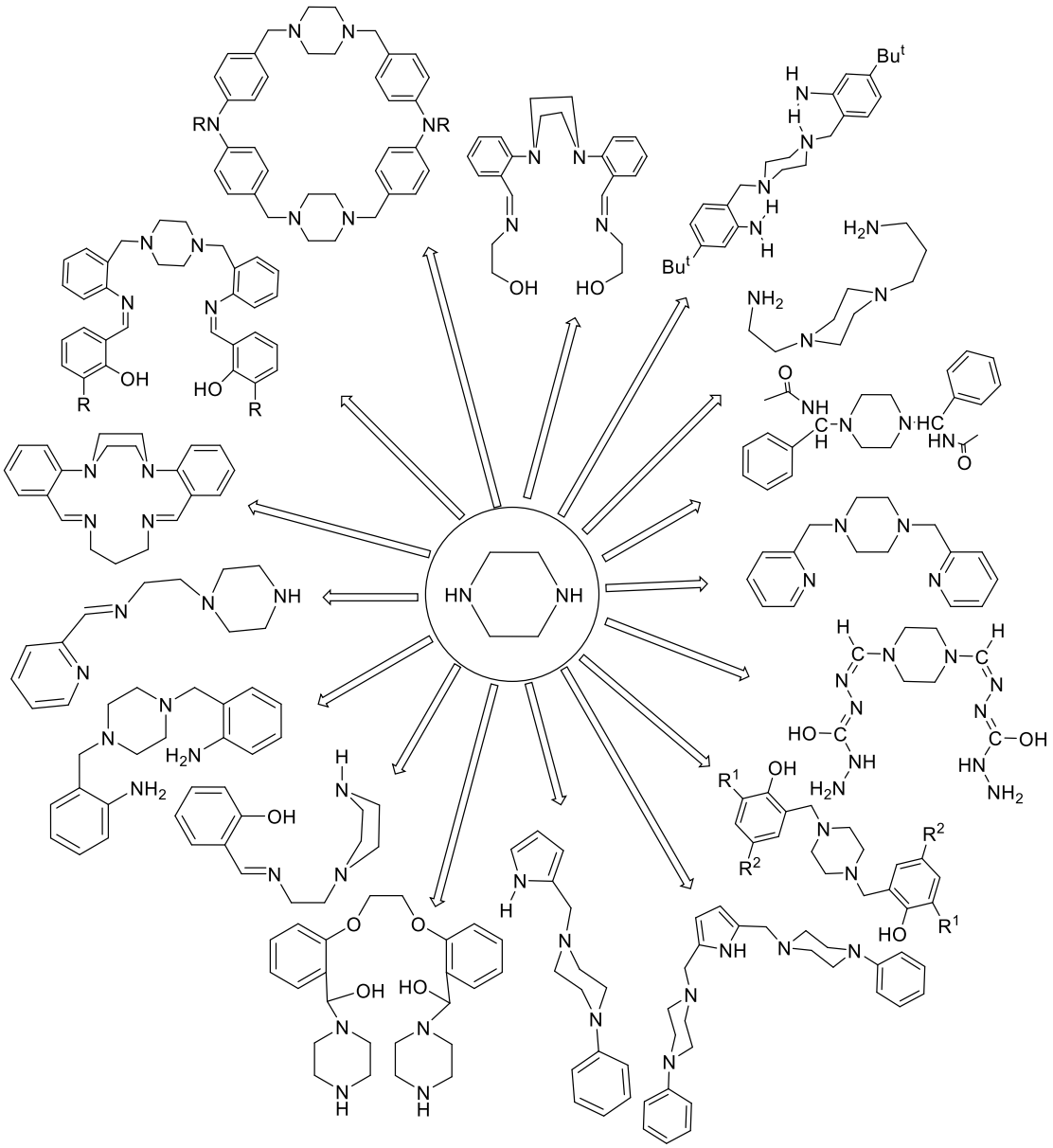

Figure1.2: Structures of ligands derived from piperazine

Since substitution at N-atom of piperazine makes them versatile ligands,[33] they are used to bind either one- or two-metal ions in different conformation environments. Boat conformation is preferred in monometallic complexes binding to one metal centre resulting in a conformational strain upon the piperazine ring.[34]While in bimetallic complexes binding to two metal ions allows the piperazine stable chair

conformation. In general, Substitution on piperazine ring nitrogen is made with suitable moieties for increasing the tacticity and increased binding possibilities of ligands. For example, ligand 1,4-bis(2-pyridylmethyl)piperazine reported by Ostremiar *et al.*was able to bind with iron in two different denticity i.e.as a tetradentate or bidentate ligand.[35] Thus potential of the ligands based on piperazine ring can be shown to generate a diverse series of different metal complexes.

Piperazine is considered as the structural component during screening of drugs and have been designated for many successful applications in biochemistry and medicinal field.[36]The piperazine scaffold is regarded as the active core and is frequently observed in naturally occurring bioactive compounds across a variety of naturally occurring medicines.[13] A large number of potent commercially available drugs like fluphenazine,flunarizine, lomerizine,cinnarizine, HIV protease, crixivan,ciprofloxacin, etc. contain a piperazine core are good examples of bioactive piperazine derived compounds.[37]Owing the presence of polar nitrogen atom in the piperazine ring it confers bioactivity to its derivatives by increasing the favourable interactions with bio molecules[7]and play major rolein the biochemical processes in living cells. Moreover, many of the enzymes have heterocycles as coenzymes for their active functioning.[6] These nitrogen sites are responsible in water solubility of the organic moleculesand thereby playing an active role in the bioavailability. Also, piperazine derived compounds are extensively used in drug discovery because they permit synthetic medicinal chemist to design such molecules in which basicity is retained.

The major role of this privileged structure, in medicinal chemistry, is to furnish a path to build up a library of compounds based on piperazine structural motif and screen them against an array of different receptors[12] for different therapeutic areas.[13]Among a wide verities of currently available drugs, few examples that contain piperazine unit are shown in the figure 1.3.[38–42]

Antidepressant drugs containing piperazine core are amoxapine[43,44]buspirone[45,46], befuraline.[47] The drugs that possess anticancer activity is imatinib with a piperazine moiety. Imatinib[48] effectiveness has been proved in treatment of Chronic Myeloid Leukemia (CML) and it also act as synthetic tyrosine kinase inhibitor. Ranolazine[49,50]

and trimetazidine[51] are class of antianginal drugs used to treat angina, a symptom for heart attack and give immediate relief form angina attack.

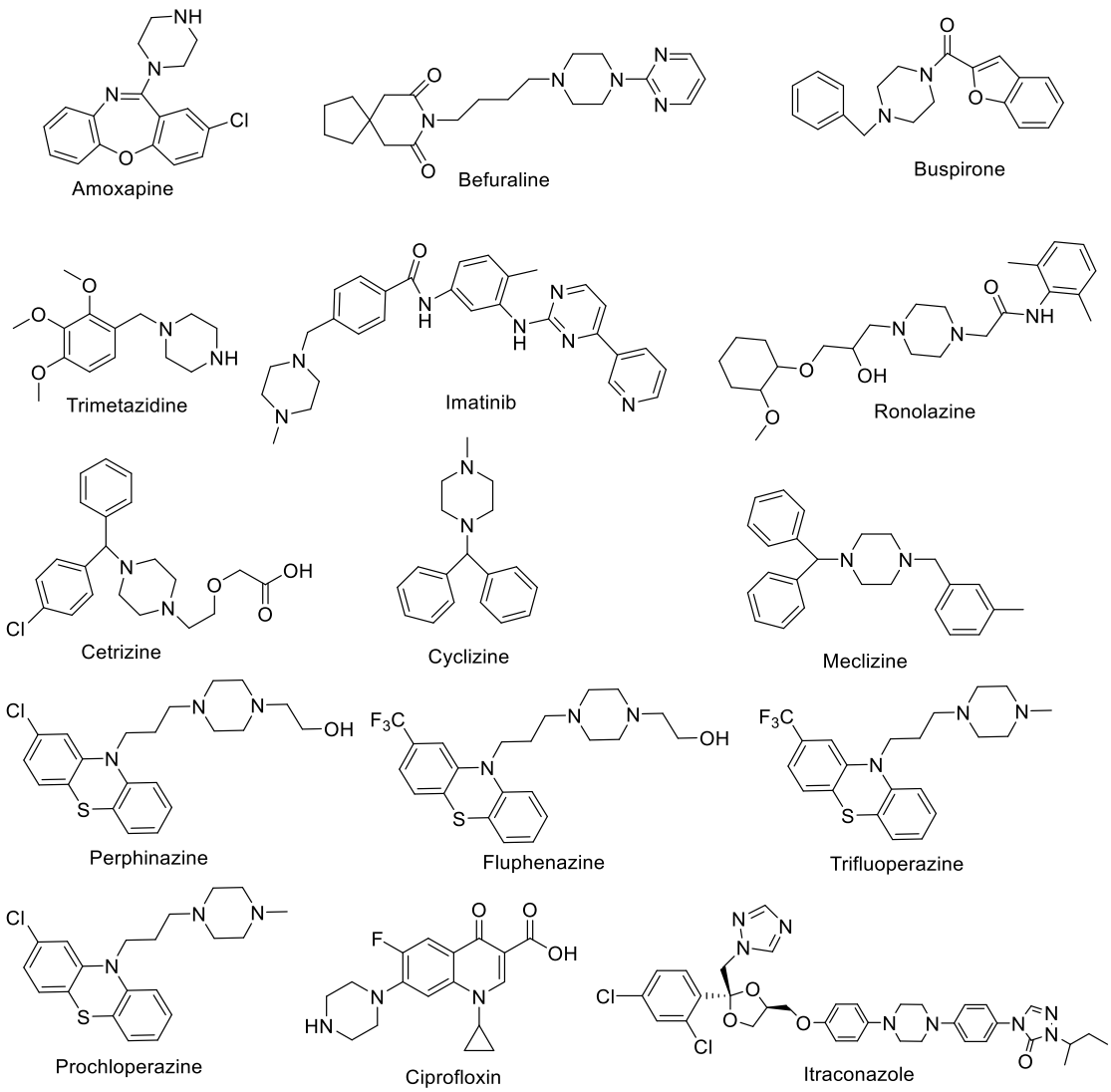

Figure 1.3: Structures and name of marketed drugs containing piperazine moiety

Cetrizine[52], cyclizine[53] and meclizine are class of antihistamine drugs which are used to treat allergic symptoms like hives, sneezing, a runny nose and watery eyes by blocking effect of histamines. All the three drugs have structural similarity and possess piperazine nucleus as backbone unit. Perphinazine[54], fluphenazine, trifluperazine, prochloroparazine are antipsychotic class of drugs, used to treat symptoms of psychosis like delusions, confused thoughts, paranoia or hallucinations. Antibiotics ciprofloxin[55] is a fluoroquinolone derived compound containing piperazine moiety and have broad spectrum activity in therapeutics because several

pathogens which are resistance to other drugs, are susceptible to ciprofloxin. Itraconazole[56]is an antifungal drug containing triazole moiety with built in piperazine unit possess broad spectrum activity againstseveral systemic fungal pathogens.

1.2 Review of Literature

1.2.1 Phenylpiperazines ring-based ligands

Asymmetric phenyl piperazines have been synthesized by Vibhor *et al.*[57] from chlorinationof *bis*-ethanolamine to*bis*-(β-chloroethyl)amine which were condensed with a suitable aromatic primary amine. Liu *et al.*[58] has also followed a similar way to synthesize monosubstituted and disubstituted compounds by reacting with alkyl halides. Preparation of piperazine derivative bearing phenyl ring in the middle is a keyprecursor for the preparation of macrocyclic ligands (Figure 1.4).[59]

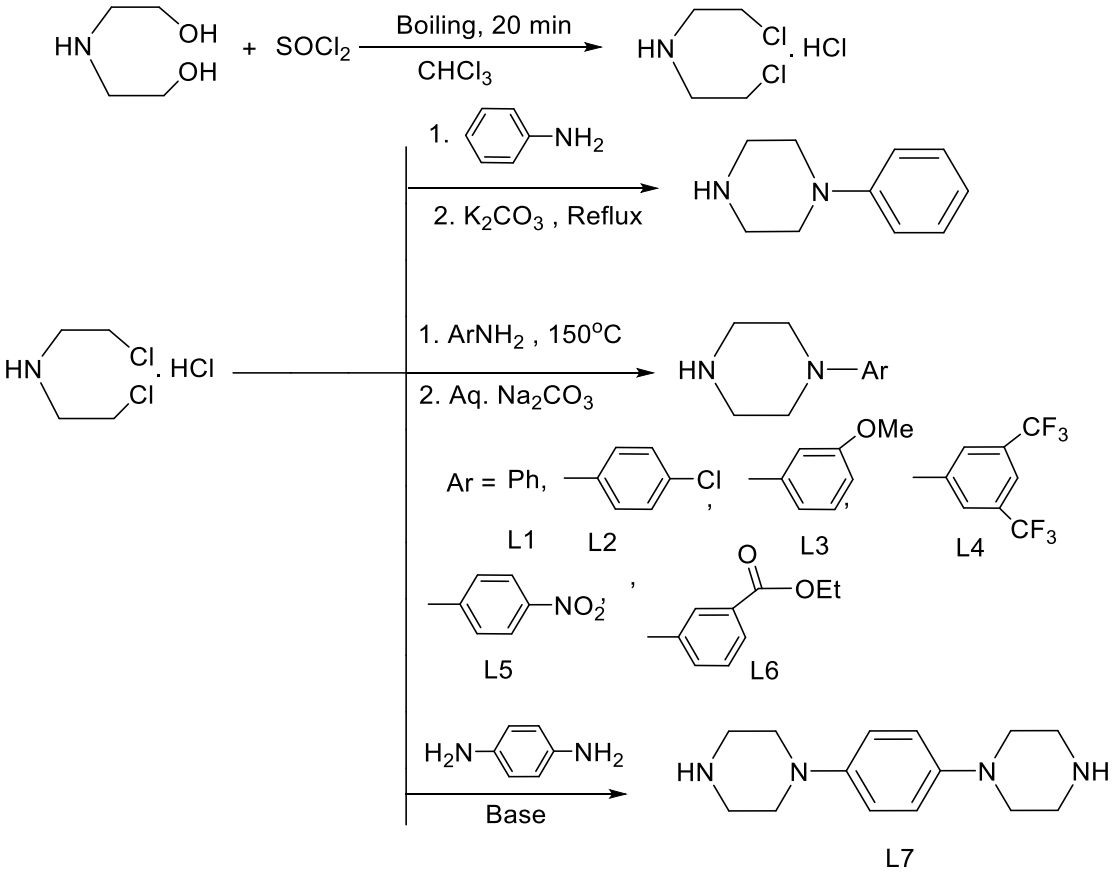

Figure1.4: Synthesis of substituted phenylpiperazine

1.2.2 Amino-alkyl/benzyl and di-acetamide piperazine ring base ligands and complexes

Tetradentate amino-alkyl piperazines with varying chain length have been shown to act asprecursor for further substitutiontoSchiff Base metal complexes. Bis(3-aminopropyl)piperazine and bis(2-aminoethyl)piperazine have symmetric substitutionboth side while preparation of an asymmetrical N,N'-(2-aminoethyl)(3-aminopropylpiperazine(L8) has been given by Kaypour *et al.*[60]by puttinglinear amines having different length with amine group protection (Figure 1.5).

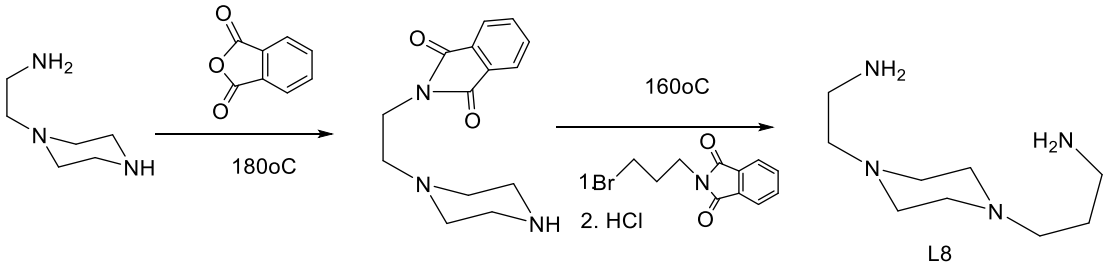

Figure1.5: Synthesis and structure ofligand L8

Substituted benzylamine incorporating piperazine ring (L9) has been synthesized by Lloyd *et al.*[61]by the rection of 2-nitro-4-*tert*-butylbenzylbromide with piperazine followed by reduction (Figure 1.6).

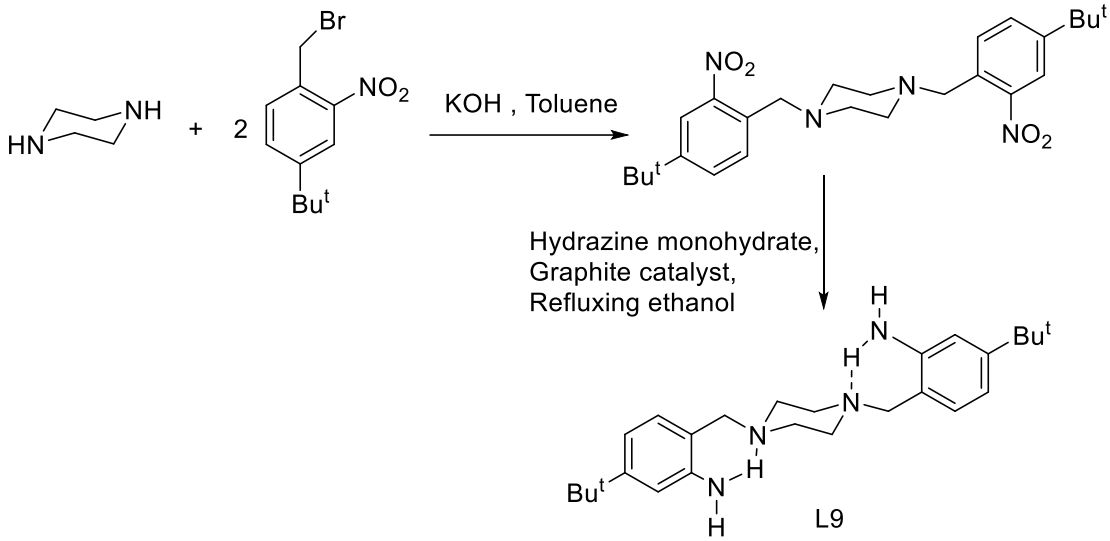

Figure1.6: Synthetic procedure of substituted amino-benzylpiperazine

Diacetamide based Mannich base piperazine ligand (L10)have beendescribedby Babu *et al.*[62] which is prepared by the condensing benzylaldehyde, acetamide and piperazine. Metal complexes of the ligands have been prepared using Cu^{2+}, Ni^{2+}, Co^{2+} and Zn^{2+} metals (Figure 1.7).

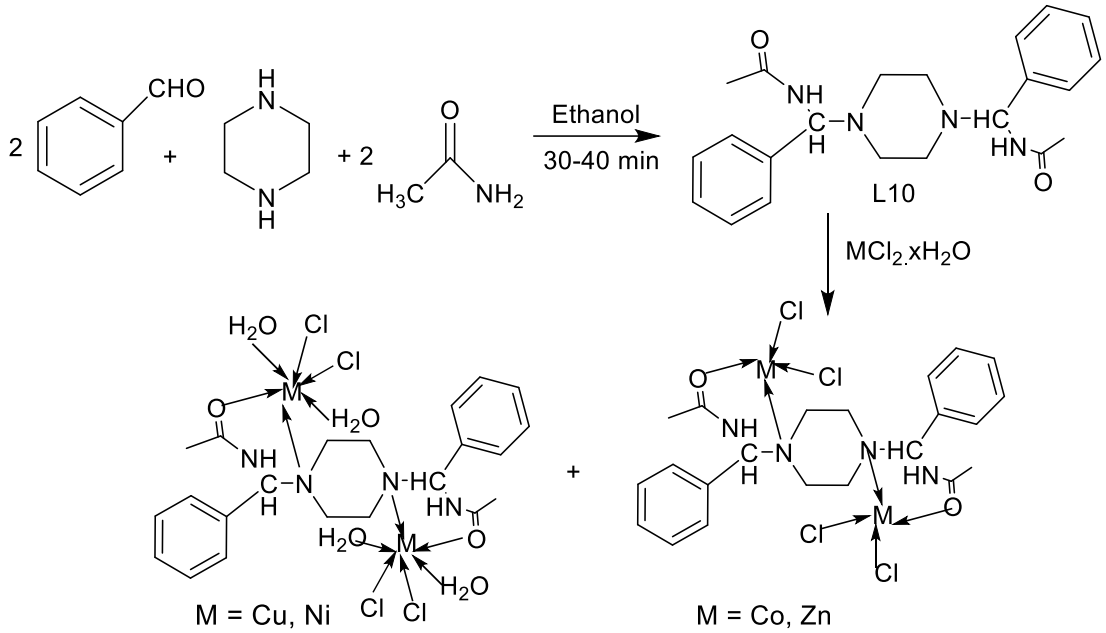

Figure1.7: Synthesis of piperazine derived ligand and their complexes

1.2.3 Pyridyl piperazine based ligands and complexes

Pyridine appended piperazine are the range of ligands that have been used for various applications [63] These ligands are prepared by treating piperazine with 2-picolyl chloride (Figure 1.8).[64]Substituted pyridyl compounds have also beensynthesized by Schatz *et al.*[65]and Massoud et al.[66] by following the similarprocedure.

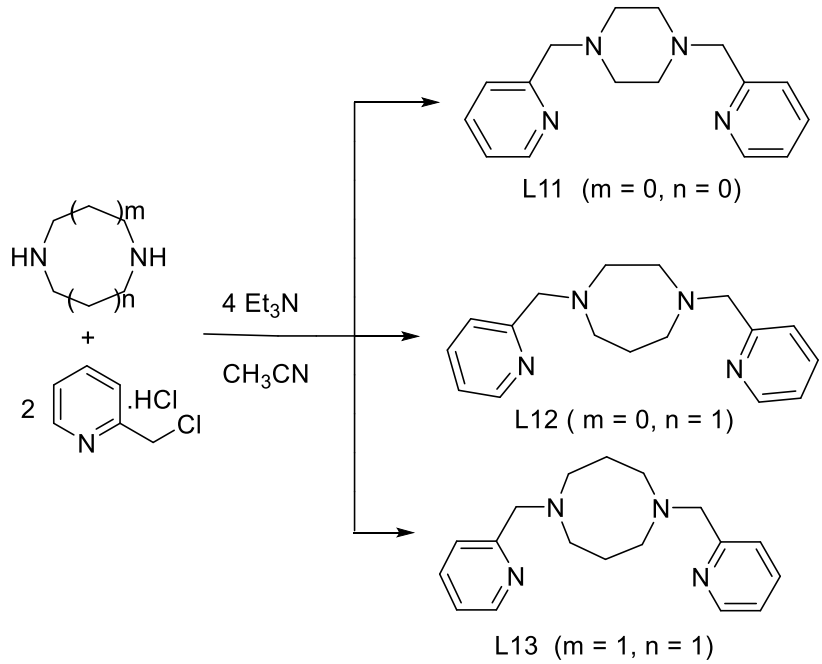

Figure1.8: Synthesis of bispyridyl piperazine and their higher ring analog

Tetra-dentate pyridine based ligand L11 are also employed by Ratilainena *et al.*[67] for the different transition metal complexes such as copper, cobalt, manganese and silver employing metal salts with different anions and their structures have been explained (Figure 1.9,1.10).

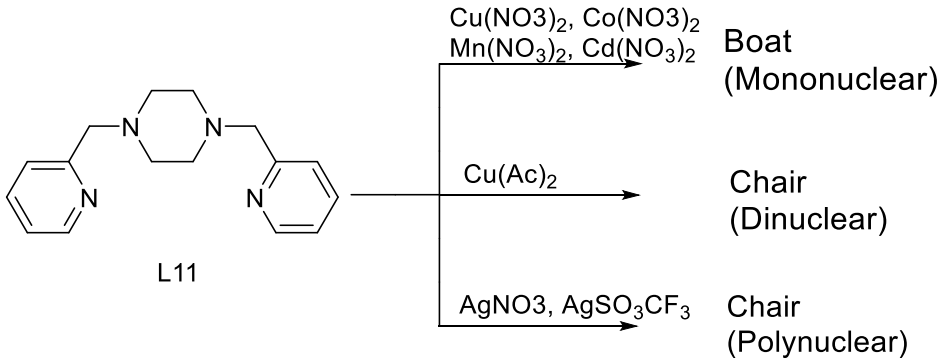

Figure1.9: Different metal complexes of ligand L11

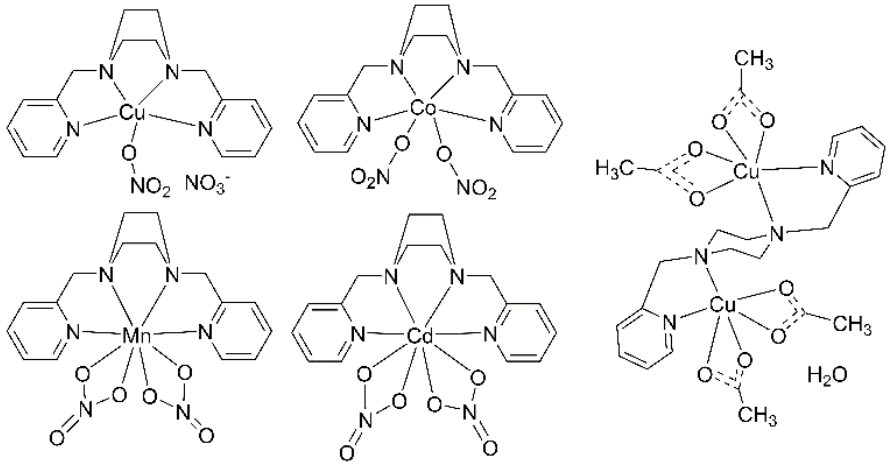

Figure 1.10: Structure of metal complexes of ligandL11

Analogue to pyridyl appended piperazine ligands, diaza-cycloalkanes based and other similar ligands (Figure 1.12)and their manganese complexes (Figure 1.11)have been prepared Saravanan *et al.*[68] with the important use in olefinic oxidation with effect of ring size having significant effect in catalytic activity.

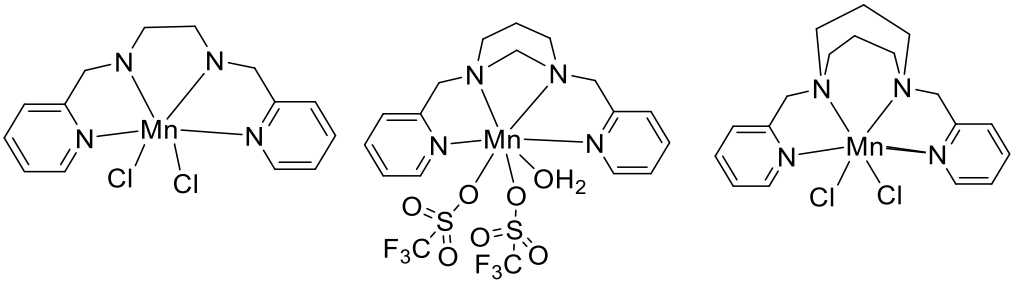

Figure 1.11: Manganese complexes of L20, L18, L13

Peroxy manganese complexes of the various ligands (L11, L12, L14, L15 and L18) synthesized by Gieger *et al.*[69] have been testedimportant in catalytically promoted oxidation of small molecule using manganese as the active centre. These complexes have different coordination number ranging from six to eight coordination which also have influence in catalytic activity owing steric hindrance. Binding affinity of ligands L17, L19 and L20 with actenides has been invegigated by Ogden *et al.*[70]in methanolic solution.

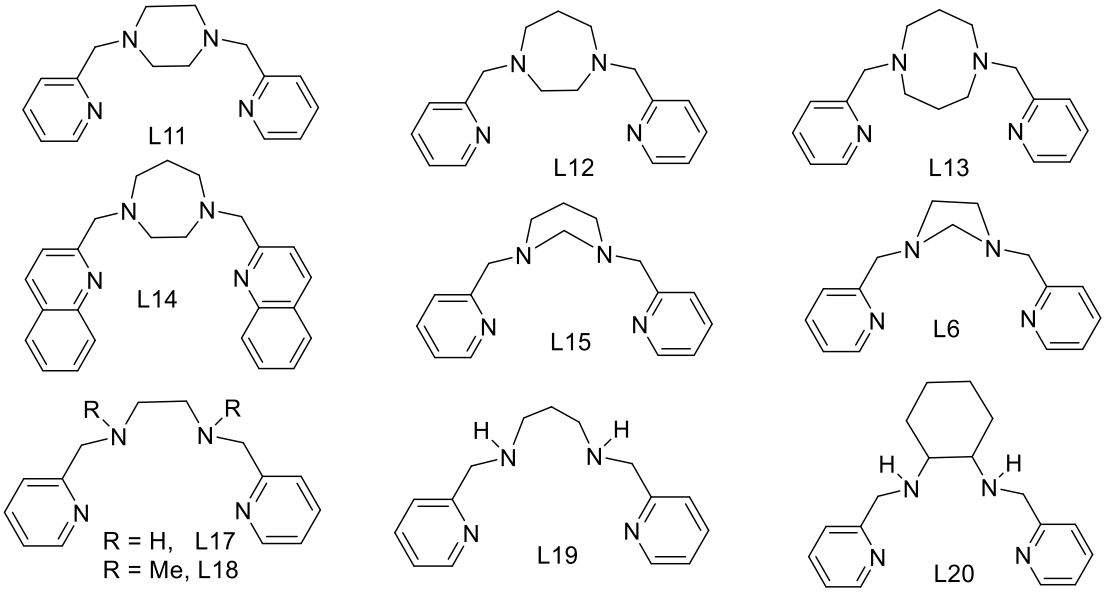

Figure1.12: Structure of bispyridyl/quinolyl ligands

Limberg *et al.*[35] have utilized the ligand bis-2-pyridylmethylpiperazine L11 to show the effect of boat and chair conformers on complexation and coordination environment by preparing four different iron complexes (Figure 1.13). This is important to observe that role of solvent polarity, oxidation state of metal ion, and co-anions of metal salts are essentially involved as key factors in deciding the coordination environment around the ligands and metal ion. Boat conformation binding of piperazine derivatives in L8 has also been provedwith structures reported by Ostremeier *et al.*[71]Isobutyl group forces piperazines (L22)to coordinates in boat conformation with iron (Figure 1.14).

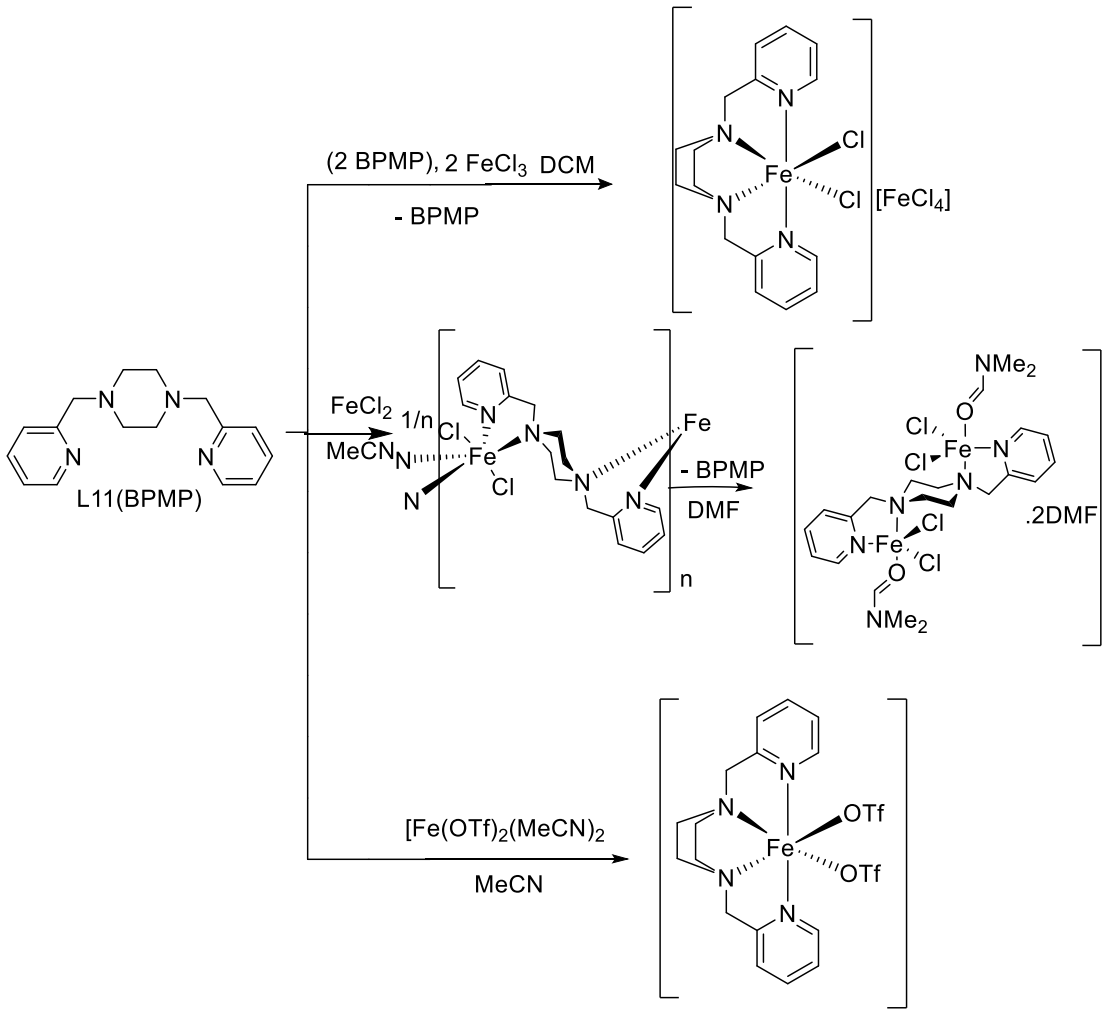

Figure1.13: Synthesis and structure of iron complexes of L11in different geometrical conformations

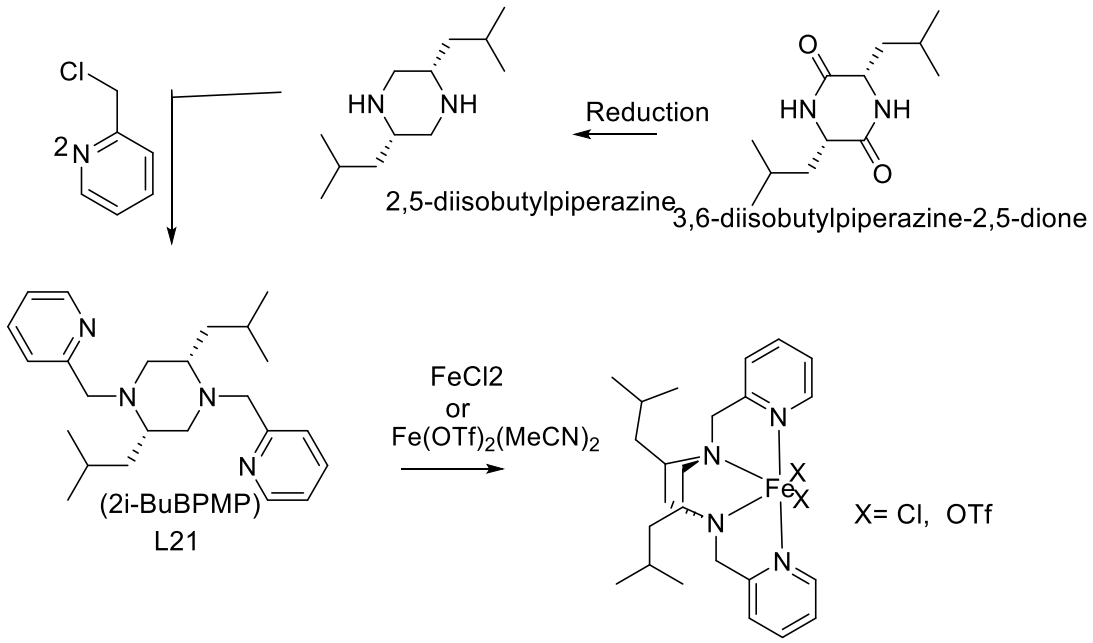

Figure1.14: Synthesis of [($^{2i\text{-}Bu}$BPMP)Fe(Cl)$_2$] and [($^{2i\text{-}Bu}$BPMP)Fe(OTf)$_2$]

1.2.4 Diformyl piperazine bis(carbohydrazone) based ligands and complexes

Sulekh Chandra *et al.*[72] has prepared Schiff base type 1,4-diformylpiperazine*bis*(carbohydrazone) (L22) (Figure 1.15), its dinuclear copper complexes and their EPR studies have been done. Magnetic studies are important to know about the coordination environment around the metal ion (Figure 1.16).

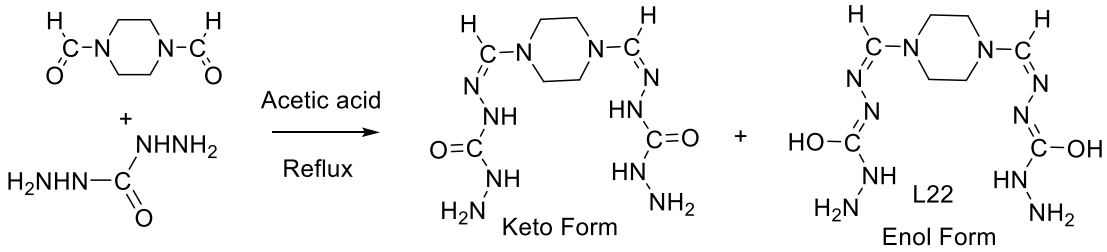

Figure1.15: Synthesis of 1,4-diformylpiperazine*bis*(carbohydrazone)

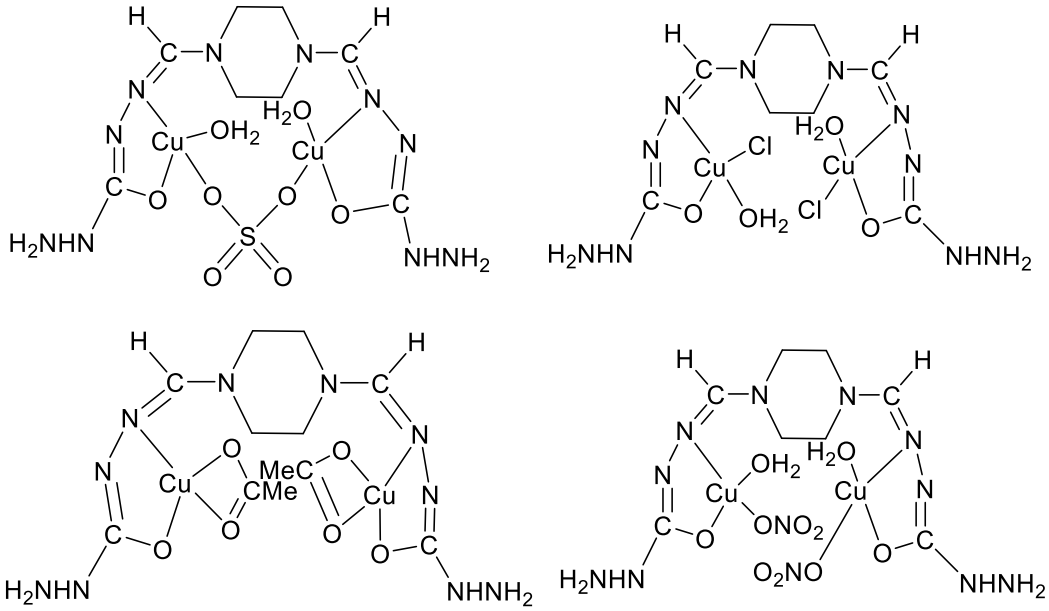

Figure1.16: Structure of the complexes of ligand L22

1.2.5 Hydroxybenzyl piperazine based ligandsand complexes

Ligands based on substituted *bis*-2-hydroxybenzyl with the homopiperazine and piperazine ring at the middle(Figure 1.17) have been studied and their complexes have been synthesized by Hancock *et al.*[73,74].

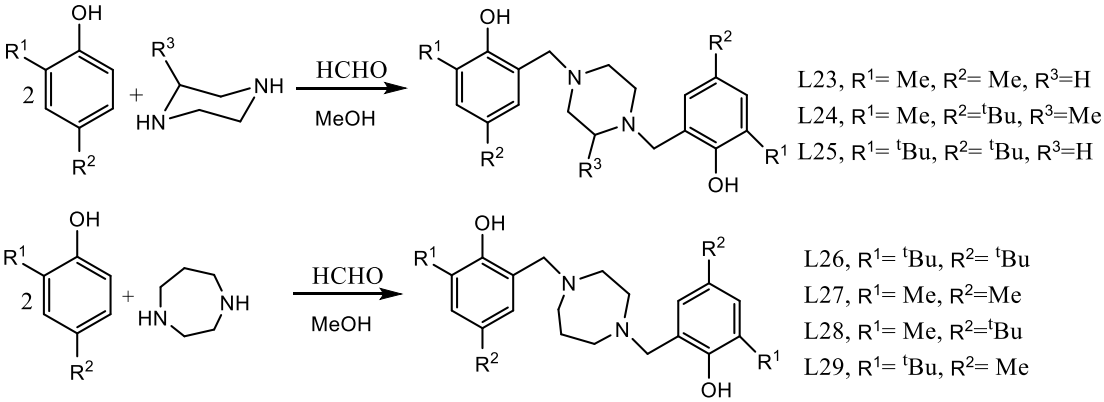

Figure1.17: Synthetic procedure of *bis*-2-hydroxy benzylpiperazine/homopiperazine ligands

Synthesis and characterization of aluminum complexes of hydroxybenzylpiperazine ligands have been done by Fulton *et al.*[75]They have synthesized both monometallic and bimetallic aluminum methyl complexes by treating of L25 with $AlMe_3$(Figure 1.18).

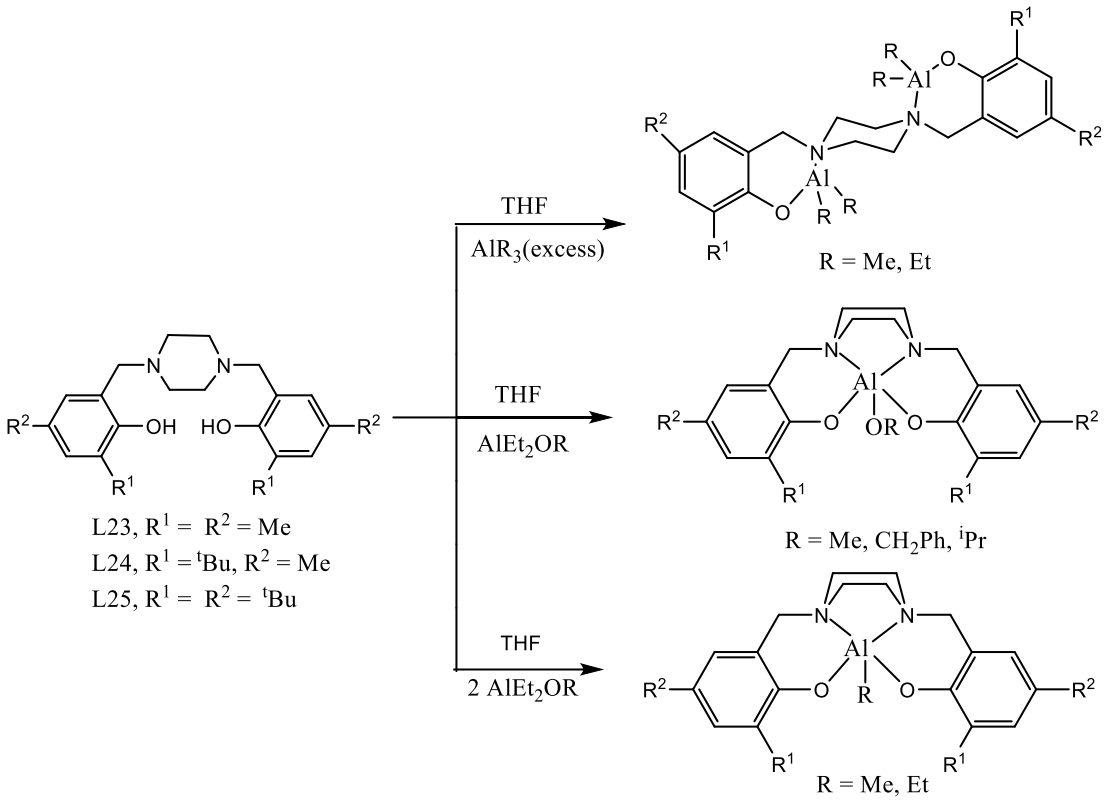

Figure1.18: Synthetic procedure of Al complexes of hydroxy-benzylpiperazine ligands

Similar and dinuclear[76]andmononuclear[77]aluminum complexes have also been prepared by Li and Chen *et al.*[78] with littlechanges in the structure of ligand. In the complexes, the aluminium ions are stabilized by phenolate ligands. Guo *et al.*[79] have reported structures and spectroscopic characterization of Cu^{2+} complexes of homopiperazine based*bis*-2-hydroxybenzyl ligand(L29) (Figure 1.19).

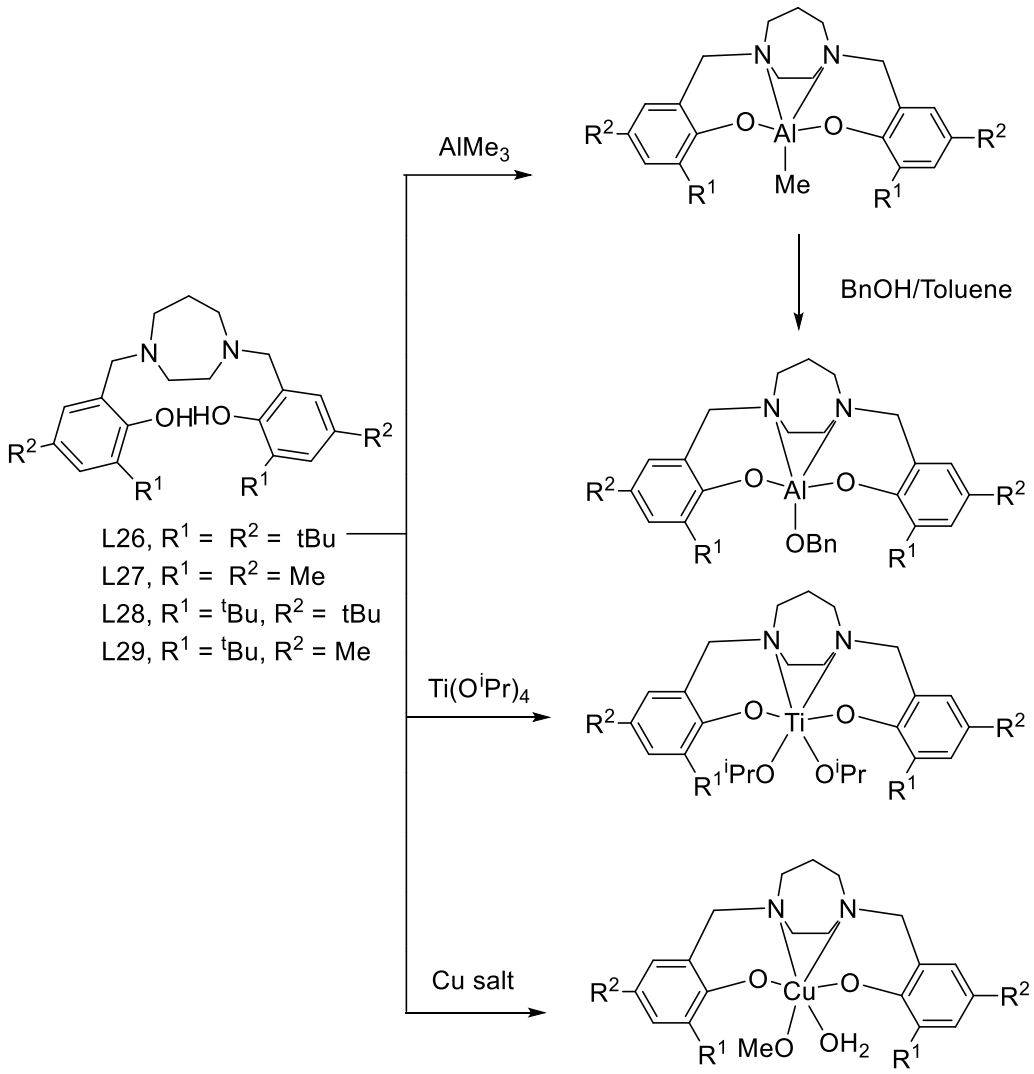

Figure1.19: Synthesis of Al, Ti and Cu complexes of homopiperazine based*bis*-2-hydroxybenzyl ligands

Mohanty *et al.*[80]have synthesized palladium complexes of similar ligands(L30,31) having different position of alkyl group (Figure 1.20) and they have used these complexes as catalysts in cross coupling reactions which are phosphine free diamino-diol based catalysts.

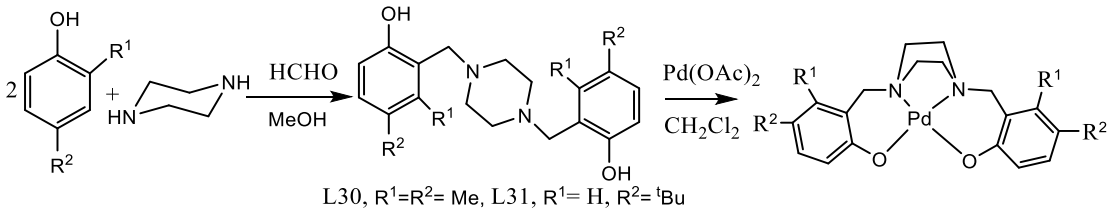

Figure1.20: Synthetic procedure of ligands L30, L31 and their Pd complexes

1.2.6 Pyrrole-piperazine based ligands and complexes

Piperazine pyrrole combination in ligands (L32 and L33) and their aluminum complexes have been praparedby Hu *et al.*[81]which are both nitrogen based heterocycles (Figure 1.21). Metal salt and ligand stoichiometry play a key role in deciding the number of ligands around the metal ions. Mixed ligands complexes were also prepared using some other co-ligands and effect of moistures have also been observed in these complexes (Figure 1.22 and 1.23).

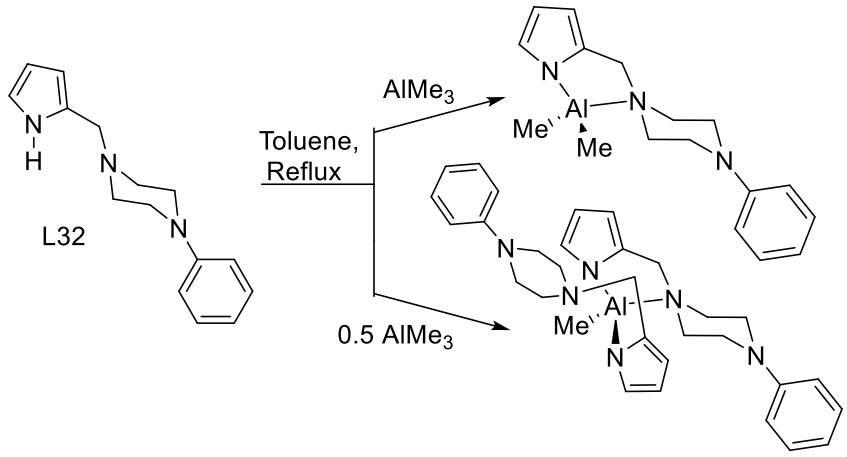

Figure1.21: Aluminium complexes of pyrrole piperazine based ligand L32

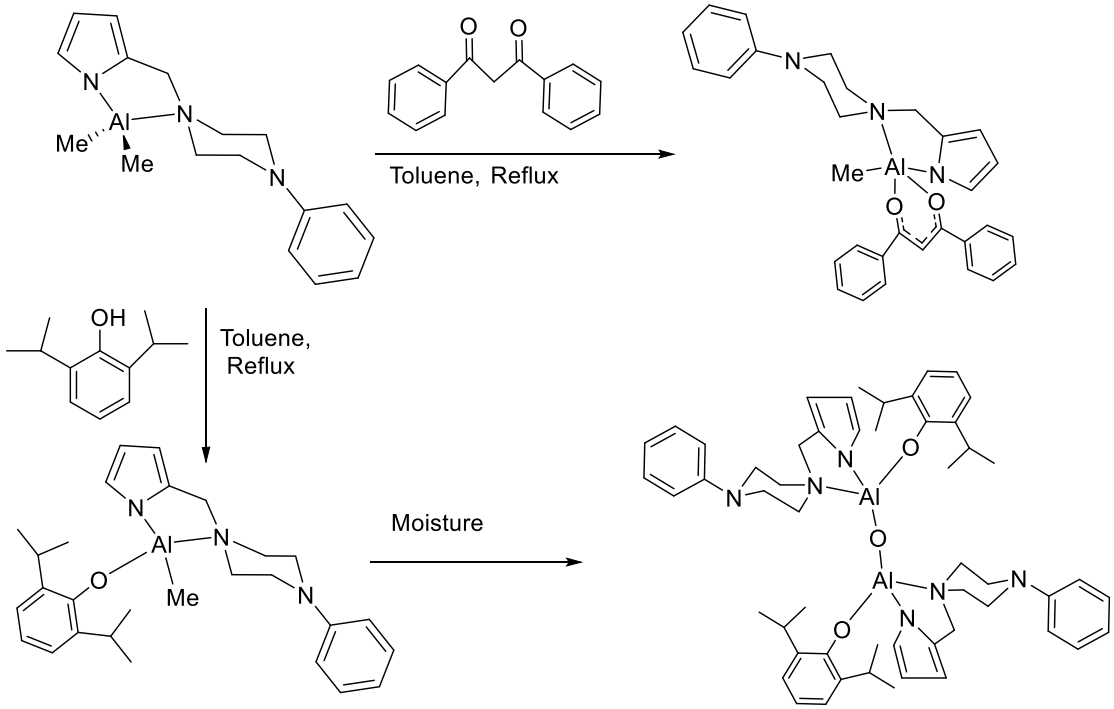

Figure1.22: Pyrrole piperazine ligand complexes of [$AlMe_2$(L32)]

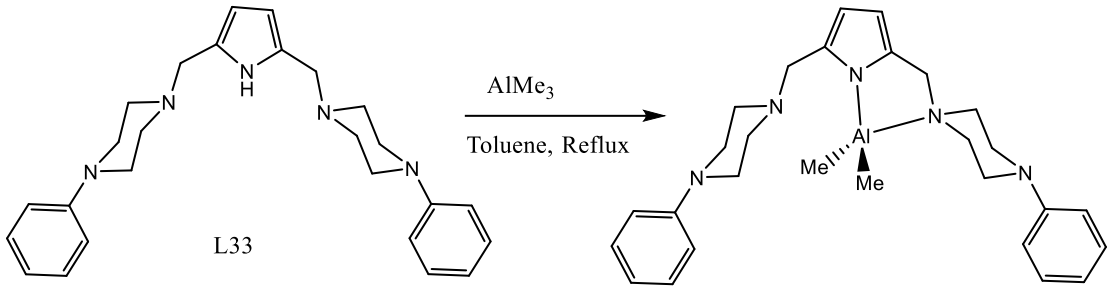

Figure1.23: Synthesis of metal complex of L33

Ligand based on dibenzo-dihydroxy-bispiperazine-dioxododecane(L34) and their Cu^{2+} and Zn^{2+} metal complexes has been prepared by Bhat *et al.*[82]to explore their biological activities (Figure 1.24). Non-ionic nature of these complexes has octahedral coordination around copper and zinc metal ions. Cyclic voltammetry,viscosity measurements and UV–vis, fluorescence methods have been used to study DNA binding calf thymus DNA.

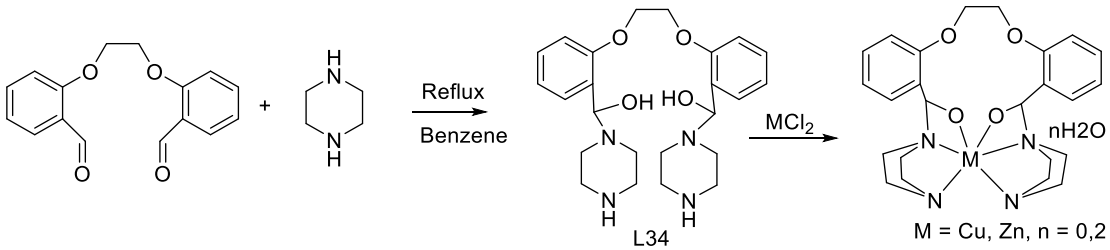

Figure1.24: Synthesis of L34 and its metal complexes

1.2.7 Schiff Base based piperazine ligands and complexes

Schiff Base ligands containing piperazine ring contains additional imine type bond available for metal binding. The asymmetric Schiff base ligand (Figure 1.25) based on salicylaldehyde and aminoethyl piperazine, (L35) has been prepared byMukhopadhyay *et al.*[83]. This ligand is used by Pait *et al.*[84]to prepare three copper complexes $[Cu(L35)(H_2O)_2(NO_3)](NO_3)$, $[Cu(L35)(N_3)(ClO_4)]$ and $[Cu_2(L35)(\mu\text{-}1,3\text{-}NCS)_2](ClO_4)_2.2H_2O$. These complexes have been tested for anticancer activity and protein binding studies.

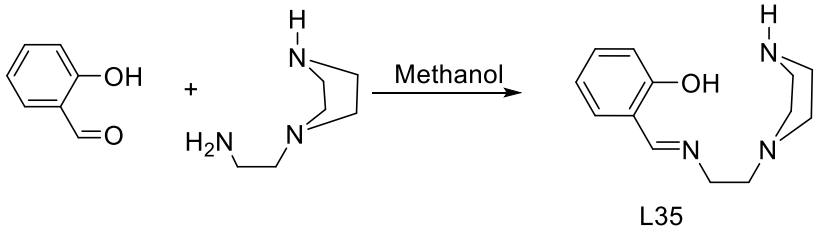

Figure1.25: Synthesis of Schiff Base ligand (L35)

In place of salicylaldehyde using pyridine carbaldehyde,ligand L36is obtained. Zinc, cadmium and mercury complexes of this tetradentate ligand has been prepared and structurally characterized by Purkit *et al*[85] (Figure 1.26).

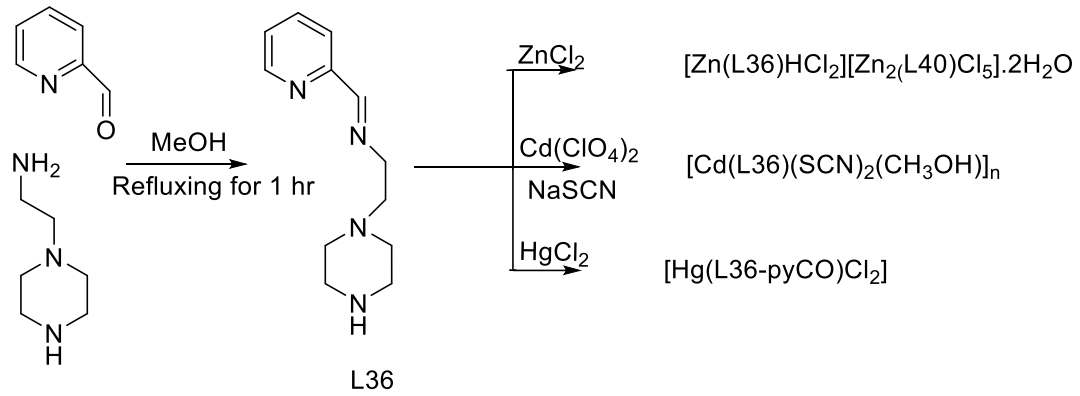

Figure1.26: Synthetic procedure of ligand and its complexes

Macrocyclic Schiff base type ligands (L37-39) and their manganese complexes have been prepared by Keypour *et al.*[60] by 1+1 templated direct cyclocondensation of or 2,6-pyridinedicarbaldehyde or 2,6-diacetylpyridine (Figure 1.27) with the (2-aminoethyl)(3-aminopropyl)piperazine or 1,4-bis(3-aminopropyl)piperazine and these ligands and complexes are characterized by FAB (Fast Atom Bombardment) mass and elemental analysis.

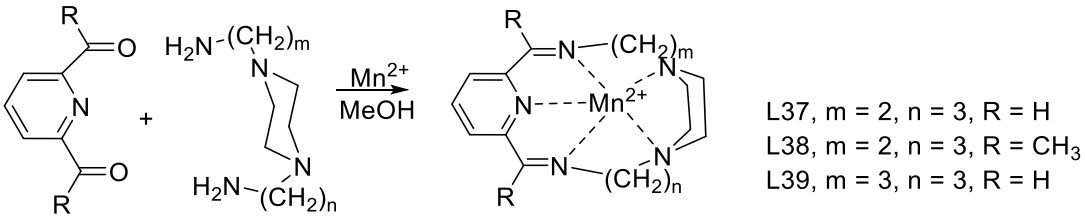

Figure1.27: Templated synthesis of macrocyclic Schiff base type ligands and manganese complexes

The aminobenzylpiperazinebased ligand (L40) has been prepared (Figure 1.28) by the reaction of 2-nitrobenzylchloride and piperazine followed by nitro group reduction using zinc by Keypour *et al.*[86] Their corresponding Mn^{2+} and Zn^{2+} macrocyclic complexes have also been prepared by the 1+1 templated cyclocondensation of ligand L40 and diacetylpyridine or pyridinedicarbaldehyde.

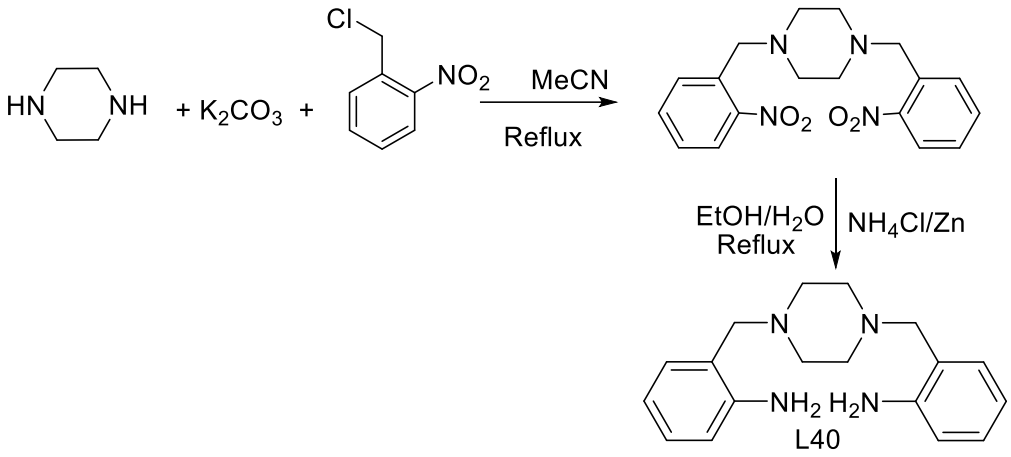

Figure1.28: Synthesis of ligand L40

The ligand L40act as precursor for further modification to Schiff Base ligand (L41-43) by reacting it with substituted salicylaldehyde in ethanol solvent (Figure 1.29).[87,88] The cobalt and copper complexes of these ligands have also been prepared and characterized (Figure 1.30).

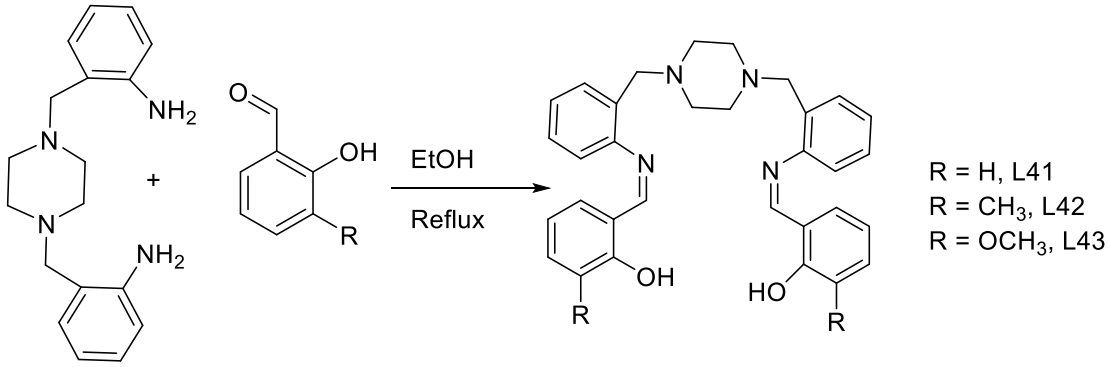

Figure1.29: Synthetic procedure of hexadentate N_4O_2 Schiff base ligands

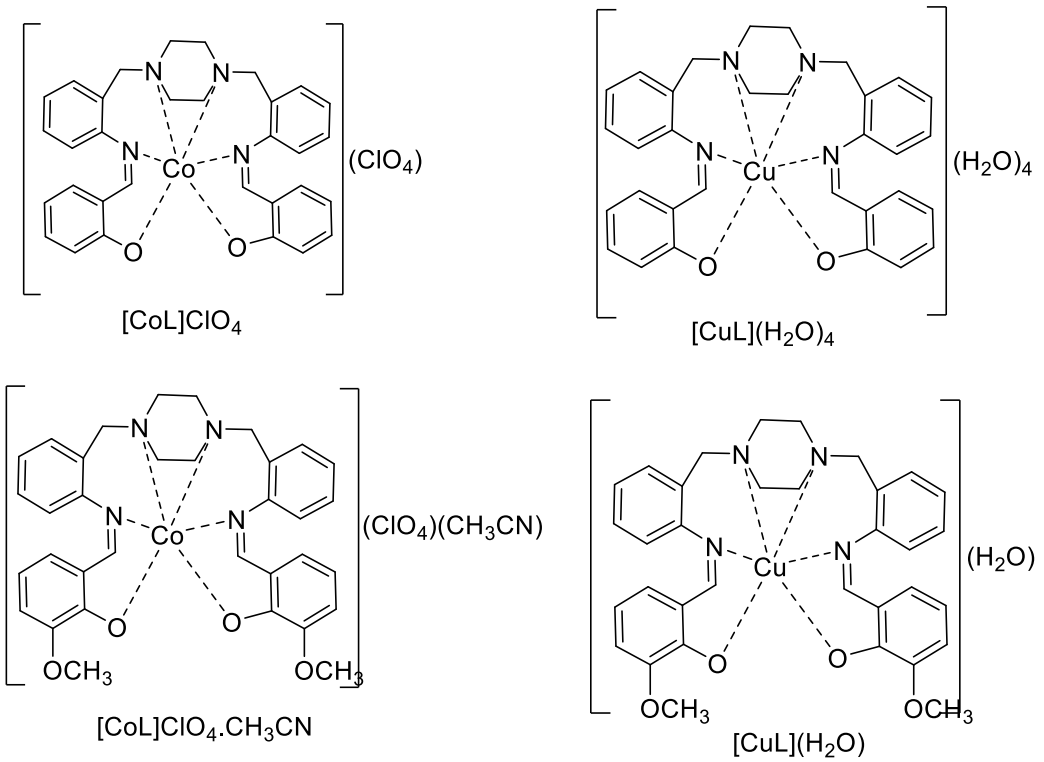

Figure1.30: Schiff base complexes of ligand L43

In a different approach, using piperazine and 2-fluorobenzaldehydeKeypour *et al.*[86] synthesized a ligand L44 (Figure 1.31)which were further converted to macrocyclic ligands with diamine and amino-alkanol [89] in one-pot cyclocondensation reaction resulting in ligands L45 and L46 through 1+1 and 2+2 cycloaddition reaction (Figure 1.32). Different metal complexes of ligand (L45) with zinc, cobalt and nickel have been synthesized and characterized by the reaction of the ligand (L45) and a respective metal salt.

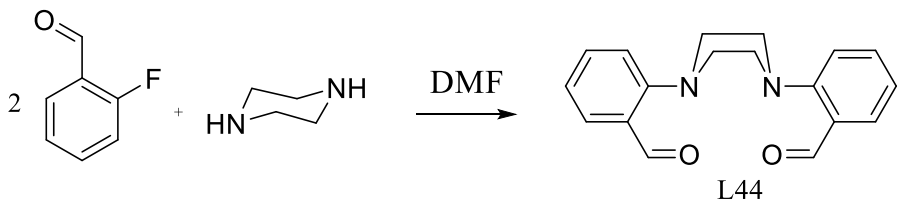

Figure1.31: Process of synthesis of ligand L44

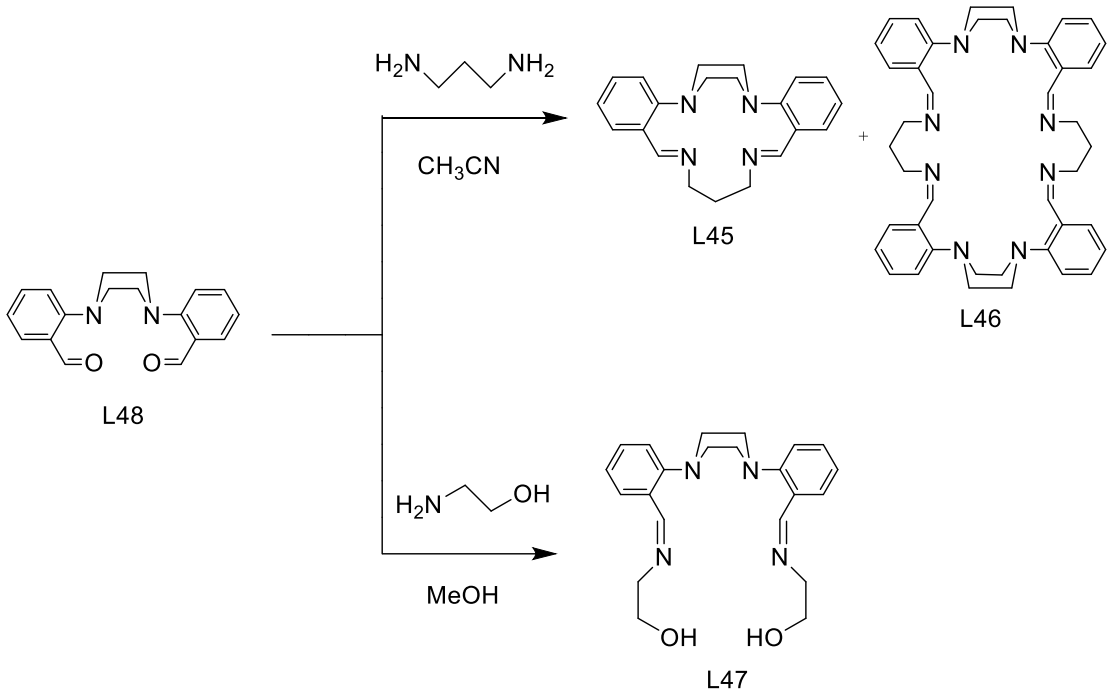

Figure1.32: Synthetic procedure of macrocyclic ligands L45, L46 and L47

El-Sherif *et al.* by adopting a different approach prepared another hexadentate ligand 1,4-*bis*[(2-hydroxybenzaldehyde)propyl]piperazine (L48) and its complexes by the reaction of salicylaldehyde with1,4-*bis*(3-aminopropyl)piperazine using ethanol as solvent (Figure 1.33).[90]

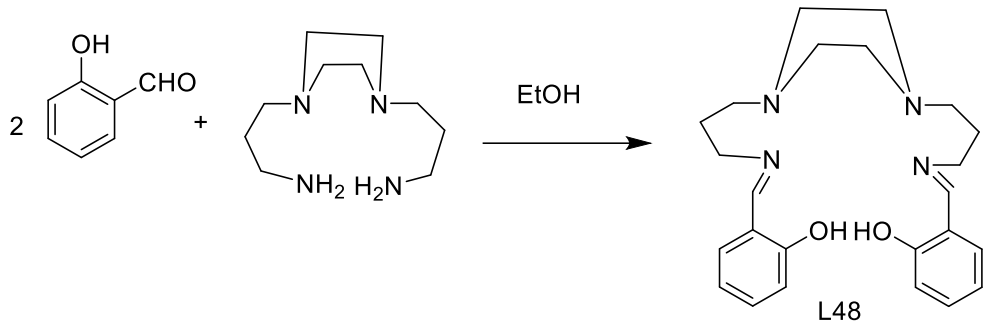

Figure1.33: Synthesis of ligand (L48)

Macrocycle ligand(L49) has been prepared in a four steps reaction by Nishant *et al.*[91] Ligand is synthesized by mixing 5-amino salicylic acid, formaldehyde and piperazine in ethanolic solutionfollowed by chlorination with $SOCl_2$, which further treated with ethylenediamine and finally give the macrocyclic ligand (Figure 1.34).

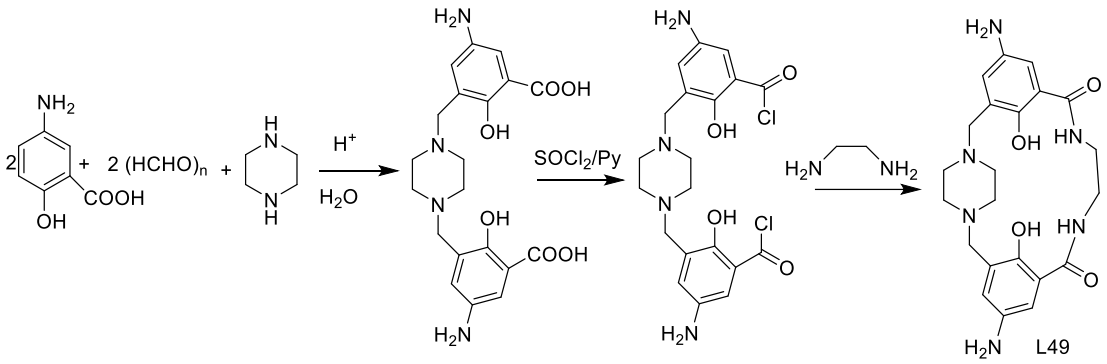

Figure1.34: Synthesis of macrocycle ligand (L49)

1.2.8 Carboxyphenylmethylene piperazine based ligands and complexes

A flexible piperazine containing ligand has been prepared by Hawes *et al.*[92]This ligand is utilized to build a porous coordination material which show selective CO_2uptake after solvent exchange and thermal activation. The ligand N,N-*bis*(1,4-carboxyphenylmethylene)piperazine (L50) is prepared in three steps reaction by treating4-bromomethyl benzoate with piperazine followed by hydrolysis (Figure 1.35).

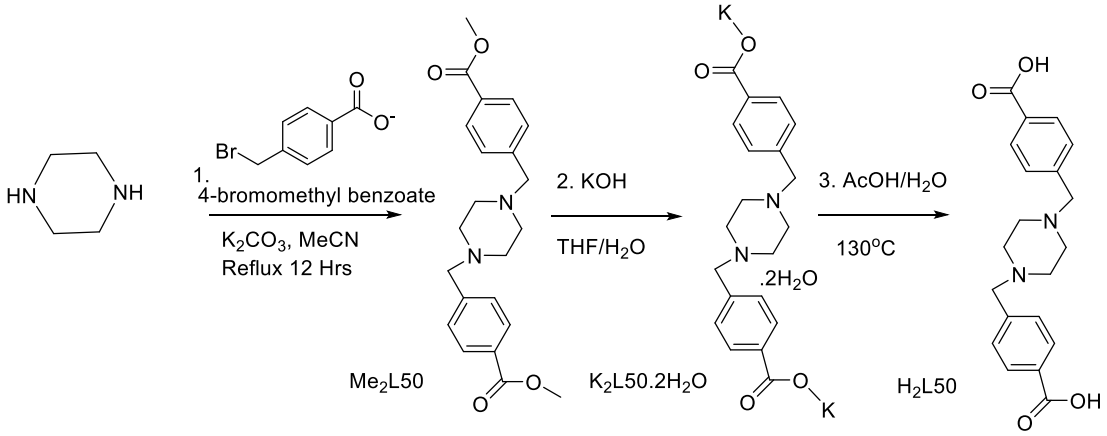

Figure1.35: Synthetic procedure of Me_2L50, $K_2L50.2H_2O$ and H_2L50

Application of piperazine ring-based ligands and complexes

1.2.9 Anti-microbial activity of ligands and complexes

Anti-bacterial activity of aryl piperazine derivatives (Figure 1.36) has been studied by Vibhor *et al.*[57] and Chaudhary *et al.*[93] using the standard drug ampicillin against four strains i.e. *E. coli, S. aureus, P. aeruginosa* and *S. epidermidis* respectively. Compounds exhibit moderate activity compared to the standard, while excellent activity against *S. aureusis* is shown by 1-(4-chlorophenyl)-4-propylpiperazine (L51) and against *P. aeruginosa. by* 1-(4-methylphenyl)-4-propylpiperazine (L52).

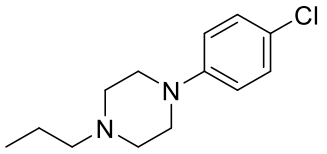

1-(4-chlorophenyl)-4-propylpiperazine

L51

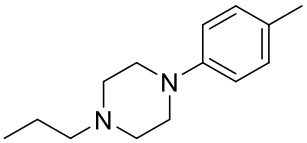

1-(4-methylphenyl)-4-propylpiperazine

L52

Figure1.36: Compounds having antimicrobial activity

Biological activity of cobalt, nickel, copper and zinc complexes of L9 has been given by Babu *et al.*[62] The metal complexes have shown higher anti-microbial action than the respective ligand and this was explained by chelation theory(Figure 1.37).

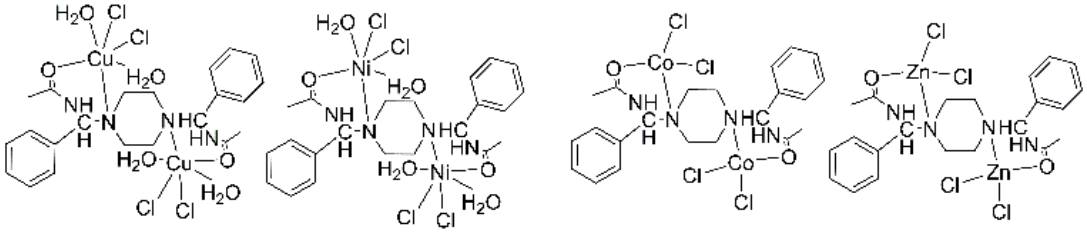

Figure 1.37: Copper, nickel, cobalt and zinc complexes exhibiting antibacterial and antifungal activity

Cytotoxic activity and antibacterial action of the Mn^{2+} and Zn^{2+} complexes of macrocyclic Schiff-base ligands have been analyzed.[87](Figure 1.38)Cytotoxic analysis studies indicated effectiveness of zinc complex was more as compared to doxorubicinstandard, and showing their potential to treat glioblastoma(a brain cancer). The analysis of anti-bacterial actionindicated that the manganese complex exhibit higher activity against *B. thuringiensis*, *Pectobacterium SP.* and *S. saprophyticus* thanstandards tobramycin and tetracycline.

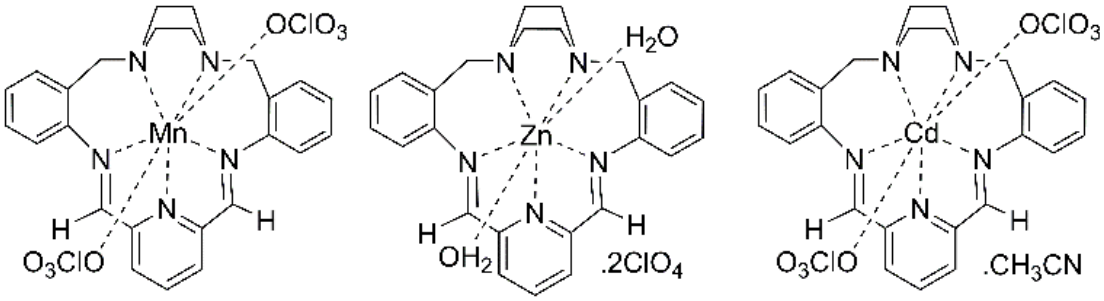

Figure1.38: Mn and Zn complexes possessing cytotoxic and antibacterial activities

Ligand L48 and its nickel copper and cobalt complexes (Figure 1.39) have been tested for antimicrobial application against selected bacteriaand fungi using disc selection

method. Antibacterial activity indicates that these complexes have high activity against the selected types of bacteria stain as compared to the free ligand.[90]

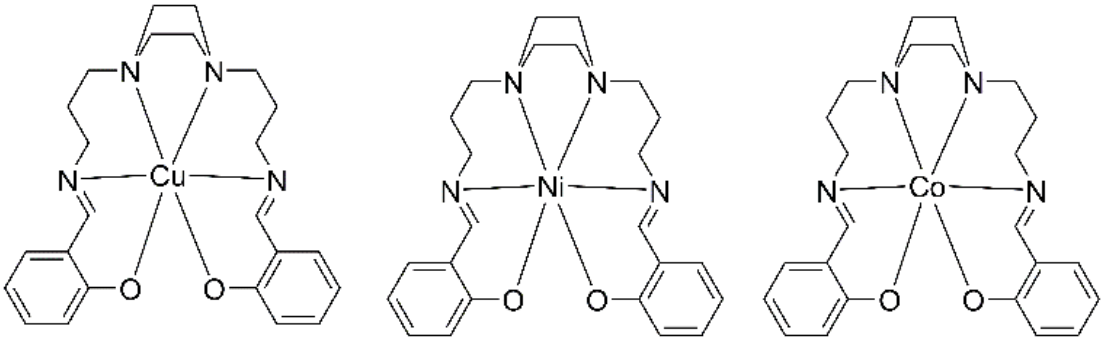

Figure1.39: Copper, nickel and cobalt complexes of L48possessing anti-microbial activity

1.2.10 DNA binding, protein binding, and anti-cancer activity of ligands and complexes

An important role in drug therapy is shown by the molecules which bind to plasma proteins as this binding provides a platform for molecules to act as drug and have an effect on the metabolic modification of ligands.

Copper complexes of asymmetric Schiff Base ligand (L35) were analyzed for protein binding and anti-cancerous studies by Pait *et al.*[84] BSA and metal complexes interaction in buffer solution has been studied by fluorescence and UV–Vis spectroscopy methods. The results indicate that tryptophan (amino acid residue in BSA) fluorescence quenching ability of complexes is strong mainly through static quenching. Anti-migratory, anti-proliferativeand cytotoxic activities have shown by all the complexes and all were active against human breast cancer cell line (Figure 1.40).

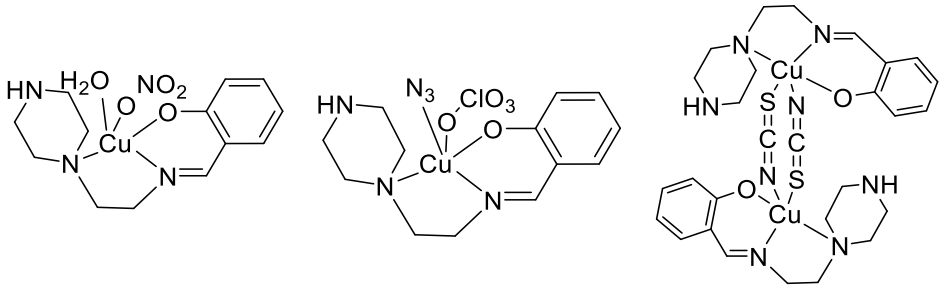

Figure1.40: Complexes of ligand L35for protein binding and cytotoxic activity (Uncoordinated ions and moleculesare omitted for simplicity)

Copper and zinc complexes of the ligand based on dibenzodihydroxybispiperazine (L34) as [L34Cu], [L34Zn] have been analyzed by Bhat *et al.*[82] for interaction with CT-DNA (Calf Thymus-DNA) using fluorescence, UV–vis,viscosity and cyclic voltammetry measurements (Figure 1.41). Results indicated that complexes interaction to CT-DNA have different affinities and thus they are groove binders. In vitro antimicrobial activity against fungi strain*A.niger, A. brassicicola*, and bacterial strain*P. aeruginosa, E. coli* were also carried out with these complexes. Result of antimicrobial action indicated zinc complexes was more active against both bacterial and fungal strains.

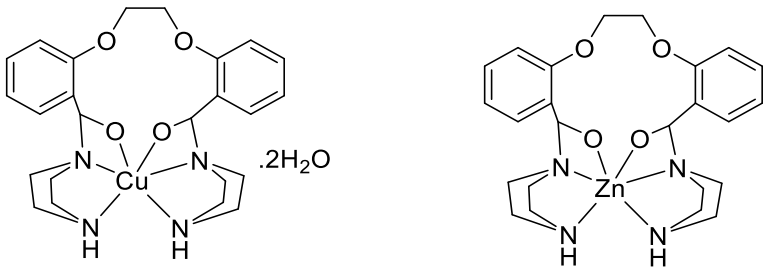

Figure1.41: Copper and zinc complexes of L34possessing anti-microbial activity

Mn^{2+} and Zn^{2+} complexes with ligands L41 L45 and its cytotoxic and antibacterial properties have been done by Keypour *et al.*[86] (Figure 1.42)

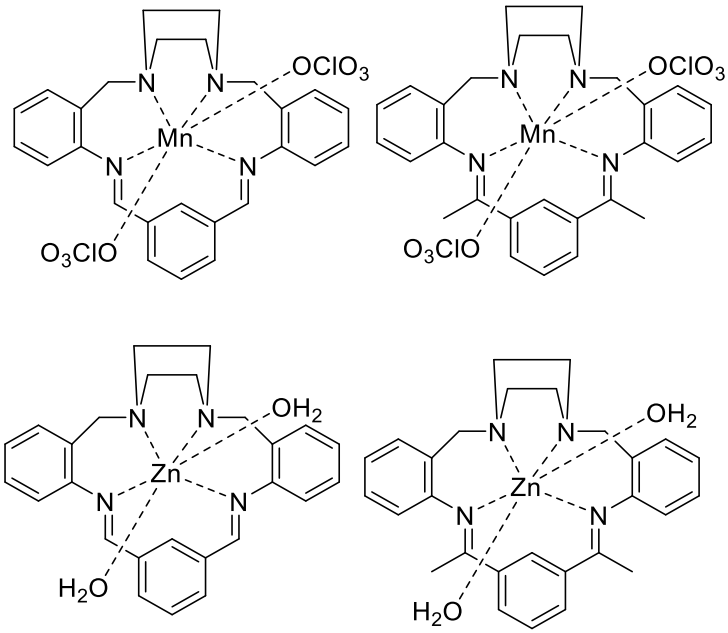

Figure1.42: Metal complexes exhibiting anti-microbial activity

1.2.11 Antioxidant activity of ligands and complexes

Antioxidants are compounds that inhibit oxidation that generates free radicals leading to chain reactions that affect the organism and their cells. Thiols and ascorbic acid are common antioxidants which are used to terminate these chain reactions. Plants and animals have a complex system of overlapping antioxidants to balance this oxidative stress, such as glutathione and enzymes produced internally.

Antioxidant properties of piperazine based molecules containing methylxanthine moiety have been studied by Andonova *et al.*[94], Pietrzycka *et al.*[95], Sloczyska *et al.*[96] and Kimura *et al.*[40]. In vitro antioxidant activity has been tested mainly by DPPH (Diphenylpcrylhydrazyl), ABTS (2,2'-azino-bis(3-ethylbenzothiazoline-6-sulfonic acid) and FRAP (Ferric ion reducing antioxidant power) methods. They have shown effect of various substituent groups attached to the piperazine ring (Figure 1.43).

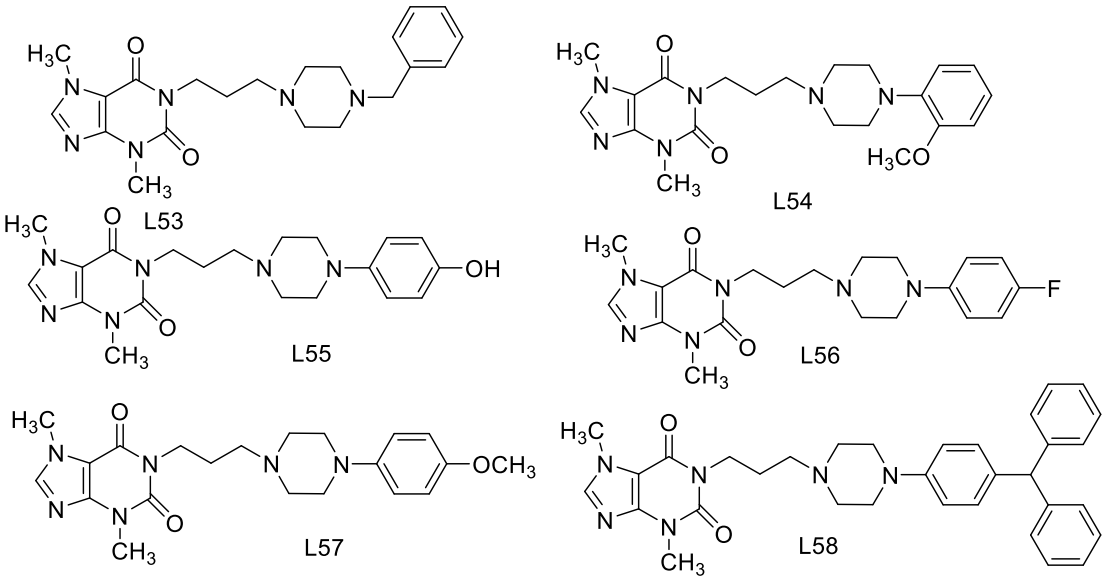

Figure1.43: Compounds having antioxidant activity

Anti-oxidant activity of Schiff bases type 1-(2-ketoiminoethyl)piperazines (Figure 1.44) have been described by Salga *et al*. The assay of these compounds showed significant inhibitory activities on hAChE (human acetylcholinesterase) by one of the compounds bearing hydroxo groups on the phenyl ring. The acute oral toxicity, antioxidant activities and molecular docking studies were also performed of these compounds.[97]

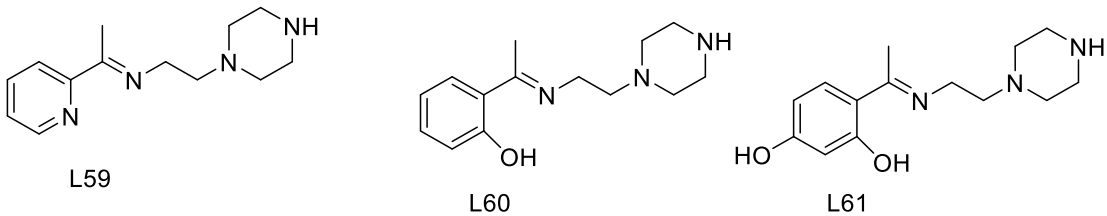

Figure1.44: Antioxidant compounds with various functional group

1.2.12 Catalytic applications of ligands and complexes

The main factors which are used to control reactions are temperature, pressure concentration of reactants and time duration. By increasing the temperature and pressure enables reactions to proceed at a higher rate of production but to maintain such condition it becomes more expensive. A catalyst accelerates the rate of reactions, and hence enabling to proceed them under the favorable pressure, temperature and other thermodynamic conditions.

Fulton *et al.*[75] have used aluminum complexes of hydroxybenzylpiperazine based ligands (L25) as catalyst in the ROP (ring-opening polymerization) of lactide and caprolactone with limited success**.** Similarlymononuclear[77] and dinuclear aluminum complexes[76]synthesized by Chen *et al.*[78] have been used as catalysts in the ε-Caprolactone polymerization (Figure 1.45 and 1.46).

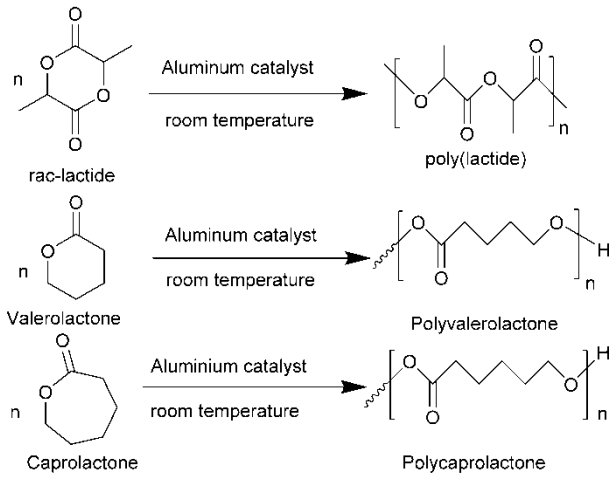

Figure1.45: Ring-opening polymerization of different cyclic polyesters by aluminium complex

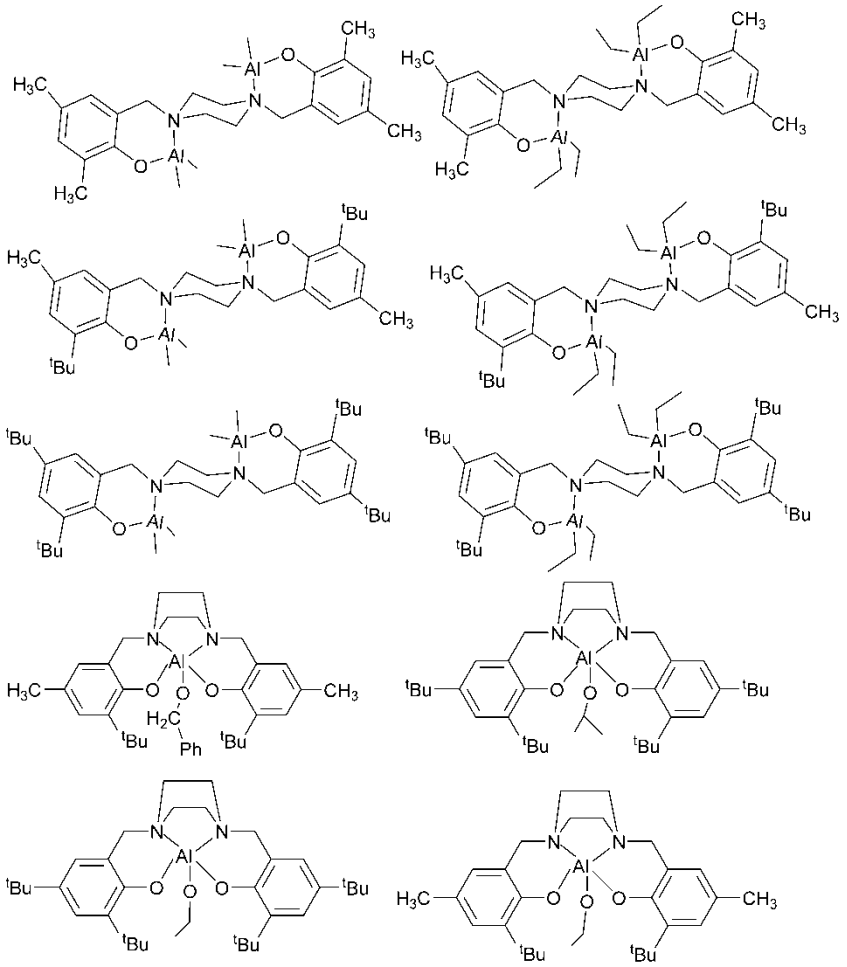

Figure 1.46:Structure of aluminium complexes used as ROP catalysts

Mn^{2+} complexes have been used as a catalyst for alkene epoxidation by Saravanan *et al.*[68]Out of several complexes prepared by them, effect of ring size on catalyst efficiency have been explained (Figure 1.47).

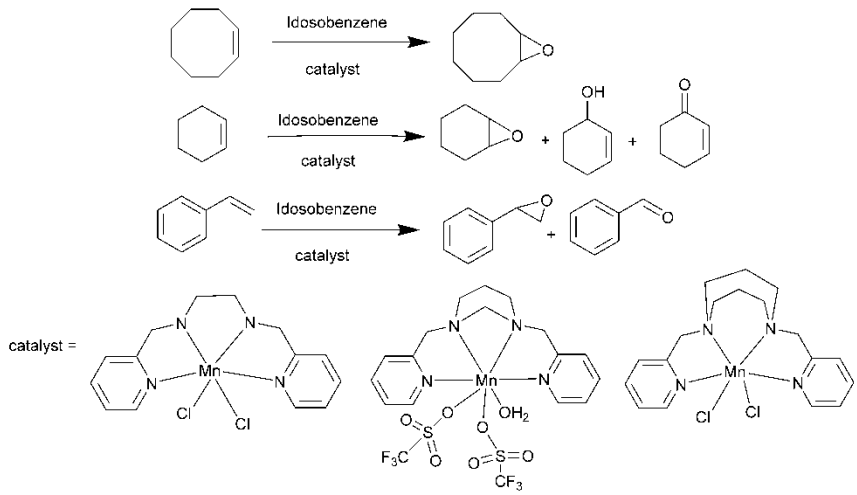

Figure 1.47: Manganese complexes catalyzed epoxidation of alkene

Palladium complexes of ligands (L30,31) have been preparedandused as catalysts in Suzuki–Miyaura reactions. The catalyst is used to catalyze cross coupling reaction based on phenylboronic acid and aryl bromides (Figure 1.48).[80]

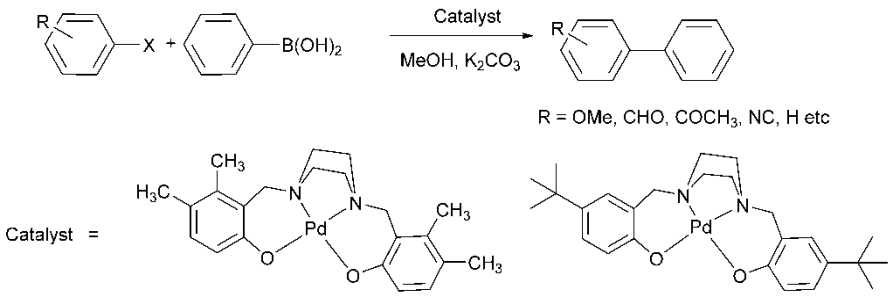

Figure1.48: Cross coupling reaction catalyzed by palladium complexes

1.2.13 Metal organic frameworks (MOFs) of ligands and complexes

MOF's[98,99]are a class of coordination polymers[100] with organic linkers connecting clusters or metal ions so as to form one dimensional chains, two dimensional sheets or 3D blocks.[101] Metal Organic Framework (MOF'S) are the compounds in which interaction between ligand to metal produce porous coordination networks which may result in record setting surface areas.[102] For the construction of MOFs two major components are required, the organic linker acting as the ligand[103] and a metal ion or cluster as the point of attachment. The attachment point can be at the corner or at the sides. Both the ligand and the metal contribute to exceptional crystallinity, tuneable porosity and structural diversity. The denticity of the ligand and the spatial position of the ligating atoms as well as the geometry and coordination number of the metal ion determine the shape and size of the pores of the material. In addition to metal ions, secondary building units (SBUs) consisting of inorganic polynuclear clusters can also be connected by organic linkers via strong bonds.[104,105] By virtue of their unique design, polynuclear cluster nodes, or SBUs, can introduce extra stability due the presence of strong and directional covalent bonds within the bulk material compared to weak nondirectional bond found in metal ions bound to neutral organic donor linkers. Selection from a library of units with predetermined topologies result in engineered materials with special applications in catalysis, gas storage, sensing and drug delivery system.[106,107]

Solvothermal synthesis has remained to be the most common method for the synthesis of MOFs with the solvent molecules occupying the pores.[108–110] Templated synthesis

of zeolites or use of metal binding solvents like N,N-dimethylformamide[111–113] and water are also widely exploited.[114,115] Recent advances in the microwave-assisted solvothermal synthesis has proved helpful in tackling the major drawback of it being slow and problems related to scaling up.[116–121] Solvent free methods are reported using proligands which convert into suitable organic linkers upon heating.[122–125] MOF films and composites are also constructed using chemical vapor deposition method.[126–130]

The structure of these MOFs can be best explained by X-ray crystallography techniques since conventional methods like IR or NMR may sometime fail to elucidate the actual structure. The MOF's application includes sensors[131,132], catalysis[133], separation[134,135] and storage of gases[136–140] and others.[141]

Pyromellitate coordination polymers having piperazine unit has been synthesized and structurally characterized by Ganesan *et al.*[142]. Hydrothermal methods have been employed for the preparation of two new coordination polymers of the pyromellitic acid ($C_{10}H_6O_8$), [$Zn_2(H_2O)$(pyromellitate)(piperazine)] and [$Cd_4(H_2O)_2$(pyromellitate)$_2$(piperazine)$_3$], in the presence of piperazine. Both the coordination polymers exhibit photoluminescence at room temperature. They have employed piperazine and aminopropyl piperazine which ligate metal ion and have direct influence in the photoluminescence properties of the polymer formed.

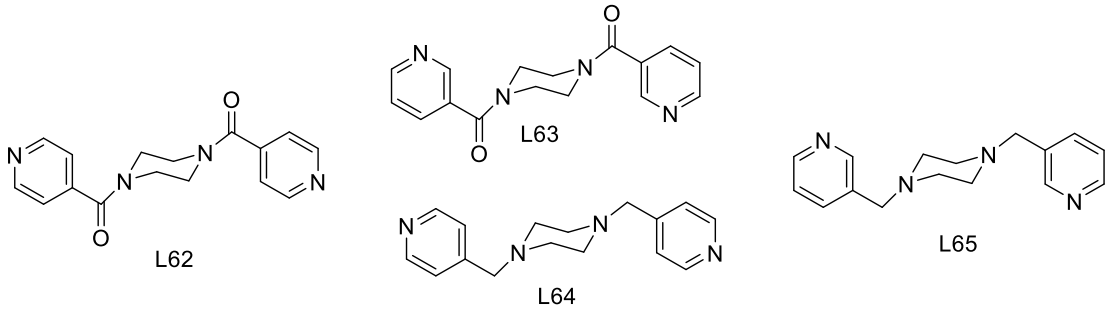

Figure1.49: Pyridyl piperazine based ligands used in MOFs

Metal ligands based polymeric material containing flexible bispyridylmethylpiperazine (L64) and divalent metal isophthalate tethers have been given by Martin *et al.*[145]Structural chemistry of metal coordination polymers incorporating *bis*(4-pyridylmethyl)piperazine and para aromatic dicarboxylate ligands with zinc and cadmium have been given by Farnum *et al.*[146,147](Figure 1.49).

Study of cadmium linked bis(4-pyridylformyl)piperazine(L62) coordination polymers, 3,5-connected binodal lattice and layered nets have been done by Lucas *et al.*[148]and selectivity between rare fsc(fully self-connected) and simple chain network topologies have been given by Mizzi *et al.*[149]When an aqueous solution of cadmium salt is slowly diffused to the methanolic solutions of L62, crystalline coordination polymer is generated in which the nature of the counter anion is responsible for dimensionality and topology. Binding of N-atom of pyridyl nitrogen and O-atom of amide carbonyl in $[Cd(L62)Cl_2]_n$ and $[Cd(L62)(NO_3)_2]_n$ have resulted in 2-D coordination polymer layers Similar layer motifs formation is also shown by $[(Cd(L62)\ (H_2O)_2)(ClO_4)_2(L62)_3H_2O]_n$. Blue-violet luminescence is shown by all the species on ultraviolet light exposure (Figure 1.50).

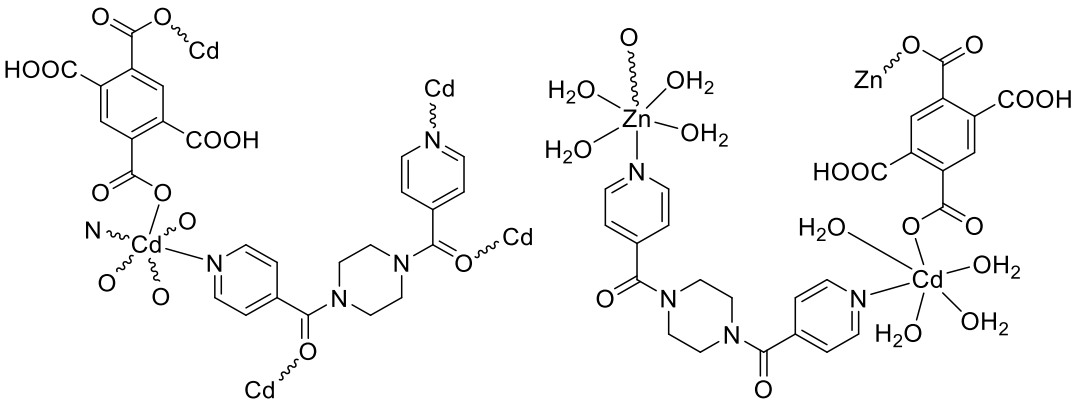

Figure1.50: Metal organic frameworks of pyridyl piperazine with cadmium and zinc

Structural dynamics and coordination chemistry of long and flexible ligand containing piperazine had also been given by Hawes *et al.*[150] Ligand had been internally functionalizedandused in the preparation of porous coordination polymers with Co^{2+}, Cd^{2+}, and Ag^{2+} metalions. Linear conformation is adopted by the ligand in poly-[Cd(L64a)(terephthalate)] and poly-[Co(L64a)(isophthlate)].

Selective CO_2 uptake and it's structural chemistry of a permeableMOF of ligand L50 has been done by Hawes *et al.*[92] They synthesized and characterized flexible piperazine-derived ligands containing carboxylic acid and demonstrated its utility in how the formation of porous coordination polymer occurs. In complex $[Zn_3(L50)_2(OH)_2]\cdot 2DMF\cdot 0.5H2O$, the ligand backbone is encouraged to adopt a bowed form through template action by the H-bond interaction of guest molecules. The complex shows selective affinity for CO_2 after activation by methanol exchange

and evacuation, adsorbing 77 cm^3/ g CO_2 at 25 bar and 273 K. These results provide a further motivation for the research of internally functionalized non-identical ligands in framework synthesis (Figure 1.51).

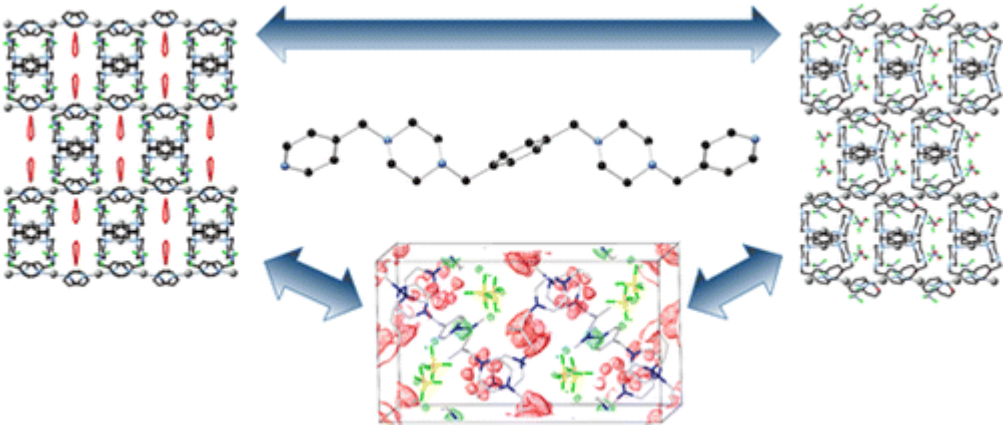

Figure1.51: Metal organic frameworks for selective CO_2 uptake

1.3 Literature Gap

At this juncture it will be interesting to know how piperazine bearing molecules behave in our body. How they interact with the large biomolecules? Do they form covalent bonds as an electrophile attacking the biomolecules and become parts of a cascading signaling chain or form hydrogen bonds or other noncovalent interactions filling pockets or grooves to have an allosteric effect on the working of other biomolecules? The intriguing binding atoms placed conveniently in these molecules arouse the curiosity how these molecules will interact with metal ions present in the vicinity?

Such questions thrust our research and this thesis towards a controlled study of a series of piperazine based towards metal binding, and their bioactivity.Literature study reveals that, work has been done mostly on pyridyl or hydroxybenzyl appended piperazines with symmetrical substitution. Much work can still be done by preparing the unsymmetrical derivative of piperazine along with other coordination moiety. New methodology or new synthetic routs can be uncovered for the synthesis of the molecules. Organic groups containing suitable donor atoms can be linked to the piperazine ring through linkers like formaldehyde or suitable epoxides, which will lead to synthesis of new ligands. Metal complexes synthesized from piperazine based ligands have shown various applications but still the data is lacking for complete

analysis of DNA binding, protein binding, antioxidant, and anti-microbial property of these complexes. Metal ligand interaction studies are also of limited nature where only a few MOF are reported but they can be further exploited for interesting applications.

1.4 Objectives

- To synthesize ligands based on piperazine ring
- To synthesize few transition metal complexes of the synthesized ligands.
- To characterize the synthesized ligands and complexes by common spectroscopic technique like IR, UV-vis, NMR, MS etc.
- To monitor biological activities such as antimicrobial, antioxidant, DNA binding and protein binding activity of synthesized ligands and their metal complexes
- To corroborate the experimental results with computational properties of the synthesized molecules.

1.5 Proposed Methodology

The ligands will be synthesized according to the standard procedure reported. First, substituted anilines will be synthesized or purchased directly. Secondly, diethanolamine will be converted to its halogen derivative by treating them with hydrobromic acid for the bromo derivative and with thionyl chloride for synthesis of the chloro derivative respectively. Reaction of the substituted anilines with these dihalo-amines under basic condition in presence of potassium carbonate will produce the corresponding ligands (Figure 1.52).

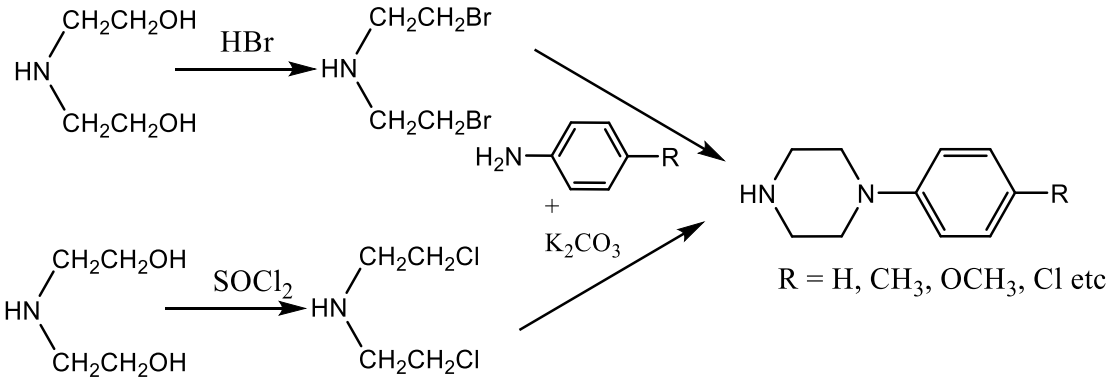

Figure 1.52: Synthetic Scheme (1) for ligands

Many substituents are possible at the phenyl ring, of which methyl, methoxy and chloro groups are chosen for the present purpose for their bioactivity. Starting with the corresponding substituted aniline the desired ligand could be synthesized.

A different set of ligands could also be synthesized by substitution at the second nitrogen atom of the phenylpiperazines. Aliphatic substituents like methyl or ethyl could be introduced in the initial steps. The diethanolamine on reaction with alkyl iodide like methyl iodide or ethyl iodide in presence of potassium carbonate will produce the N-methyl diethanolamine or N-ethyl diethanolamine. These can be used further through halogenation and cyclization with substituted aniline to produce the desired ligand molecule (Figure 1.53).

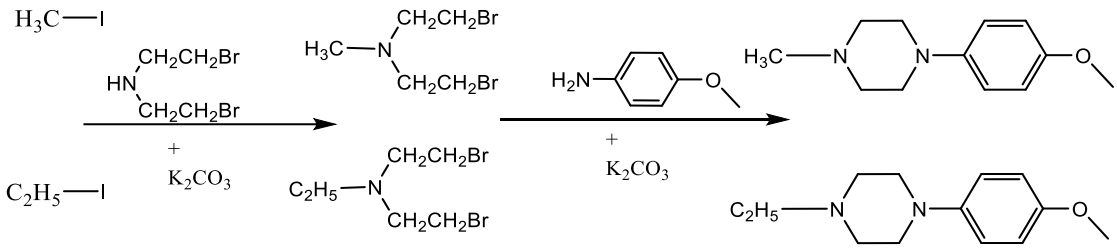

Figure 1.53: Synthetic Scheme (2) for ligands

Another way of synthesis involve reaction of piperazine with suitable alkyl dihalide to produce substituted dipiperazine derivatives which on further reaction with functionalized benzylchloride produces substitution in both N atom of piperazine (Figure 1.54).

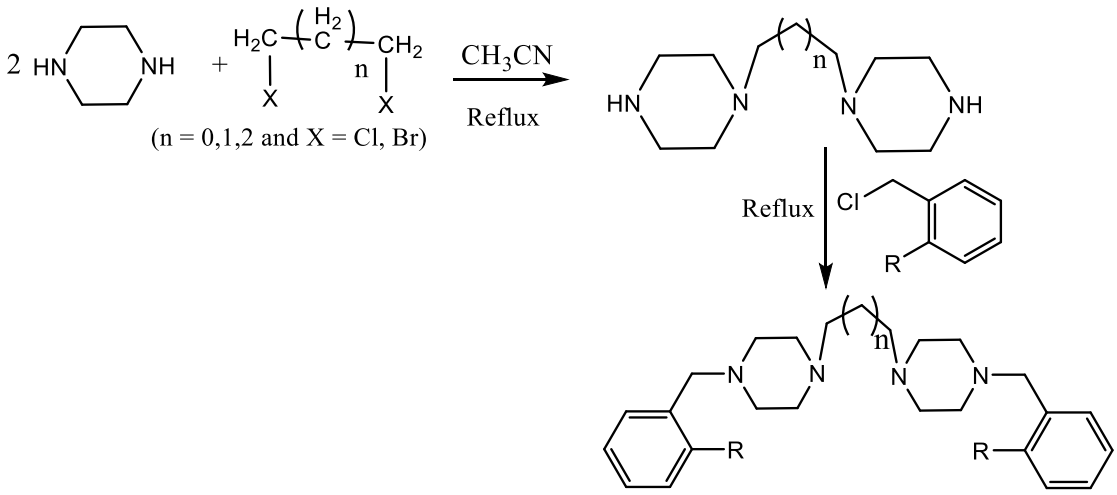

R = OH, OCH_3, NH_2, $N(CH_3)_2$ etc

Figure 1.54: Synthetic scheme (3) for ligands

Metal complexes with these ligands will be synthesized by reacting metal salts with these ligands in a suitable solvent. Metal chloride, nitrate or acetate salts can be used for this purpose (Figure 1.55).

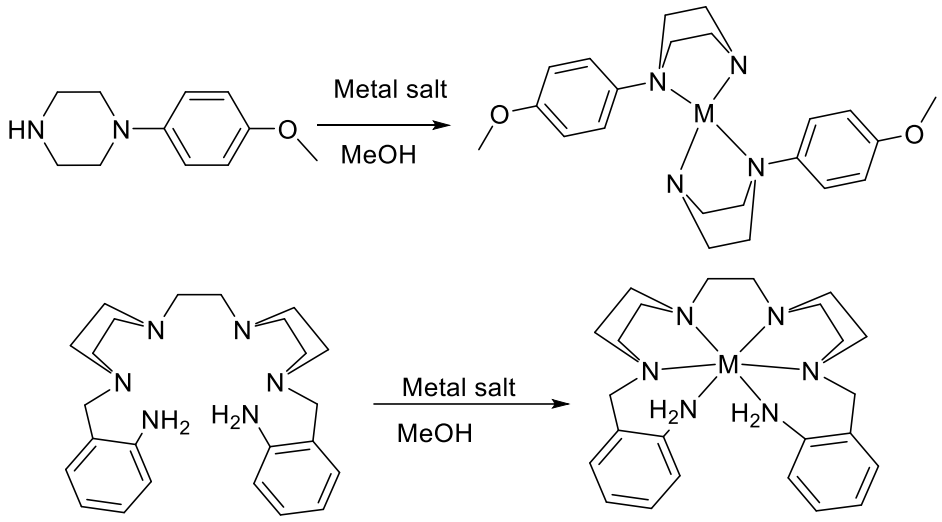

Figure 1.55: Synthetic scheme for metal complexes

Transition metals complexes with the newly synthesized ligands will be prepared and extensively characterized by different spectroscopic methods including, UV-vis, FT-IR, ESI-MS, and Structural characterization will be performed through X-ray diffraction of single crystals grown of the metal complexes.

1.6 References:

(1) Young, D. W. *Heterocyclic Chemistry*; Longman: London ; New York, 1975.

(2) Yang, S. M.; Malaviya, R.; Wilson, L. J.; Argentieri, R.; Chen, X.; Yang, C.; Wang, B.; Cavender, D.; Murray, W. V. Simplified Staurosporine Analogs as Potent JAK3 Inhibitors. *Bioorganic Med. Chem. Lett.***2007**, *17* (2), 326–331. https://doi.org/10.1016/j.bmcl.2006.10.062.

(3) Schmidt, A. W.; Reddy, K. R.; Knölker, H. J. Occurrence, Biogenesis, and Synthesis of Biologically Active Carbazole Alkaloids. *Chem. Rev.***2012**, *112* (6), 3193–3328. https://doi.org/10.1021/cr200447s.

(4) Shaquiquzzaman, M.; Verma, G.; Marella, A.; Akhter, M.; Akhtar, W.; Khan, M. F.; Tasneem, S.; Alam, M. M. Piperazine Scaffold: A Remarkable Tool in Generation of Diverse Pharmacological Agents. *Eur. J. Med. Chem.***2015**, *102*, 487–529. https://doi.org/10.1016/j.ejmech.2015.07.026.

(5) Asif, M. Piperazine and Pyrazine Containing Molecules and Their Diverse Pharmacological Activities. **2015**, *01* (01), 5–11. https://doi.org/10.7439/ijasr.

(6) Nekrasov, D. D. Biological Activity of 5- and 6-Membered Azaheterocycles and Their Synthesis from 5-Aryl-2,3-Dihydrofuran-2,3-Diones. (Review). *Chem. Heterocycl. Compd.***2001**, *37* (3), 263–275. https://doi.org/10.1023/A:1017505929583.

(7) Todorovic, A.; Haskell-Luevano, C. A Review of Melanocortin Receptor Small Molecule Ligands. *Peptides*. 2005. https://doi.org/10.1016/j.peptides.2004.11.024.

(8) Keywor, D. A. Ionization Constants for Some Piperazine Derivatives. **1969**, No. September 1959, 1355–1356.

(9) Khalili, F.; Henni, A.; East, A. L. L. PKa Values of Some Piperazines at (298, 303, 313, and 323) K. *J. Chem. Eng. Data***2009**, *54* (10), 2914–2917. https://doi.org/10.1021/je900005c.

(10) Jouve A Gras, A.; Benyamine, R. The current treatment of angina pectoris. Trial of new piperazine derivatives. *Vie Med.***1963**, *44*, 115–120.

(11) Rathi, A. K.; Syed, R.; Shin, H. S.; Patel, R. V. Piperazine Derivatives for Therapeutic Use: A Patent Review (2010-Present). *Expert Opin. Ther. Pat.***2016**, *26* (7), 777–797. https://doi.org/10.1080/13543776.2016.1189902.

(12) Horton, D. A.; Bourne, G. T.; Smythe, M. L. The Combinatorial Synthesis of Bicyclic Privileged Structures or Privileged Substructures. *Chem. Rev.***2003**, *103* (3), 893–930. https://doi.org/10.1021/cr020033s.

(13) Al-Ghorbani, M.; Bushra Begum, A.; Zabiulla, Z.; Mamatha, S. V.; Khanum, S. A. Piperazine and Morpholine: Synthetic Preview and Pharmaceutical Applications. *Res. J. Pharm. Technol.***2015**, *8* (5), 611–628. https://doi.org/10.5958/0974-360X.2015.00100.6.

(14) Phillips, O. A.; Udo, E. E.; Samuel, S. M. Synthesis and Structure-Antibacterial Activity of Triazolyl Oxazolidinones Containing Long Chain Acyl Moiety. *Eur. J. Med. Chem.***2008**, *43* (5), 1095–1104. https://doi.org/10.1016/j.ejmech.2007.07.006.

(15) Lohray, B. B.; Lohray, V. B.; Srivastava, B. K.; Gupta, S.; Solanki, M.; Pandya, P.; Kapadnis, P. Novel 4-N-Substituted Aryl Pent-2-Ene-1,4-Dione

Derivatives of Piperazinyloxazolidinones as Antibacterials. *Bioorganic Med. Chem. Lett.***2006**, *16* (6), 1557–1561. https://doi.org/10.1016/j.bmcl.2005.12.025.

(16) Foroumadi, A.; Ghodsi, S.; Emami, S.; Najjari, S.; Samadi, N.; Faramarzi, M. A.; Beikmohammadi, L.; Shirazi, F. H.; Shafiee, A. Synthesis and Antibacterial Activity of New Fluoroquinolones Containing a Substituted N-(Phenethyl)Piperazine Moiety. *Bioorganic Med. Chem. Lett.***2006**, *16* (13), 3499–3503. https://doi.org/10.1016/j.bmcl.2006.03.103.

(17) Foroumadi, A.; Emami, S.; Mansouri, S.; Javidnia, A.; Saeid-Adeli, N.; Shirazi, F. H.; Shafiee, A. Synthesis and Antibacterial Activity of Levofloxacin Derivatives with Certain Bulky Residues on Piperazine Ring. *Eur. J. Med. Chem.***2007**, *42* (7), 985–992. https://doi.org/10.1016/j.ejmech.2006.12.034.

(18) Gan, L.; Fang, B.; Zhou, C. Synthesis of Azole-Containing Piperazine Derivatives and Evaluation of Their Antibacterial , Antifungal and Cytotoxic Activities. **2010**, *31* (12), 3684–3692. https://doi.org/10.5012/bkcs.2010.31.12.3684.

(19) Watkins, W. J.; Chong, L.; Cho, A.; Hilgenkamp, R.; Ludwikow, M.; Garizi, N.; Iqbal, N.; Barnard, J.; Singh, R.; Madsen, D.; et al. Quinazolinone Fungal Efflux Pump Inhibitors. Part 3: (N-Methyl)Piperazine Variants and Pharmacokinetic Optimization. *Bioorganic Med. Chem. Lett.***2007**, *17* (10), 2802–2806. https://doi.org/10.1016/j.bmcl.2007.02.047.

(20) Upadhayaya, R. S.; Sinha, N.; Jain, S.; Kishore, N.; Chandra, R.; Arora, S. K. Optically Active Antifungal Azoles: Synthesis and Antifungal Activity of (2R,3S)-2-(2,4-Difluorophenyl)-3-(5-{2-[4-Aryl-Piperazin-1-Yl]-Ethyl} -Tetrazol-2-Yl/1-Yl)-1-[1,2,4]-Triazol-1-Yl-Butan-2-Ol. *Bioorganic Med. Chem.***2004**, *12* (9), 2225–2238. https://doi.org/10.1016/j.bmc.2004.02.014.

(21) Rokosz, L. L.; Huang, C. Y.; Reader, J. C.; Stauffer, T. M.; Chelsky, D.; Sigal, N. H.; Ganguly, A. K.; Baldwin, J. J. Surfing the Piperazine Core of Tricyclic Farnesyltransferase Inhibitors. *Bioorganic Med. Chem. Lett.***2005**, *15* (24), 5537–5543. https://doi.org/10.1016/j.bmcl.2005.08.074.

(22) Chen, J.; Lu, M.; Jing, Y.; Dong, J. The Synthesis of L-Carvone and Limonene Derivatives with Increased Antiproliferative Effect and Activation of ERK

Pathway in Prostate Cancer Cells. *Bioorganic Med. Chem.***2006**, *14* (19), 6539–6547. https://doi.org/10.1016/j.bmc.2006.06.013.

(23) Shami, P. J.; Saavedra, J. E.; Bonifant, C. L.; Chu, J.; Udupi, V.; Malaviya, S.; Carr, B. I.; Kar, S.; Wang, M.; Jia, L.; et al. Antitumor Activity of JS-K [O 2 - (2 , 4-Dinitrophenyl) Diazeniumdiolates in Vitro and in Vivo. *Metab. Clin. Exp.***2006**, 4356–4366.

(24) Guo, C.; Tong, R.; Li, K. Chloroalkyl Piperazine and Nitrogen Mustard Porphyrins : Synthesis and Anticancer Activity. **2004**, *12*, 2469–2475. https://doi.org/10.1016/j.bmc.2004.01.045.

(25) Kumar, S.; KumAhmed Kamala, R. Ramua, V. T. Remarkable DNA Binding Affinity and Potential Anticancer Activity of Pyrrolo [2,1-c][1,4] Benzodiazepine – Naphthalimide Conjugates Linked through Piperazine Side-Armed Alkane Spacers. **2008**, *16*, 7218–7224. https://doi.org/10.1016/j.bmc.2008.06.034.

(26) Kumar, S.; Kumar, N.; Roy, P.; Sondhi, S. M. Efficient Synthesis of Heterocyclic Compounds Derived from 2 , 6- Dioxopiperazine Derivatives and Their Evaluation for Anti- Inflammatory and Anticancer Activities. **2014**, 3953–3969. https://doi.org/10.1007/s00044-014-0969-1.

(27) Smits, R. A.; Lim, H. D.; Hanzer, A.; Zuiderveld, O. P.; Guaita, E.; Adami, M.; Coruzzi, G.; Leurs, R.; Esch, I. J. P. De. Fragment Based Design of New H 4 Receptor - Ligands with Anti-Inflammatory Properties in Vivo. *J. Med. Chem.***2008**, *51* (Scheme 1), 2457–2467. https://doi.org/10.1021/jm7014217.

(28) Penjišević, J.; Šukalović, V.; Andrić, D.; Kostić-Rajačić, S.; Šoškić, V.; Roglić, G. 1-Cinnamyl-4-(2-Methoxyphenyl)Piperazines: Synthesis, Binding Properties, and Docking to Dopamine (D2) and Serotonin (5-HT1A) Receptors. *Arch. Pharm. (Weinheim).***2007**, *340* (9), 456–465. https://doi.org/10.1002/ardp.200700062.

(29) Yevich, J. P.; New, J. S.; Smith, D. W.; Lobeck, W. G.; Catt, J. D.; Minielli, J. L.; Eison, M. S.; Taylor, D. P.; Riblet, L. A.; Temple, D. L. Synthesis and Biological Evaluation of I-(1,2-Benzisothiazol-3-Yl)- and (1,2-Benzisoxazol-3-Yl)Piperazine Derivatives as Potential Antipsychotic Agents. **1986**, 359–369. https://doi.org/10.1021/jm00153a010.

(30) Hage, J. M. El; Serradji, C. N. Piperazine Derivatives as Iron Chelators : A Potential Application in Neurobiology. *BioMetals***2015**, *28* (6), 1043–1061. https://doi.org/10.1007/s10534-015-9889-x.

(31) Us, P.; Patentsuche. N- Substituted Piperazines, 2017.

(32) Baltzly, R.; Buck, J. S.; Lorz, E.; Schön, W. The Preparation of N-Mono-Substituted and Unsymmetrically Disubstituted Piperazines. *J. Am. Chem. Soc.***1944**, *66* (2), 263–266. https://doi.org/10.1021/ja01230a031.

(33) Dunstan, P. O.; Khan, A. M. Synthesis, Characterization and Thermochemistry of Piperazine Complexes of Bivalent Metal Bromides. **2013**, *4* (3), 250–255. https://doi.org/10.5155/eurjchem.4.3.250-254.791.

(34) Niemeyer, H. M. Conformational Equilibria in Six-Membered Rings. *J. Mol. Struct.***1979**, *57* (C), 241–244. https://doi.org/10.1016/0022-2860(79)80249-5.

(35) Ostermeier, M.; Limberg, C.; Ziemer, B. The Coordination Chemistry of Iron with the 1,4-Bis(2-Pyridyl-Methyl)Piperazine Ligand. *Zeitschrift für Anorg. und Allg. Chemie***2006**, *632* (7), 1287–1292. https://doi.org/10.1002/zaac.200600003.

(36) Bentley, A. O.; Driver, J. E.; Atherden, L. M. *Bentley and Driver's Textbook of Pharmaceutical Chemistry*; Oxford medical publications; Oxford U.P., 1969.

(37) Young, D. W. *Heterocyclic Chemistry / D. W. Young*; Longman: London ; New York, 1975.

(38) Malviya, M.; Kumar, Y. C. S.; Mythri, R. B.; Venkateshappa, C.; Subhash, M. N.; Rangappa, K. S. Muscarinic Receptor 1 Agonist Activity of Novel N-Aryl Carboxamide Substituted 3-Morpholino Arecoline Derivatives in Alzheimer's Presenile Dementia Models. *Bioorg. Med. Chem.***2009**, *17* (15), 5526—5534. https://doi.org/10.1016/j.bmc.2009.06.032.

(39) Ryckebusch, A.; Debreu-Fontaine, M.-A.; Mouray, E.; Grellier, P.; Sergheraert, C.; Melnyk, P. Synthesis and Antimalarial Evaluation of New N1-(7-Chloro-4-Quinolyl)-1,4-Bis(3-Aminopropyl)Piperazine Derivatives. *Bioorg. Med. Chem. Lett.***2005**, *15* (2), 297–302. https://doi.org/10.1016/j.bmcl.2004.10.080.

(40) Kimura, M.; Masuda, T.; Yamada, K.; Kawakatsu, N.; Kubota, N.; Mitani, M.; Kishii, K.; Inazu, M.; Kiuchi, Y.; Oguchi, K.; et al. Antioxidative Activities of

Novel Diphenylalkyl Piperazine Derivatives with High Affinities for the Dopamine Transporter. *Bioorg. Med. Chem. Lett.***2004**, *14* (16), 4287–4290. https://doi.org/https://doi.org/10.1016/j.bmcl.2004.05.091.

(41) Dauzonne, D.; Gillardin, J. M.; Lepage, F.; Pointet, R.; Rissé, S.; Lamotte, G.; Demerseman, P. Synthesis and Some CNS Activities of New Benzofuranylacryloylpiperazines. *Eur. J. Med. Chem.***1995**, *30* (1), 53–59. https://doi.org/https://doi.org/10.1016/0223-5234(96)88209-2.

(42) Kossakowski, J.; Krawiecka, M.; Kuran, B. Synthesis of Conformationally Constrained Aryl- or Heteroarylpiperazinyl Derivatives of Selected Imides as 5-HT1A Receptor Ligands. *Molecules* . 2006. https://doi.org/10.3390/11080615.

(43) Fulton, A.; Norman, T.; Burrows, G. D. Ligand Binding and Platelet Uptake Studies of Loxapine, Amoxapine and Their 8-Hydroxylated Derivatives. *J. Affect. Disord.***1982**, *4* (2), 113–119. https://doi.org/10.1016/0165-0327(82)90041-6.

(44) Jan A. Fawcett, M.D., and Howard M. Kravitz, D. O. Amoxapine - An Antidepressant With Some Neuroleptic Properties? *Pharmacother. J. Hum. Pharmacol. Drug Ther.***1982**.

(45) Karen L. Goa and Alan Ward. Buspirone A Preliminary Review of Its Pharmacological Properties and Therapeutic. *Drugs Aging***1993**, *3* (5), 441–459. https://doi.org/10.2165/00002512-199303050-00006.

(46) Eison, A. S.; Temple, D. L. Buspirone: Review of Its Pharmacology and Current Perspectives on Its Mechanism of Action. *Am. J. Med.***1986**, *80* (3 SUPPL. 2), 1–9. https://doi.org/10.1016/0002-9343(86)90325-6.

(47) Gastpar, M.; Gastpar, G.; Gilsdorf, U. Befuraline, Its Safety and Efficacy in Depressed Inpatients. *Pharmacopsychiatry***1985**, *18* (6), 351–355. https://doi.org/10.1055/s-2007-1017396.

(48) Brazzelli, V.; Grasso, V.; Borroni, G. Imatinib, Dasatinib and Nilotinib: A Review of Adverse Cutaneous Reactions with Emphasis on Our Clinical Experience. *J. Eur. Acad. Dermatology Venereol.***2013**, *27* (12), 1471–1480. https://doi.org/10.1111/jdv.12172.

(49) Shaquiquzzaman, M.; Verma, G.; Marella, A.; Akhter, M.; Akhtar, W.; Khan,

M. F.; Tasneem, S.; Alam, M. M.; Anton, F.; Burch, E. A.; et al. Ranolazine: A Contemporary Review. *Drugs***2015**, *2015* (2), 1–9. https://doi.org/10.1161/01.CIR.0000139333.83620.5D.

(50) Antzelevitch, C.; Belardinelli, L.; Zygmunt, A. C.; Burashnikov, A.; Di Diego, J. M.; Fish, J. M.; Cordeiro, J. M.; Thomas, G. Electrophysiological Effects of Ranolazine, a Novel Antianginal Agent with Antiarrhythmic Properties. *Circulation***2004**, *110* (8), 904–910. https://doi.org/10.1161/01.CIR.0000139333.83620.5D.

(51) McClellan, K. J.; Plosker, G. L. Trimetazidine: A Review of Its Use in Stable Angina Pectoris and Other Coronary Conditions. *Drugs***1999**, *58* (1), 143–157. https://doi.org/10.2165/00003495-199958010-00016.

(52) Campoli-Richards, D. M.; Buckley, M. M. T.; Fitton, A. Cetirizine: A Review of Its Pharmacological Properties and Clinical Potential in Allergic Rhinitis, Pollen-Induced Asthma, and Chronic Urticaria. *Drugs***1990**, *40* (5), 762–781. https://doi.org/10.2165/00003495-199040050-00009.

(53) Bassett, K. E.; Schunk, J. E.; Crouch, B. I. Cyclizine Abuse by Teenagers in Utah. *Am. J. Emerg. Med.***1996**, *14* (5), 472–474. https://doi.org/10.1016/S0735-6757(96)90156-4.

(54) Schnabel, A.; Eberhart, L. H.; Muellenbach, R.; Morin, A. M.; Roewer, N.; Kranke, P. Efficacy of Perphenazine to Prevent Postoperative Nausea and Vomiting: A Quantitative Systematic Review. *Eur. J. Anaesthesiol.***2010**, *27* (12), 1044–1051. https://doi.org/10.1097/EJA.0b013e32833b7969.

(55) Sharma, P. C.; Jain, A.; Jain, S.; Pahwa, R.; Yar, M. S. Ciprofloxacin: Review on Developments in Synthetic, Analytical, and Medicinal Aspects. *J. Enzyme Inhib. Med. Chem.***2010**, *25* (4), 577–589. https://doi.org/10.3109/14756360903373350.

(56) Bailey, E. M.; Krakovsky, D. J.; Rybak, M. J. The Triazole Antifungal Agents: A Review of Itraconazole and Fluconazole. *Pharmacother. J. Hum. Pharmacol. Drug Ther.***1990**, *10* (2), 146–153. https://doi.org/10.1002/j.1875-9114.1990.tb02561.x.

(57) Jain, V. K.; Jain, B.; Sharma, U. K.; Saha, D. Synthesis, Characterization and Antimicrobial Screening of Some 4-Substituted 1(4-Substituted

Phenyl)Piperazine Derivatives. *Int. J. Curr. Pharm. Res.***2011**, *3* (1), 66–70.

(58) Liu, K. G.; Robichaud, A. J. A General and Convenient Synthesis of N-Aryl Piperazines. **2006**, *46* (2005), 8543. https://doi.org/10.1016/j.tetlet.2005.09.092.

(59) Anastasiadis, C.; Hogarth, G.; Wilton-Ely, J. D. E. T. Functionalised Dithiocarbamate Complexes: Complexes Based on Indoline, Indole and Substituted Piperazine Backbones - X-Ray Crystal Structure of [Ni(S2CNC3H6C6H4)2]. *Inorganica Chim. Acta***2010**, *363* (13), 3222–3228. https://doi.org/10.1016/j.ica.2010.05.061.

(60) Keypour, H.; Rezaeivala, M.; Valencia, L.; Pérez-Lourido, P. Synthesis and Crystal Structure of Mn(II) Complexes with Novel Macrocyclic Schiff-Base Ligands Containing Piperazine Moiety. *Polyhedron***2008**, *27* (14), 3172–3176. https://doi.org/10.1016/j.poly.2008.07.012.

(61) Lloyd, J.; Vatsadze, S. Z.; Robson, D. A.; Blake, A. J.; Mountford, P. New Titanium Imido Complexes Containing Piperazine-Based Diamido-Diamine Ligands. *J. Organomet. Chem.***1999**, *591* (1–2), 114–126. https://doi.org/10.1016/S0022-328X(99)00447-7.

(62) Babu, K.; Pitchai, P. The New Transition Metal Complexes of N,N'-(Piperazine-1,4di(Bisphenylmethylene)) Diacetamide and Their Biological Activity. **2014**, *4* (1), 145–151.

(63) Niu, Y.; Hou, H.; Wei, Y.; Fan, Y.; Zhu, Y.; Du, C.; Xin, X. A Linear Piperazine-Pyridine Ligand and Its Hg Coordination Polymer. *Inorg. Chem. Commun.***2001**, *4* (7), 358–361. https://doi.org/10.1016/S1387-7003(01)00213-1.

(64) Halfen, J. A.; Uhan, J. M.; Fox, D. C.; Mehn, M. P.; Que, L. Copper(II) Complexes of Pyridyl-Appended Diazacycloalkanes: Synthesis, Characterization, and Application to Catalytic Olefin Aziridination. *Inorg. Chem.***2000**, *39* (21), 4913–4920. https://doi.org/10.1021/ic000664+.

(65) Schatz, M.; Becker, M.; Thaler, F.; Hampel, F.; Schindler, S.; Jacobson, R. R.; Tyeklár, Z.; Murthy, N. N.; Ghosh, P.; Chen, Q.; et al. Copper(I) Complexes, Copper(I)/O2reactivity, and Copper(II) Complex Adducts, with a Series of Tetradentate Tripyridylalkylamine Tripodal Ligands. *Inorg. Chem.***2001**,

40(10), 2312–2322. https://doi.org/10.1021/ic000924n.

(66) Mautner, F. A.; Soileau, J. B.; Bankole, P. K.; Gallo, A. A.; Massoud, S. S. Synthesis and Spectroscopic Characterization of Dicyanamido-Cu(II) Complexes. Part 21For Part 1 See Ref. [1].: Crystal Structure of the Complexes of Tris[2-(2-Pyridylethyl)]Amine, Tris(2-Pyridylmethyl)Amine and 1,4-Bis[2-(2-Pyridylethyl)]Piperazine. *J. Mol. Struct.***2008**, *889* (1–3), 271–278. https://doi.org/10.1016/j.molstruc.2008.02.015.

(67) Ratilainen, J.; Airola, K.; Frohlich, R. Synthesis of a Tetradentate Piperazine Ligand and a Structural Study of Its Coordination Compounds. *Polyhedron***1999**, *18*, 2265–2273. https://doi.org/10.1016/s0277-5387(99)00117-5.

(68) Saravanan, N.; Palaniandavar, M. Manganese(II) Complexes of Pyridyl-Appended Diazacyclo-Alkanes: Effect of Ligand Backbone Ring Size on Catalytic Olefin Oxidation. *Inorganica Chim. Acta***2012**, *385*, 100–111. https://doi.org/10.1016/j.ica.2012.01.009.

(69) Geiger, R. A.; Chattopadhyay, S.; Day, V. W.; Jackson, T. A. A Series of Peroxomanganese(III) Complexes Supported by Tetradentate Aminopyridyl Ligands: Detailed Spectroscopic and Computational Studies. *J. Am. Chem. Soc.***2010**, *132* (8), 2821–2831. https://doi.org/10.1021/ja910235g.

(70) Ogden, M. D.; Sinkov, S. I.; Lumetta, G. J.; Nash, K. L. Affinity of An(VI) for N4-Tetradentate Donor Ligands: Complexation of the Actinyl(VI) Ions with N4-Tetradentate Ligands. *J. Solution Chem.***2012**, *41* (4), 616–629. https://doi.org/10.1007/s10953-012-9827-2.

(71) Ostermeier, M.; Limberg, C.; Herwig, C.; Ziemer, B. Stabilizing the Boat Conformation of Piperazines Coordinated to Iron (II): Iso-Butyl Substituents Lead to Robust Oxidation Catalysts via Hyperconjugation. *Zeitschrift fur Anorg. und Allg. Chemie***2009**, *635* (12), 1823–1830. https://doi.org/10.1002/zaac.200900275.

(72) Chandra, S.; Jain, D.; Sharma, A. K. EPR, Mass, Electronic, IR Spectroscopic and Thermal Studies of Bimetallic Copper(II) Complexes with Tetradentate Ligand, 1,4-Diformyl Piperazine Bis(Carbohydrazone). *Spectrochim. Acta - Part A Mol. Biomol. Spectrosc.***2009**, *71* (5), 1712–1719.

https://doi.org/10.1016/j.saa.2008.06.028.

(73) Hancock, S. L.; Mahon, M. F.; Kociok-Kohn, G.; Jones, M. D. Homopiperazine and Piperazine Complexes of ZrIV and Hf IV and Their Application to the Ring-Opening Polymerisation of Lactide. *Eur. J. Inorg. Chem.***2011**, No. 29, 4596–4602. https://doi.org/10.1002/ejic.201100589.

(74) Hancock, S. L.; Jones, M. D.; Langridge, C. J.; Mahon, M. F. Al(Iii)-Homopiperazine Complexes and Their Exploitation for the Production of Polyesters. *New J. Chem.***2012**, *36* (9), 1891–1896. https://doi.org/10.1039/c2nj40300e.

(75) Johnstone, N. C.; Aazam, E. S.; Hitchcock, P. B.; Fulton, J. R. Synthesis of Aluminium Complexes Bearing a Piperazine-Based Ligand System. *J. Organomet. Chem.***2010**, *695* (2), 170–176. https://doi.org/10.1016/j.jorganchem.2009.10.016.

(76) Li, W.; Wu, W.; Wang, Y.; Yao, Y.; Zhang, Y.; Shen, Q. Bimetallic Aluminum Alkyl Complexes as Highly Active Initiators for the Polymerization of ε-Caprolactone. *Dalt. Trans.***2011**, *40* (43), 11378. https://doi.org/10.1039/c1dt11380a.

(77) Li, W.; Yao, Y.; Zhang, Y.; Shen, Q. Aluminum Complexes Stabilized by Piperazidine-Bridged Bis(Phenolate) Ligands: Syntheses, Structures, and Application in the Ring-Opening Polymerization of μ-Caprolactone. *Chinese J. Chem.***2012**, *30* (3), 609–615. https://doi.org/10.1002/cjoc.201100438.

(78) Chen, L.; Li, W.; Yuan, D.; Zhang, Y.; Shen, Q.; Yao, Y. Syntheses of Mononuclear and Dinuclear Aluminum Complexes Stabilized by Phenolato Ligands and Their Applications in the Polymerization of ε-Caprolactone: A Comparative Study. *Inorg. Chem.***2015**, *54* (10), 4699–4708. https://doi.org/10.1021/acs.inorgchem.5b00022.

(79) Guo, Y.-M.; Du, M.; Wang, G.-C.; Bu, X.-H. Structural and Spectral Studies of Some Coordination Complexes of a Phenol-Functionalized Diazamesocyclic Ligand 1,4-Bis-(3-Tert-Butyl-5-Methyl-2-Hydroxybenzyl)-1,4-Diazacycloheptane (H2L). *J. Mol. Struct.***2002**, *643* (1–3), 77–83. https://doi.org/10.1016/S0022-2860(02)00405-2.

(80) Mohanty, S.; Suresh, D.; Balakrishna, M. S.; Mague, J. T. Phosphine Free

Diamino-Diol Based Palladium Catalysts and Their Application in Suzuki-Miyaura Cross-Coupling Reactions. *J. Organomet. Chem.***2009**, *694* (13), 2114–2121. https://doi.org/10.1016/j.jorganchem.2009.02.019.

(81) Hu, T.; Wu, M.; Wu, S.; Hu, C.; Lin, C.; Datta, A.; Lin, T.; Huang, J. Synthesis, Characterization and Reactivity Study of Aluminum Compounds Incorporating Bi- and Tri-Dentate Pyrrole–Piperazine Ligands. *RSC Adv.***2016**, *6*, 16331–16339. https://doi.org/10.1039/C6RA01694D.

(82) Bhat, I. ul H.; Tabassum, S. Synthesis of New Piperazine Derived Cu(II)/Zn(II) Metal Complexes, Their DNA Binding Studies, Electrochemistry and Anti-Microbial Activity: Validation for Specific Recognition of Zn(II) Complex to DNA Helix by Interaction with Thymine Base. *Spectrochim. Acta - Part A Mol. Biomol. Spectrosc.***2009**, *72* (5), 1026–1033. https://doi.org/10.1016/j.saa.2008.12.037.

(83) Mukhopadhyay, S.; Mandal, D.; Ghosh, D.; Goldberg, I.; Chaudhury, M. Equilibrium Studies in Solution Involving Nickel(II) Complexes of Flexidentate Schiff Base Ligands: Isolation and Structural Characterization of the Planar Red and Octahedral Green Species Involved in the Equilibrium. *Inorg. Chem.***2003**, *42* (25), 8439–8445. https://doi.org/10.1021/ic0346174.

(84) Pait, M.; Kundu, B.; Kundu, S. C.; Ray, D. Copper(II) Complexes of Piperazine Based Ligand: Synthesis, Crystal Structure, Protein Binding and Evaluation of Anti-Cancerous Therapeutic Potential. *Inorganica Chim. Acta***2014**, *418* (Ii), 30–41. https://doi.org/10.1016/j.ica.2014.04.019.

(85) Purkait, S.; Aullón, G.; Zangrando, E.; Chakraborty, P. Group 12 Metal Complexes of (2-Piperazine-1-Yl-Ethyl)-Pyridin-2-Yl-Methylene-Amine: Rare Participation of Terminal Piperazine N in Coordination Leads to Structural Diversity. *Dalt. Trans.***2017**, *46* (7), 2184–2195. https://doi.org/10.1039/C6DT04578B.

(86) Keypour, H.; Rezaeivala, M.; Ramezani-Aktij, A.; Bayat, M.; Dilek, N.; Ünver, H. New Macrocyclic Schiff Base Complexes Incorporating a Homopiperazine Unit: Synthesis of Some Co(II), Ni(II),Cu(II) and Zn(II) Complexes and Crystal Structure and Theoretical Studies. *J. Mol. Struct.***2016**, *1115*, 180–186. https://doi.org/10.1016/j.molstruc.2016.02.071.

(87) Keypour, H.; Mahmoudabadi, M.; Shooshtari, A.; Bayat, M.; Ghassemzadeh, M.; Hosseinzadeh, L.; Mohsenzadeh, F.; Harms, K. Synthesis and Characterization of Two New N4O2 Macroacyclic Schiff-Base Ligands Containing Piperazine Moiety and Mononuclear Co(III) and Cu(II) Complexes, Spectral, X-Ray Crystal Structural, Theoretical Studies, Cytotoxic and Antibacterial Properties. *Polyhedron***2017**, *129* (Iii), 189–198. https://doi.org/10.1016/j.poly.2017.03.035.

(88) Keypour, H.; Mahmoudabadi, M.; Shooshtari, A.; Hosseinzadeh, L.; Mohsenzadeh, F.; Gable, R. W. Synthesis of Mn(II) and Zn(II) Complexes with New Macrocyclic Schiff-Base Ligands Containing Piperazine Moiety: Spectroscopic, Structural, Cytotoxic and Antibacterial Properties. *Polyhedron***2017**, *127* (Ii), 345–354. https://doi.org/10.1016/j.poly.2017.02.008.

(89) Rezaeivala, M. Schiff Base Ligand Containing Piperazine Moiety and Related Mn (II), Cu (II), Ni (II) And. **2017**. https://doi.org/10.22036/icr.2016.46261.

(90) El-Sherif, A. A.; Shehata, M. R.; Shoukry, M. M.; Barakat, M. H. Synthesis, Characterization, Equilibrium Study and Biological Activity of Cu(II), Ni(II) and Co(II) Complexes of Polydentate Schiff Base Ligand. *Spectrochim. Acta - Part A Mol. Biomol. Spectrosc.***2012**, *96*, 889–897. https://doi.org/10.1016/j.saa.2012.07.047.

(91) Nishat, N.; Haq, M. M.; Ahamad, T.; Kumar, V. Synthesis , Spectral and Antimicrobial Studies of a Novel Macrocyclic Ligand Containing a Piperazine Moiety and Its Binuclear Metal Complexes. **2017**, *8972* (December). https://doi.org/10.1080/00958970600791400.

(92) Hawes, C. S.; White, K. F.; Abrahams, B. F.; Knowles, G. P.; Chaffee, A. L.; Batten, R.; Turner, D. R. Piperazine-Derived Porous Coordination Polymer †. *CrystEngComm***2015**, *17*, 2196–2203. https://doi.org/10.1039/C4CE02547D.

(93) Chaudhary, P.; Kumar, R.; Verma, A. K.; Singh, D.; Yadav, V.; Chhillar, A. K.; Sharma, G. L.; Chandra, R. Synthesis and Antimicrobial Activity of N-Alkyl and N-Aryl Piperazine Derivatives. *Bioorganic Med. Chem.***2006**, *14* (6), 1819–1826. https://doi.org/10.1016/j.bmc.2005.10.032.

(94) Andonova, L.; Zheleva-Dimitrova, D.; Georgieva, M.; Zlatkov, A. Synthesis and Antioxidant Activity of Some 1-Aryl/Aralkyl Piperazine Derivatives with Xanthine Moiety at N4. *Biotechnol. Biotechnol. Equip.***2014**, *28* (6), 1165–1171. https://doi.org/10.1080/13102818.2014.979978.

(95) Pietrzycka, A.; Stepniewski, M.; Waszkielewicz, A. M.; Marona, H. Preliminary Evaluation of Antioxidant Activity of Some 1-(Phenoxyethyl)-Piperazine Derivatives. *Acta Pol. Pharm.***2006**, *63* (1), 19–24.

(96) Słoczyńska, K.; Pańczyk, K.; Waszkielewicz, A. M.; Marona, H.; Pękala, E. In Vitro Mutagenic, Antimutagenic, and Antioxidant Activities Evaluation and Biotransformation of Some Bioactive 4-Substituted 1-(2-Methoxyphenyl)Piperazine Derivatives. *J. Biochem. Mol. Toxicol.***2016**, *30* (12), 593–601. https://doi.org/10.1002/jbt.21826.

(97) Salga, S. M.; Ali, H. M.; Abdullah, M. A.; Abdelwahab, S. I. Synthesis, Characterization, Acetylcholinesterase Inhibition, Molecular Modeling and Antioxidant Activities of Some Novel Schiff Bases Derived from 1-(2-Ketoiminoethyl)Piperazines. **2011**, 9316–9330. https://doi.org/10.3390/molecules16119316.

(98) Zhou, H. C. J.; Kitagawa, S. Metal-Organic Frameworks (MOFs). *Chem. Soc. Rev.***2014**, *43* (16), 5415–5418. https://doi.org/10.1039/c4cs90059f.

(99) Zhou, H. C.; Long, J. R.; Yaghi, O. M. Introduction to Metal-Organic Frameworks. *Chem. Rev.***2012**, *112* (2), 673–674. https://doi.org/10.1021/cr300014x.

(100) Batten, S. R.; Champness, N. R.; Chen, X. M.; Garcia-Martinez, J.; Kitagawa, S.; Öhrström, L.; O'Keeffe, M.; Suh, M. P.; Reedijk, J. Coordination Polymers, Metal-Organic Frameworks and the Need for Terminology Guidelines. *CrystEngComm***2012**, *14* (9), 3001–3004. https://doi.org/10.1039/c2ce06488j.

(101) Seth, S.; Matzger, A. J. Metal–Organic Frameworks: Examples, Counterexamples, and an Actionable Definition. *Cryst. Growth Des.***2017**, *17* (8), 4043–4048. https://doi.org/10.1021/acs.cgd.7b00808.

(102) Biradha, K.; Ramanan, A.; Vittal, J. J. Coordination Polymers Versus Metal−Organic Frameworks. *Cryst. Growth Des.***2009**, *9* (7), 2969–2970. https://doi.org/10.1021/cg801381p.

(103) Zhao, X. L.; Sun, W. Y. The Organic Ligands with Mixed N-/O-Donors Used in Construction of Functional Metal-Organic Frameworks. *CrystEngComm***2014**, *16* (16), 3247–3258. https://doi.org/10.1039/c3ce41791c.

(104) Furukawa, H.; Cordova, K. E.; O'Keeffe, M.; Yaghi, O. M. The Chemistry and Applications of Metal-Organic Frameworks. *Science (80-.).***2013**, *341* (6149), 1230444–12. https://doi.org/10.1126/science.1230444.

(105) Shi, Z.; Li, G.; Wang, L.; Gao, L.; Chen, X.; Hua, J.; Feng, S. Two Three-Dimensional Metal-Organic Frameworks from Secondary Building Units of Zn8(OH)4(O2C-)12 and Zn2(OH)(O2C-)3: [Zn2(OH)(Btc)] 2(4,4′-Bipy) and Zn2(OH)(Btc)(Pipe). *Cryst. Growth Des.***2004**, *4* (1), 25–27. https://doi.org/10.1021/cg034084+.

(106) Zhao, H.; Jin, Z.; Su, H.; Jing, X.; Sun, F.; Zhu, G. Targeted Synthesis of a 2D Ordered Porous Organic Framework for Drug Release. *Chem. Commun.***2011**, *47* (22), 6389–6391. https://doi.org/10.1039/c1cc00084e.

(107) Taleghani, S.; Mirzaei, M.; Eshtiagh-Hosseini, H.; Frontera, A. Tuning the Topology of Hybrid Inorganic–Organic Materials Based on the Study of Flexible Ligands and Negative Charge of Polyoxometalates: A Crystal Engineering Perspective. *Coord. Chem. Rev.***2016**, *309*, 84–106. https://doi.org/10.1016/j.ccr.2015.10.004.

(108) O. M. Yaghi and H. Li. Hydrothermal Synthesis of a Metal-Organic Framework Containing Large Rectangular Channels. *J. Am. Chem. Soc.***1995**, *117* (41), 10401–10402.

(109) Ni, Z.; Masel, R. I. Rapid Production of Metal−Organic Frameworks via Microwave-Assisted Solvothermal Synthesis. *J. Am. Chem. Soc.***2006**, *128* (38), 12394–12395. https://doi.org/10.1021/ja0635231.

(110) Gao, J.; Huang, C.; Lin, Y.; Tong, P.; Zhang, L. In Situ Solvothermal Synthesis of Metal–Organic Framework Coated Fiber for Highly Sensitive Solid-Phase Microextraction of Polycyclic Aromatic Hydrocarbons. *J. Chromatogr. A***2016**, *1436*, 1–8. https://doi.org/10.1016/j.chroma.2016.01.051.

(111) Israr, F.; Chun, D.; Kim, Y.; Kim, D. K. High Yield Synthesis of Ni-BTC Metal–Organic Framework with Ultrasonic Irradiation: Role of Polar Aprotic DMF Solvent. *Ultrason. Sonochem.***2016**, *31*, 93–101.

https://doi.org/10.1016/j.ultsonch.2015.12.007.

(112) Goesten, M. G.; Magusin, P. C. M. M.; Pidko, E. A.; Mezari, B.; Hensen, E. J. M.; Kapteijn, F.; Gascon, J. Molecular Promoting of Aluminum Metal–Organic Framework Topology MIL-101 by N , N -Dimethylformamide. *Inorg. Chem.***2014**, *53* (2), 882–887. https://doi.org/10.1021/ic402198a.

(113) Clausen, H. F.; Poulsen, R. D.; Bond, A. D.; Chevallier, M.-A. S.; Iversen, B. B. Solvothermal Synthesis of New Metal Organic Framework Structures in the Zinc–Terephthalic Acid–Dimethyl Formamide System. *J. Solid State Chem.***2005**, *178* (11), 3342–3351. https://doi.org/10.1016/j.jssc.2005.08.013.

(114) Sánchez-Sánchez, M.; Getachew, N.; Díaz, K.; Díaz-García, M.; Chebude, Y.; Díaz, I. Synthesis of Metal–Organic Frameworks in Water at Room Temperature: Salts as Linker Sources. *Green Chem.***2015**, *17* (3), 1500–1509. https://doi.org/10.1039/C4GC01861C.

(115) Ibarra, I. A.; Bayliss, P. A.; Pérez, E.; Yang, S.; Blake, A. J.; Nowell, H.; Allan, D. R.; Poliakoff, M.; Schröder, M. Near-Critical Water, a Cleaner Solvent for the Synthesis of a Metal–Organic Framework. *Green Chem.***2012**, *14* (1), 117–122. https://doi.org/10.1039/C1GC15726D.

(116) Taddei, M.; Dau, P. V.; Cohen, S. M.; Ranocchiari, M.; Van Bokhoven, J. A.; Costantino, F.; Sabatini, S.; Vivani, R. Efficient Microwave Assisted Synthesis of Metal-Organic Framework UiO-66: Optimization and Scale Up. *Dalt. Trans.***2015**, *44* (31), 14019–14026. https://doi.org/10.1039/c5dt01838b.

(117) Lin, Z.; Wragg, D. S.; Morris, R. E. Microwave-Assisted Synthesis of Anionic Metal-Organic Frameworks under Ionothermal Conditions. *Chem. Commun.***2006**, *4* (19), 2021–2023. https://doi.org/10.1039/b600814c.

(118) Klinowski, J.; Almeida Paz, F. A.; Silva, P.; Rocha, J. Microwave-Assisted Synthesis of Metal-Organic Frameworks. *Dalt. Trans.***2011**, *40* (2), 321–330. https://doi.org/10.1039/c0dt00708k.

(119) Amo-Ochoa, P.; Givaja, G.; Miguel, P. J. S.; Castillo, O.; Zamora, F. Microwave Assisted Hydrothermal Synthesis of a Novel CuI-Sulfate-Pyrazine MOF. *Inorg. Chem. Commun.***2007**, *10* (8), 921–924. https://doi.org/10.1016/j.inoche.2007.04.024.

(120) Babu, R.; Roshan, R.; Kathalikkattil, A. C.; Kim, D. W.; Park, D. W. Rapid,

Microwave-Assisted Synthesis of Cubic, Three-Dimensional, Highly Porous MOF-205 for Room Temperature CO2 Fixation via Cyclic Carbonate Synthesis. *ACS Appl. Mater. Interfaces***2016**, *8* (49), 33723–33731. https://doi.org/10.1021/acsami.6b12458.

(121) Dong, X. Liu, W. Shi, Y. Huang, W. Metal–Organic Framework MIL-53(Fe): Facile Microwave-Assisted Synthesis and Use as a Highly Active Peroxidase Mimetic for Glucose Biosensing. *RSC Adv.***2015**, *5* (23), 34999–35009. https://doi.org/10.1039/C4RA15891A.

(122) Shekhah, Y. Belmabkhout, K. Adil, P. Bhatt, A. J. Cairns, O. A Facile Solvent-Free Synthesis Route for the Assembly of a Highly CO2 Selective and H2S Tolerant NiSIFSIX Metal-Organic Framework. **2011**. https://doi.org/10.1039/b000000x.

(123) Pichon, A.; Lazuen-Garay, A.; James, S. L. Solvent-Free Synthesis of a Microporous Metal-Organic Framework. *CrystEngComm***2006**, *8* (3), 211–214. https://doi.org/10.1039/b513750k.

(124) Lanchas, M.; Arcediano, S.; Aguayo, A. T.; Beobide, G.; Castillo, O.; Cepeda, J.; Vallejo-Sánchez, D.; Luque, A. Two Appealing Alternatives for MOFs Synthesis: Solvent-Free Oven Heating vs. Microwave Heating. *RSC Adv.***2014**, *4* (104), 60409–60412. https://doi.org/10.1039/c4ra09743b.

(125) Crawford, D.; Casaban, J.; Haydon, R.; Giri, N.; McNally, T.; James, S. L. Synthesis by Extrusion: Continuous, Large-Scale Preparation of MOFs Using Little or No Solvent. *Chem. Sci.***2015**, *6* (3), 1645–1649. https://doi.org/10.1039/c4sc03217a.

(126) Stassen, I.; Campagnol, N.; Fransaer, J.; Vereecken, P.; De Vos, D.; Ameloot, R. Solvent-Free Synthesis of Supported ZIF-8 Films and Patterns through Transformation of Deposited Zinc Oxide Precursors. *CrystEngComm***2013**, *15* (45), 9308–9311. https://doi.org/10.1039/c3ce41025k.

(127) Reinsch, H. “Green” Synthesis of Metal-Organic Frameworks. *Eur. J. Inorg. Chem.***2016**, *2016* (27), 4290–4299. https://doi.org/10.1002/ejic.201600286.

(128) Faÿ, S.; Kroll, U.; Bucher, C.; Vallat-Sauvain, E.; Shah, A. Low Pressure Chemical Vapour Deposition of ZnO Layers for Thin-Film Solar Cells: Temperature-Induced Morphological Changes. *Sol. Energy Mater. Sol.*

*Cells***2005**, *86* (3), 385–397. https://doi.org/10.1016/j.solmat.2004.08.002.

(129) Yeung, K. S.; Lam, Y. W. A Simple Chemical Vapour Deposition Method For Depositing Thin TiO2 Films. *Thin Solid Films***1983**, *109* (2), 169–178.

(130) Stassen, I.; Styles, M.; Grenci, G.; Van Gorp, H.; Vanderlinden, W.; De Feyter, S.; Falcaro, P.; De Vos, D.; Vereecken, P.; Ameloot, R. Chemical Vapour Deposition of Zeolitic Imidazolate Framework Thin Films. *Nat. Mater.***2016**, *15* (3), 304–310. https://doi.org/10.1038/nmat4509.

(131) Kumar, P.; Deep, A.; Kim, K. H. Metal Organic Frameworks for Sensing Applications. *TrAC Trends Anal. Chem.***2015**, *73*, 39–53. https://doi.org/10.1016/j.trac.2015.04.009.

(132) Lian, X.; Yan, B. Phosphonate MOFs Composite as Off-On Fluorescent Sensor for Detecting Purine Metabolite Uric Acid and Diagnosing Hyperuricuria. *Inorg. Chem.***2017**, *56* (12), 6802–6808. https://doi.org/10.1021/acs.inorgchem.6b03009.

(133) Valvekens, P.; Vermoortele, F.; De Vos, D. Metal-Organic Frameworks as Catalysts: The Role of Metal Active Sites. *Catal. Sci. Technol.***2013**, *3* (6), 1435–1445. https://doi.org/10.1039/c3cy20813c.

(134) He, Y. C.; Yang, J.; Kan, W. Q.; Zhang, H. M.; Liu, Y. Y.; Ma, J. F. A New Microporous Anionic Metal-Organic Framework as a Platform for Highly Selective Adsorption and Separation of Organic Dyes. *J. Mater. Chem. A***2015**, *3* (4), 1675–1681. https://doi.org/10.1039/c4ta05391e.

(135) Pan, L.; Olson, D. H.; Ciemnolonski, L. R.; Heady, R.; Li, J. Separation of Hydrocarbons with a Microporous Metal-Organic Framework. *Angew. Chemie - Int. Ed.***2006**, *45* (4), 616–619. https://doi.org/10.1002/anie.200503503.

(136) Liu, Y.; Wang, Z. U.; Zhou, H. C. Recent Advances in Carbon Dioxide Capture with Metal-Organic Frameworks. *Greenh. Gases Sci. Technol.***2012**, *2* (4), 239–259. https://doi.org/10.1002/ghg.1296.

(137) R. James, M. J. Keogh, W.D. Heitz, C. Cross-Linked, Water Insoluble Poly(N-Glycidyl-Piperazine. U.S. Patent No. 4018721, 1977.

(138) Das, A.; Choucair, M.; Southon, P. D.; Mason, J. A.; Zhao, M.; Kepert, C. J.; Harris, A. T.; D'Alessandro, D. M. Application of the Piperazine-Grafted CuBTTri Metal-Organic Framework in Postcombustion Carbon Dioxide

Capture. *Microporous Mesoporous Mater.***2013**, *174*, 74–80. https://doi.org/10.1016/j.micromeso.2013.02.036.

(139) Sumida, K.; Rogow, D. L.; Mason, J. A.; McDonald, T. M.; Bloch, E. D.; Herm, Z. R.; Bae, T. H.; Long, J. R. Carbon Dioxide Capture in Metal-Organic Frameworks. *Chem. Rev.***2012**, *112* (2), 724–781. https://doi.org/10.1021/cr2003272.

(140) Rosi, N. L.; Eckert, J.; Eddaoudi, M.; Vodak, D. T.; Kim, J.; O'Keeffe, M.; Yaghi, O. M. Hydrogen Storage in Microporous Metal-Organic Frameworks. *Science (80-.).***2003**, *300* (5622), 1127–1129. https://doi.org/10.1126/science.1083440.

(141) Silva, P.; Vilela, S. M. F.; Tomé, J. P. C.; Almeida Paz, F. A. Multifunctional Metal-Organic Frameworks: From Academia to Industrial Applications. *Chem. Soc. Rev.***2015**, *44* (19), 6774–6803. https://doi.org/10.1039/c5cs00307e.

(142) Ganesan, S. V.; Natarajan, S. Synthesis and Structures of New Pyromellitate Coordination Polymers with Piperazine as a Ligand. *Inorg. Chem.***2004**, *43* (1), 198–205. https://doi.org/10.1021/ic034836p.

(143) Wang, H.; Liu, Y.; Li, M.; Huang, H.; Xu, H. M.; Hong, R. J.; Shen, H. Multifunctional TiO2nanowires-Modified Nanoparticles Bilayer Film for 3D Dye-Sensitized Solar Cells. *Optoelectron. Adv. Mater. Rapid Commun.***2010**, *4* (8), 1166–1169. https://doi.org/10.1039/b000000x.

(144) Blake, K. M.; Lucas, J. S.; Laduca, R. L. Zinc Pyromellitate Coordination Polymers with Bis(Pyridylmethyl)Piperazine Tethers: A Rare Binodal Network and a New Simple Self-Penetrated Topology. *Cryst. Growth Des.***2011**, *11* (4), 1287–1293. https://doi.org/10.1021/cg1015109.

(145) Martin, D. P.; Braverman, M. A.; LaDuca, R. L. Two- and Three-Dimensional Divalent Metal Isophthalate Coordination Polymers Incorporating Flexible Bispyridylmethylpiperazine Tethers: Structure Direction through Coordination Geometry Preferences, Carboxylate Binding Mode, and Ligand Conformation. *Cryst. Growth Des.***2007**, *7* (12), 2609–2619. https://doi.org/10.1021/cg700664u.

(146) Farnum, G. A.; Murray, N. H.; Laduca, R. L. Parallel Chain Polyrotaxane , Layer , and Diamondoid Divalent Metal Coordination Polymers Containing

Para Aromatic Dicarboxylate and Bis (4-Pyridylmethyl)Piperazine Ligands. *Inorganica Chim. Acta***2013**, *406*, 65–72. https://doi.org/10.1016/j.ica.2013.07.002.

(147) Layer, T.; Topologies, S.; Robinson, M. E.; Mizzi, J. E.; Staples, R. J.; Laduca, R. L. Structural Chemistry and Properties of Metal Oxalates Containing a Long-Spanning Dipyridyl Ligand : Chain , Interpenetrated Structural Chemistry and Properties of Metal Oxalates Containing a Long-Spanning Dipyridyl Topologies. **2015**. https://doi.org/10.1021/acs.cgd.5b00040.

(148) Lucas, J. S.; Pochodylo, A. L.; LaDuca, R. L. Cadmium Bis(4-Pyridylformyl)Piperazine Coordination Polymers: Layered Nets and a Novel 3,5-Connected Binodal Lattice. *CrystEngComm***2010**, *12* (10), 3310–3317. https://doi.org/10.1039/c0ce00117a.

(149) Mizzi, J. E.; Laduca, R. L. Divalent Metal Pyromellitate Coordination Polymers Containing Bis(4-Pyridylformyl)Piperazine: Selection between Simple Chain and Rare Fsc Network Topologies. *Inorganica Chim. Acta***2014**, *421*, 183–190. https://doi.org/10.1016/j.ica.2014.05.038.

(150) Hawes, C. S.; Hamilton, S. E.; Hicks, J.; Knowles, G. P.; Chaffee, A. L.; Turner, D. R.; Batten, S. R. Coordination Chemistry and Structural Dynamics of a Long and Flexible Piperazine-Derived Ligand. *Inorg. Chem.***2016**, *55* (13), 6692–6702. https://doi.org/10.1021/acs.inorgchem.6b00933.

CHAPTER 2

SYNTHESIS AND CHARACTERIZATION OF PIPERAZINE RING BASED LIGANDS

This chapter give details of synthetic procedure of ligands, their characterization via physical and spectroscopic measurements. All the results obtained were analyzed and discussed.

2.1 Synthesis and characterization of ligands

Materials and methods:

Chemicals required for the study were purchased from commercial sources and were used as received. Precursor *bis*-chloroethylaminewas synthesized in bulk amount by standard procedure reported in the literature.[1] All the ligands were characterized by using different physical and spectroscopictechniques such as FTIR, UV-vis,^{1}H NMR and mass spectrometry. Melting points were measured using capillary method. UV-visible absorption spectra were recorded on Shimadzu UV-1800 in the wavelength range 800-200 nm. Shimadzu FTIR 8400 spectrometer with diamond ATR was used to record IR in the range 400-4000 cm^{-1}. For recording ^{1}H NMR spectra Brucker Advance II 400 NMR Spectrometer was used with d^{6}–DMSO/$CDCl_3$ as solvents with tetra methyl silane (TMS) as the internal standard. XEVO G2-XS QTOF ESI-Mass Spectrometer was used for analyzing mass spectra using $CHCl_3$/DMSO as solvents. Synthetic scheme and structure of ligands has been described in figure 2.1-2.14.

2.1.1 Synthesis of *1-(2-pyridyl)-piperazine (HL1)*

21 mmol (2g) of 2-aminopyridine and 21 mmol (3g) of *bis*-chloroethylamine were dissolvedin 30 ml of n-butanol and refluxed on magnetic stirrer for 8 hours in 80-90°C. After then 25 mmol (3.03gm) of potassium carbonate was added in the mixture and refluxed for next 10 hours. The progress of the reaction was continuously checked by TLC. At the end mixture was cooled down and filtered.The filtrate was kept for 1-2 days and the product was collected after filtration and drying the precipitates.Physical state ***semisolid,*** color ***white***, yield70%. **UV-vis (λ, nm)** 259 **FTIR (ν in cm^{-1})** 3345 (N-H Str.), 1498, 1504 (C=C Str.), 3104 (C–H Str.), 1305 (Ar-N Str.). **^{1}H NMR (δ, ppm)** 2.49 (s, 1H, -NH), 3.55(t, 2H, -CH_2), 3.37 (t, 2H, -CH_2), 6.40 (d, 1H, Ar-H), 6.81(t, 1H, Ar-H), 7.98 (t, 1H, Ar-H), 8.81(d, 1H, Ar-H).**Mass (m/z)** 327(2M+H^{+}).

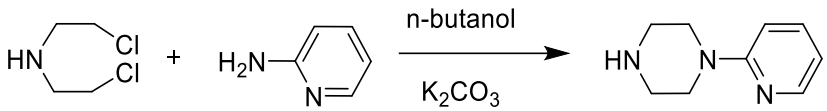

Figure 2.1:Synthesis and structure of 1-(2-pridyl)-piperazine (HL1)

2.1.2 Synthesis of *1-(3-pyridyl)-piperazine* (HL2)

Ligand HL2 was synthesized by similarprocedure as reported for HL1 using 21 mmol (2g) of 3-aminopyridine and 21 mmol (3g) of *bis*-chloroethylamine. The ligand was obtained after complete removal of the solvent under vacuum. Physical state ***oily liquid,*** color ***brown***, yield72%. **UV-vis (λ, nm)** 250, 334 **FTIR (ν in cm^{-1})** 3447 (N-H Str.), 1498, 1642 (C=C Str.), 2962 (C–H Str.),1341 (Ar-N Str.) **^{1}H NMR (δ, ppm)** 2.48 (s, 1H, -NH), 3.41 (t, 2H, -CH_2), 3.50 (t, 2H, -CH_2), 6.89 (d, 1H, Ar-H), 7.58 (d, 1H, Ar-H), 7.56 (t, 1H, Ar-H), 8.18 (s, 1H, Ar-H).

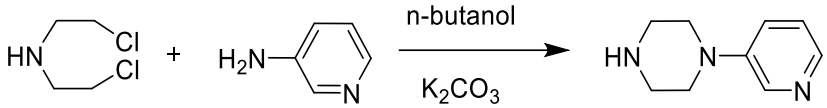

Figure 2.2:Synthesis and structure of 1-(3-pyridyl)-piperazine (HL2)

2.1.3 Synthesis of *1-(4-pyridyl)-piperazine(HL3)*

Ligand HL3 was synthesized by similarprocedure as reported for HL1using 21 mmol (2g) of 4-aminopyridine and 21 mmol (3g) of *bis*-chloroethylamine. The ligand was obtained after complete removal of the solvent under vacuum. Physical state ***oily liquid,*** color ***brown,*** Yield 68%. **UV-vis (λ, nm)** 227, 299 **FTIR (ν in cm^{-1})** 3344 (N-H Str.), 1498, 1550 (C=C Str.), 2947 (C–H Str.),1201 (Ar-N Str.) **^{1}H NMR (δ,ppm)** 2.49 (s, 1H, -NH) 3.89 (t, 2H, -CH_2),3.33 (t, 2H, -CH_2), 6.84 (d, 1-H, Ar-H), 8.52(d, 2H, Ar-H) 6.84 (d, 1H, Ar-H)**Mass(m/z)**327 (2M+H^+).

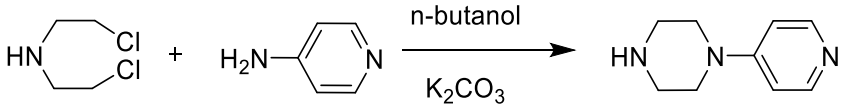

Figure 2.3:Synthesis and structure of 1-(4-pyridyl)-piperazine (HL3)

2.1.4 Synthesis of *1-(phenyl)-piperazine (HL4)*

Ligand HL4 was synthesized by similarprocedure as reported for HL1using 21 mmol (1.95 g) of aniline and 21 mmol (3g) of *bis*-chloroethylamine. Physical state ***solid***, color***white***, m. pt. 175°C, yield 80%. **UV-vis (λ, nm)** 231, 289 **FTIR (ν in cm^{-1})** 3344 (N-H Str.), 1498, 1593 (C=C Str.), 2922 (C–H Str.),1321 (Ar-N Str.) **^{1}H NMR**

(δ,ppm) 3.38(s, 1H, -NH), 3.1(t, 2H, $-CH_2$), 2.59(t, 2H, $-CH_2$), 7.11(d, 2H, Ar-H) 6.61(t, 1H, Ar-H)6.64(t, 2H, Ar-H) Mass **(m/z)** 163 ($M+H^+$).

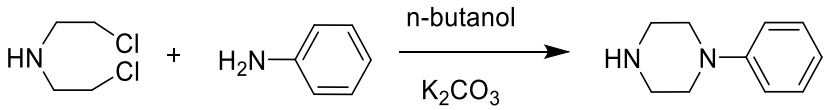

Figure 2.4:Synthesis and structure of 1-(phenyl)-piperazine (HL4)

2.1.5Synthesis of *1-(2-methoxy phenyl)-piperazine (HL5)*

Ligand HL5was synthesized by similarprocedure as reported forHL1using 21 mmol (2.58 g) of o-anisidine and 21 mmol (3g) of *bis*-chloroethylamine. Physical state ***solid***, color ***black***, m. pt. 192°C, yield80%. **UV-vis (λ, nm)** 240, 306 **FTIR (ν in cm^{-1})** 3277 (N-H Str.), 1510,1497 (C=C Str.), 2926 (C–H Str.), 1301 (Ar-N Str.) **^{1}H NMR (δ, ppm)** 3.84 (s, 1H, -NH), 3.25 (t, 2H, $-CH_2$) 3.14(t, 2H, $-CH_2$) 2.55 (s, 3H, $-CH_3$), 6.61 (d, 1H, Ar-H) 6.67 (t, 1H, Ar-H,) 6.87 (t, 1H, Ar-H), 6.76 (d, 1H, Ar-H) **Mass(m/z)** 385 ($2M+H^+$).

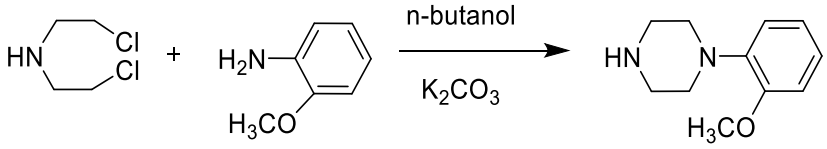

Figure 2.5:Synthesis and structure of 1-(2-methoxy phenyl)-piperazine(HL5)

2.1.6 Synthesis of *1-(4-methoxy phenyl)-piperazine (HL6)*

Ligand HL6was synthesized by similarprocedure as reported forHL1using 21 mmol (2.58 g) of p-anisidine and 21 mmol (3g) of *bis*-chloroethylamine. Physical state ***solid***, color ***dark violet***, m. pt. 195°C, yield 70%. **UV-vis (λ, nm)** 244, 287 **FTIR (ν in cm^{-1})** 3277 (N-H Str.), 1510,1497 (C=C Str.), 2926 (C–H Str.), 1301 (Ar-N Str.) **^{1}H NMR (δ, ppm)** 3.7 (s, 1H, -NH), 3.40 (t, 2H, $-CH_2$),3.2 (t, 2H, $-CH_2$), 2.55 (s, 3H, $-CH_3$), 6.97 (d, 2H, Ar-H) 6.85 (d, 2H, Ar-H).

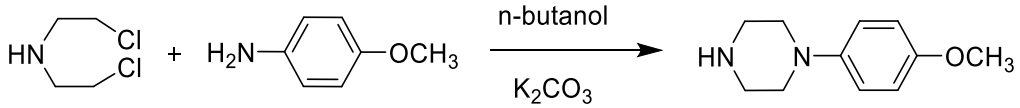

Figure 2.6:Synthesis and structure of 1-(4-methoxy phenyl)-piperazine(HL6)

2.1.7Synthesis of *1-(3-hydroxyphenyl)-piperazine (HL7)*

Ligand H7was synthesized by similarprocedure as reported forHL1using 21 mmol (2.28 g) of 3-aminophenol and 21 mmol (3g) of *bis*-chloroethylamine. Physical state ***solid,*** color ***black***, m. pt. 187°C, yield 90%. **UV-vis (λ, nm)** 242, 284 **FTIR (ν in cm-**

^{1}**)** 3232 (N-H Str.), 1593,1498 (C=C Str.), 2956 (C–H Str.)1346 (Ar-N Str.) **^{1}H NMR(δ, ppm)** 4.1(s, 1H, -OH),3.6 (s, 1H, -NH), 3.25 (t, 2H, -CH_2), 3.14(t, 2H, -CH_2), 6.78 (d, 1H, Ar-H) 6.86 (t, 1H, Ar-H) 7.02(s, 1H, Ar-H) 6.98 (d, 1H, Ar-H) **Mass(m/z)**179 ($M+H^+$).

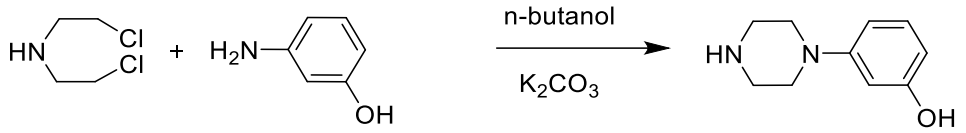

Figure 2.7:Synthesis and structure of 1-(3-hydroxyphenyl)-piperazine(HL7)

2.1.8Synthesis of *1-(4-hydroxyphenyl)-piperazine (HL8)*

Ligand HL8was synthesized by similarmethod as reported forHL1 using 21 mmol (2.28 g) of 4-aminophenol and 21 mmol (3g) of *bis*-chloroethylamine. Physical state ***solid,*** color ***black***, m. pt. 190°C, yield 80%. **UV-vis (λ, nm)** 283, 298 **FTIR (ν in cm^{-1})** 3261 (N-H Str.) 1599,1506 (C=C Str.), 2955 (C–H Str.), 1357 (Ar-N Str.) **^{1}H NMR(δ, ppm)**3.81 (s, 1H, -OH), 3.67 (s, 1H, -NH) 3.40 (t, 2H, -CH_2), 2.92 (t, 2H, -CH_2), 6.82 (t, 2H, Ar-H), 6.66 (d, 2H, Ar-H) **Mass(m/z)** 179 ($M+H^+$).

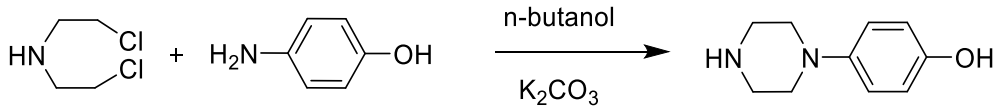

Figure 2.8:Synthesis and structure of 1-(4-hydroxyphenyl)-piperazine(HL8)

2.1.9 Synthesis of *1,4-bisethanol piperazine(H_2L9)*

In 30 ml of propanol 1.032 gm (12 mmol) of piperazine was dissolved with 1.932 gm (24 mmol) of chloroethanol and 3.21 gm of potassium carbonate (24 mmol) was added and refluxed for 8 hours under 60-70°C. The progress of reaction was monitored by TLC. After that reaction mixture was cooleddown and filtered. The filtrate was allowed to stand for overnight. A white crystalline solid appears which was filtered and dried. Recrystallization of the dried product was done with hot methanol. Physical state ***solid***, color ***shiny transparent***, m. pt. 170°C, yield 80%. **UV-vis (λ, nm)** 213 **FTIR (ν in cm^{-1})**3122 (O–H Str.) 2816 (C–H Str.) 1329 (C–NStr.) 1301 (C–C Str.) **^{1}H NMR (δ, ppm)**2.51(t, 2H, -CH_2), 2.35(t, 2H, -CH_2), 4.37(t, 2H, -CH_2), 3.46(t, 2H, -CH_2)**Mass(m/z)** 175 ($M+H^+$).

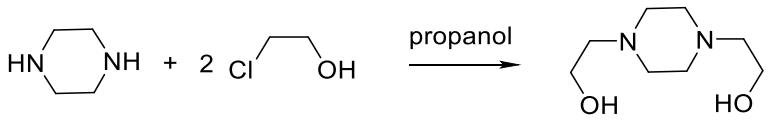

Figure 2.9:Synthesis and structure of 1,4-bisethanol piperazineH_2L9

2.1.10 Synthesis of *bis-(1-phenylethanol) piperazine (H_2L10)*

15 mmol (1.29 g) of piperazine in ethanol was added dropwise to ethanolic solution of styrene oxide (3.6 g, 30 mmol). The reaction mixture was refluxed for 8 hours at 60-70ºC. A white colored solid was obtained which was filtered and dried. TLC was done at regular interval to check the progress of reaction. Recrystallization was done by using hot ethanol. Physical state ***solid***, color ***white***,m. pt. 190°C,yield 85%. **UV-vis (λ, nm)** 213, 253 **FTIR (ν in cm^{-1})**3371 (O–H Str.), 2939,2823 (C–H Str.), 1315 (C–N Str.) **^{1}H NMR (δ, ppm)** 2.79(t, 2H, -CH_2), 2.89(d, 2H, -CH_2), 3.8(t, 1H, -CH), 7.30(d, 2H, Ar-H), 7.36(t, 3H, Ar-H) **Mass(m/z)**327 ($M+H^+$).

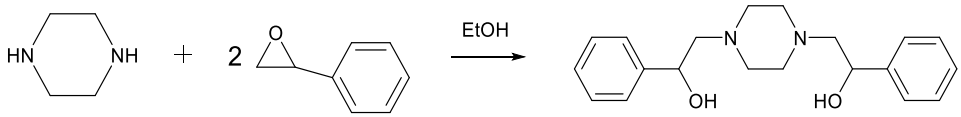

Figure 2.10:Synthesis and structure of bis (1-phenylethanol) piperazine H_2L10

2.1.11 Synthesis of *3,3'-(1-bis(2 hydroxyethyl)amino)butan-2-ol) piperazine (H_6L11)*

Asolution of epichlorohydrin (3.70g, 40 mmol) in methanol (15ml) taken in a beaker was added drop wise to another solution of piperazine(1.72g,20 mmol) in methanol (30 ml) taken in an RBF. The mixture was stirred mechanically using a magnetic stirrer for 72 hours at -5ºC. White colored precipitates appeared at the end of reaction. The remaining methanol in the RBF was evaporated using rotavapor. The compound thus obtained act as intermediate and was named as (*bis*-(1-chlorobutan-2-ol)) piperazine.

10 mmol (2.70 g) of (*bis*-(1-chlorobutan-2-ol)) piperazine was then dissolved in acetonitrile and to the solution 20 mmol (2.10 g) of diethanolamine and 20 mmol (2.76 g) potassium carbonatewere added. The mixture was then refluxed at 70-80 ºC for 48 hours. The final ligand was in the form of transparent liquid. Any remaining solvent was evaporated using rotavapor. The progress of the reaction was analyzed by

TLC. Physical state ***oily liquid***, color ***colorless***, yield 65%. **UV-vis (λ, nm)** 224 **FTIR (ATR ν in cm^{-1})**3304 (O–H Str.), 2927,2937 (CH Str.), 1329 (C–N Str.) **^{1}H NMR (δ, ppm)** 4.2 (s, -OH), 2.72 (t, 4H, -CH_2), 1.96 (d, 2H, -CH_2), 3.80 (m, 1H, -CH), 2.10 (d, 2H, -CH_2), 3.46 (t, 2H, -CH_2), 3.56 (t, 2H, -CH_2) **Mass(m/z)**409 (M+H$^+$).

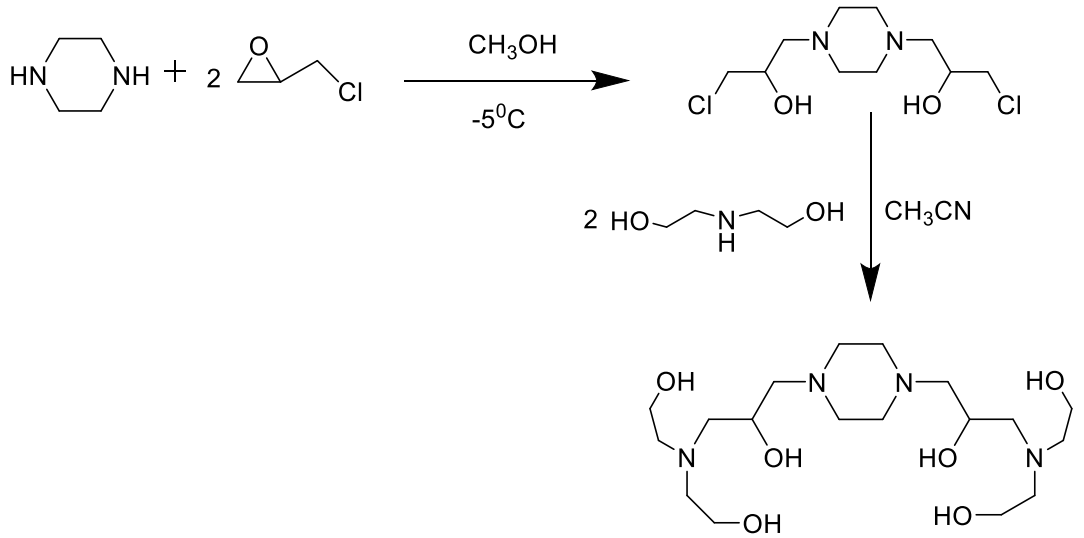

Figure 2.11:Synthesis and structureof H_6L11

2.1.12 Synthesis of *3,3'-(piperazine-1,4-diyl)bis(1-((2-hydroxyethyl)(methyl)amino) propan-2-ol) (H_4L12)*

Ligand H_4L12 was synthesized by similarprocedure as reported forH_6L11 using 10 mmol (2.70 g) of (*bis*-(1-chlorobutan-2-ol)) piperazine and 20 mmol (1.50 g) of N-methyl ethanolamine. Physical state ***oily liquid***, color ***colorless***, yield 55%.**UV-vis (λ, nm)** 210 **FTIR (ν in cm^{-1})**3383 (O–H Str.), 2937,2816 (CH Str.), 1309 (C–N Str.) **^{1}H NMR (δ, ppm)**2.7 (t, 4H, -CH_2), 2.32 (d, 2H, -CH_2),2.39 (d, 2H, -CH_2), 3.58 (m, 1H, -CH), 3.48 (t, 2H, -CH_2), 4.3 (t, 2H, -CH_2), 2.91 (s, 3H, -CH_3) **Mass(m/z)**349 (M+H$^+$).

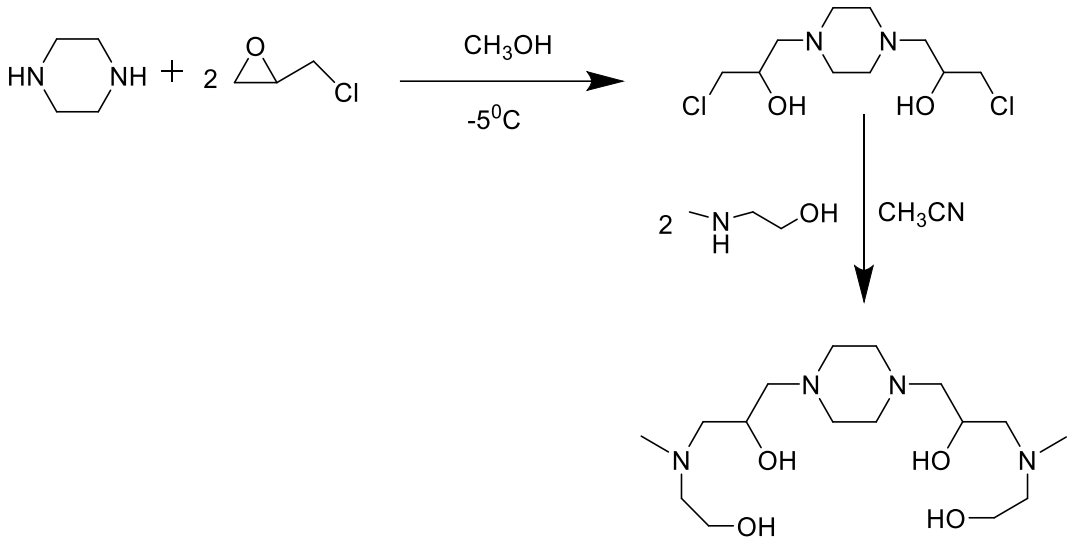

Figure 2.12:Synthesis and structureof H_4L12

2.1.13 Synthesis of *3,3'-(piperazine-1,4-diyl)bis(1-(ethyl)(2-hydroxyethyl)(amino)propan-2-ol) (H_4L13)*

Ligand H_4L13 was synthesized by similarprocedure as reported forH_6L11using 10 mmol (2.70 g) of (*bis*-(1-chlorobutan-2-ol)) piperazine and 20 mmol (1.78 g) of N-ethyl ethanolamine.Physical state ***oily liquid***, color ***colorless***, yield 70%.**UV-vis (λ, nm)** 210 **FTIR (ν in cm^{-1})**3371 (O–H Str.), 2939,2823 (CH Str.), 1315 (C–N Str.) **^{1}H NMR (δ, ppm)**2.72 (t, 4H, $-CH_2$), 2.32 (d, 2H, $-CH_2$),2.39 (d, 2H, $-CH_2$), 2.44 (m, 1H, -CH), 3.41 (t, 2H, $-CH_2$),4.6 (t, 2H, $-CH_2$), 1.1 (q, 2H, $-CH_2$), 0.91 (t, 3H, $-CH_3$),**Mass(m/z)**377($M+H^+$).

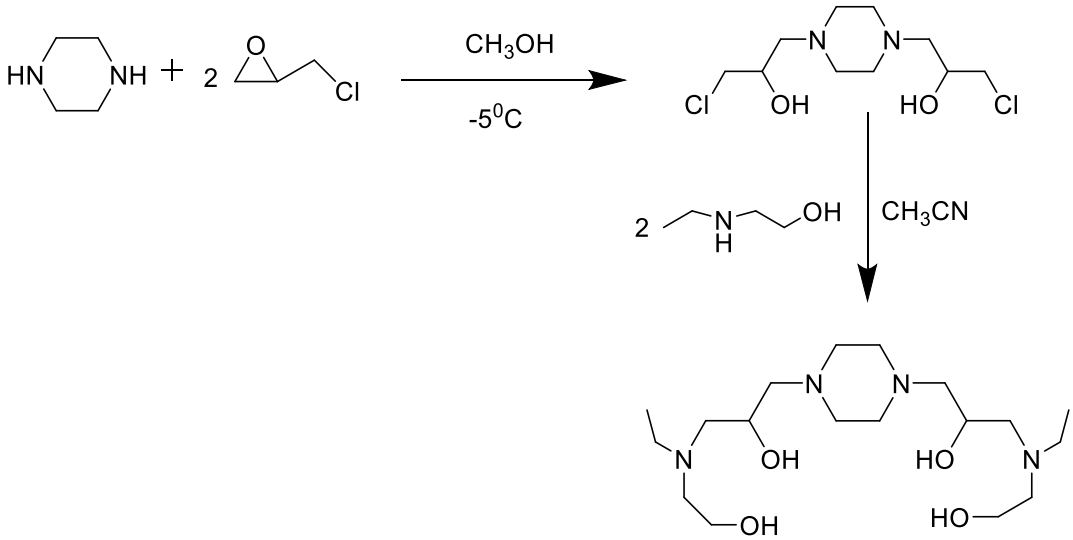

Figure 2.13:Synthesis and structureof H_4L13

2.1.14 Synthesis of *3,3'-(piperazine-1,4-diyl)bis(1-(ethyl)(2-hydroxyethyl)(amino)propan-2-ol) (H_4L14)*

Ligand H_4L14 was synthesized by similarprocedure as reported forH_6L11using 10 mmol (2.70 g) of (*bis*-(1-chlorobutan-2-ol)) piperazine and 20 mmol (3.02 g) of N-benzyl ethanolamine.Physical state ***oily liquid***, color ***colorless***, yield 70%.**UV-vis (λ, nm)** 237 **FTIR (ν in cm^{-1})**3371 (O–H Str.), 2939,2823 (CH Str.), 1315 (C–N Str.) **^{1}H NMR (δ, ppm)**2.2 (t, 4H, $-CH_2$), 3.7 (d, 2H, $-CH_2$), 3.8 (d, 2H), 3.1 (m, 1H, -CH), 2.9 (t, 2H, $-CH_2$), 3.6 (t, 2H, $-CH_2$), 1.9 (s, 2H, $-CH_2$), 6.9 (t, 2H, Ar-H),7.25 (d, 2H, Ar-H), 7.15 (m, 1H, Ar-H)**Mass(m/z)**501($M+H^+$).

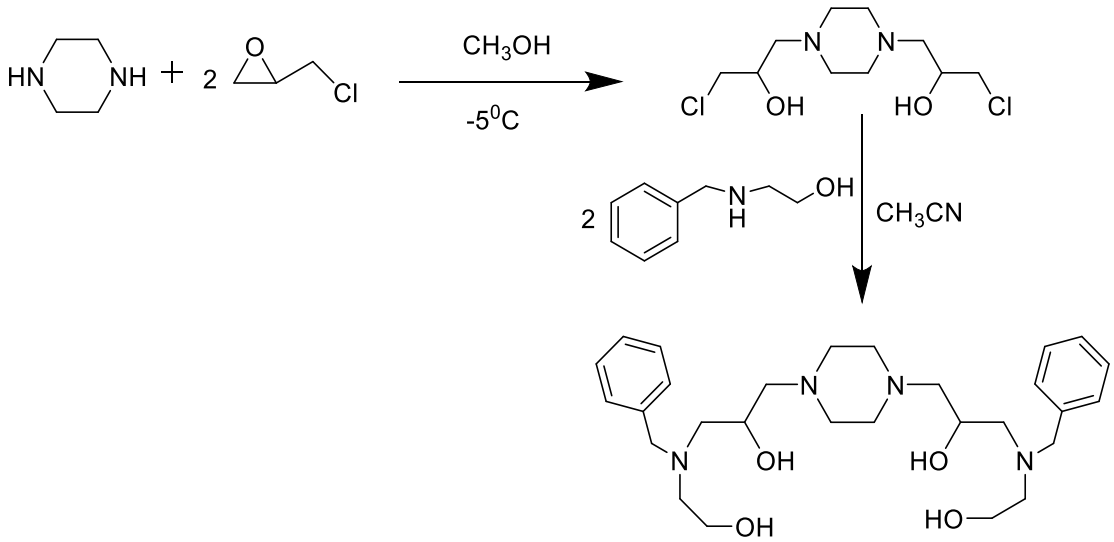

Figure 2.14:Synthesis and structureof H_4L14

2.2 Results and discussions

The ligands were synthesized using three different approaches (Figure 2.15). In first case diethanolamine was chlorinated to obtain *bis*-chloroethylamine which was then condensed with a range of suitable aromatic amine to obtain series of ligands (HL1-HL8). In the second approach, piperazine was directly treated with hydroxy alkyl chloride to yield symmetrically disubstituted ligand (H_2L9). By using the ring opening reaction, In the third approach piperazine was reacted with suitable epoxide (styrene oxide) which yielded ligand H_2L10 or its halo derivative (epichlorohydrin) to give an intermediate in 48 hours under the ice-cold conditions (-5^{0}C). This intermediate was then treated with suitable secondary amine for another 48 hours under the refluxing condition which yields the multidentate ligands (H_6L11-H_4L14). Physical state of

these ligands very from oily liquid to semisolid to solid in different molecules. Ligands such as HL4, HL5, HL6, H_2L9 and H_2L10 were thermally stable and non-hygroscopic solids in nature. Solubility of these ligands were tested in methanol, water, chloroform, DMF, DMSO Tris buffer (pH 7.4).

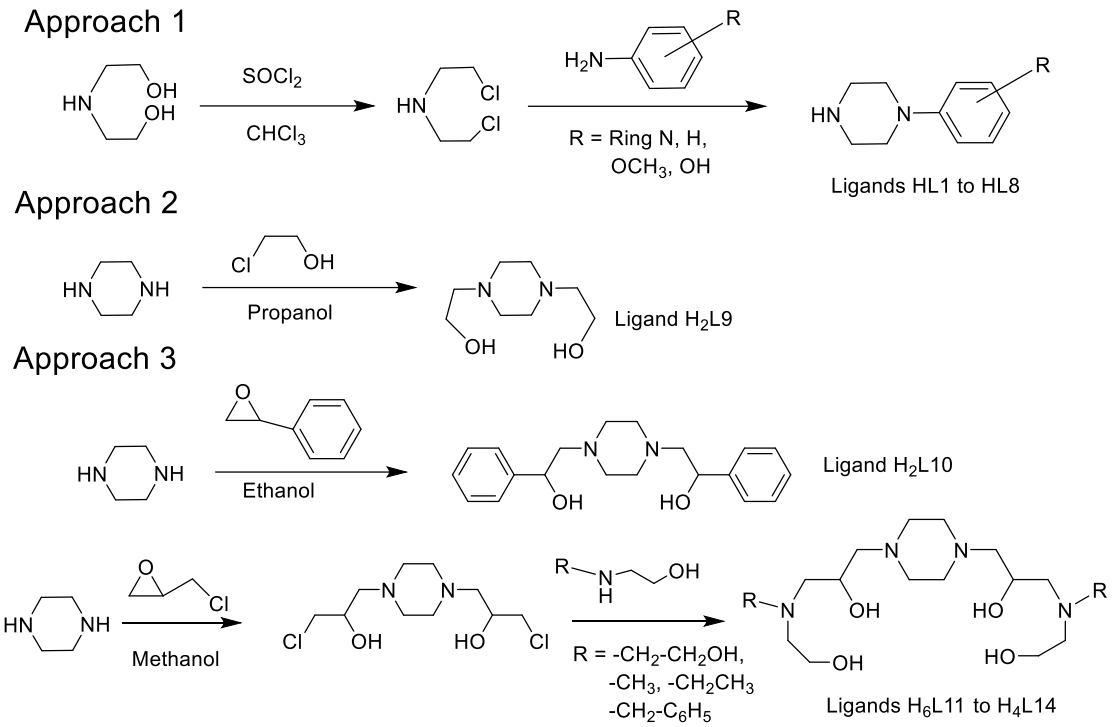

Figure 2.15:Synthetic approaches for various ligands

2.2.1 UV-vis analysis

The UV-vis absorption spectra of piperazine ring-based ligands were recorded in the range of 800- 200 nm at 10^{-3}M concentration using methanol as solvent. 90% methanolic solution was also used to record absorption spectra where solubility in 100% methanol was not observed. The $\pi \rightarrow \pi^*$ transitionsbands were clearly observed in those ligands only in which aromatic ring was present in the ligand skelton. Effect of substitution on aromatic ring was also observed in ligands HL5-HL8 as compared to HL4. Since both methoxy and hydroxy groups are electron donating group and stabilize the ring, $\pi \rightarrow \pi^*$ absorption wavelength was increased and it was established that ortho and para-substitution have similar effect while it was different in meta and

para-substitution (HL7 and HL8). The observed UV–vis spectrum peaks of the ligands along with their structures have been shown in table 2.1.[1]

UV-vis spectra of three ligands which contain isomeric pyridyl ring substitution at one side of piperazine ring were recorded using methanol as solvent. HL1 show maximum absorbance at 258 nm with the molar extinction coefficient of 1.41 x 10^3Lmol^{-1}cm^{-1}whereas the other two isomeric ligands show absorbance at 255, 330 nm and 226, 299nm with the molar extinction coefficient of 1.44 x 10^3, 0.57 x $10^3$and 0.91 x 10^3, 0.64 x 10^3Lmol^{-1}cm^{-1} respectively (Figure 2.16). These transitions correspond to π→π* and n→π* electronic transition owing the presence of aromatic ring in the ligand skelton. In case of fourth ligand which has a simple phenyl ring in the ligand HL4 this electronic transition occurs at 231 and 289 nm with the extinction coefficient of 2.45 x 10^3 and 1.48 x 10^3Lmol^{-1}cm^{-1}indicative the type of π→π* and n→π* transition (Figure 2.17).

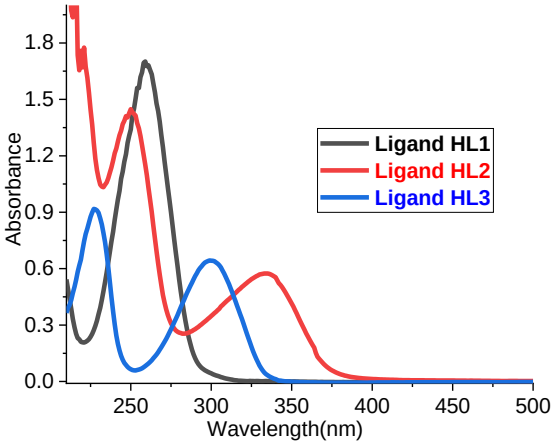

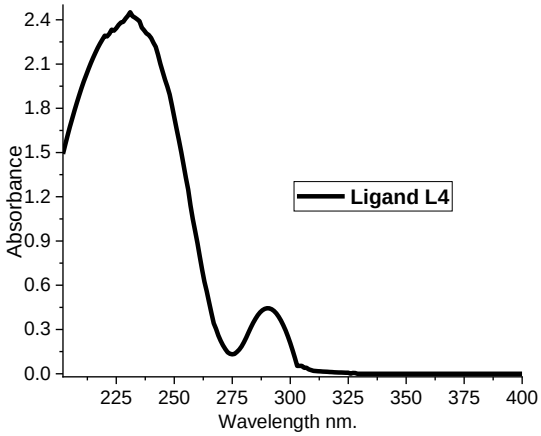

Figure 2.16: UV-vis spectra of ligands HL1-L3 Figure 2.17: UV-vis spectra of ligand HL4

In case of ligands which contain isomeric anisidine substituent (Ligands HL5 and HL6) at the piperazine ring absorption occur at 240, 306 nm and 244, 287 nm with the molar extinction coefficient of 1.14 x 10^3,0.30 x 10^3 and 1.14 x $10^3$and 0.92 x 10^3,0.30 x 10^3 Lmol^{-1}cm^{-1}which also owe the π→π* and n→π*type of electronic transition (Figure 2.18). Whereas isomeric phenolic ligands HL7 and HL8 have absorption maxima at 242, 284 nm with 1.85 x 10^3, 0.82 x 10^3 and 283, 298 nm with 1.25 x 10^3,1.31 x 10^3 Lmol^{-1}cm^{-1}corresponding to above similar transitions (Figure 2.19).

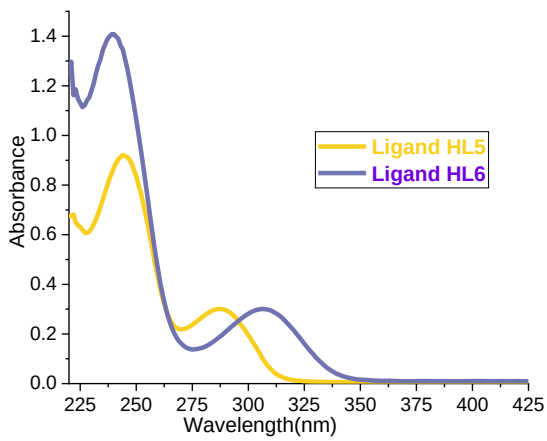

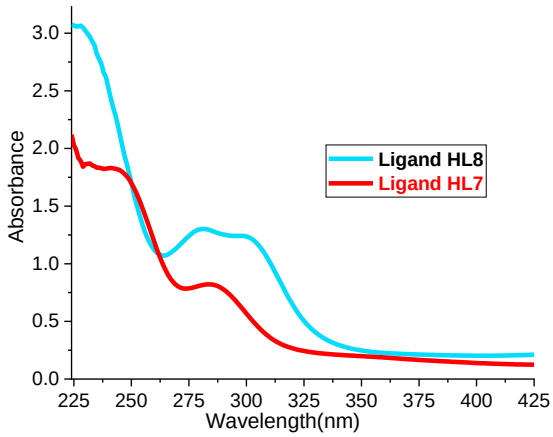

Figure 2.18: UV-vis spectra of ligands HL5-HL6 Figure 2.19: UV-vis spectra of ligands HL7-HL8

The other ligand 1,4-bisethanol piperazineH_2L9 which has absence of aromatic ring show absorbance only at the wavelength of 213 nm with extinction coefficient 2.40 x $10^3 Lmol^{-1}cm^{-1}$indicated and confirmed only presence of n-σ* type of electronic transition where as in case of similar ligand bis (1-phenylethanol) piperazine H_2L10 which have presence of additional aromatic ring with similar sigma skelton as the ligand H_2L9 show a broad peak at 253 nm (Ɛ = 0.27 x $10^3 Lmol^{-1}cm^{-1}$)along with 213 nm with extinction coefficient 2.40 x $10^3 Lmol^{-1}cm^{-1}$indicative the presence of π to π* transition (Figure 2.20). In case of multidentate ligands which owe to absence of pi bonds or aromatic ring (H_6L11, H_4L12 and H_4L13) show absorption peak at the range of 210-224 nm while the analogue ligand H_4L14 with aromatic ring show broad peak at 237 nm (Figure 2.21).

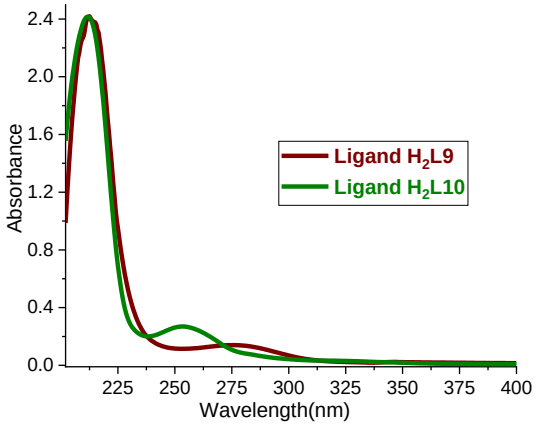

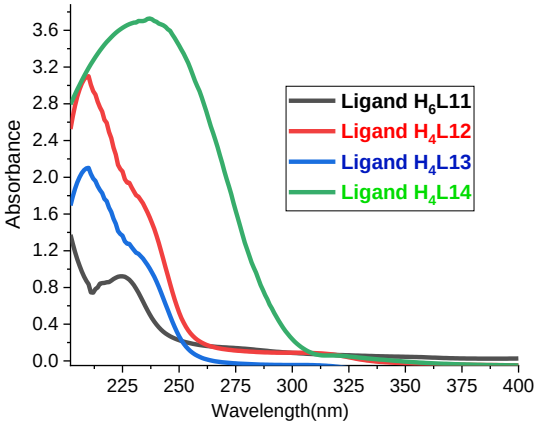

Figure 2.20 UV-vis spectra of ligands H_2L9-H_2L10 Figure 2.21 UV-vis spectra of ligands H_6L11-H_4L14

Table 2.1: Maximum absorption wavelength with molar extinction coefficient and type of transition of synthesized ligands

Ligand Code	Structure	Wavelength (λ_{max}, nm)	Molar Extinction Coefficient (ε $Lmol^{-1}cm^{-1}$)	Transitions
HL1	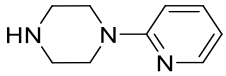	259	1.70×10^3	$\pi \rightarrow \pi^*$
HL2	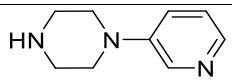	250, 334	1.44×10^3, 0.57×10^3	$\pi \rightarrow \pi^*$, $n \rightarrow \pi^*$
HL3	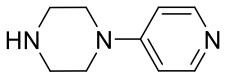	227, 299	0.91×10^3, 0.64×10^3	$\pi \rightarrow \pi^*$, $n \rightarrow \pi^*$
HL4	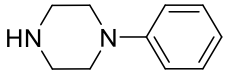	231, 289	2.45×10^3, 1.48×10^3	$\pi \rightarrow \pi^*$, $n \rightarrow \pi^*$
HL5	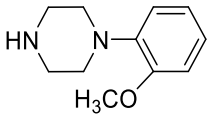	240, 306	1.408×10^3, 0.30×10^3	$\pi \rightarrow \pi^*$, $n \rightarrow \pi^*$
HL6	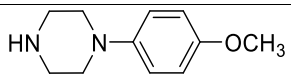	244, 287	0.30×10^3, 0.92×10^3	$\pi \rightarrow \pi^*$, $n \rightarrow \pi^*$
HL7	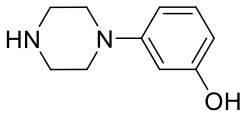	242, 284	0.82×10^3, 1.85×10^3	$\pi \rightarrow \pi^*$, $n \rightarrow \pi^*$
HL8	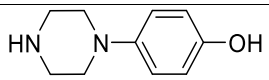	283, 298	1.25×10^3, 1.31×10^3	$\pi \rightarrow \pi^*$, $n \rightarrow \pi^*$
H_2L9	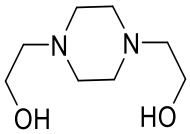	213	2.40×10^3	$n \rightarrow \sigma^*$
H_2L10	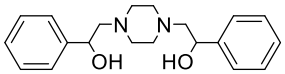	213, 253	0.26×10^3, 2.40×10^3	$\pi \rightarrow \pi^*$, $n \rightarrow \pi^*$
H_6L11	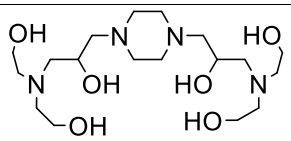	224	0.92×10^3	$n \rightarrow \sigma^*$
H_4L12	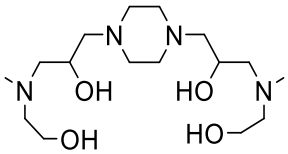	210	2.10×10^3	$n \rightarrow \sigma^*$
H_4L13	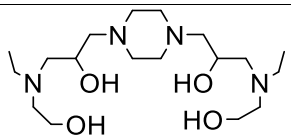	210	3.18×10^3	$n \rightarrow \sigma^*$

H_4L14	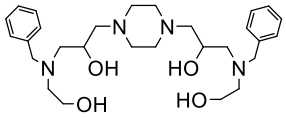	227	3.72×10^3	$\pi \rightarrow \pi^*$

2.2.2 FTIR analysis

Fourier Transform Infra-Red (FTIR) spectroscopy is a time saving, non-destructive and rapid techniquecapable to detect presence or absenceof a range of functional groups sensitive to molecular changes.[2,3] Any changes in the absorption pattern characteristics infers changes in the composition of molecules.[4] All ligands were characterized by FTIR technique and showed significant vibrational peaks of desired functional groups and selected bond frequencies.

Since the ligands have specific functional group along with their other bonds active in the IR region. Comparative studies are helpful in showing the variation in the bond frequencies along with their structures.

In the IR spectra of ligands (HL1-HL8) a strong band appeared in the region of 3350-3260 cm^{-1} corresponding N-H Stretching of piperazine ring unsubstituted secondary amine group. While the presence of bands near 1400-1600 cm^{-1} in these ligands were evidence to C=C stretching owing the presence of aromatic ring. Other important C–N and C–H stretching were also indicated in the region of 1300-1360 cm^{-1} and 2930-3100 cm-1. While in other ligands which did not contain aromatic ring or C=C type fragment, absence of band near 1400-1600 cm^{-1} were in good agreement the support structure of ligands as absence of peaks in this region makes the comparative studies of these ligands with each other having quite different ligand backbone skelton. The ligands that contain -OH functional group (HL6, HL7, H_2L9, H_2L10, H_6L11-H_4L14) broad absorption peak in the region of ~3300 cm^{-1} was observed. These IR interpretations were more useful in the explaining the metal complexing behavior of these ligands. IR analysis with selected bond frequencies of all piperazine based ligands along with their structures are as follows (Table 2.2):

Table 2.2: Selected bond frequencies (cm^{-1}) of ligands

Ligand Code	Structure	N-H Str.	O–H Str.	C=C(Ar) Str.	C–N Str.	C–H (Ar/sp^3) Str.
HL1	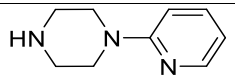	3345	-	1498,1504	1305	3104
HL2	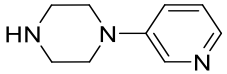	3477	-	1498,1642	1341	2962
HL3	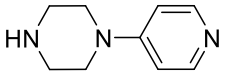	3344	-	1498,1550	1201	2947
HL4	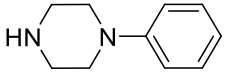	3344	-	1498,1593	1321	2922
HL5	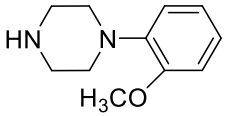	3277	-	1510,1497	1301	2926
HL6	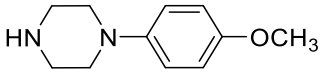	3277	-	1510,1497	1301	2926
HL7	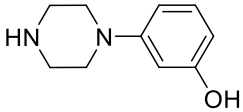	3232	-	1593,1498	1346	2956
HL8	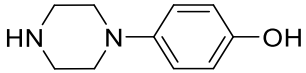	3261	-	1599,1506	1357	2955
H_2L9	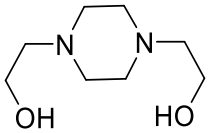	-	3122	-	1329	-

H_2L10	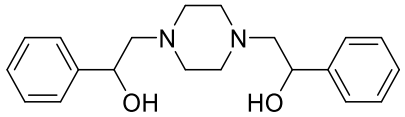	-	3371	1440	1315	2923
H_6L11	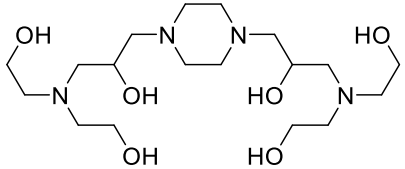	-	3304	-	1329	2927
H_4L12	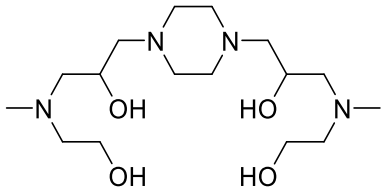	-	3383	-	1309	2937
H_4L13	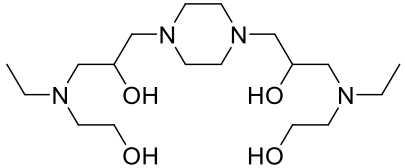	-	3371	-	1315	2939
H_4L14	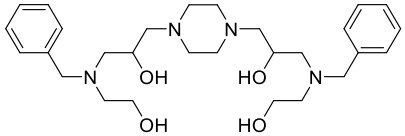	-	3367	1448	1313	2931

2.3.3 Mass spectral analysis

Ligands were also analyzed by mass spectrometry by using direct mass under +ve ionization mode. Molecular ion peak of the corresponding ligand is observed at the $M+H^+$ (M = Molecular mass) which confirm the structure of the ligand. Additionally, interpretation of fragmentation pattern of the also support the structure of the ligand.[5-8] Mass spectra of ligands HL1-HL8 have been represented in figure 2.22-2.27 with the structure that represent to molecular ion peaks while for other ligands fragmentation patternsare discussed in detail.

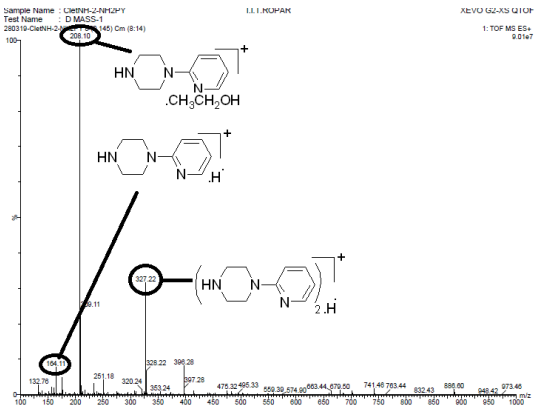

Figure 2.22: Mass spectra of ligand HL1

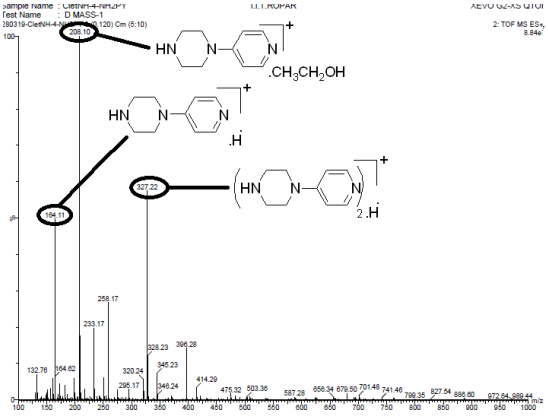

Figure 2.23: Mass spectra of ligand HL3

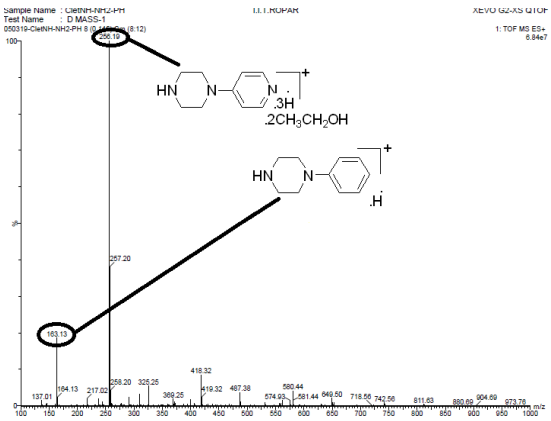

Figure 2.24: Mass spectra of ligand HL4

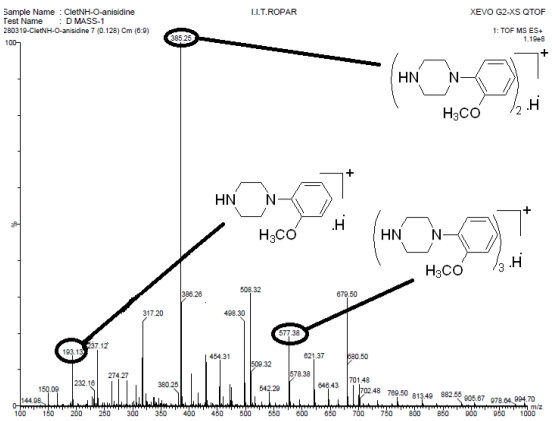

Figure 2.25: Mass spectra of ligand HL5

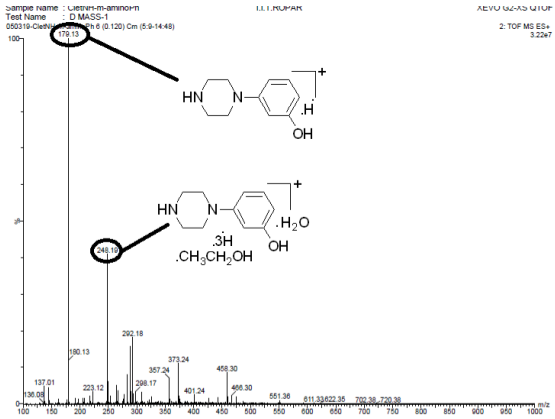

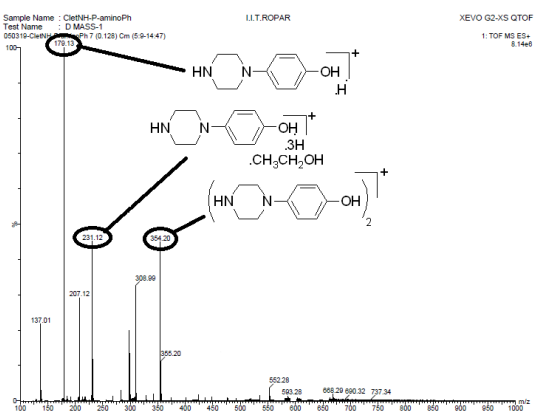

Figure 2.26: Mass spectra of ligand HL7 Figure 2.27: Mass spectra of ligand HL8

In the mass spectra of ligand H_2L9, molecular ion peak representing to molecular mass of ligand is shown at m/z 175 $[M+H^{\cdot}]^+$. The ligand shows very less fragmentation pattern as there is only dominant peak of ligands molecular mass only. A small peak at m/z 219 corresponds to ligand coupled with CH_3-CH_2-OH. Another low intensity peak at m/z 157 represents the loss of water molecule which is very common fragmentation pattern of alcohols (Figure 2.28 and 2.29).

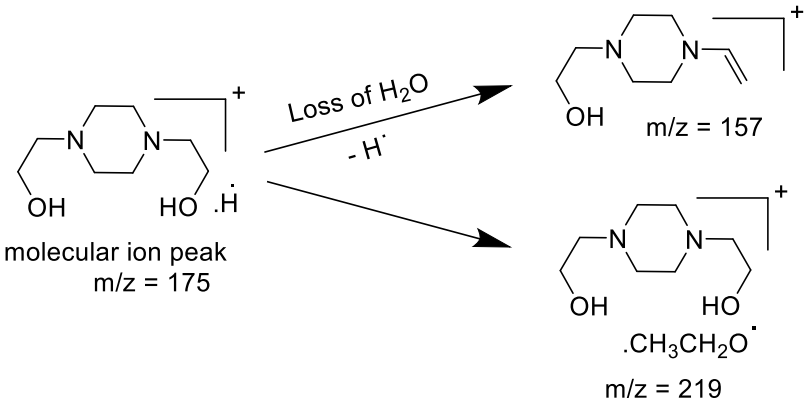

Figure 2.28 Proposed fragmentation pathway of ligand H_2L9

In the mass spectra of ligand H_2L10, molecular ion peak representing to molecular mass of ligand is shown at m/z 327 $[M+H^{\cdot}]^+$. The ligand shows very less fragmentation pattern as there is few dominant peaks of ligands mass spectral fragmentation. Another medium intensity peak at m/z 309 represents the loss of water molecule which is very common fragmentation pattern of alcohols. To this further loss of styrene fragment or direct loss of one arm from the ligand result in another intermediate species corresponding m/z at 207 (Figure 2.30 and 2.31). Since there is

one more alcoholic group which is susceptible to be lost as water molecule m/z at 189 correspond to this species which comes through water loss from m/z 207 or from m/z 327 by the loss of one arm and one water from second arm. Thus, ligand show fair fragmentation pattern which is in agreement in the evidence of given proposed structure of ligand.

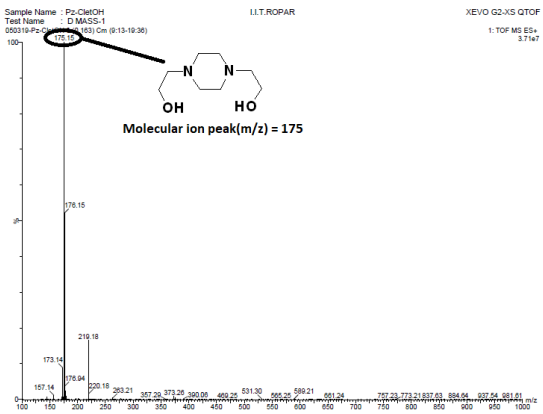

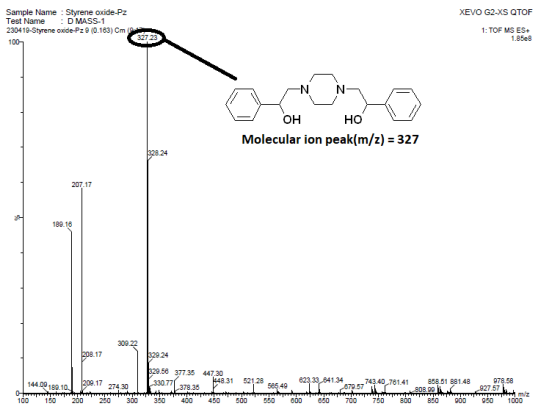

Figure 2.29: Mass spectra of ligand H_2L9 Figure 2.30: Mass spectra of ligand H_2L10

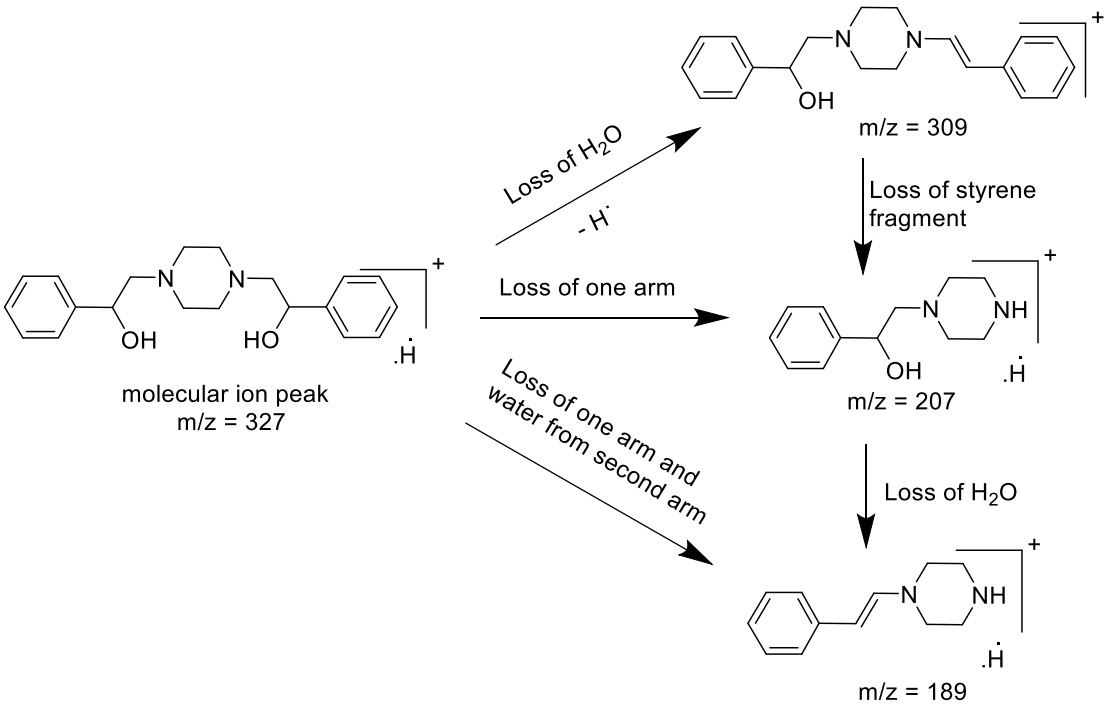

Figure 2.31 Proposedfragmentation pathwayof ligand H_2L10

In the mass spectra of multidentate ligand H_6L11, molecular ion peak representing to molecular mass of ligand is shown at m/z 409 $[M+H^{\cdot}]^+$ and 431 $[M+Na^{\cdot}]^+$. The ligand shows quite remarkable fragmentation pattern as there is dominant peaks of ligands mass spectral fragmentation which were explainable in two ways wowing to the symmetry of molecule. In the first pathway initial loss of ethyl alcohol branch from one side results in the species corresponding to m/z 322. Further loss of $-NH_2$ gives the species belonging to m/z 304. Again, the loss of ethyl alcohol results m/z at 276. Another medium intensity peak at m/z 309 represents the loss of water molecule which is very common fragmentation pattern of alcohols (Figure 2.32 and 2.33).

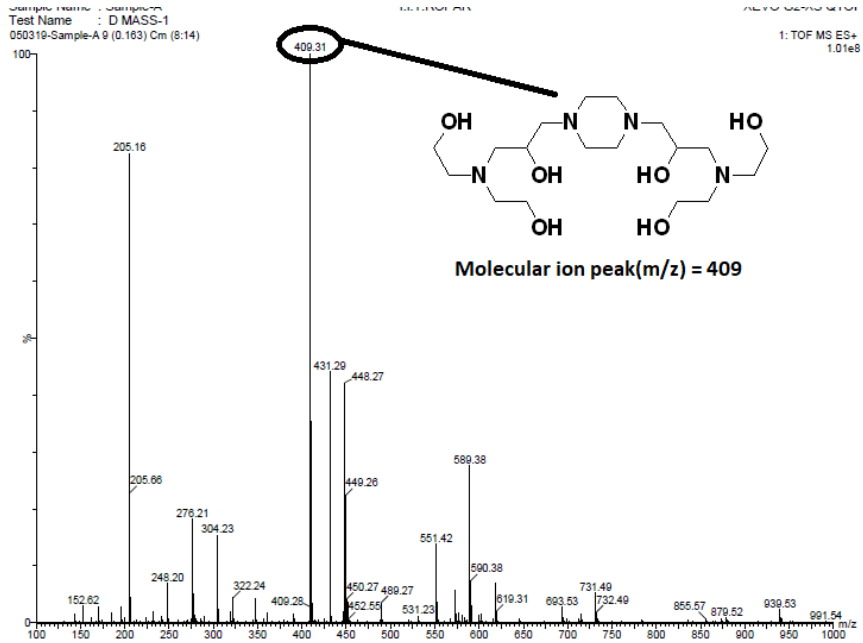

Figure 2.32: Mass spectra of ligand H_6L11

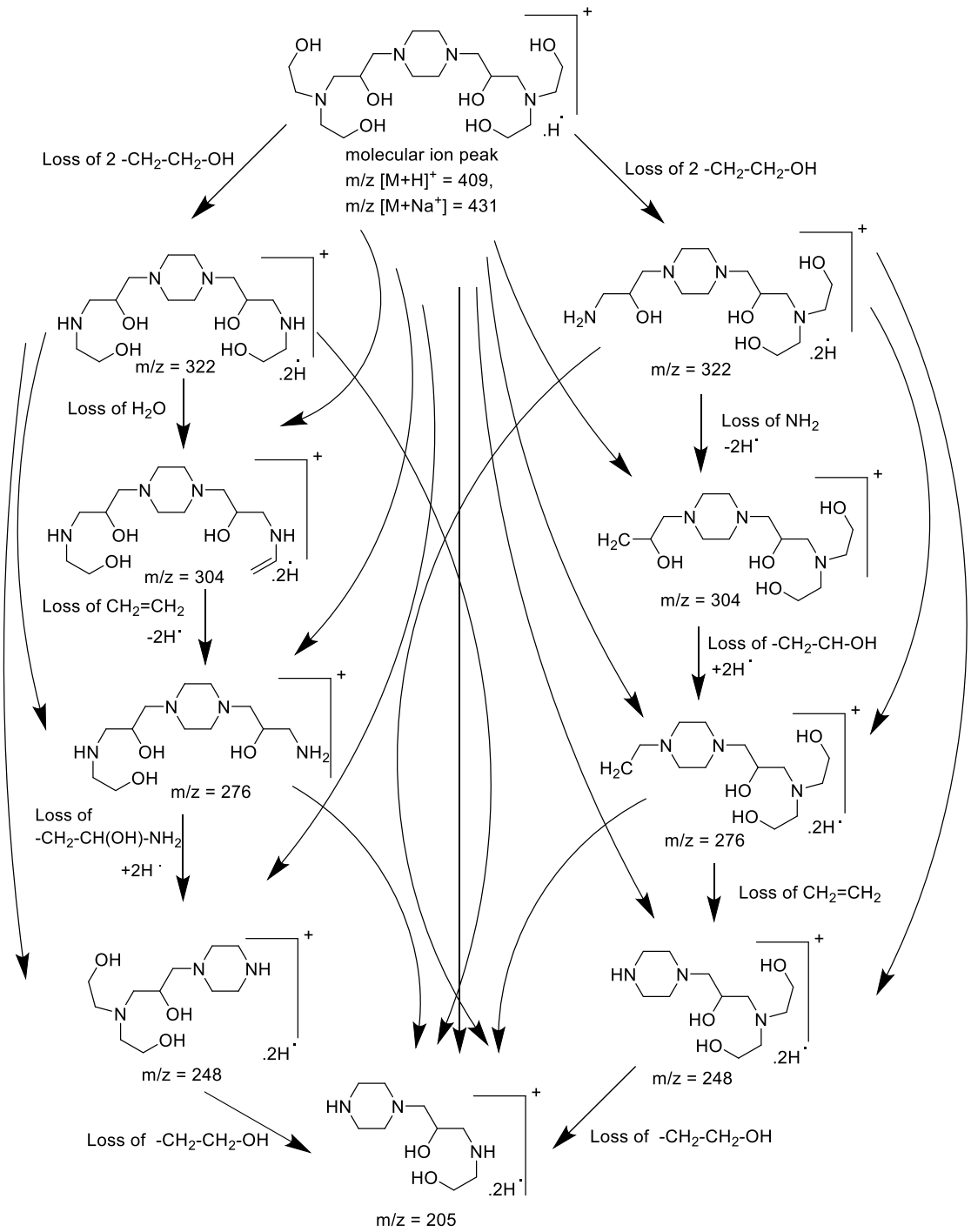

Figure 2.33Proposedfragmentation pathwaysof ligand H_6L11

In the mass spectra of multidentate ligand H_4L12, molecular ion peak representing to molecular mass of ligand is shown at m/z 339 [M+H·]+, 371 [M+Na·]+, 545 [M+CH_2-CH_2-OH·]+. The mass spectrum matched well with the expected fragmentation pattern of the ligand. In the first pathway initial loss of two water molecule results in the

species corresponding to m/z 312. Further loss of two water molecule in two steps represents the peaks m/z at 292 and 274. Continued loss of half fragment from the species at 274, results in another intermediate species corresponding to m/z at 137. In the alternative pathway direct loss of two HO-CH_2-CH_2-NH-CH_3 fragments gives the intermediate species corresponding to m/z at 274. To this further loss of NH_2-CH-OH gives peak at 218 from where loss of CH_2-NH-CH_3 fragment shows the peak at m/z 276 and at the end loss of two waterfrom m/z 276 return backs to m/z 137 which is also explainable by first fragmentation pattern (Figure 2.34 and 2.35). Thus, ligand show fair fragmentation pattern which is in agreement in the evidence of given proposed structure of ligand.

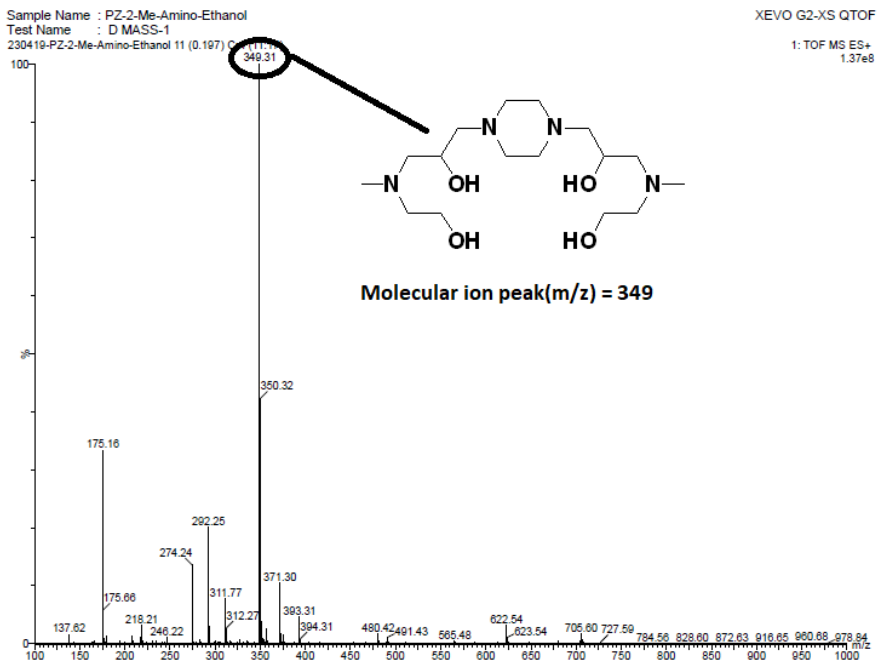

Figure 2.34: Mass spectra of ligand H_4L12

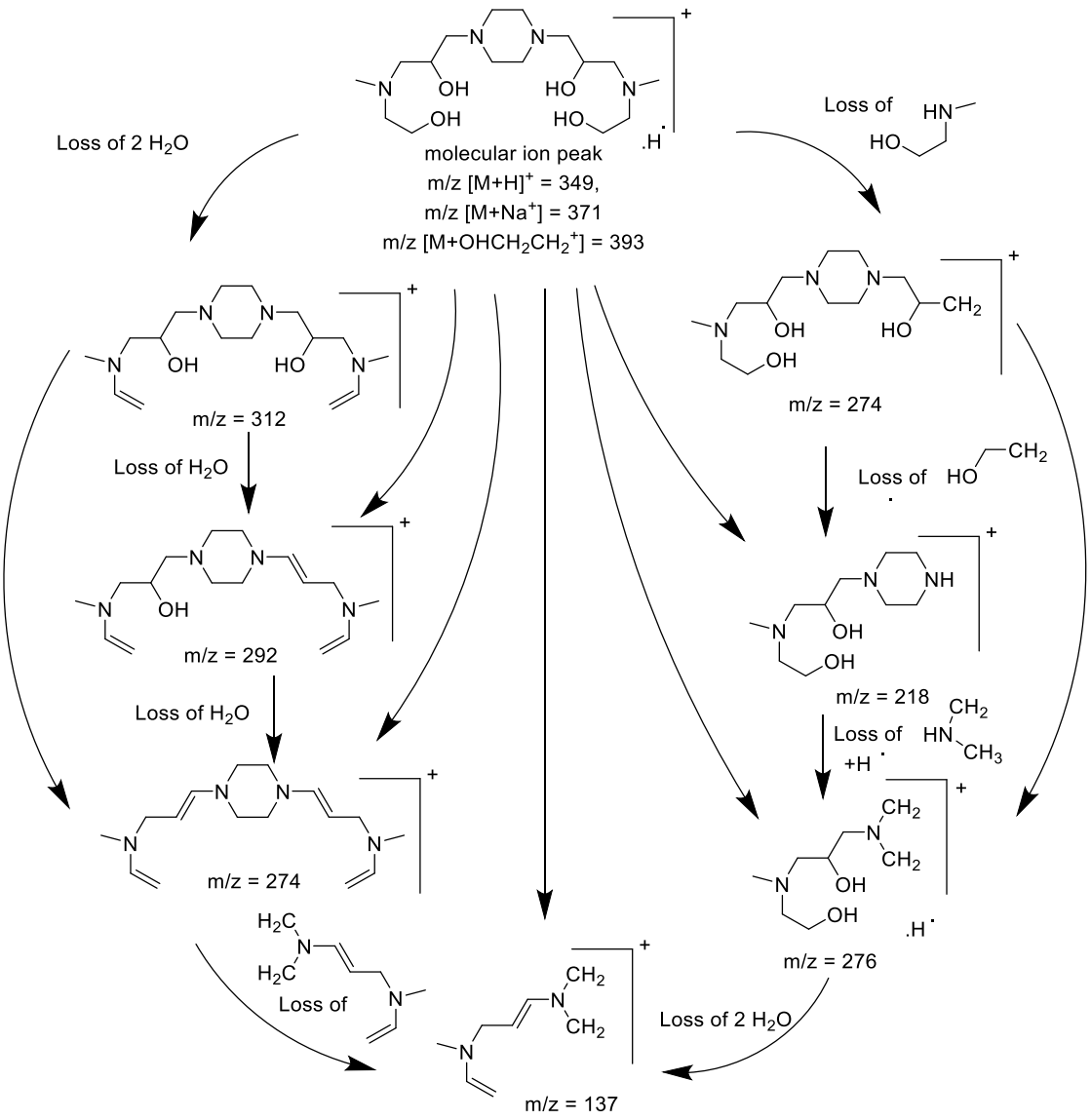

Figure 2.35 Proposedfragmentation pathwaysof ligand H_4L12

In the mass spectra of multidentate ligand H_4L13, molecular ion peak representing to molecular mass of ligand is shown at m/z 377 $[M+H^{\cdot}]^+$, 399 $[M+Na^{\cdot}]^+$. The mass spectrum matched well with the expected fragmentation pattern of the ligand.In the first pathway initial loss of two ethyl alcohol fragment results in the species corresponding to m/z 331. Further loss of CH_2-CH_2-N and CH_2-CH_3 fragments gives the species belonging to m/z 260whereas loss of onlyCH_2-CH_2-N fragment gives the peak at m/z 288. Again, the loss of CH_2-CH-OH molecule results m/z at 232. In the alternate pathway direct loss of HO-CH_2-CH_2-N-CH_2-CH_3also gives the intermediate species corresponding to m/z at 288.To this further loss of CH_2-CH(HO)-CH_2

fragment or direct loss of one arm from the ligand result in another intermediate species corresponding m/z at 232. Continued loss of CH_2-NH-CH_2 fragment which is exact half of original ligand gives m/z at 189 (Figure 2.36 and 2.37). Thus, ligand show fair fragmentation pattern which is in agreement in the evidence of given proposed structure of ligand.

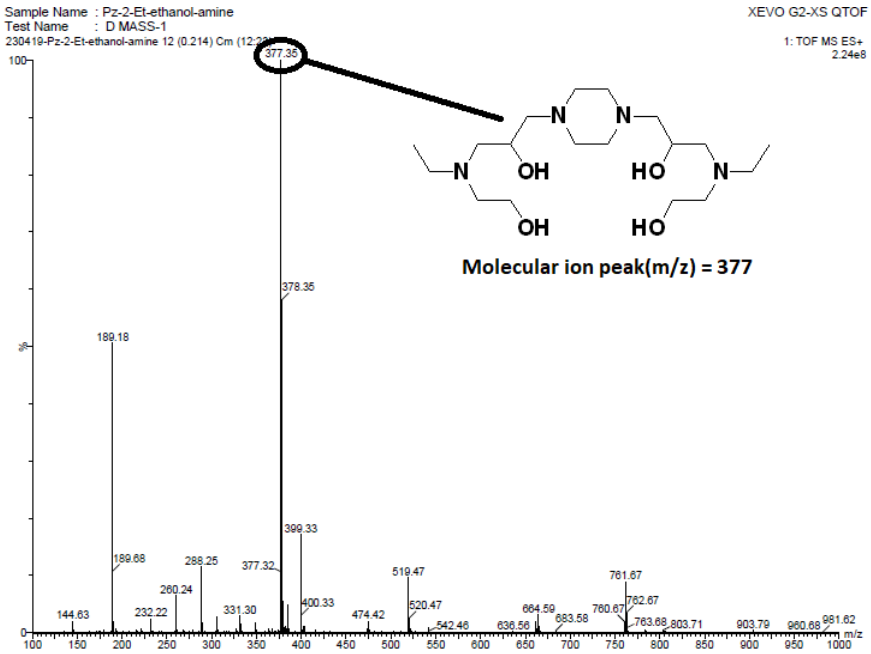

Figure 2.36: Mass spectra of ligand H_4L13

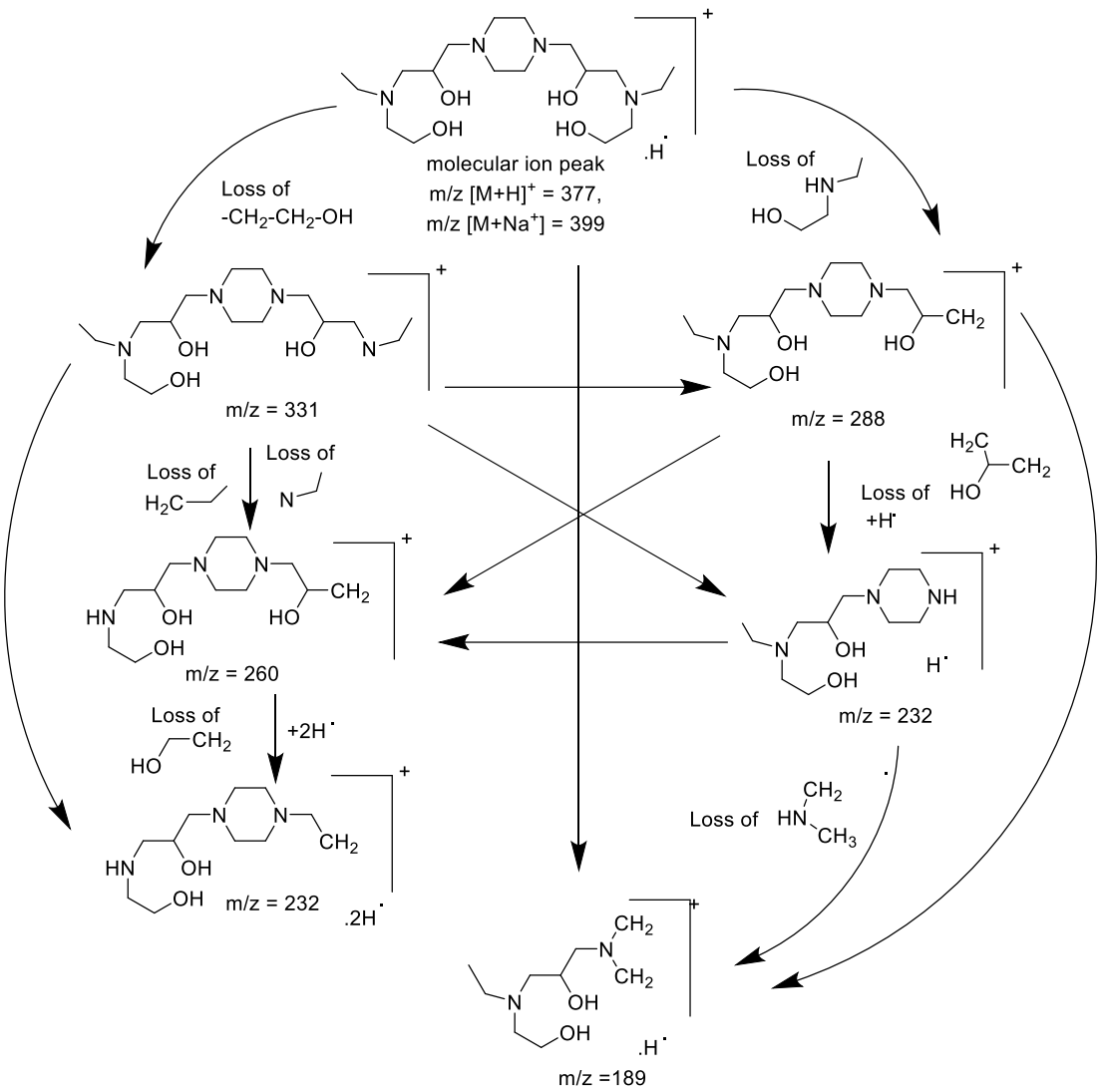

Figure 2.37 Proposedfragmentation pathwaysof ligand H_4L13

In the mass spectra of multidentate ligand H_4L14, molecular ion peak representing to molecular mass of ligand is shown at m/z 501 $[M+H^{\cdot}]^+$, 523 $[M+Na^{\cdot}]^+$545 $[M+CH_2\text{-}CH_2\text{-}OH^{\cdot}]^+$. The mass spectrum matched well with the expected fragmentation pattern of the ligand.In the first pathway initial loss of subsequent loss of ethyl alcohol fragment results in the species corresponding to m/z 455 and 411. Farther loss of exact half fragments m/z 411 gives the species belonging to m/z 206, from where loss of twoCH_2 fragment gives the peak at m/z 178. In the alternate pathway direct loss of two HO-CH_2-CH_2 and benzyl fragments gives the intermediate species corresponding to m/z at 368. To this further loss of NH_2-$CH_2$and HO gives peak at 321 from where loss of CH_2-CH fragment shows the peak at m/z 278 and loss of CH_2-NH-CH_2

fragment which is exact half of original ligand gives m/z at 251.Peak The loss of one more HO-CH_2-$CH_2$from m/z return backs to m/z 206 which is also explainable by first fragmentation pattern (Figure 2.38 and 2.39). Thus, ligand show fair fragmentation pattern which is in agreement in the evidence of given proposed structure of ligand.

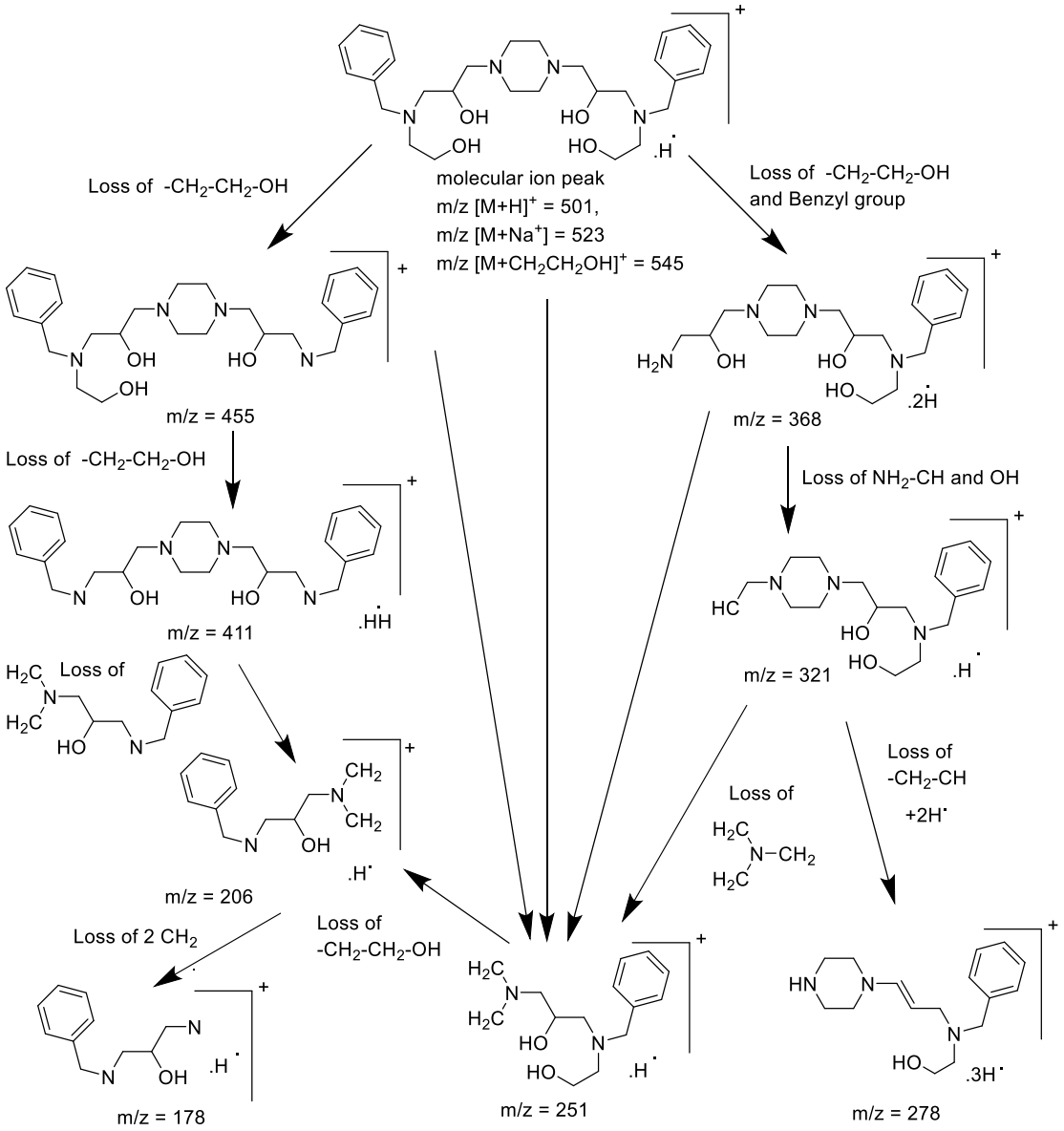

Figure 2.38Proposedfragmentation pathways of ligand H_4L14

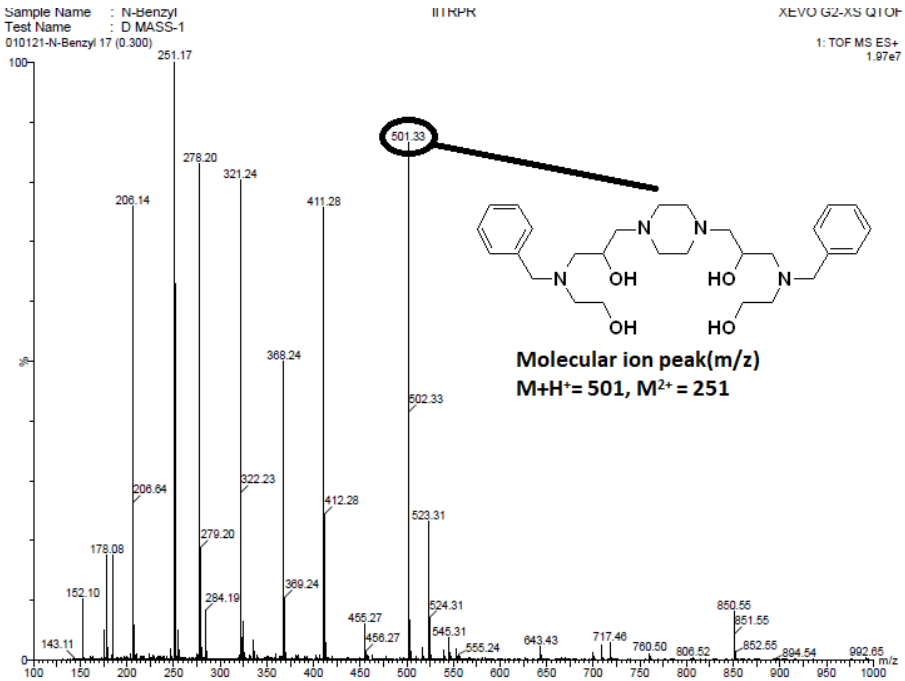

Figure 2.39: Mass spectra of ligand H_4L14

2.3.4 ^{1}H NMR Analysis:

All ligands were also analyzed by ^{1}H NMR spectroscopy. Observed proton peaks were in agreement with the structure of the ligand. NMR data for ligands HL1- HL8 is discussed in the tabular form (Table 2.3) while for all other ligands, it is discussed in detail.

Table 2.3: Observed proton peaks in NMR for ligands HL1 to HL8

Ligands	NH	Ha	Hb	Hc	Hd	He	Hf	Hg
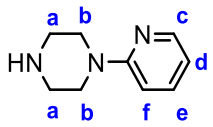	2.49 (t)	3.37 (t)	3.55 (t)	6.40 (d)	7.98 (t)	6.81 (t)	8.81 (d)	-
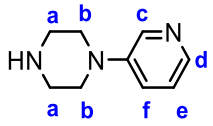	2.48 (t)	2.50 (t)	3.41 (t)	6.89 (d)	7.56 (t)	7.58 (d)	8.18 (s)	-
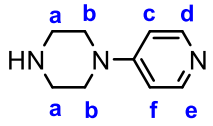	2.49 (t)	3.33 (t)	3.89 (t)	6.84 (d)	8.52 (d)	8.52 (d)	6.84 (d)	-

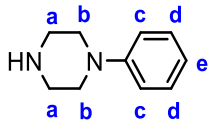	3.38	2.59 (t)	3.1 (t)	7.11 (d)	6.64 (t)	6.61 (t)	-	-
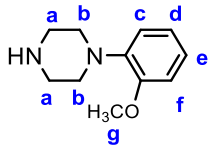	3.84 (m)	3.14 (t)	3.25 (t)	6.61 (d)	`6.87 (t)	`6.67 (t)	6.76 (d)	2.55 (s)
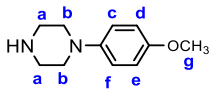	3.7 (m)	3.2 (t)	3.40 (t)	6.97 (d)	`6.97 (t)	`6.85 (t)	6.85 (d)	2.55 (s)
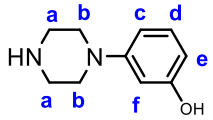	3.6 (m)	3.14 (t)	3.25 (t)	6.78 (d)	`6.86 (t)	6.98 (d)	7.02 (s)	-
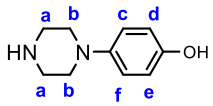	3.67 (m)	3.41 (t)	2.92 (t)	6.78 (d)	`6.86 (t)	6.98 (d)	7.02 (s)	-

In the NMR spectra of H_2L9, there are four types of protons, except -OH which is exchangeable, all other protons are expected to have triplet splitting of signal. Piperazine ring $-CH_2$type two signal were shown at up field 2.3 ppm marked as a. whereas other two signal were shown slight down field at 3.5 and 4.4 ppm marked as b and c (Figure 2.40). Thus, NMR spectra is also good agreement of proposed structure of ligand.

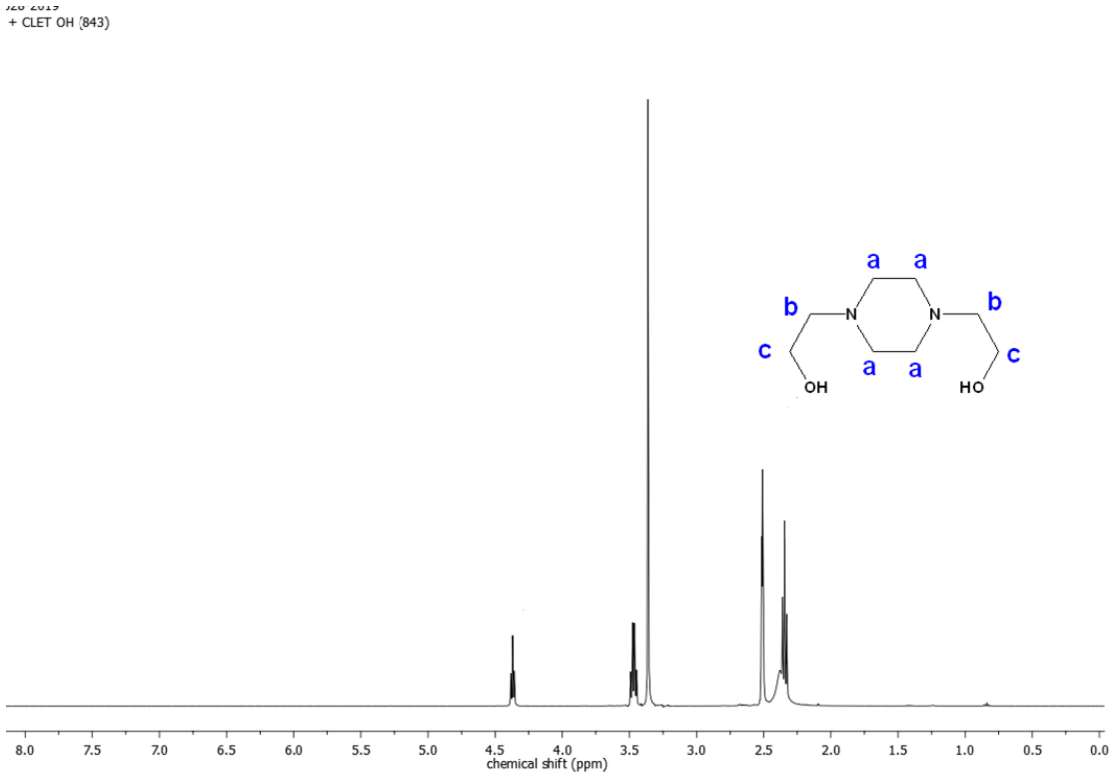

Figure 2.40: NMR Spectra of ligand H_2L9

In the NMR spectra of H_2L10, there are eight types of protons, except -OH which is exchangeable, all other protons are expected to have triplet (proton type a), doublet (proton type b), triplet (proton type c) and multiplate (proton type d, e and f) splitting of signals. Piperazine ring $-CH_2$type two signal were shown at up field 2.7 ppm marked as a. whereas other second signal is shown slight down field at 3.5 with doublet marked as b. Type c signal is shown at 3.8 ppm with triplet. Aromatic protons marked as d, e and f comes in the range of 7.2-7.5 ppm (Figure 2.41).Thus, NMR spectra is also good agreement of proposed structure of ligand.

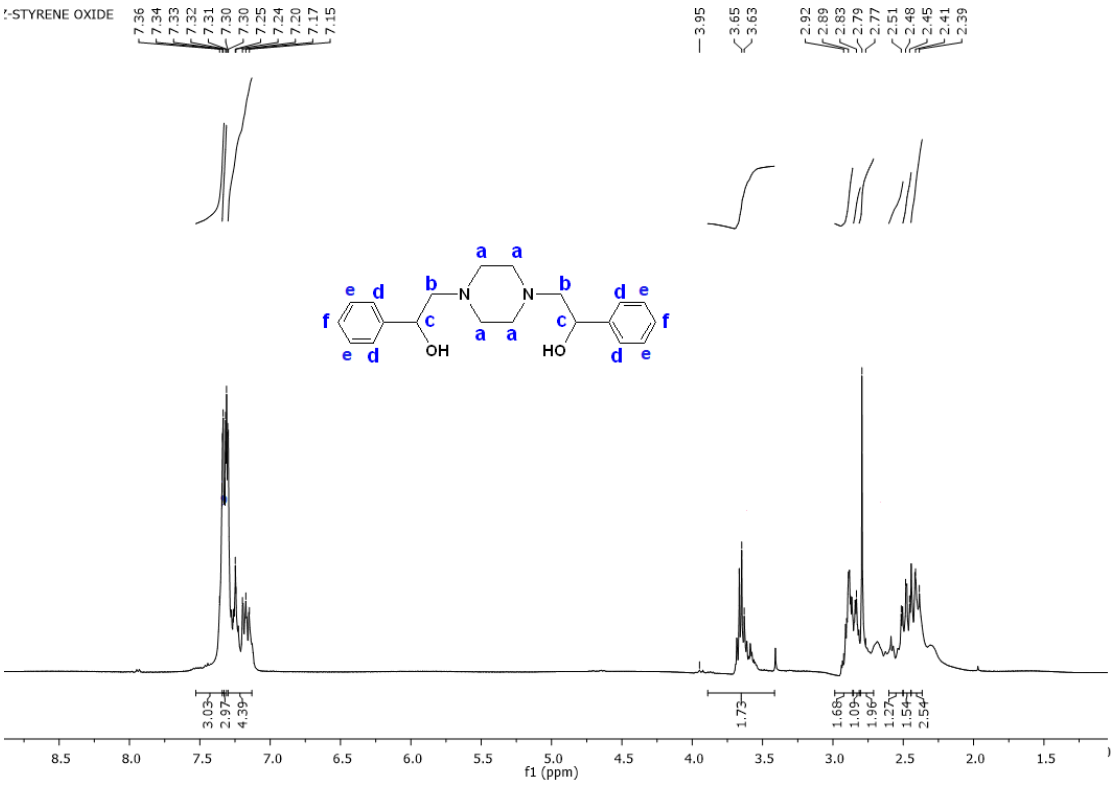

Figure 2.41: NMR Spectra of ligand H_2L10

In NMR spectra of ligandH_6L11 -OH broad peak is visible at 4.2 ppm due to presence of 6 -OH group in the ligand. Protons marked as a show triplet at the 2.7 ppm. While the protons marked as b and d show doublet at the up-field value of 1.96 and 2.1 ppm. Protons marked as c show slight downfield with multiplate splitting at 3.8 ppm. The other two protons marked as f and g both show triplet at the value of 3.46 and 3.56 ppm. Since there were no aromatic protons in the ligand no any peak is observed in the aromatic region (Figure 2.42).Thus, NMR spectra is also good agreement of proposed structure of ligand.

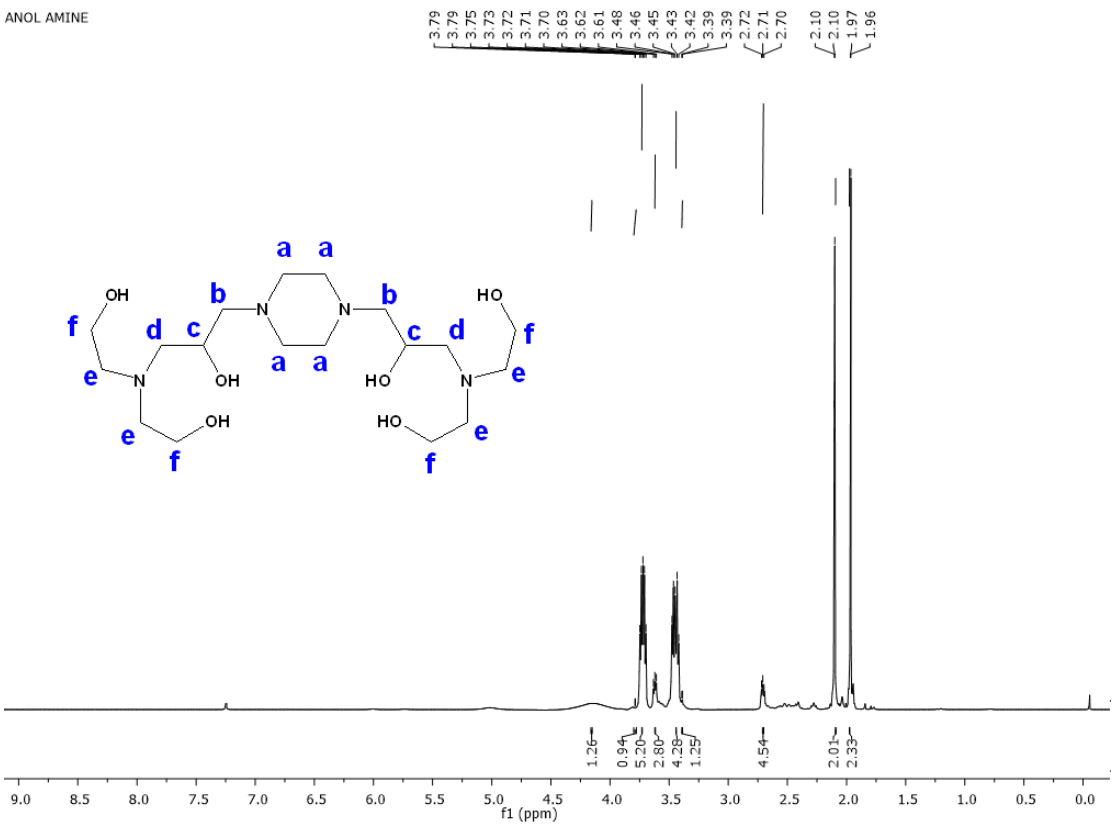

Figure 2.42: NMR Spectra of ligand H_6L11

In NMR spectra of ligandH_4L12 -OH broad peak is not visible still owing to the presence of 4 -OH group in the ligand. Protons marked as a show triplet at the 2.7 ppm. While the protons marked as b and d show doublet at the up-field value of 2.32 and 2.39 ppm. Protons marked as c show slight downfield with multiplate splitting at 3.58 ppm. The other two protons marked as e and f both show triplet at the value of 3.8 and 4.3 ppm. Proton marked as g show sharp singlet 2.9 ppm. Since there were no aromatic protons in the ligand no any peak is observed in the aromatic region (Figure 2.43).Thus, NMR spectra is also good agreement of proposed structure of ligand.

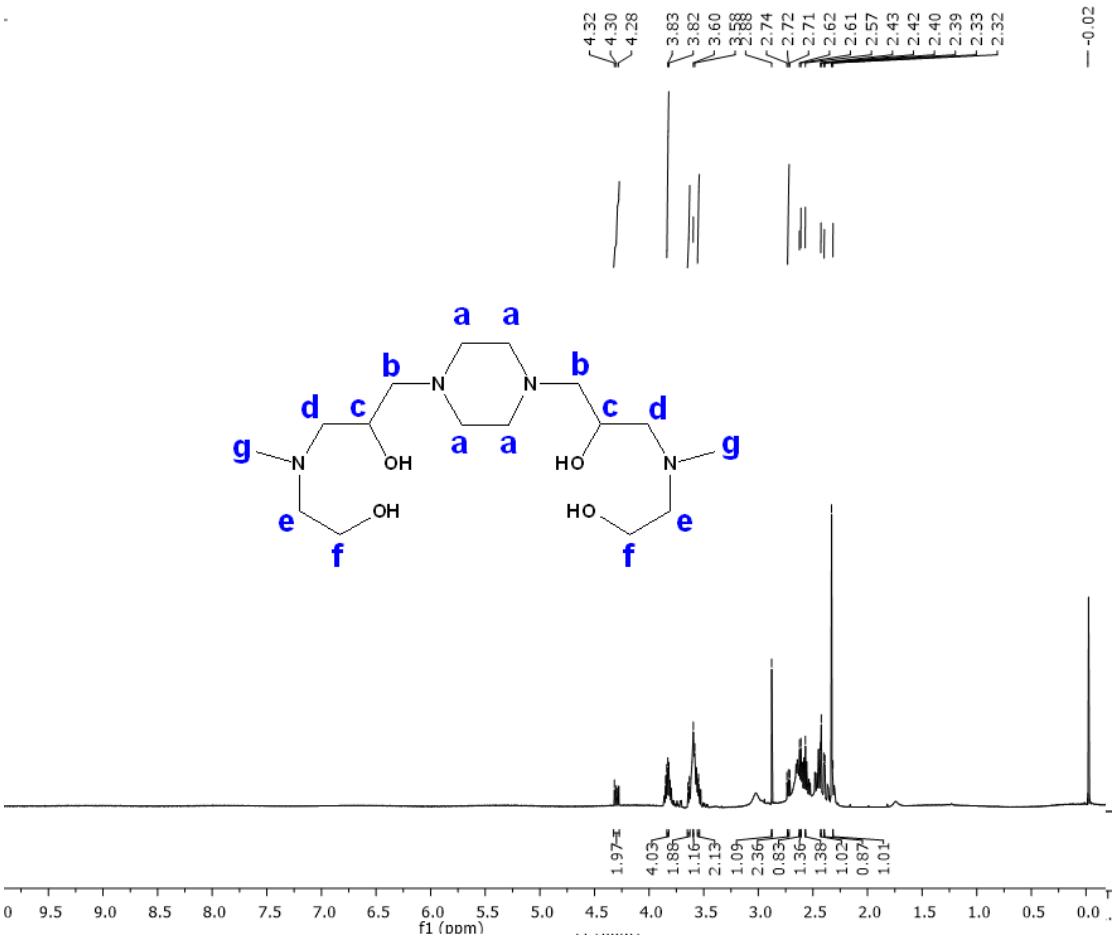

Figure 2.43: NMR Spectra of ligand H_4L12

In NMR spectra of ligandH_4L13 -OH broad peak is not visible still owing to the presence of 4 -OH group in the ligand. Protons marked as a show triplet at the 2.7 ppm. While the protons marked as b and d show doublet at the up-field value of 2.32 and 2.39 ppm. Protons marked as c show slight downfield with multiplate splitting at 2.4 ppm. The other two protons marked as e and f both show triplet at the value of 3.4 and 4.6 ppm. Proton marked as g and h show sharp quartet and triplet at up field value 1.1 and 0.9 ppm. Since there were no aromatic protons in the ligand no any peak is observed in the aromatic region (Figure 2.44).Thus, NMR spectra is also good agreement of proposed structure of ligand.

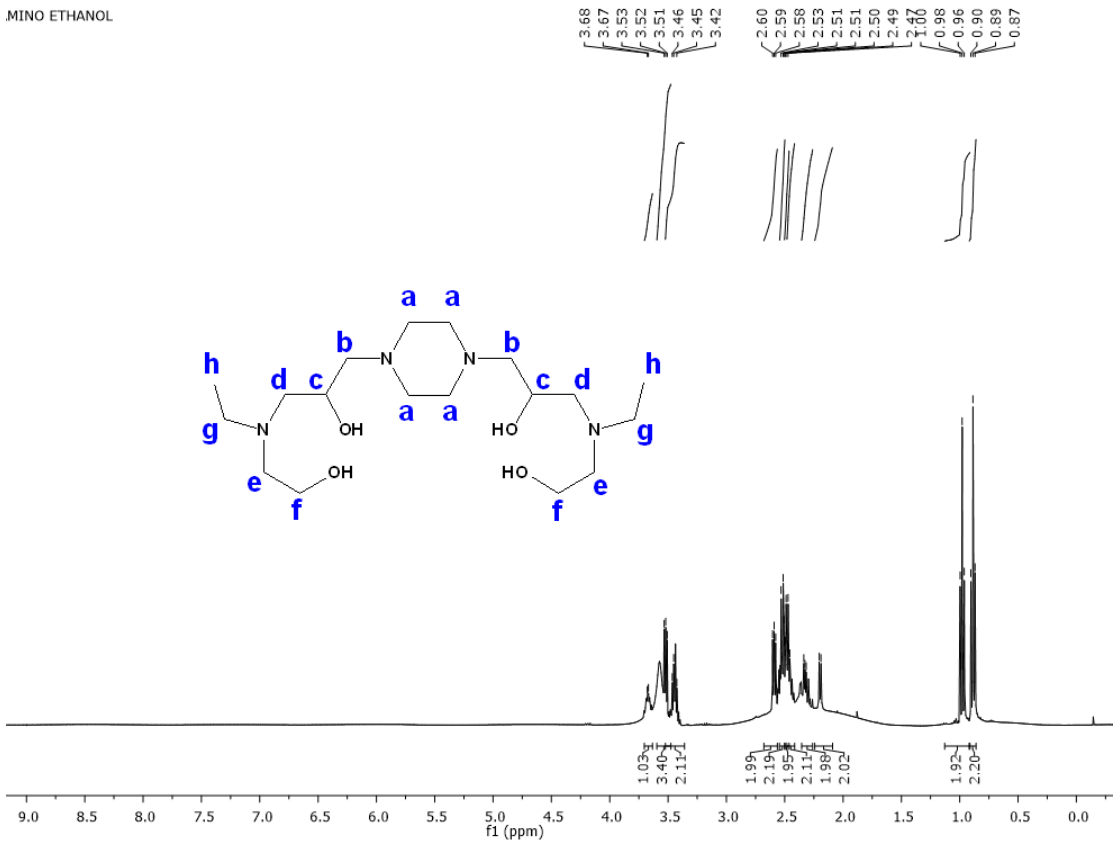

Figure 2.44: NMR Spectra of ligand H_4L13

In NMR spectra of ligandH_4L14 -OH broad peak is not visible still owing to the presence of 4 -OH group in the ligand. Protons marked as a show triplet at the 2.2 ppm. While the protons marked as b and d show doublet at the up-field value of 3.7 and 3.8 ppm. Protons marked as c show slight downfield with multiplate splitting at 3.1 ppm. The other two protons marked as e and f both show triplet at the value of 2.9 and 3.6 ppm. Proton marked as g show singlet at up field value 1.9 ppm. Since there were present aromatic protons marked as h, i and j in the ligand show peaks is observed in the aromatic region 6.9-7.3 ppm (Figure 2.45).Thus, NMR spectra is also good agreement of proposed structure of ligand.

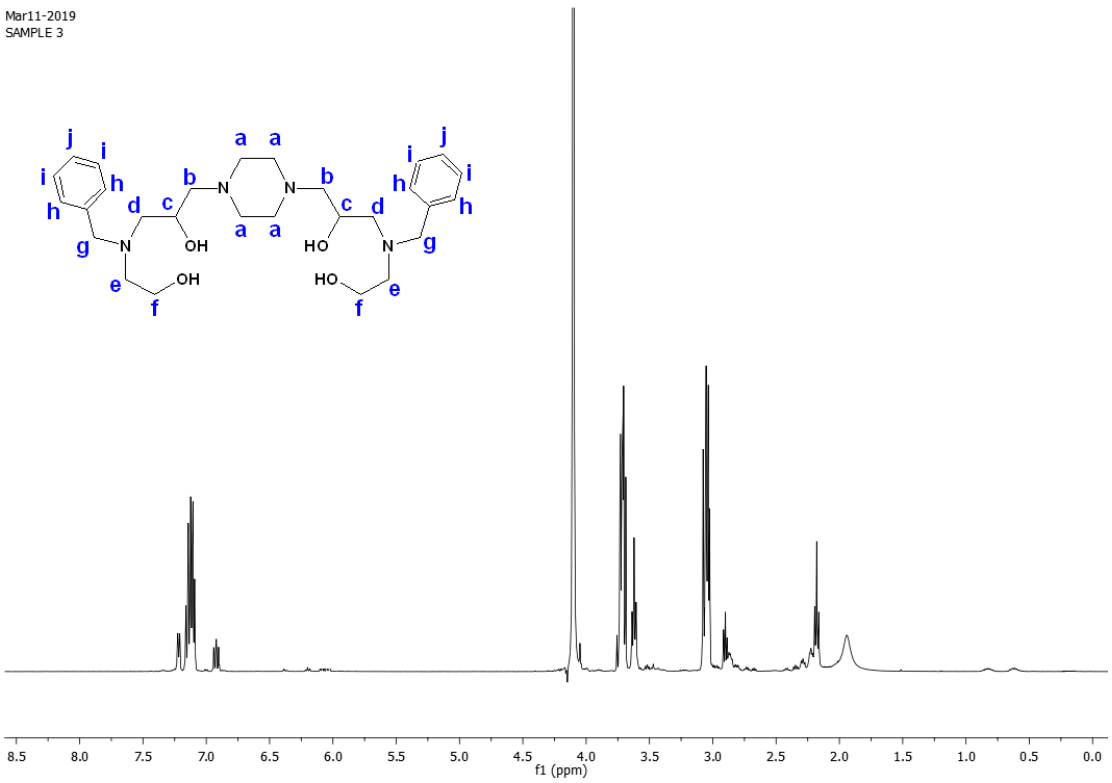

Figure 2.45: NMR Spectra of ligand H_4L14

2.3 Conclusion:

In this chapter, we described synthetic procedure and different spectroscopic characterization of ligands based on piperazine ring. Ligands were synthesized under varying conditions like use of different solvents, wide range of temperature conditions, different precursors and a range of substituted aliphatic or aromatic amine. Substitution on one nitrogen atom at the piperazine ring is brought by condensing aromatic amines with *bis*-chloroethyl amine resulting in the formation of series of ligands (HL1-HL8). Direct condensation of piperazine with chloroethanol resulted in ligand H_2L9 where as H_2L10 was obtained by ring opening rection of epoxides in which styrene oxide was reacted with piperazine resulting in the formation of ligand. In other method ring opening rection of piperazine with epichlorohydrin was carried out under ice cold condition and product thus obtained was used as precursor which was further condensed with substituted aliphatic amine resulting in the formation of four multidentate ligands H_6L11, H_4L12- H_4L14.

All ligands were characterized by spectroscopic methods *viz*. FT-IR, UV-vis, NMR and Mass spectrometry to support the proposed structure of the synthesized ligands.

UV spectroscopy identifies various electronic transitions as π→π* or n→π* or n→σ*which were significant and also absence of π→π* wavelength is ligands without aromatic ring were in good agreement. IR supports the presence of major functional group present in these ligands. Mass spectrometry evidently support the structure of these ligands in which base peak corresponds to the m/z value which is for molecular mass of these ligands in most of the cases. NMR is much sensitive technique and relates numbers of proton and their environment in the neighborhood. Further these ligands act as potential molecules for metal complexes formation which have been discussed in the next chapter.

2.4 References:

(1) Jain, V.K.; Jain B.; Sharma, U.K.; Saha, D.I. Synthesis, characterization and antimicrobial screening of some 4-substituted-1-(4-substituted phenyl) piperazine derivatives. *Int J Curr Pharm Res*. **2011**, *3* (1),66-70.

(2) Sharma, Y.R. Elementary organic spectroscopy. *S. Chand Publishing***2007**.

(3) Amir, R.M.; Muhammad, F.; Muhammad, A.; Khan, I.; Khan, M.R.; Pasha, I.; Nadeem, M. Application of Fourier transform infrared (FTIR) spectroscopy for the identification of wheat varieties. *J Food Sci Technol***2013**, *50* (5), 1018–1023.

(4) Faghihzadeh, F.; Anaya, N.M.; Schifman, L.A.; Craver, V.O. Fourier transform infrared spectroscopy to assess molecular-level changes in microorganisms exposed to nanoparticles, *Nanotechnol. Environ. Eng.***2016**, *1* (1), 1-16.

(5) Silverstein, R.M.; Bassler, G. C. Spectrometric identification of organic compounds. *Journal of Chemical Education* **1962**, *39*, 546.

(6) Mahmoud, W.H.; Deghadi, R.M.; Mohamed G.G.; Preparation, geometric structure, molecular docking thermal and spectroscopic characterization of novel Schiff base ligand and its metal chelates, *J Therm Anal Calorim***2017**, *127*, 2149–2171.

(7) Alaghaz, A.N.M. and Ammar, R.A., New dimeric cyclodiphosph (V) azane complexes of Cr (III), Co (II), Ni (II), Cu (II), and Zn (II): Preparation,

characterization and biological activity studies. *European journal of medicinal chemistry*, **2010**, *45*(4), 1314-1322.

(8) Chandra, S.; Jain, D.; Sharma, A. K. EPR, Mass, Electronic, IR Spectroscopic and Thermal Studies of Bimetallic Copper(II) Complexes with Tetradentate Ligand, 1,4-Diformyl Piperazine Bis(Carbohydrazone). *Spectrochim. Acta - Part A Mol. Biomol. Spectrosc.***2009**, *71* (5), 1712–1719.

2.5 Annexure:

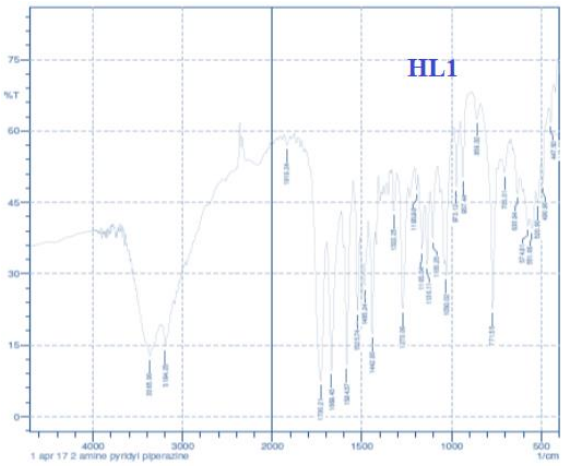

Annexure 2(a): IR spectra of HL1

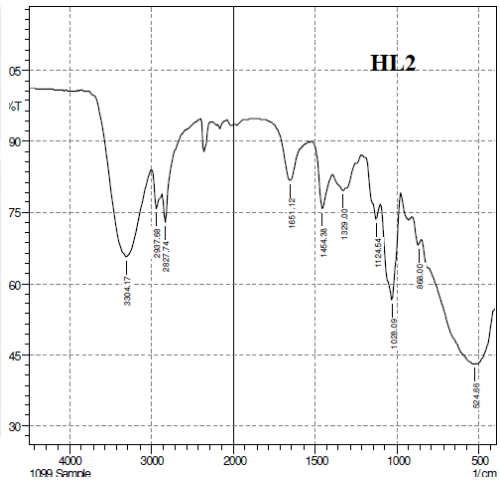

Annexure 2(b): IR spectra of HL2

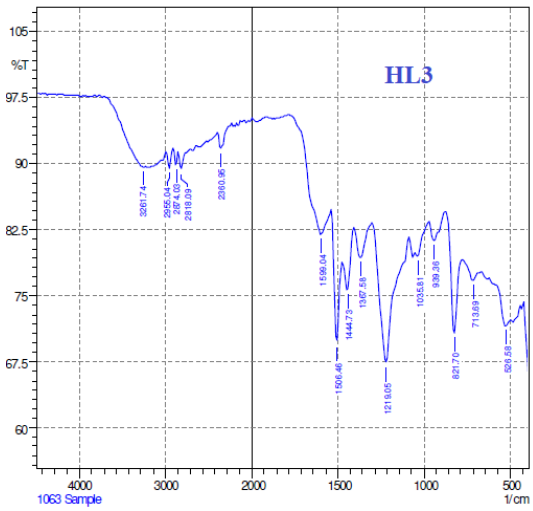

Annexure 2(c): IR spectra of HL3

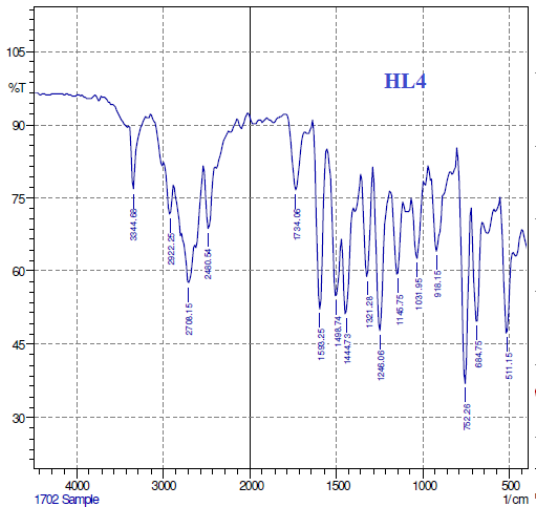

Annexure 2(d): IR spectra of HL4

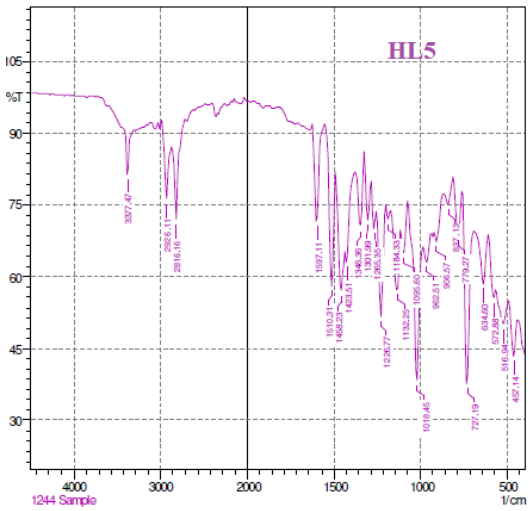

Annexure 2(e): IR spectra of HL5

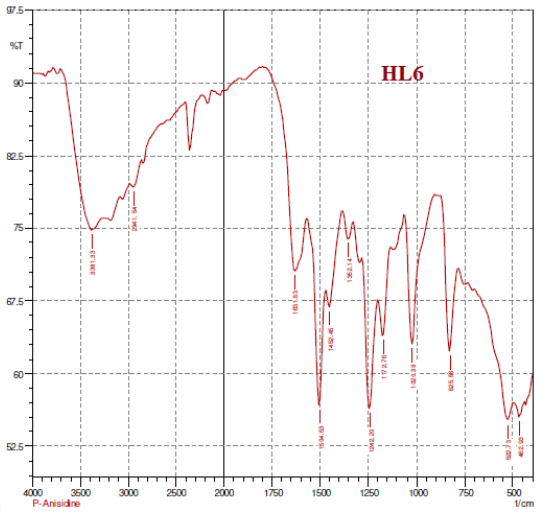

Annexure 2(f): IR spectra of HL6

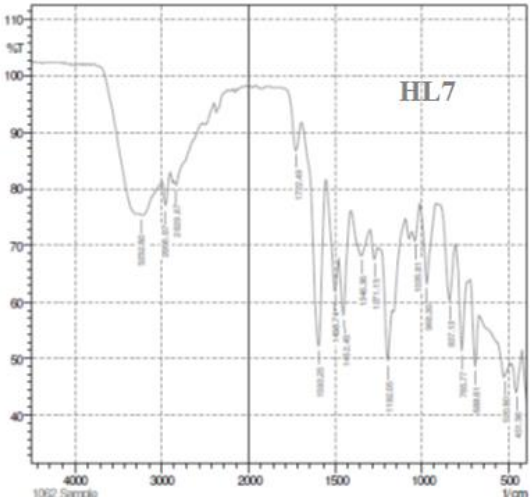

Annexure 2(g): IR spectra of HL7

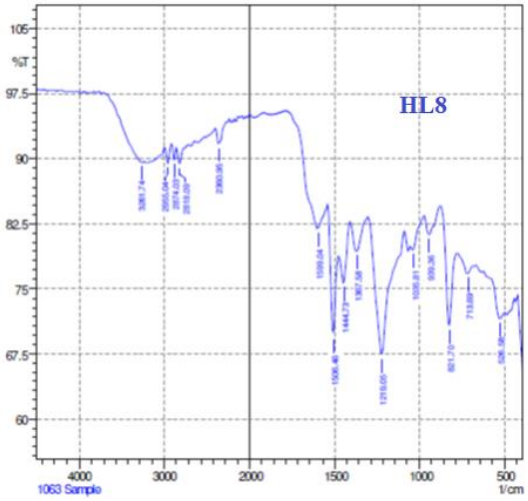

Annexure 2(h): IR spectra of HL8

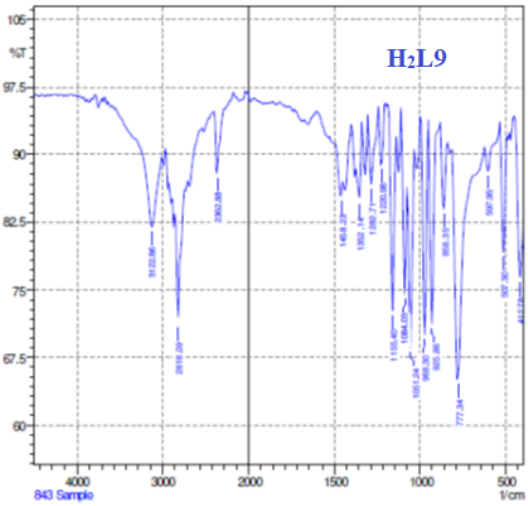

Annexure 2(i): IR spectra of H_2L9

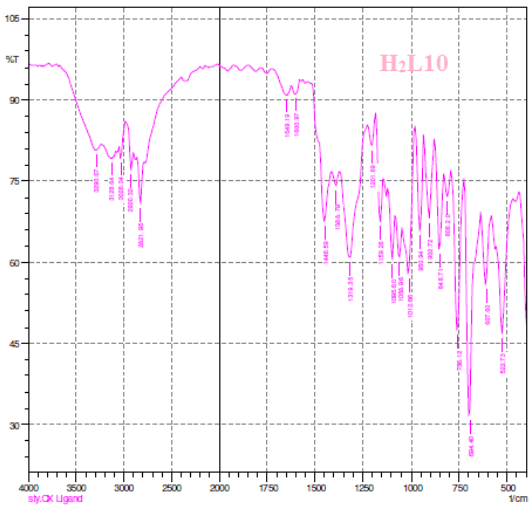

Annexure 2(j): IR spectra of H_2L10

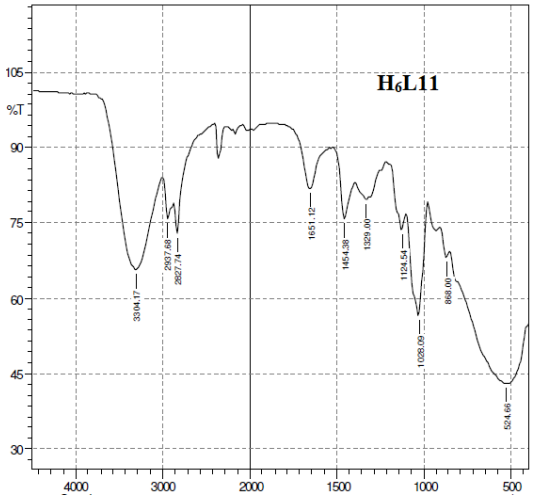

Annexure 2(k): IR spectra of H_6L11

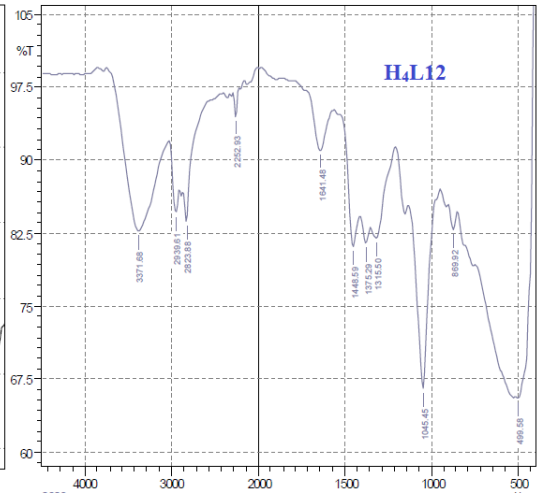

Annexure 2(l): IR spectra of H_4L12

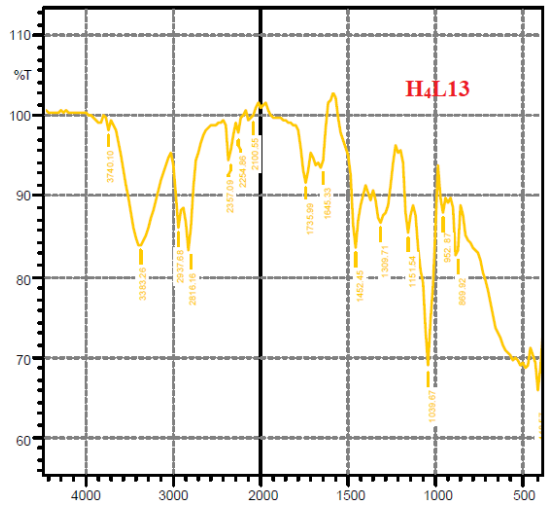

Annexure 2(m): IR spectra of H_4L13

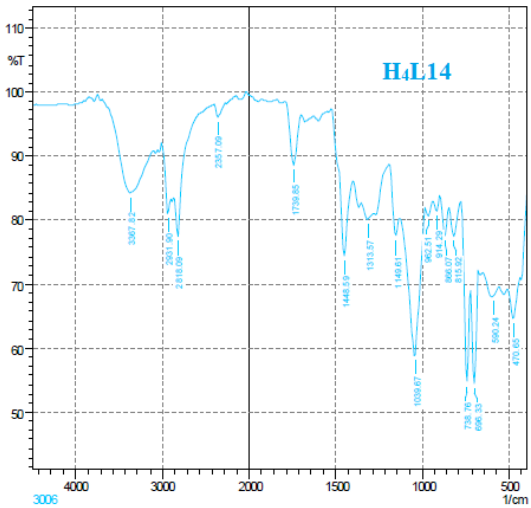

Annexure 2(n): IR spectra of H_4L14

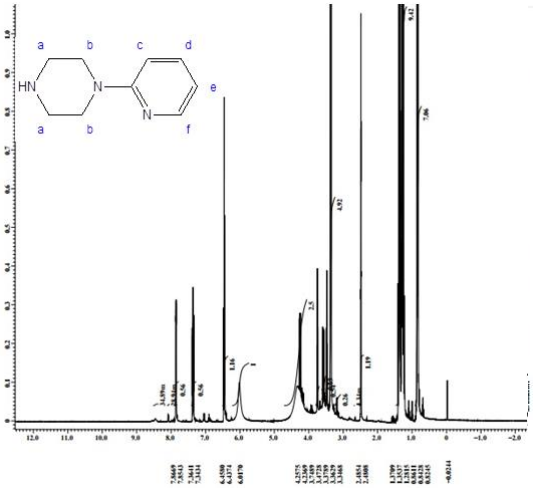

Annexure 2(o): NMR spectra of HL1

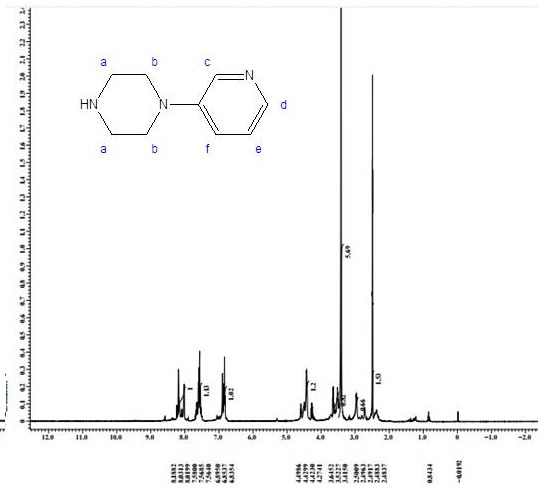

Annexure 2(p): NMR spectra of HL2

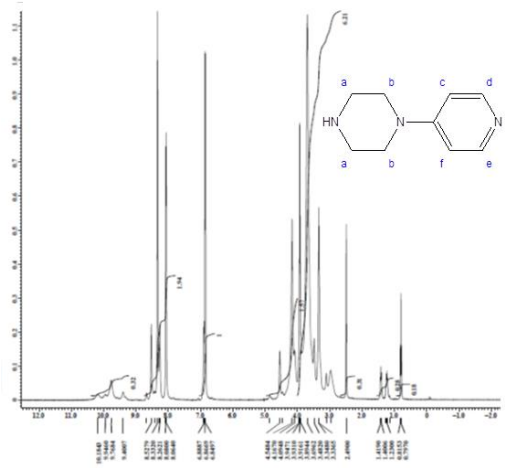

Annexure 2(q): NMR spectra of HL3

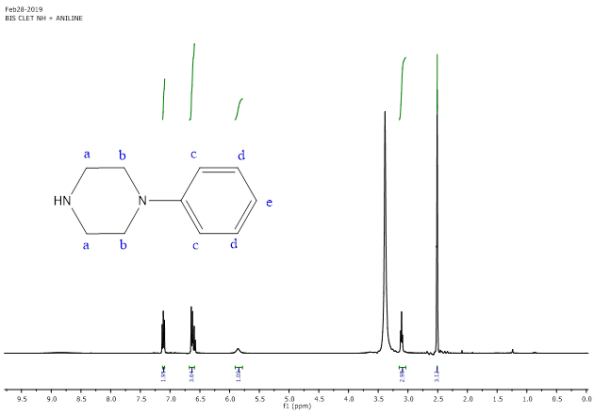

Annexure 2(r): NMR spectra of HL4

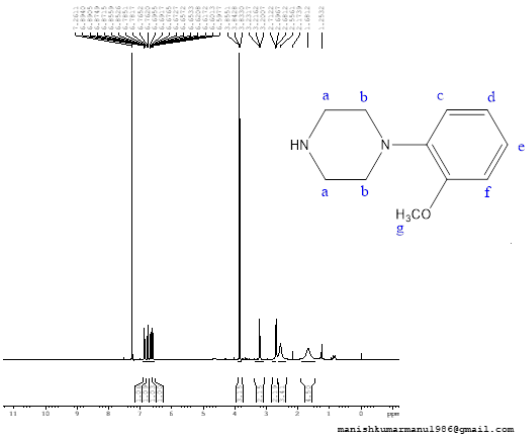

Annexure 2(s): NMR spectra of HL5

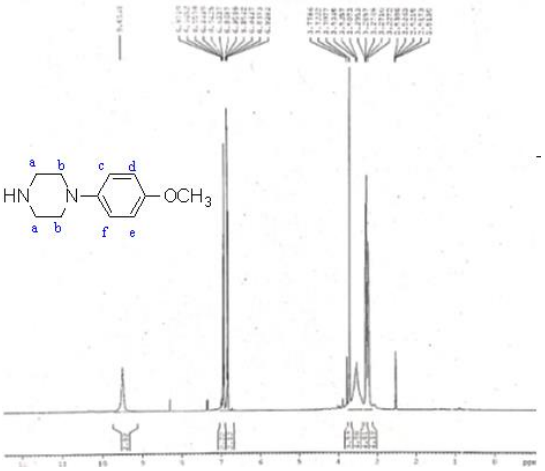

Annexure 2(t): NMR spectra of HL6

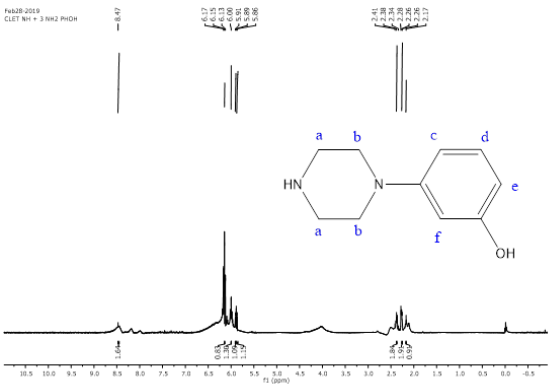

Annexure 2(u): NMR spectra of HL7

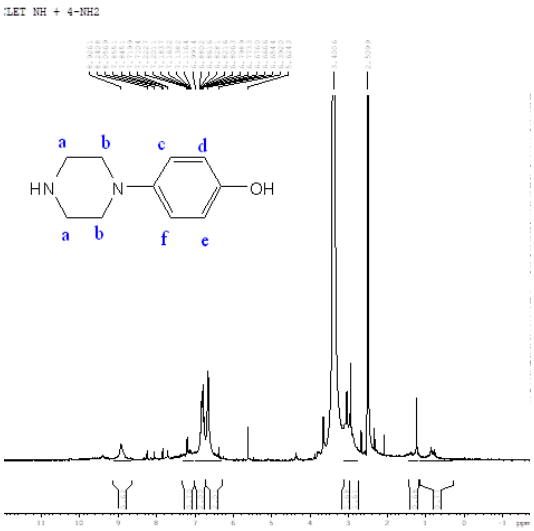

Annexure 2(v): NMR spectra of HL8

CHAPTER 3

SYNTHESIS AND CHARACTERIZATION OF TRANSITION METAL COMPLEXES OF PIPERAZINE RING BASED LIGANDS

This chapter give details of synthetic procedure of copper and cobalt metal complexes and their structures of piperazine ring-based ligands, their characterization via physical and spectroscopic measurements.

3.1 Synthesis, characterization and structure of complexes

3.1.1 Metal complex of copper with 1-(2-pyridyl)-piperazine $[Cu(L1)_2(H_2O)_2]$

0.17 g (1 mmol) of the cupric chloride dihydrate was added to a solution of 0.32 g (2 mmol) of ligand HL1 in 20 ml of methanol. The solution was then refluxed under 50-70°C for four hours and kept in a water bath to evaporate the solvent. The final product was dried in vacuum. Physical state ***hygroscopic solid***, color ***lightgreen***, m. pt. 255°C, yield 65%. **FTIR (ν in cm^{-1})** 3319 (M–OH_2 Str.), 3051 (C–H Str.), 1657 (C=C Str.), 1299 (C–N Str.), 489 (Cu–N Vib.) **UV-vis (λ, nm)** 208, 233, 302 **Mass(m/z)** 424, 327, 254, 208, 164.

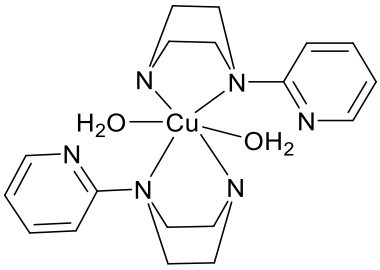

Figure 3.1: Proposed structure of complex as $[Cu(L1)_2(H_2O)_2]$

3.1.2 Metal complex of copper with 1-(3-pyridyl)-piperazine $[Cu(L2)Cl(H_2O)_2(CH_3OH)].2CH_3OH$

CuL2 was synthesized by similar procedure as reported for CuL1. Physical state ***semi solid***, color ***dark brown***,m. pt. 245°C, yield 68%. **FTIR (ν in cm^{-1})** 3344 (M–OH_2 Str.), 2922 (C–H Str.), 1627 (C=C Str.), 1340 (C–N Str.), 474 (Cu–N Vib.) **UV-vis (λ, nm)** 258, 334 **Mass(m/z)** 390, 327, 258, 226, 200, 164.

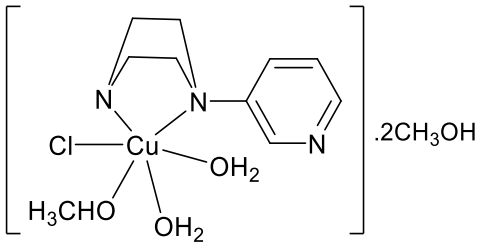

Figure 3.2: Proposed structure of complex as $[Cu(L2)Cl(H_2O)_2(CH_3OH)].2CH_3OH$

3.1.3 Metal complex of copper with 1-(4-pyridyl)-piperazine $[Cu(L3)Cl(H_2O)(CH_3OH)_2].3H_2O$

CuL3 was synthesized by similar procedure as reported for CuL1.Physical state ***semi solid***, color ***light green***,m. pt. 250°C, yield 78%. **FTIR (ν in cm^{-1})** 3402 (M–OH_2 Str.), 2922 (C–H Str.), 1631 (C=C Str.), 1260 (C–N Str.), (Cu–N Vib.) **UV-vis (λ, nm)** 209, 269 **Mass (m/z)** 396, 327, 295, 258, 164.

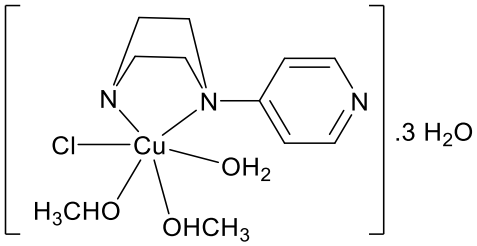

Figure 3.3: Proposed structure of complex as $[Cu(L3)Cl(H_2O)(CH_3OH)_2].3H_2O$

3.1.4 Metal complex of copper with 1-(phenyl)-piperazine $[CuL4(CH_3OH)(NO_3)(H_2O)_2]$

In the 20 ml of methanol 0.16 g (1 mmol) of the cupric nitrate trihydrate and 0.12 g (0.5 mmol) of ligand HL4 were added. The solution mixture was then refluxed for three hours and was kept in a water bath to evaporate the solvent. The final product was dried in vacuum. Physical state ***solid***, color ***light green***,m. pt. 258°C, yield 60%. **FTIR (ν in cm^{-1})** 3344 (M–OH_2 Str.), 2922 (C–H Str.), 1631 (C=C Str.), 1269 (C–N Str.), 497 (Cu–N Vib.) **UV-vis (λ, nm)** 222, 307, 384 **Mass (m/z)** 356, 318, 294, 256, 163.

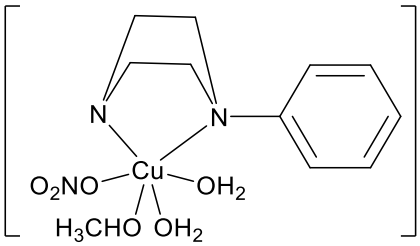

Figure 3.4: Proposed structure of complex as $[CuL4(CH_3OH)(NO_3)(H_2O)_2]$

3.1.5 Metal complex of copper with 1-(2-methoxy phenyl)-piperazine $[Cu(L5)_2(H_2O)_2].2H_2O$

CuL5 was synthesized by similar procedure as reported for CuL4 using 2 mmol (0.38 g) of o-anisidine and 1 mmol (0.17 g) of cupric chloride dihydrate. Physical state ***solid***, color ***light blue***,m. pt. 275°C, yield 60%. **FTIR (ν in cm^{-1})** 3383 (M–OH_2 Str.), 2935 (C–H Str.), 1508 (C=C Str.), 1242 (C–N Str.), 422 (Cu–N Vib.) **UV-vis (λ, nm)** 222, 275 **Mass (m/z)** 518, 453, 438, 395, 338, 292.

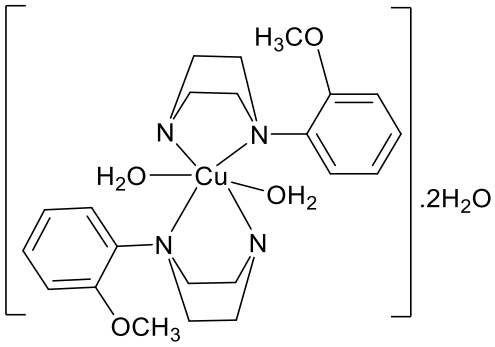

Figure 3.5: Proposed structure of complex as $[Cu(L5)_2(H_2O)_2].2H_2O$

3.1.6 Metal complex of copper with 1-(4-methoxy phenyl)-piperazine $[Cu(L6)(H_2O)(Cl)(CH_3OH)_2].4H_2O$

CuL6 was synthesized by similar procedure as reported for CuL4 using 2 mmol (0.38 g) of p-anisidine and 1 mmol (0.17 g) of cupric chloride dihydrate. Physical state ***solid***, color ***light green***,m. pt. 265°C, yield 60% **FTIR (ν in cm^{-1})** 3327 (M–OH_2 Str.), 3163 (C–H Str.), 1506 (C=C Str.), 1249 (C–N Str.), 470 (Cu–N Vib.) **UV-vis (λ, nm)** 269, 392 **Mass (m/z)** 443, 390, 354, 177.

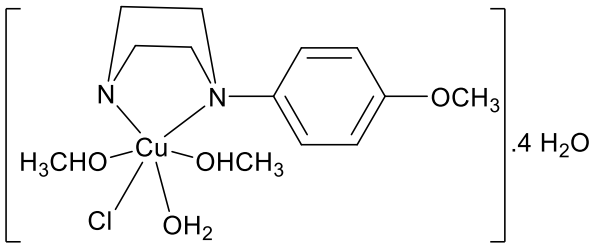

Figure 3.6: Proposed structure of complex as $[Cu(L6)(H_2O)Cl(CH_3OH)_2].4H_2O$

3.1.7 Metal complex of copper with 1-(3-hydroxyphenyl)-piperazine $[Cu(L7)(H_2O)(Cl)(CH_3OH)_2]$

CuL7 was synthesized by similar procedure as reported for CuL4using 2 mmol (0.33 g) of m-aminophenol and 1 mmol (0.17 g) of cupric chloride dihydrate. Physical state

solid, color ***dark green***,m. pt. 280°C, yield 60% **FTIR (ν in cm^{-1})**3344 (M–OH_2 Str.), 3138 (C–H Str.), 1609 (C=C Str.), 1278 (C–N Str.), 488 (Cu–N Vib.) **UV-vis (λ, nm)** 213, 246, 285 **Mass (m/z)** 343, 274, 213, 163.

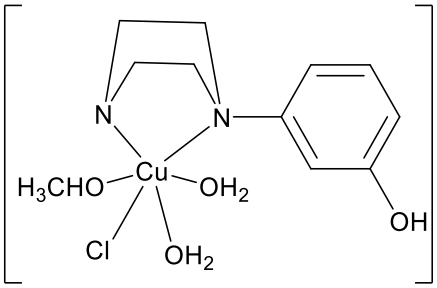

Figure 3.7: Proposed structure of complex as [Cu(L7)(H_2O)(Cl)(CH_3OH)$_2$]

3.1.8 Metal complex of copper with 1-(4-hydroxyphenyl)-piperazine[Cu(L8)(H_2O)$_2$(CH_3OH)(Cl)]

CuL8 was synthesized by similar procedure as reported for CuL4 using 2 mmol (0.33 g) of p-aminophenol and 1 mmol (0.17 g) of cupric chloride dihydrate. Physical state ***solid***, color ***dark green***,m. pt. 275°C, yield 60% **FTIR (ν in cm^{-1})** 3333 (M–OH_2 Str.), 3130 (C–H Str.), 1603 (C=C Str.), 1250 (C–N Str.), 438 (Cu–N Vib.) **UV-vis (λ, nm)** 223, 285, 363 **Mass(m/z)** 357, 339, 274, 247, 185, 213.

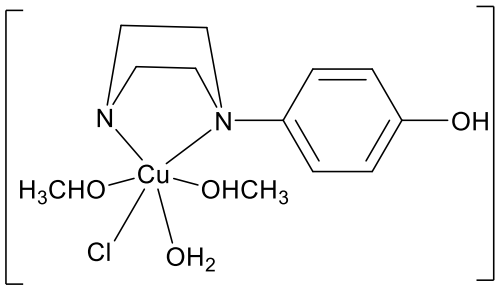

Figure 3.8: Proposed structure of complex as [Cu(L8)(H_2O)$_2$(CH_3OH)(Cl)]

3.1.9 Metal complex of cobalt with 1,4-bisethanol piperazine [CoL9(H_2O)$_2$]

0.174 g (1 mmol) of ligand was added to 0.238 g(1 mmol) cobalt chloride hexahydrate in 20ml of methanol. The solution was then refluxed under 50-70°C for four hours. The reaction mixture was filtered and filtrate was kept for 2-3 days. A bluish white colored precipitate was obtained which was filtered, washed with methanol and dried. Physical state ***solid***, color***bluish white***,m. pt. 225°C, yield 60%

FTIR (ν in cm^{-1}) 3138 (M–OH_2 Str.), 1329 (C–N Str.), 497 (Cu–N Vib.), 437 (Cu–O Vib.) **UV-vis (λ, nm)** 213.**Mass** (m/z) 268, 232, 175, 146, 139.

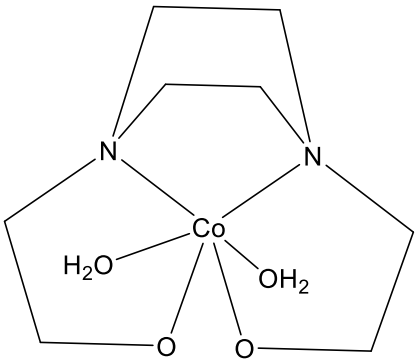

Figure 3.9: Proposed structure of complex as [CoL9(H_2O)$_2$]

3.1.10 Metal complex of copper with bis(1-phenylethan-1-ol)piperazine [Co_2(L10)(CH_3OH)$_4$(Cl)$_2$(H_2O)$_2$]

0.326 g (1 mmol) of ligand was added to 0.482g (2 mmol) cobalt chloride hexahydrate in 20ml of methanol. The solution was then refluxed under 50-70°C for four hours. The reaction mixture was filtered and filtrate was kept for 2-3 days. A light blue colored precipitate was obtained which was filtered, washed with methanol and dried. Physical state ***solid***, color ***light blue***,m. pt. 270°C, yield 60% **FTIR (ν in cm^{-1})** 3281 (M–OH_2 Str.), 3034 (C–H Str.), 1643 (C=C Str.), 1300 (C–N Str.), 509 (Cu–N Vib.), 432 (Cu–O Vib.) **UV-vis (λ, nm)** 215, 255 **Mass (m/z)** 687, 567,447, 415, 327, 309.

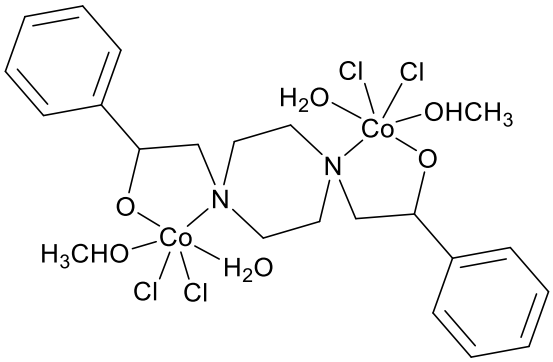

Figure: 3.10: Proposed structure of complex as [Co_2(L10)(CH_3OH)$_4$(Cl)$_2$(H_2O)$_2$]

3.1.11 Metal complex of copper with bis(1-phenylethan-1-ol)piperazine $[Cu_2(L10)(CH_3CN)Cl_2(H_2O)_5]$

0.326 g (1 mmol) of ligand was added to 0.348g (2 mmol) cupric chloride dihydrate in 20ml of acetonitrile. The solution was then refluxed under 50-70°C for four hours. The reaction mixture was cooled down. A yellow-colored precipitates appeared which were filtered, washed with acetonitrile and dried. Physical state ***solid***, color ***yellow***,m. pt. 260°C, yield 60% **FTIR (ν in cm^{-1})** 3321 (M–OH_2 Str.), 3034 (C–H Str.), 1550 (C=C Str.), 1327 (C–N Str.), 520 (Cu–N Vib.), 405 (Cu–O Vib.) **UV-vis (λ, nm)** 216, 231 and 256 **Mass (m/z)** 327, 262, 253, 220, 207, 189.

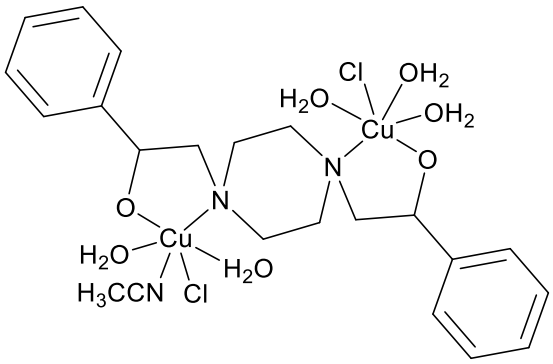

Figure: 3.11: Proposed structure of complex as $[Cu_2(L10)(CH_3CN)Cl_2(H_2O)_5]$

3.1.12 Metal complex of copper with bis(1-phenylethan-1-ol)piperazine $[Zn_2(L10)Cl_2(H_2O)_4(CH_3CN)_2]$

0.326 g (1 mmol) of ligand was added to 0.482g (2 mmol) hydrated zinc chloride in 20ml of acetonitrile. The solution was then refluxed under 50-70°C for four hours. The reaction mixture was filtered and filtrate was kept for 2-3 days. A white colored precipitate was obtained which was filtered, washed with acetonitrile and dried. Physical state ***solid***, color ***white***,m. pt. 280°C, yield 60%. **FTIR (ν in cm^{-1})** 3448 (M–OH_2 Str.), 3034 (C–H Str.), 1454 (C=C Str.), 1043 (C–N Str.), 464 (Cu–N Vib.), 430 (Cu–O Vib.) **UV-vis (λ, nm)** 210, 256 **Mass (m/z)** 679, 473, 453, 327, 309, 291.

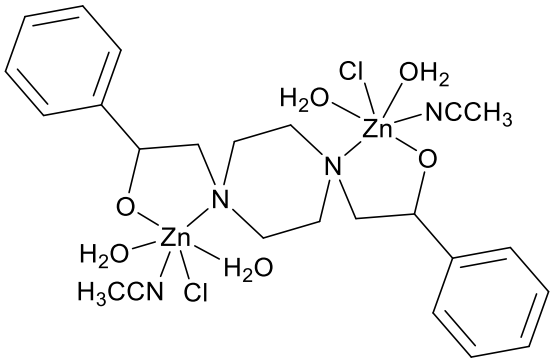

Figure: 3.12: Proposed structure of complex as $[Zn_2(L10)Cl_2(H_2O)_4(CH_3CN)_2]$

3.1.13 Metal complex of Copper with of H_3L11 $[Cu_3(L11)(H_2O)_3(CH_3OH)]CH_3OH$

In the 20 ml of methanol 0.408g (1 mmol) of ligand and 0.724g (1.5 mmol) cupric chloride dihydrate was added. The above mixture was then refluxed for 4 hours. A dark green color precipitate appeared in the end of rection. The precipitates were then filtered, washed with methanol and dried. Physical state ***solid***, color***dark green***, yield 52%. **FTIR (ν in cm^{-1})** 3336 ($M–OH_2$ Str.), 3034 (CH Str.), 1247 (C–N Str.), 453 (Cu–N Vib.), 420 (Cu–O Vib.) **UV-vis (λ, nm)** 215, 257 **Mass (m/z)** 712, 680, 626, 599, 538, 451, 409.

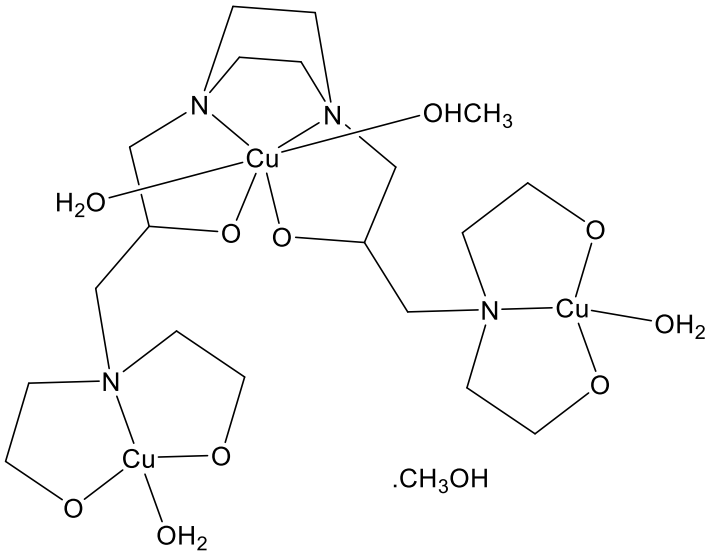

Figure: 3.13: Proposed structure of complex as $[Cu_3(L11)(H_2O)_3(CH_3OH)].CH_3OH$

3.1.14 Metal complex of copper with H_2L12 $[Cu_2(L12)(H_2O)_2]$

In the 20 ml of methanol 0.174g (0.5 mmol) of ligand and 0.255g (1.5 mmol) cupric chloride dihydrate was added. The above mixture was then refluxed for 4 hours. A green color precipitate appeared in the end of rection. The precipitates were then filtered, washed with methanol and dried.Physical state ***solid***, color ***light green***,m. pt. 280°C, yield 62%, **FTIR (ν in cm^{-1})** 3329 (M–OH_2 Str.), 2920 (C–H Str.), 1240 (C–N Str.), 449 (Cu–N Vib.), 405 (Cu–O Vib.) **UV-vis (λ, nm)** 300 **Mass (m/z)** 509, 491, 453, 410, 349.

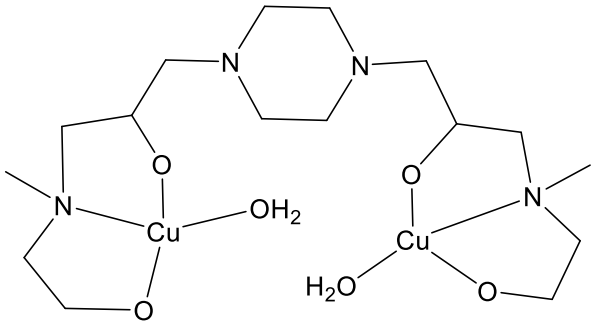

Figure 3.14: Proposed structure of complex as [Cu_2(L12)(H_2O)$_2$]

3.1.15 Metal complex of copper with H_2L13 [Cu_2(L13)(H_2O)$_2$]

In the 20 ml of methanol 0.163g (0.5 mmol) of ligand and 0.255g (1.5 mmol) cupric chloride dihydrate was added. The above mixture was then refluxed for 4 hours. A light-green color precipitate appeared in the end of rection. The precipitates were then filtered, washed with methanol and dried. Physical state ***solid***, color ***light green***,m. pt. 285°C, yield 70%, **FTIR (ν in cm^{-1})** 3340 (M–OH_2 Str.), 2979 (CH Str.), 1248 (C–N Str.), 488 (Cu–N Vib.), 415 (Cu–O Vib.) **UV-vis (λ, nm)** 268 **Mass (m/z)** 537, 499, 438, 377.

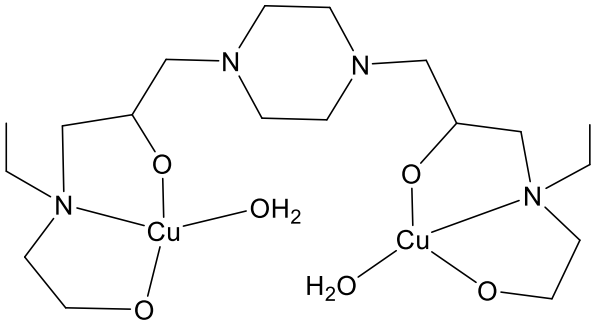

Figure: 3.15 Proposed structure of complex as [Cu_2(L13)(H_2O)$_2$]

3.1.16 Metal complex of copper with H_2L14 [$Cu_2(L14)(H_2O)_2$]

In the 20 ml of methanol 0.250g (0.5 mmol) of ligand and 0.255g (1.5 mmol) cupric chloride dihydrate was added. The above mixture was then refluxed for 4 hours. A light-yellow color precipitate appeared in the end of rection. The precipitates were then filtered, washed with methanol and dried. Physical state ***solid***, color ***yellow***,m. pt. 280°C, yield 82%, **FTIR (ν in cm^{-1})** 3160 (M–OH_2 Str.), 2936 (C–H Str.), 1247 (C–N Str.), 405 (Cu–O Vib.) 451 (Cu–N Vib.) **UV-vis (λ, nm)** 268 **Mass (m/z)** 661, 625, 562, 545, 501.

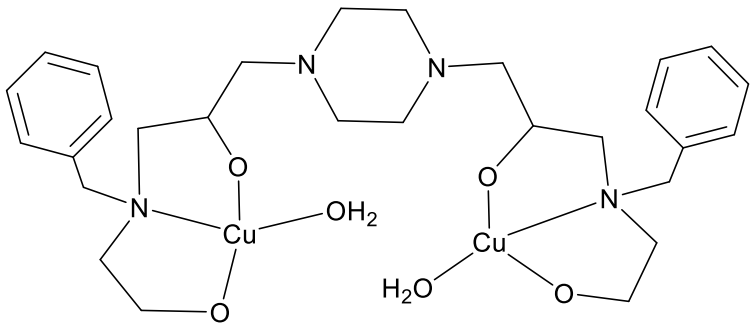

Figure: 3.16 Proposed structure of complex as [$Cu_2(L14)(H_2O)_2$]

3.2 Result and Discussion

These above metal complexes were synthesized by reacting the metal salt with the ligand in the definite stoichiometric amount in methanol/acetonitrile solvent and refluxed under 40-60°C for 3-4 hours. Resulting complexes were dried and characterised. Employing different solvents and different metal salts, resulted in the different coordination environment around the metal ion. Ligands behave bidentate (HL1-H_2L10) and polydentate (H_6L11-H_4L14) owing the presence of N and O as donor atoms.

3.2.1 UV-vis analysis:

From the UV-vis analysis binding of metal with the ligands was observed due to significant shift in the intensity (generally hyperchromic shift) as well as wavelength (bathochromic shift) from that of ligands absorption wavelength (Table 3.1).

Table 3.1: Observed maximum wavelength with molar extinction coefficient for complexes

Sr. No.	Structural Formula	Wavelength (λ_{max}, nm)	Molar Extinction Coefficient (ε, $Lmol^{-1}cm^{-1}$)
CuL1	$[Cu(L1)_2(H_2O)_2]$	208, 233, 302	2.14×10^3, 0.65×10^3, 0.33×10^3
CuL2	$[Cu(L2)Cl(H_2O)_2(CH_3OH)].2CH_3OH$	258, 334	1.87×10^3, 0.55×10^3
CuL3	$[Cu(L3)Cl(H_2O)(CH_3OH)_2].3H_2O$	209, 269	177×10^3, 0.44×10^3
CuL4	$[CuL4(CH_3OH)(NO_3)(H_2O)_2]$	222, 307, 384	2.65×10^3, 1.47×10^3, 0.78×10^3
CuL5	$[Cu(L5)_2(H_2O)_2].2H_2O$	275, 222	1.48×10^3, 3.09×10^3
CuL6	$[Cu(L6)(H_2O)(Cl)(CH_3OH)_2].4H_2O$	392, 269	1.12×10^3, 3.70×10^3
CuL7	$[Cu(L7)(H_2O)(Cl)(CH_3OH)_2]$	213,285, 246	2.78×10^3,0.90×10^3, 1.55×10^3
CuL8	$[Cu(L8)(H_2O)_2(CH_3OH)(Cl)]$	285, 223, 363	3.02×10^3,1.28×10^3,0.64×10^3
CoL9	$[CoL9(H_2O)_2]$	212, 254	1.98×10^3, 0.40×10^3
Co_2L10	$[Co_2(L10)(CH_3OH)_4(Cl)_2(H_2O)_2]$	215, 255	2.27×10^3, 0.50×10^3
Cu_2L10	$[Cu_2(L10)(CH_3CN)Cl_2(H_2O)_5]$	216, 231, 256	2.28×10^3, 1.01×10^3,0.96×10^3
Zn_2L10	$[Zn_2(L10)Cl_2(H_2O)_4(CH_3CN)_2]$	210, 256	1.77×10^3, 0.28×10^3
Cu_3L11	$[Cu_3(L11)(H_2O)_3CH_3OH].CH_3OH$	-	-
Cu_2L12	$[Cu_2(L12)(H_2O)_2]$	212, 264	3.12×10^3, 1.49×10^3
Cu_2L13	$[Cu_2(L13)(H_2O)_2]$	212, 268	2.14×10^3, 1.04×10^3
Cu_2L14	$[Cu_2(L14)(H_2O)_2]$	217, 265	0.99×10^3, 2.76×10^3

In case of copper complex of ligand HL1, CuL1 have three absorptions maximum in the UV spectra as compared to ligand. Also, the decrease in the intensity indicates the binding of metal with ligands. Low intensity peak at 302 nm arises due to LMCT transition from ligand to metal ion. Similar spectral changes were also observed in CuL2 and CuL3 as compared to HL2 and HL3 but no additional peaks were observed. A clear shift in the peaks was observed and increase and decrease in the intensity of the peaks which were significant in explaining the metal binding to the ligand (Figure 3.17-3.19).

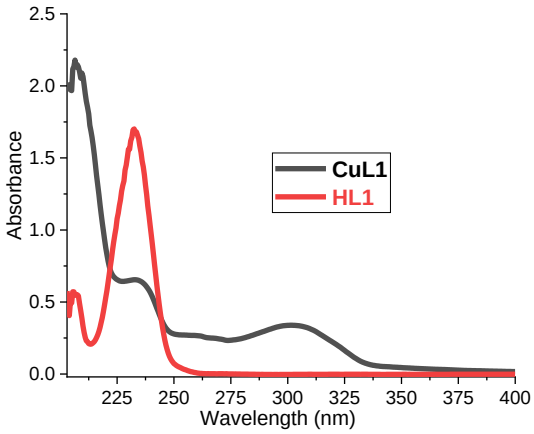

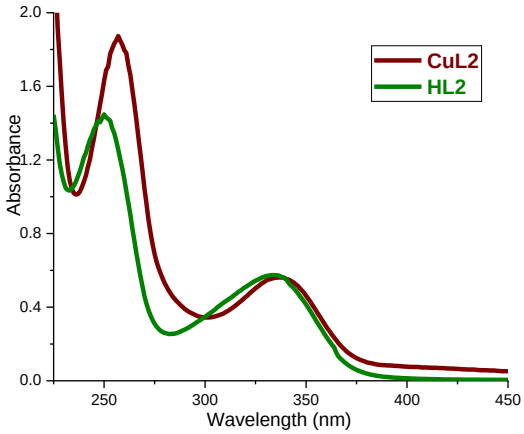

Figure 3.17: Compared UV graph of CuL1 and HL1 Figure 3.18: Compared UV graph of CuL2 and HL2

In case of CuL4, there are three absorption peaks out of which two were similar to ligand HL4 with slight shift in wavelength and intensity, while the third peak at 385 with low intensity might correspond to LMCT transition of metal complex (Figure 3.20). Thus, compared UV graph clearly indicate binding of metal ion with the ligand.

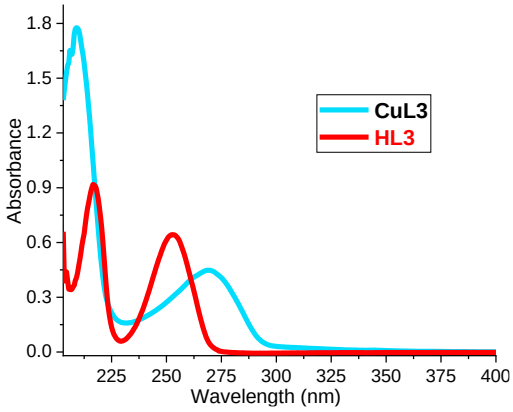

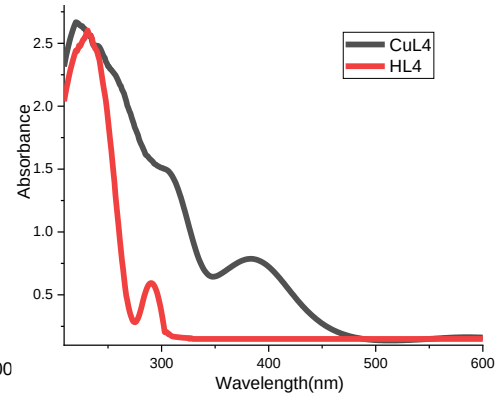

Figure 3.19: Compared UV graph of CuL3 and HL3 Figure 3.20: Compared UV graph of CuL4 and HL4

In case of complex CuL5 and CuL6, all the observed peaks in the complexes appeared with slight shift in the wavelength indicate binding of metal ion with the ligands (Figure 3.21-3.22).

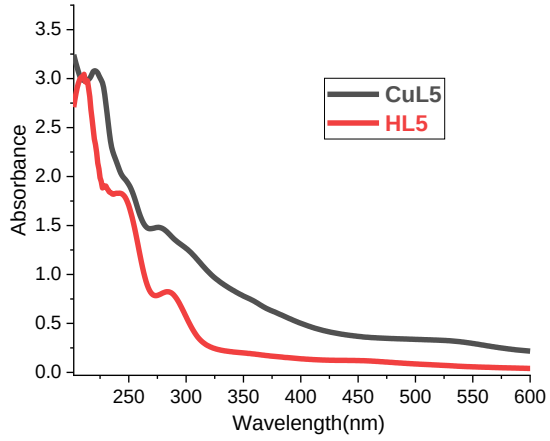

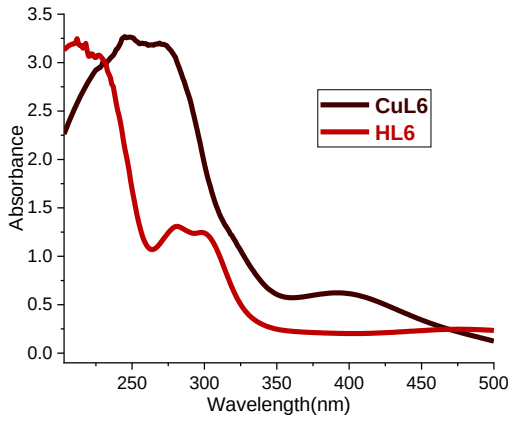

Figure 3.21: Compared UV graph of CuL5 and HL5 Figure 3.22: Compared UV graph of CuL6 and HL6

In the complexes CuL7 and CuL8, compared UV graph were also helpful to see the changes in the shift in the wavelength and intensities of the absorption of maxima (Figure 3.23-3.24).

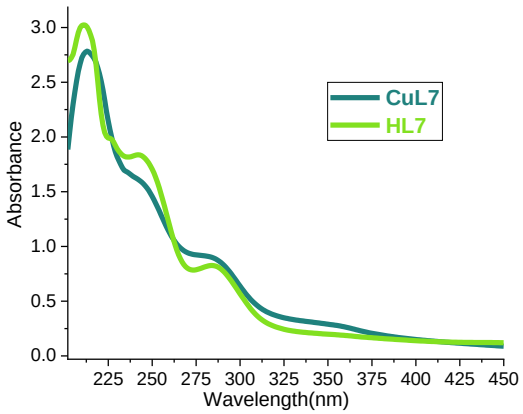

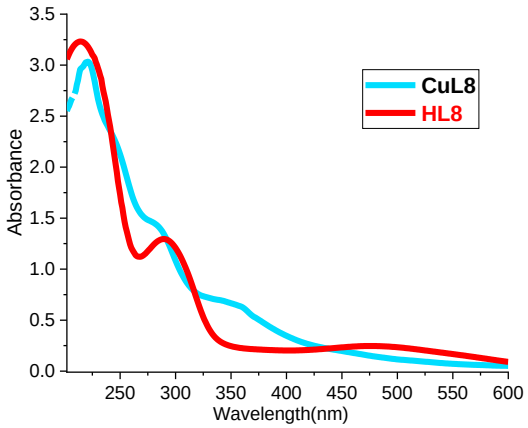

Figure 3.23: Compared UV graph of CuL7 and HL7 Figure 3.24: Compared UV graph of CuL8 and HL8

The concept of comparing two UV graph was further applied of other ligands and their complexes and quite significant inference can be drawn from the absorption pattern as indicated below (Figure 3.25-3.28).

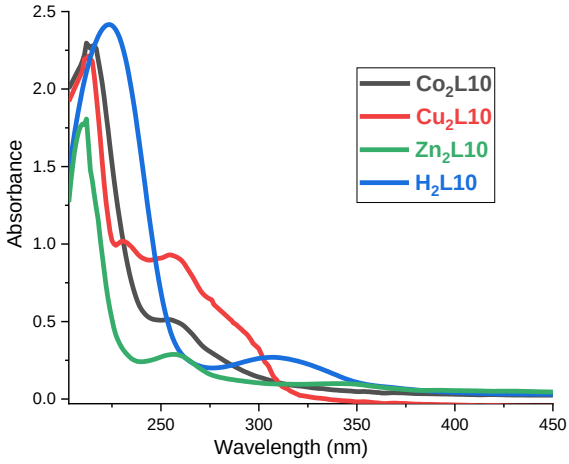

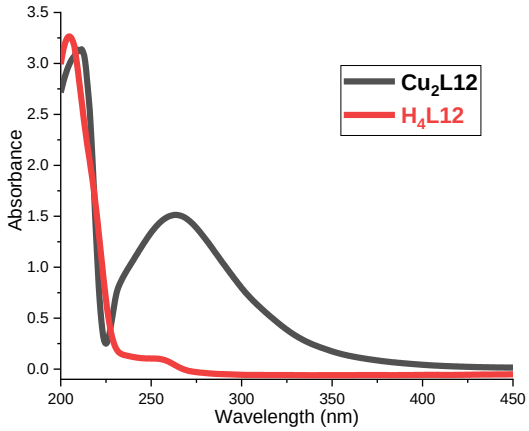

Figure 3.25: Compared UV graph of Co_2L10, Cu_2L10 and H_2L10 Figure 3.26: Compared UV graph of Cu_2L12 and H_4L12

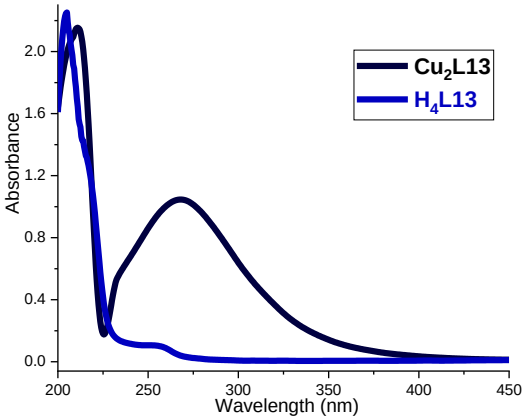

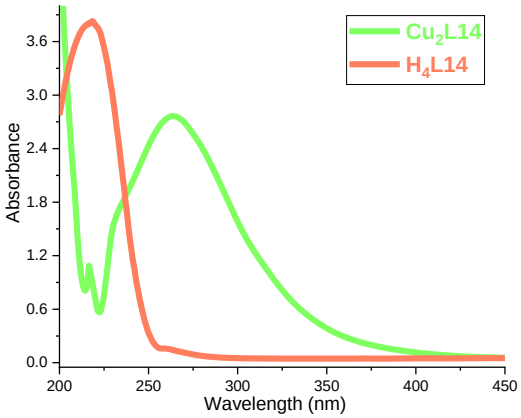

Figure 3.27: Compared UV graph of complex Cu_2L13 and H_4L13 Figure 3.28: Compared UV graph of complex Cu_2L14 and H_4L14

3.2.2 FTIR analysis:

In the non-availability of single crystal X ray data, FTIR data becomesimportant in the interpretation of binding of complex with the ligands.[1,2] Since ligands coordinated with metal, M–N and M–O peaks are important to observe in the IR spectra of metal complexes. All the complexes showed absorption peaks in the region 422 - 520 cm^{-1} corresponding to M–N type of vibrations which confirm the binding of piperazine nitrogen with metal ion. Also, the M–O type of vibration was observed in the region of 405 – 437 cm^{-1} for the complexes which involve hydroxy group binding to metal ion. Absorption bands at 3100 - 3400 cm^{-1} range in complexes indicated the presence of lattice or coordinated water. FTIR analysis with selected bond frequencies of all complexes are as described in the table 3.2.

Table 3.2: Selected frequencies (cm^{-1})of metal complexes

Complex Code	Structure	ν M–OH_2	ν M–O	ν M–N	ν C=C(Ar)	ν C–N	ν C–H (Ar/sp^3)
CuL1	$[Cu(L1)_2(H_2O)_2]$	3319	-	489	1657	1299	3051
CuL2	$[Cu(L2)Cl(H_2O)_2(CH_3OH)].2CH_3OH$	3323	-	474	1627	1340	3057
CuL3	$[Cu(L3)Cl(H_2O)(CH_3OH)_2].3H_2O$	3402	-	-	1631	1260	3184
CuL4	$[CuL4(CH_3OH)(NO_3)(H_2O)_2]$	3344	-	497	1631	1269	2922
CuL5	$[Cu(L5)_2(H_2O)_2].2H_2O$	3383	-	422	1508	1242	2935
CuL6	$[Cu(L6)(H_2O)(Cl)(CH_3OH)_2].4H_2O$	3327	-	470	1506	1249	3163
CuL7	$[Cu(L7)(H_2O)(Cl)(CH_3OH)_2]$	3344	-	488	1609	1278	3138
CuL8	$[Cu(L8)(H_2O)_2(CH_3OH)(Cl)]$	3333	-	438	1603	1250	3130
CoL9	$[CoL9(H_2O)_2]$	3122	437	497	-	1329	3138
Co_2L10	$[Co_2(L10)(CH_3OH)_4(Cl)_2(H_2O)_2]$	3281	432	509	1643	1300	3020
Cu_2L10	$[Cu_2(L10)(CH_3CN)Cl_2(H_2O)_5]$	3321	405	520	1550	1327	2920
Zn_2L10	$[Zn_2(L10)Cl_2(H_2O)_4(CH_3CN)_2]$	3448	430	464	1454	1043	-
Cu_3L11	$[Cu_3(L11)(H_2O)_3(CH_3OH)].CH_3OH$	3336	420	453	-	1051	3034
Cu_2L12	$[Cu_2(L12)(H_2O)_2]$	3329	405	449	-	1240	2990
Cu_2L13	$[Cu_2(L13)(H_2O)_2]$	3340	415	488	-	1238	2979
Cu_2L14	$[Cu_2(L14)(H_2O)_2]$	3160	405	451	1503	1247	2936

3.2.3 Mass Spectrum Analysis:

All the complexes synthesized were analyzed by direct mass using +ve ionization mode. Ligands binding to the metal ions and other coordinating co-ions or solvent molecule and structure of metal complexes have been proposed based on fragmentation pattern of the complex.[3,4] Small ligands (HL1 – HL8) binds to one copper metal ion while multidentate ligands bind two (H_2L10, H_4L12-14) and three metal ions (H_6L11) with other position occupied with solvent molecule or co ions. Proposed structure of metal complexes along with their fragmentation patterns are discussed below:

Complex $[Cu(L1)_2(H_2O)_2]$ binds with two ligands unit and two solvent water ligands in octahedral fashion which corresponds to m/z peak at 424, loss of coordinated water and pyridine ring results in intermediate ion corresponding to m/z peak at 327, further loss of piperazine ring(partial) gives another intermediate species corresponding to m/z value of 254. In the last when all coordination is removed along with metal ion, free ligand corresponding to m/z 164 is obtained. Calculated and experimental isotopic distribution is also in agreement to the proposed molecular formula of complex (Figure 3.29 and 3.31).

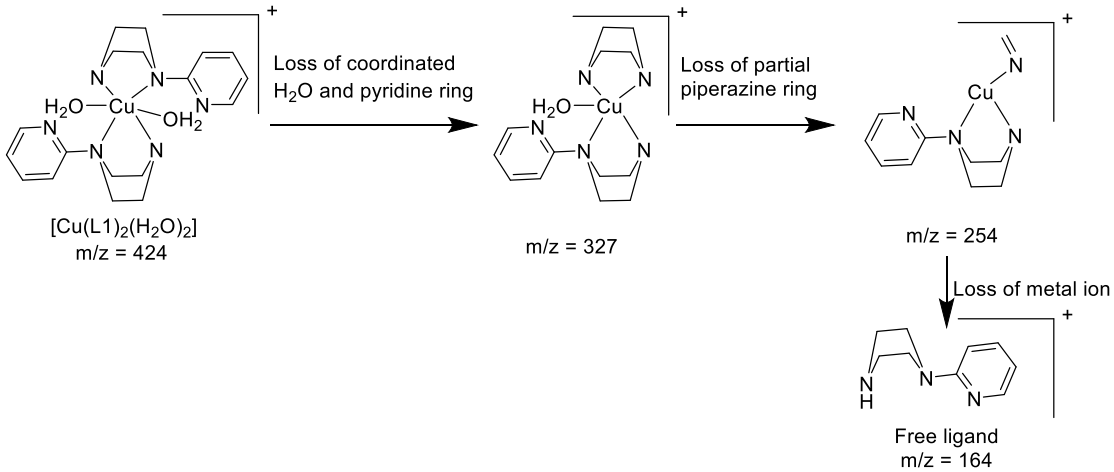

Figure 3.29: Mass spectra fragmentation of $[Cu(L1)_2(H_2O)_2]$

Complex $[Cu(L2)Cl(H_2O)_2(CH_3OH)].2CH_3OH$ binds with one ligands unit and two solvent methanol and two aqua and one chloride ligands with two uncoordinated methanol molecule in octahedral fashion which corresponds to m/z peak at 390, loss of uncoordinated methanol results in intermediate ion corresponding to m/z peak at

327 and further loss of another aqua ligand gives another intermediate species corresponding to m/z value of 309. Further loss one aqua and chloro ligands result in m/z 258. Peak at 244 indicate one with only one aqua and metal ion with ligands. Loss of piperazine arms indicate m/z at 200. In the last when all coordination is removed along with metal ion, free ligand corresponding to m/z 164 is obtained.Calculated and experimental isotopic distribution is also in agreement to the proposed molecular formula of complex (Figure 3.30 and 3.32).

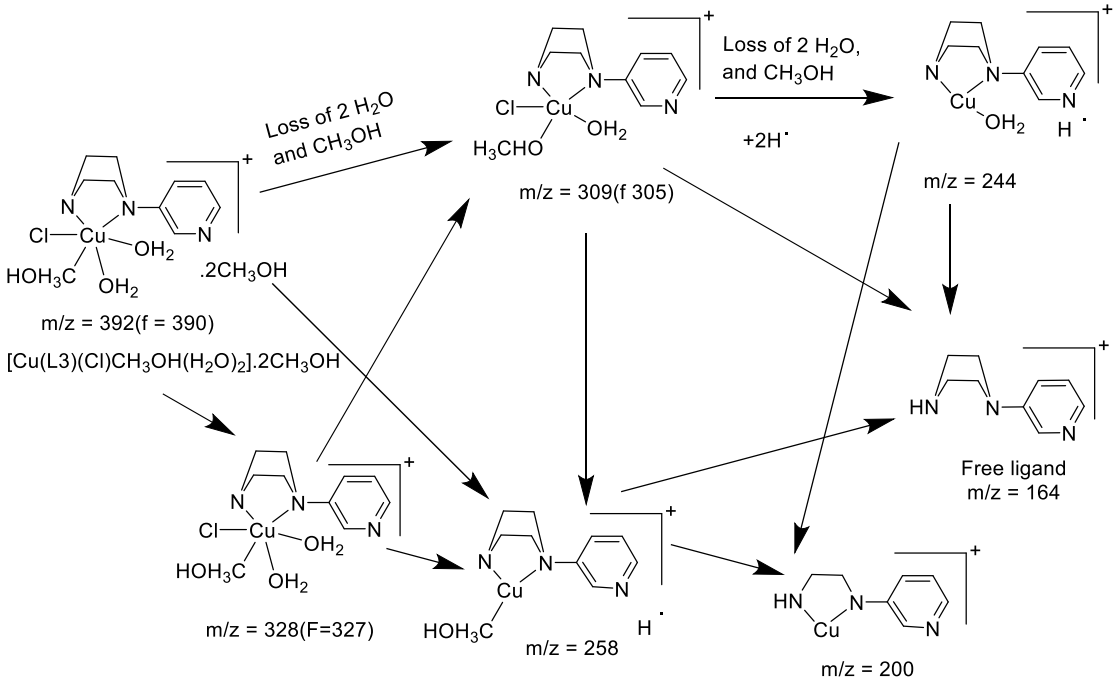

Figure 3.30: Mass spectra fragmentation of [Cu(L2)Cl(H_2O)$_2$(CH_3OH)].2CH_3OH

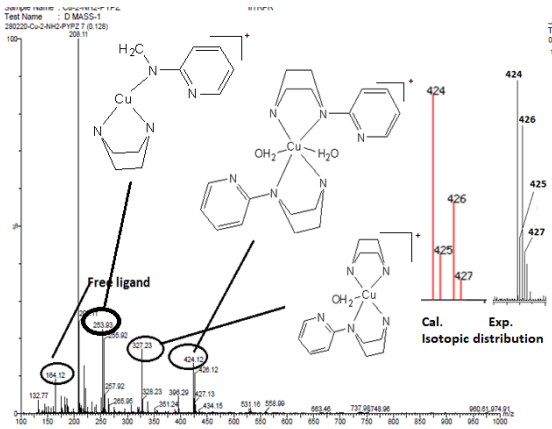

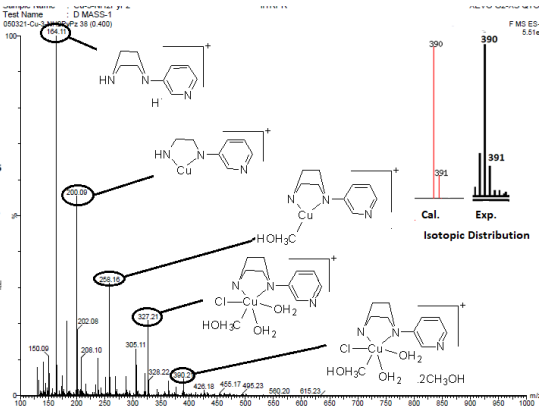

Figure 3.31: Mass spectra of [Cu(L1)$_2$(H_2O)$_2$]Figure 3.32: Mass spectra of [Cu(L2)Cl(H_2O)$_2$(CH_3OH)].2CH_3OH

Complex $[Cu(L3)Cl(H_2O)(CH_3OH)_2].3H_2O$ binds with one ligands unit and two solvent methanol, one aqua and one chloride ligands with three uncoordinated water molecule in octahedral fashion which corresponds to m/z peak at 396, loss of uncoordinated water and one methanol ligand results in intermediate ion corresponding to m/z peak at 327 and further loss of another methanol gives another intermediate species corresponding to m/z value of 295. In the second fragmentation method loss of two uncoordinated water, one methanol and chloride ligands result in species with m/z = 258. In the last when all coordination is removed along with metal ion, free ligand corresponding to m/z 164 is obtained.Calculated and experimental isotopic distribution is also in agreement to the proposed molecular formula of complex (Figure 3.33 and 3.35).

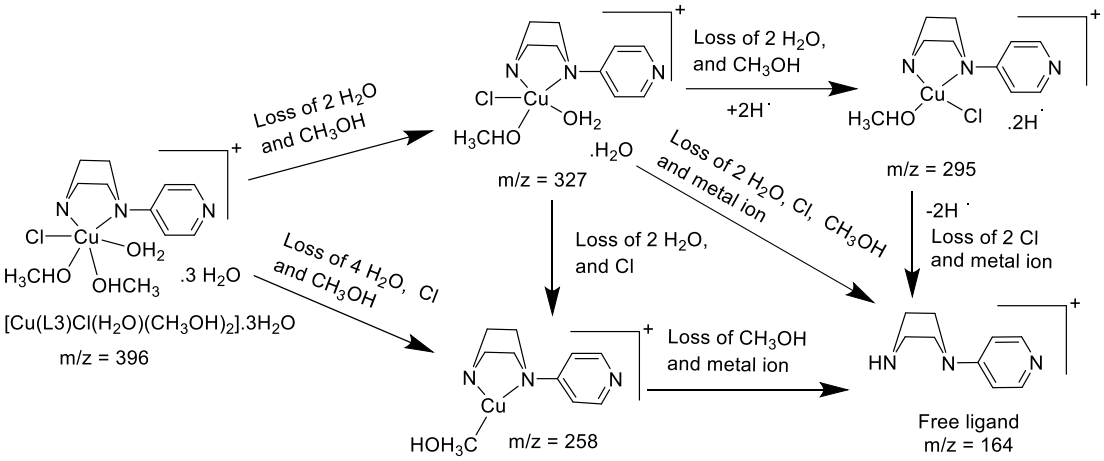

Figure 3.33: Mass spectra fragmentation of $[Cu(L3)Cl(H_2O)(CH_3OH)_2].3H_2O$

Complex $[Cu(L4)(CH_3OH)(NO_3)(H_2O)_2]$ shows m/z peak at 356 which corresponds to its molecular formula in octahedral coordination mode with two water, one methanol and one nitrate as co-ligands. Loss of two coordinated aqua ligands gives intermediate tetrahedral species which corresponds m/z to 318 and further loss of nitrate ion gives m/z to 256. Loss of only nitrate ion gives penta coordinated intermediate species corresponding to m/z to 294 in which further loss of two aqua ligands correspond to same intermediate species with m/z at 256.In the last when all coordination is removed along with metal ion, free ligand corresponding to m/z 163 is obtained. Calculated and experimental isotopic distribution is also in agreement to the proposed molecular formula of complex (Figure 3.34 and 3.36).

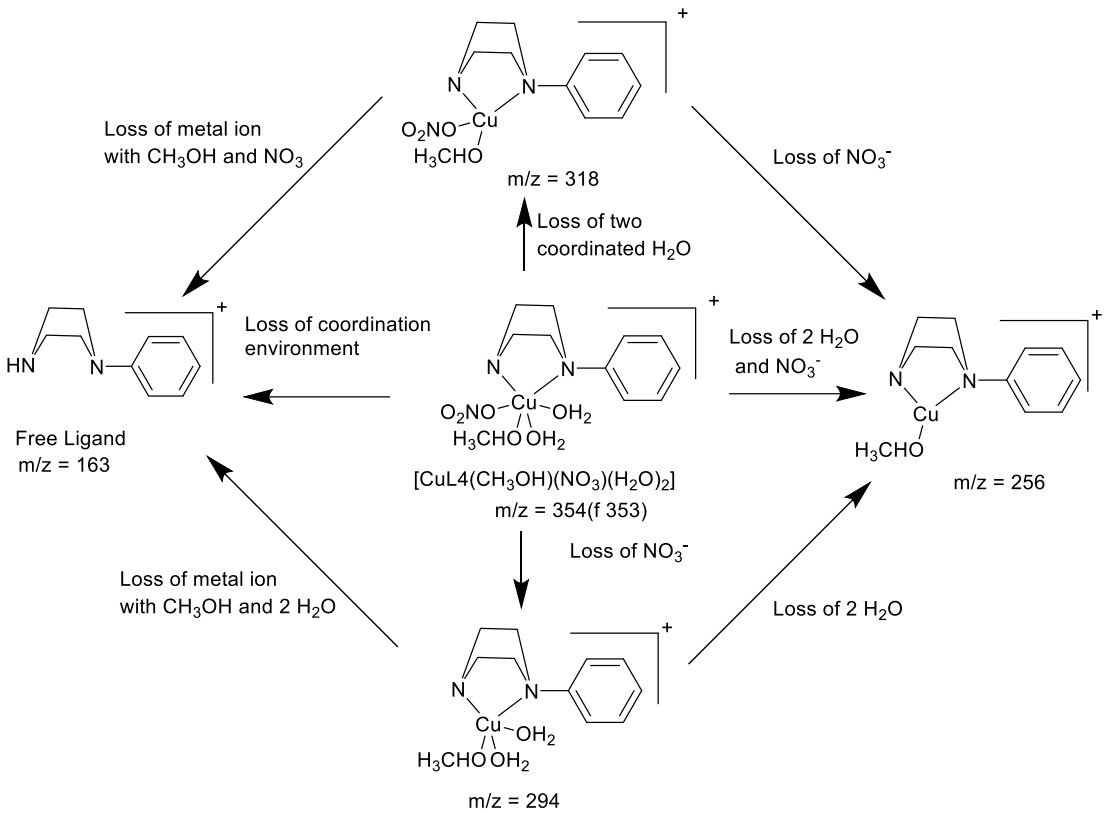

Figure 3.34: Mass spectra fragmentation of $[Cu(L4)(CH_3OH)(NO_3)(H_2O)_2]$

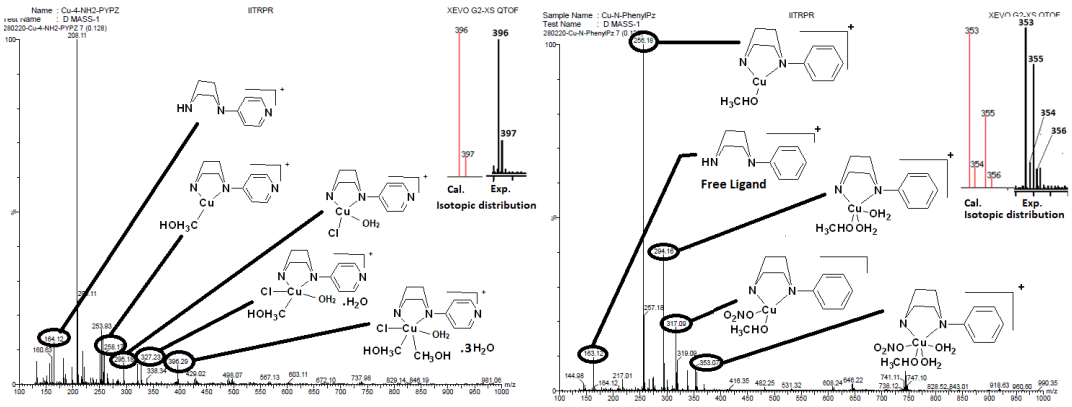

Figure 3.35: Mass spectra of $[Cu(L3)Cl_2(CH_3OH)_2].2H_2O$ Figure 3.36: Mass spectra of $[Cu(L4)(NO_3)(CH_3OH)(H_2O)_2]$

In complex $[Cu(L5)_2(H_2O)_2].2H_2O$, m/z peak at 443 corresponds to molecular formula of the complex. Further loss of three uncoordinated water molecules is indicated at m/z corresponding to 390. Loss of chloride ligand and piperazine arm results in the intermediate species corresponding to m/z at 354. Loss of coordination environment along with methoxy group of ligands results in free ligands giving m/z at

177. Calculated and experimental isotopic distribution is also in agreement to the proposed molecular formula of complex (Figure 3.37 and 3.38).

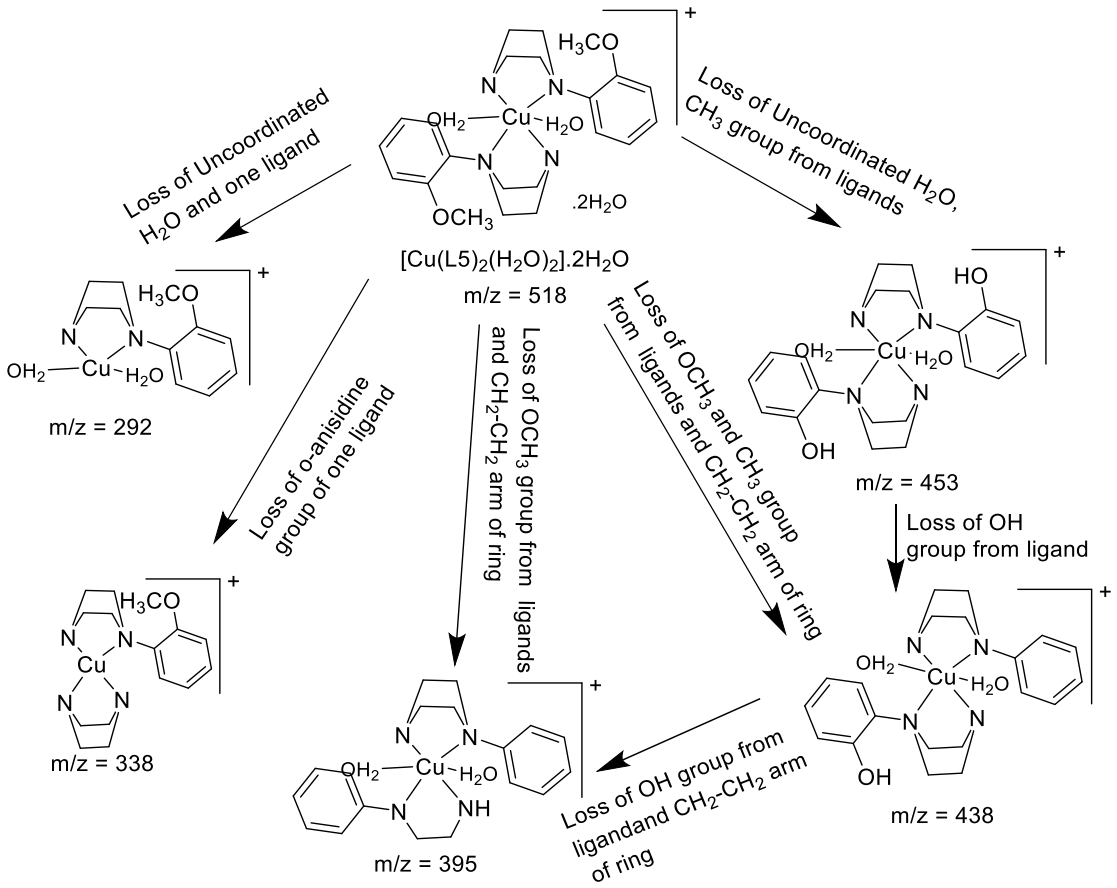

Figure 3.37: Mass spectra fragmentation of $[Cu(L5)_2(H_2O)_2].2H_2O$

In complex $[Cu(L6)(CH_3OH)_2(Cl)_2].3H_2O$, m/z peak at 443 corresponds to molecular formula of the complex. Further loss of three uncoordinated water molecules is indicated at m/z corresponding to 390. Loss of chloride ligand and piperazine arm results in the intermediate species corresponding to m/z at 354. Loss of coordination environment along with methoxy group of ligands results in free ligands giving m/z at 177. Calculated and experimental isotopic distribution is also in agreement to the proposed molecular formula of complex (Figure 3.39 and 3.40).

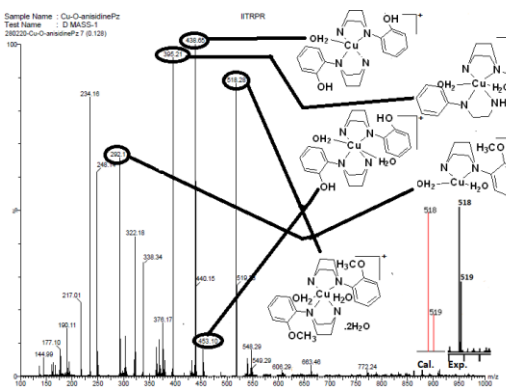

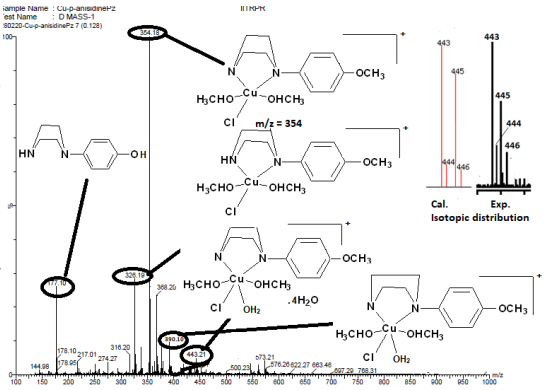

Figure 3.38: Mass spectra of $[Cu(L5)_2(H_2O)_2].2H_2O$ Figure 3.39: Mass spectra of $[Cu(L6)(CH_3OH)_2(Cl)_2].3H_2O$

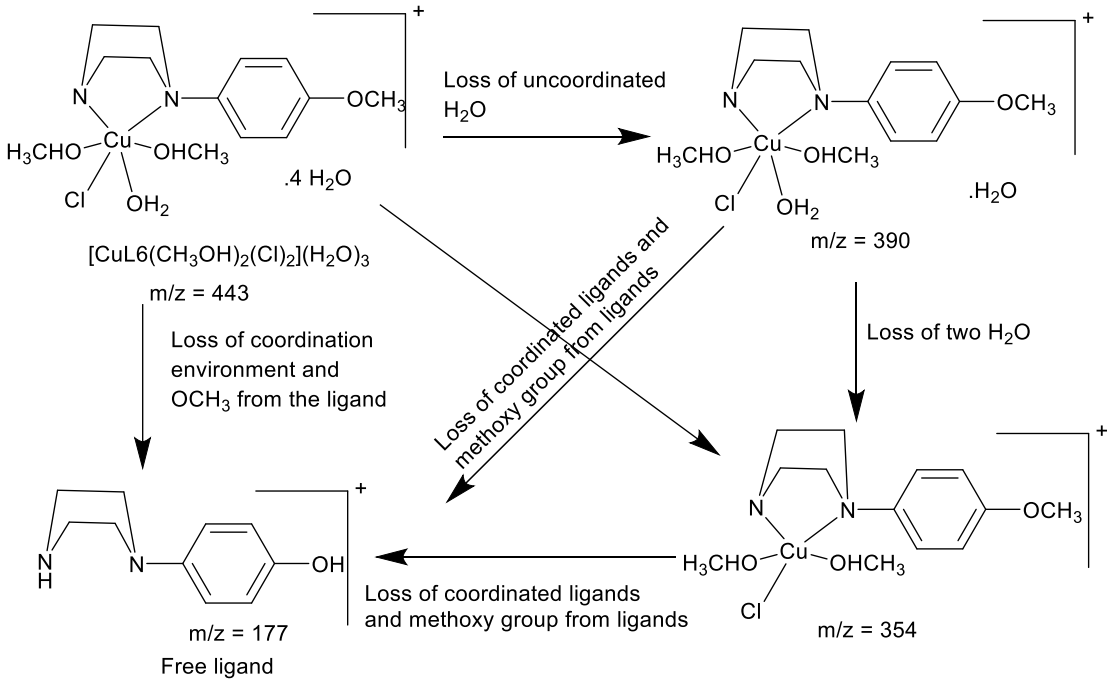

Figure 3.40: Mass spectra fragmentation of $[Cu(L6)(CH_3OH)_2(Cl)_2].3H_2O$

In complex $[Cu(L7)(CH_3OH)_2(H_2O)_2]$, m/z peak at 338 corresponds to molecular formula of the complex. Further loss of two coordinated methanol molecules and one chloride is indicated at m/z corresponding to 274. While the loss of one methanol and one aqua ligand results in the intermediate species corresponding to m/z at 247. Loss of two methanol and two aqua ligands and piperazine CH_2-CH_2 arm results in m/z corresponding to 213. Loss of coordination environment along with hydroxy group of ligands results in free ligands giving m/z at 163. Calculated and experimental isotopic distribution is also in agreement to the proposed molecular formula of complex (Figure 3.41 and 3.43).

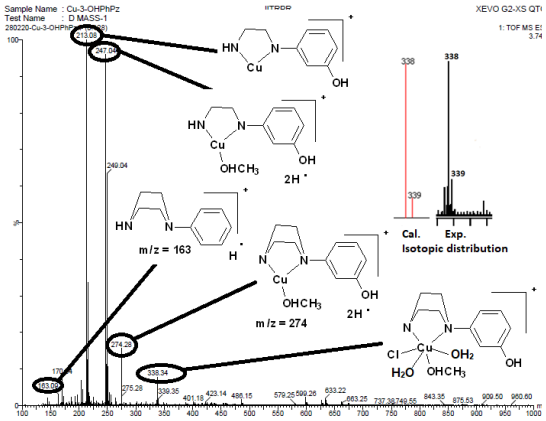

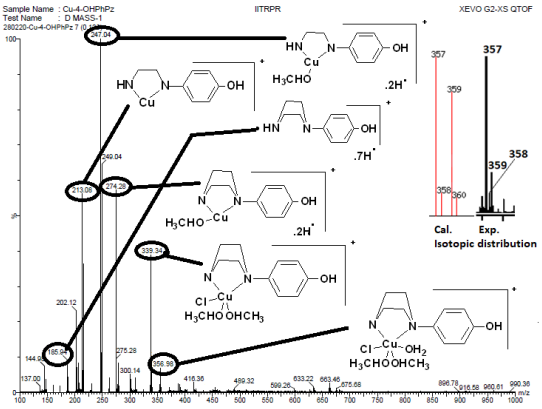

Figure 3.41: Mass spectra of [Cu(L7)(CH_3OH)Cl] Figure 3.42: Mass spectra of [Cu(L8)(CH_3OH)$_2$(H_2O)$_2$]

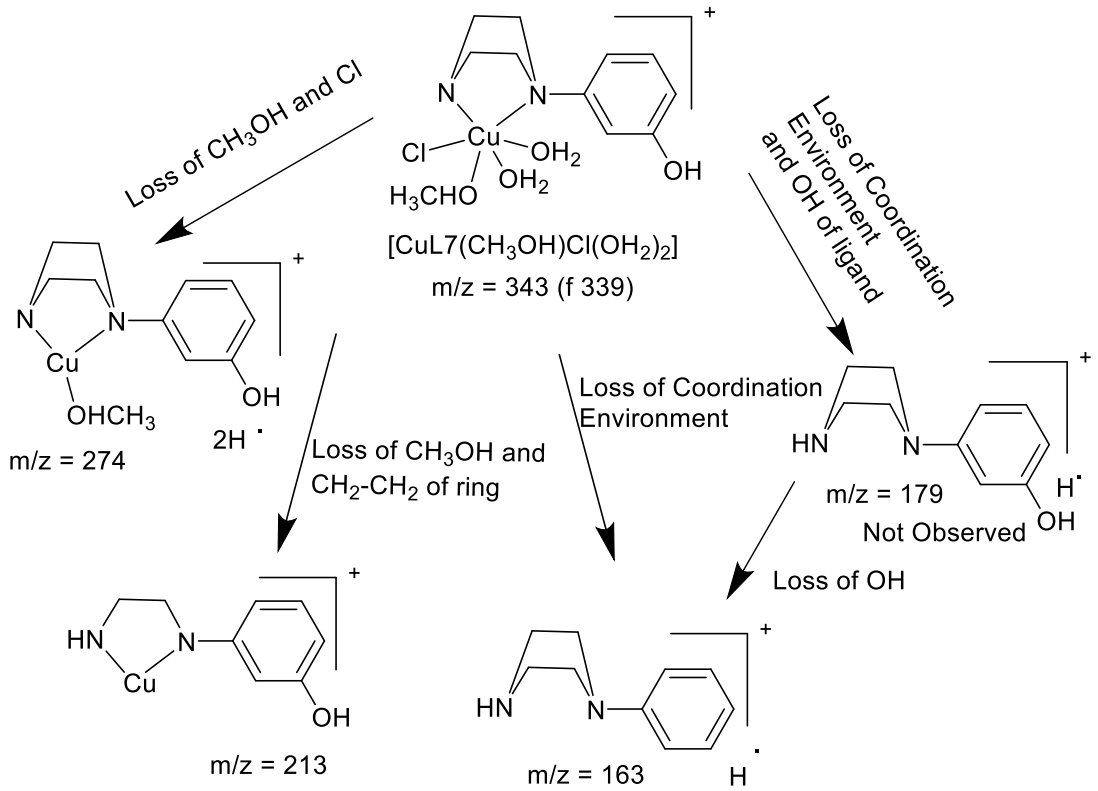

Figure 3.43: Mass spectra fragmentation of [Cu(L7)(CH_3OH)(Cl)(OH_2)$_2$]

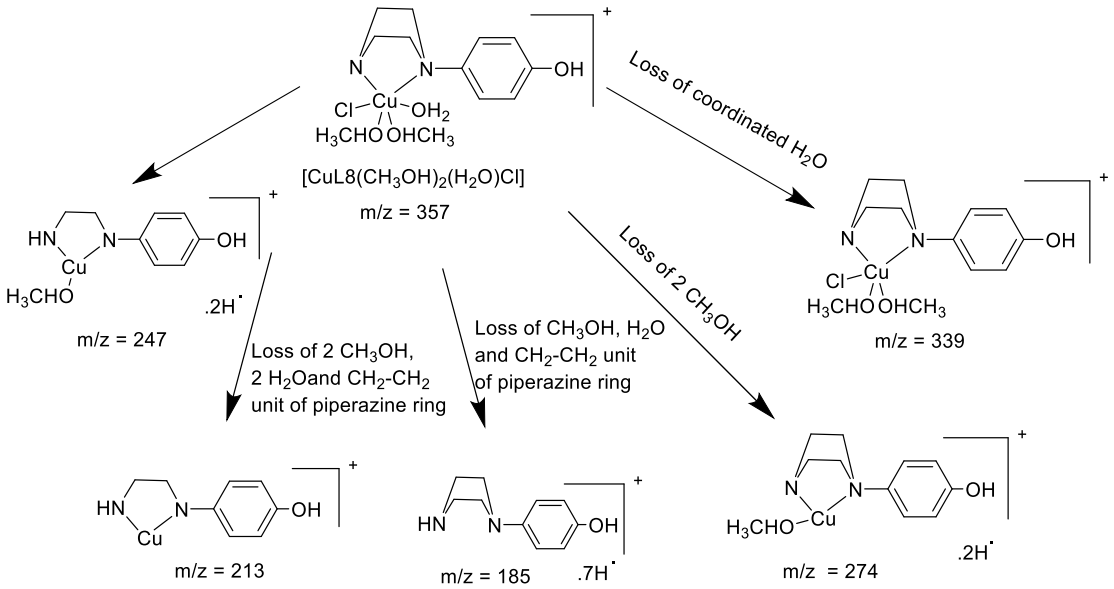

Figure 3.44: Mass spectra fragmentation of $[Cu(L8)(CH_3OH)_2(H_2O)(Cl)]$

In complex $[Cu(L8)(CH_3OH)_2(H_2O)(Cl)]$, m/z peak at 340 corresponds to molecular formula of the complex. Further loss of two coordinated methanol molecules is indicated at m/z corresponding to 276. While the loss of one methanol and one aqua ligand results in the intermediate species corresponding to m/z at 247. Loss of two methanol and two aqua ligands and piperazine CH_2-CH_2 arm results in m/z corresponding to 213. Loss of coordination environment along with hydroxy group of ligands results in free ligands is not observed. Calculated and experimental isotopic distribution is also in agreement to the proposed molecular formula of complex (Figure 3.42 and 3.44).

In complex $[Co(L9)(H_2O)_2]$, m/z peak at 267 corresponds to molecular formula of the complex. Further loss of two coordinated water molecules is indicated at m/z corresponding to 232. Loss of coordination environment along with metal ion of ligands results in free ligands is observed at m/z 175. Ligand loss of piperazine arm at 146 and two water loss in indicated at m/z 139. Calculated and experimental isotopic distribution is also in agreement to the proposed molecular formula of complex (Figure 3.44 and 3.46).

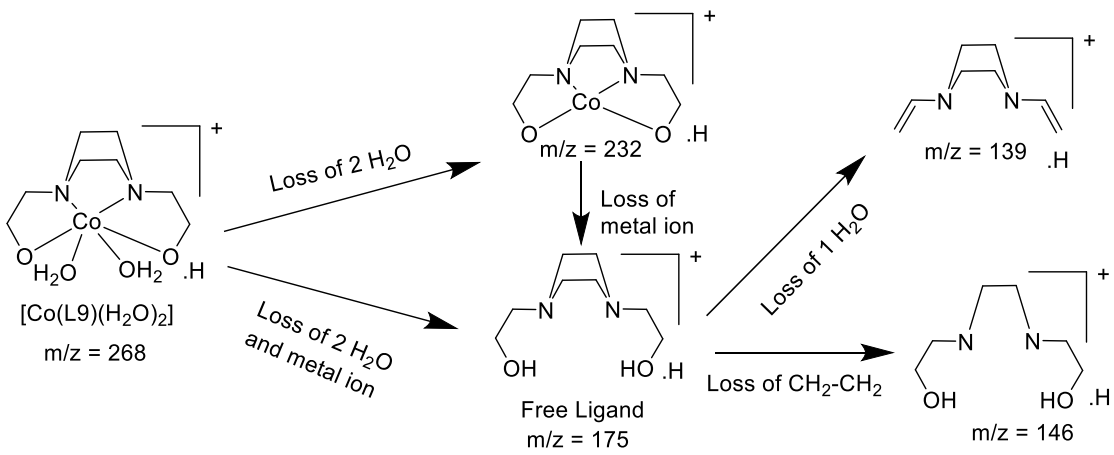

Figure 3.45: Mass spectra fragmentation of $[Co(L9)(H_2O)_2]$

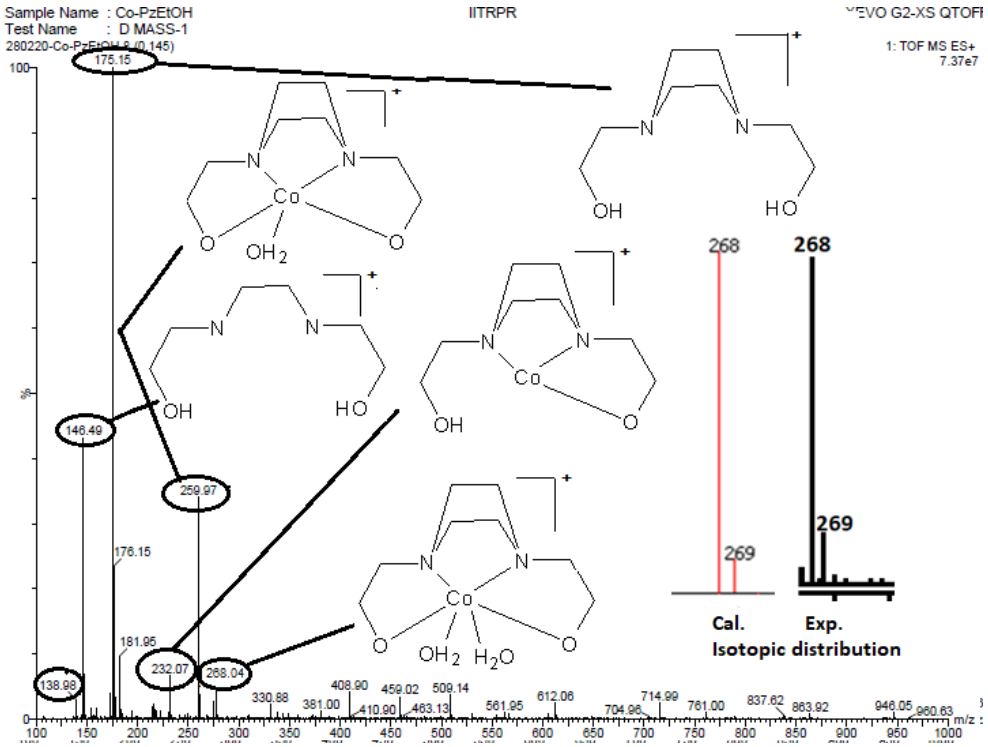

Figure 3.46: Mass spectra of $[Co(L9)(H_2O)_2]$

In complex $[Co_2(L10)Cl_4(H_2O)_2(CH_3OH)_2]$, m/z peak at 687 corresponds to molecular formula of the complex. Further loss of two coordinated methanol molecules,one chloro and two aqua ligands is indicated at m/z corresponding to 567. Further loss of two chloro results in the intermediate species corresponding to m/z at 447 and loss of two metals gives free ligand corresponding m/z at 327. Further loss of one water from ligand comes at m/z 309.In the second way, Loss of one styrene

epoxide type fragments from complex also results in m/z at 567 and subsequent loss of one more styrene epoxide type moiety gives m/z at 447. From here loss of one methanol results in m/z corresponding to 415. Loss of water from free ligands is observed at 309. Calculated and experimental isotopic distribution is also in agreement to the proposed molecular formula of complex (Figure 3.47 and 3.48).

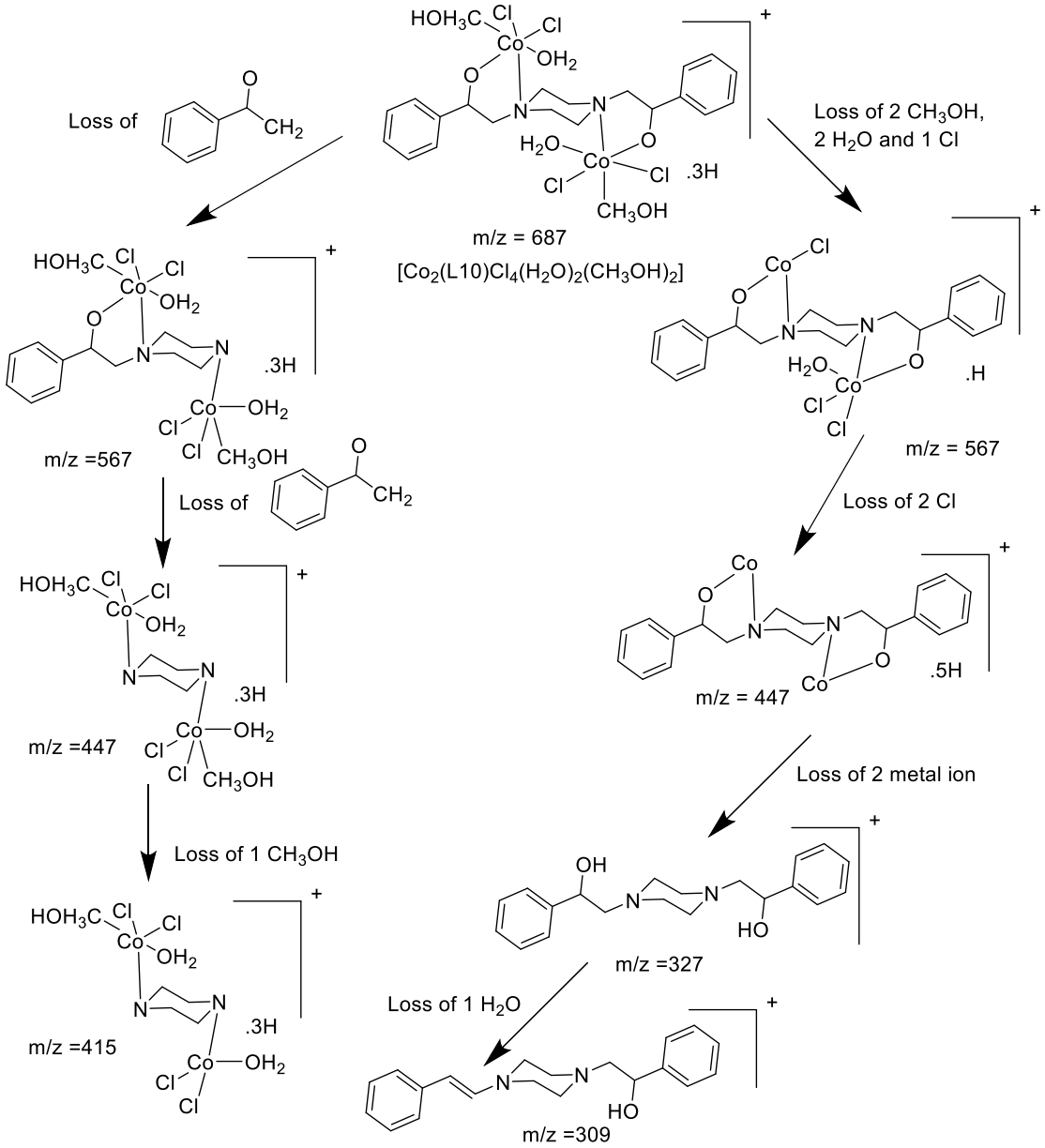

Figure 3.47: Mass spectra fragmentation of $[Co_2(L10)Cl_4(H_2O)_2(CH_3OH)_2]$

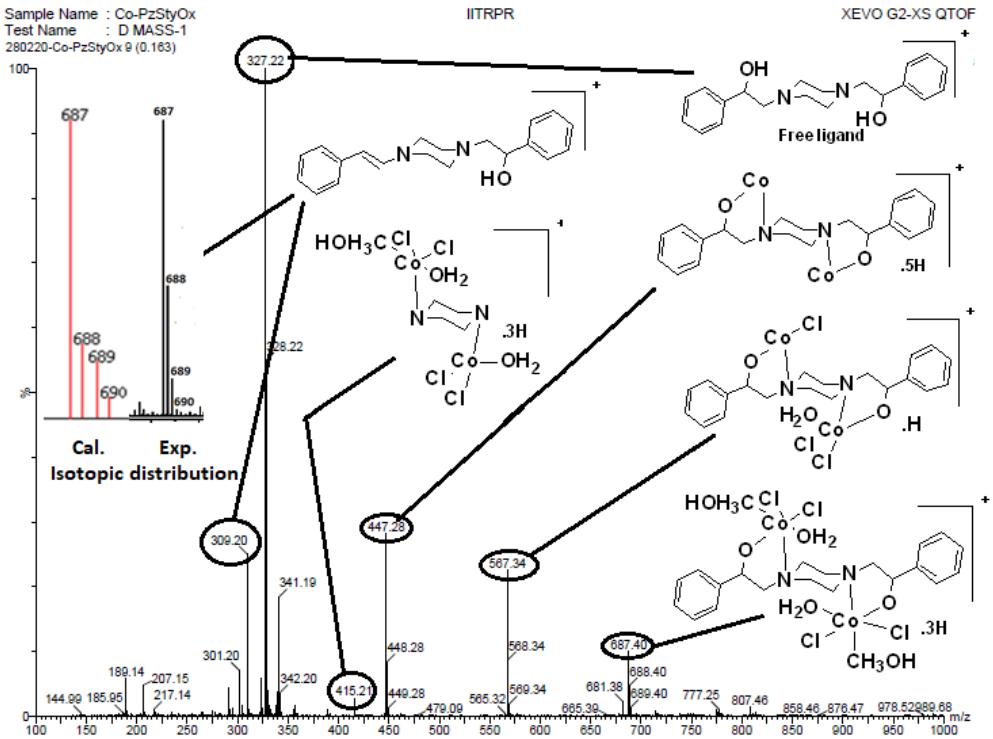

Figure 3.48: Mass spectra of[$Co_2(L10)Cl_4(CH_3OH)_2(H_2O)_2$]

In complex [$Cu_2(L10)(CH_3CN)Cl_2(H_2O)_5$], m/z peak at 327 corresponds to molecular formula of the complex with charge on the molecule taking as +2. Further loss of two coordinated chloride, one acetonitrile and one aqua ligand is indicated at m/z corresponding to 262. Loss of further aqua ligands in next steps results in the three intermediate species corresponding to m/z at 253, 220 and 189 indicating the loss of two, one and one loss in series. In case of m/z peak at 189 is also obtained results in the loss of phenyl ring of the ligand. In the second manner which the loss of all chloride and all aqua ligands remaining only with acetonitrile results in another intermediate corresponding to m/z 207 along with phenyl ring of ligand. Loss of coordination environment along with hydroxy group of ligands results in free ligands is not observed(Figure 3.49 and 3.50).

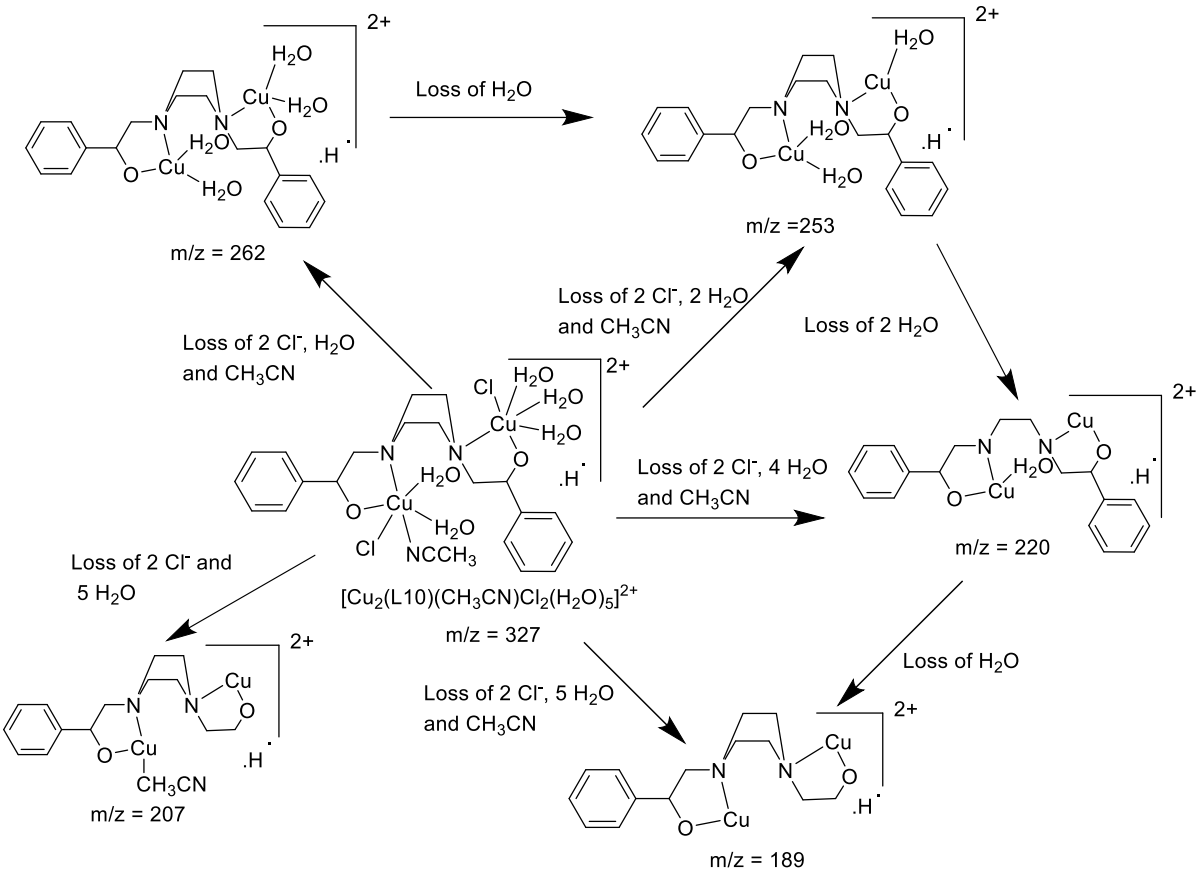

Figure 3.49: Mass spectra fragmentation of $[Cu_2(L10)(CH_3CN)Cl_2(H_2O)_5]$

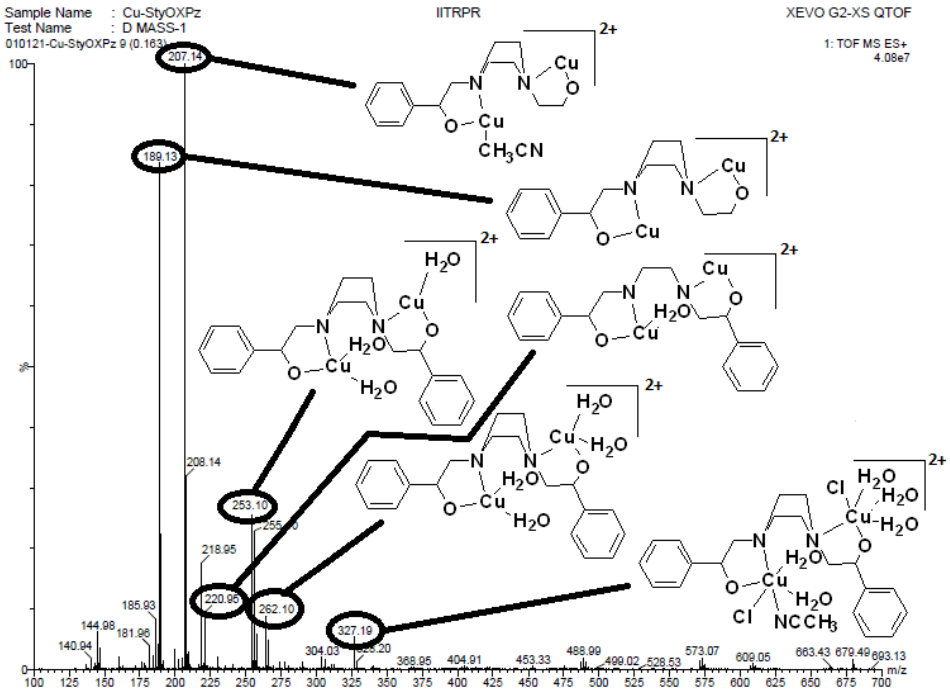

Figure 3.50: Mass spectra of $[Cu_2(L10)(CH_3CN)Cl_2(H_2O)_5]$

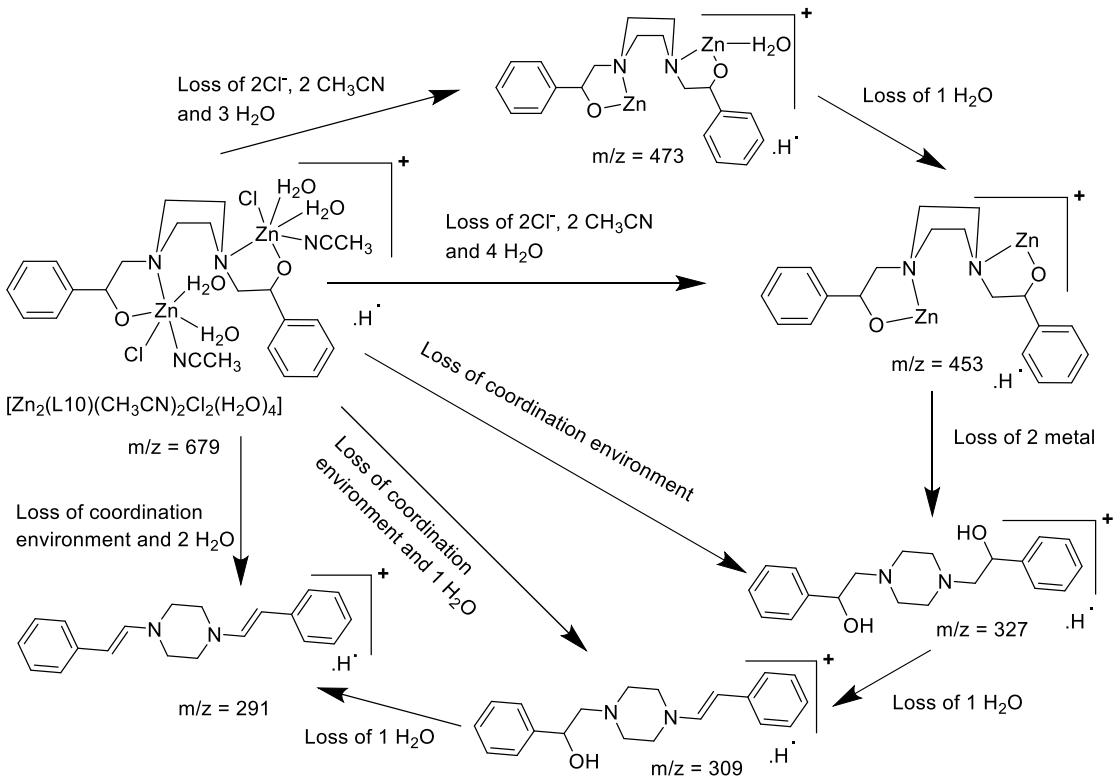

Figure 3.51: Mass spectra fragmentation of $[Zn_2(L10)Cl_2(H_2O)_4(CH_3CN)_2]$

In complex $[Zn_2(L10)Cl_2(H_2O)_2(CH_3CN)_2]$, m/z peak at 679 corresponds to molecular formula of the complex. Further loss of two coordinated acetonitrile molecules,two chloro and three aqua ligands is indicated at m/z corresponding to 473. Further loss of one more aqua ligand results in the intermediate species corresponding to m/z at 453 and loss of two metals gives free ligand corresponding m/z at 327. Further loss of one water from ligand comes at m/z 309 and that of second water 291. Calculated and experimental isotopic distribution is also in agreement to the proposed molecular formula of complex (Figure 3.51 and 3.52).

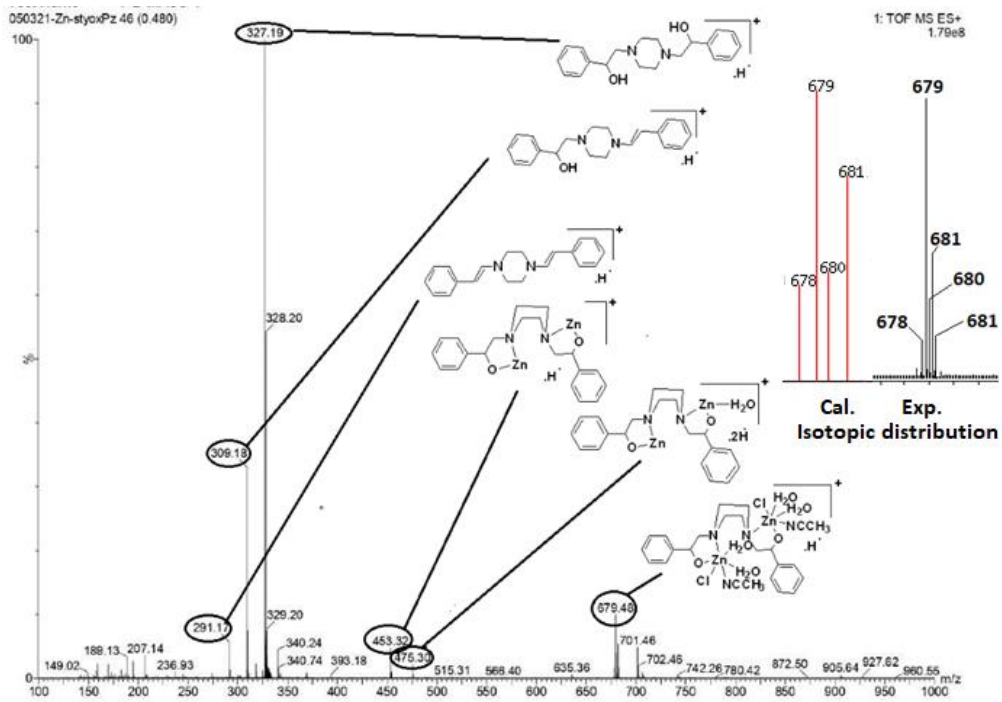

Figure 3.52: Mass spectra of $[Zn_2(L10)Cl_2(H_2O)_4(CH_3CN)_2]$

In complex $[Cu_3L11(H_2O)_3Cl]CH_3OH$,ligand L11 binds with three metal centres in with two type of coordination mode octahedral and tetrahedral with m/z peak at 712 corresponds to molecular formula of the complex.Loss of uncoordinated methanol appears in the peak which appears at m/z 680. Further loss of three coordinated water results in intermediate species corresponding to m/z 626 in which further loss of two metal ion gives m/z at 599. In another way loss of 3 H_2O, 1 Cl^- and two metal ion results m/z in 451. Also, the loss of three H_2O, 1 Cl^- and one metal ion results in m/z 538. Loss of coordination environment along with metal ion of ligands results in free ligands is observed at peak of 409 (Figure 3.53 and 3.54).

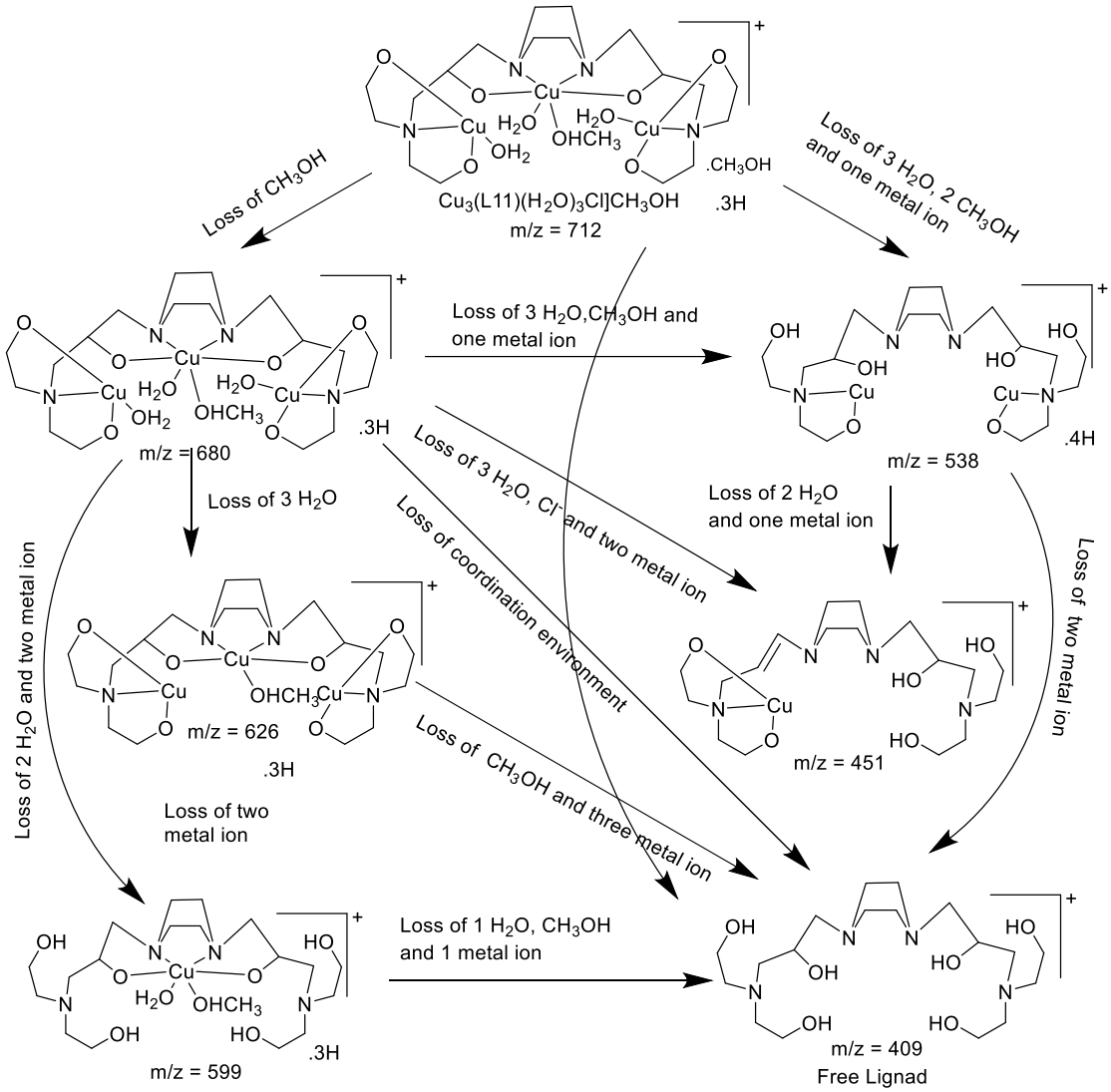

Figure 3.53: Mass spectra fragmentation of $[Cu_3(L11)(CH_3OH)(H_2O)_3].CH_3OH$

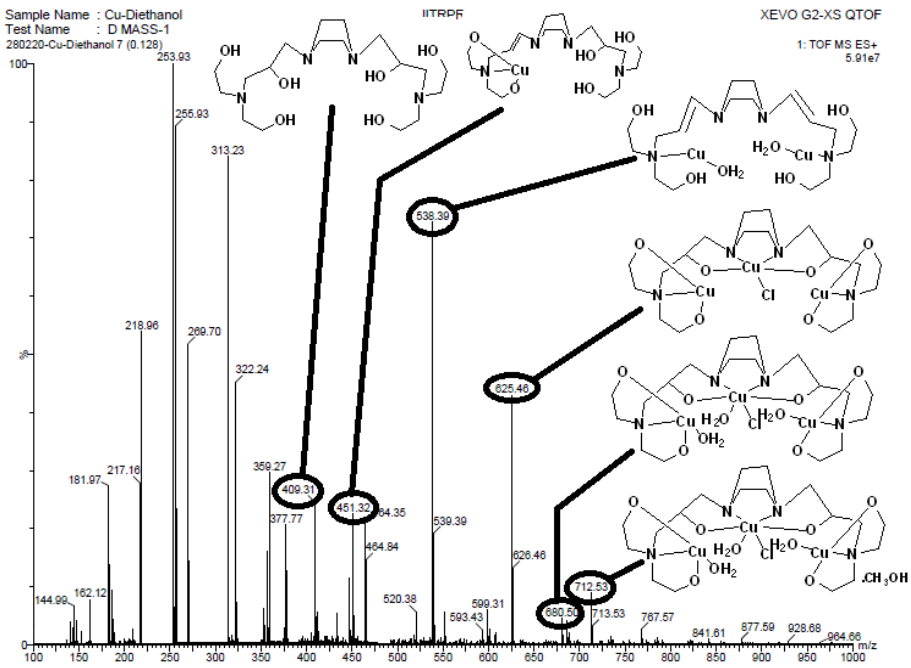

Figure 3.54: Mass spectra of $[Cu_3(L11)(CH_3OH)(H_2O)_3]CH_3OH$

In complex $[Cu_2L12(H_2O)_2]$ ligand L12 binds with two metal centres in tetrahedral coordination mode with m/z peak at 509 corresponds to molecular formula of the complex. Further loss of one coordinated water molecules is indicated at m/z corresponding to 491 subsequent loss of second coordinated water is also indicated at m/z 471. From the species at m/z 471, loss of one metal corresponds to m/z 410. And ultimately loss of coordination environment from complex to each intermediate species results in free ligands which is observed at peak of 349. Thus, fragmentation pattern is in good agreement to the proposed structure of metal complex. This structure is also supported by mass fragmentation pattern and proposed structure of other two complexes of ligands H_4L13 and H_4L14 as they have similar coordination environment around the meal ions and binds with two copper in similar tetradentate coordination mode. Calculated and experimental isotopic distribution is also in agreement to the proposed molecular formula of complex (Figure 3.55 and 3.56).

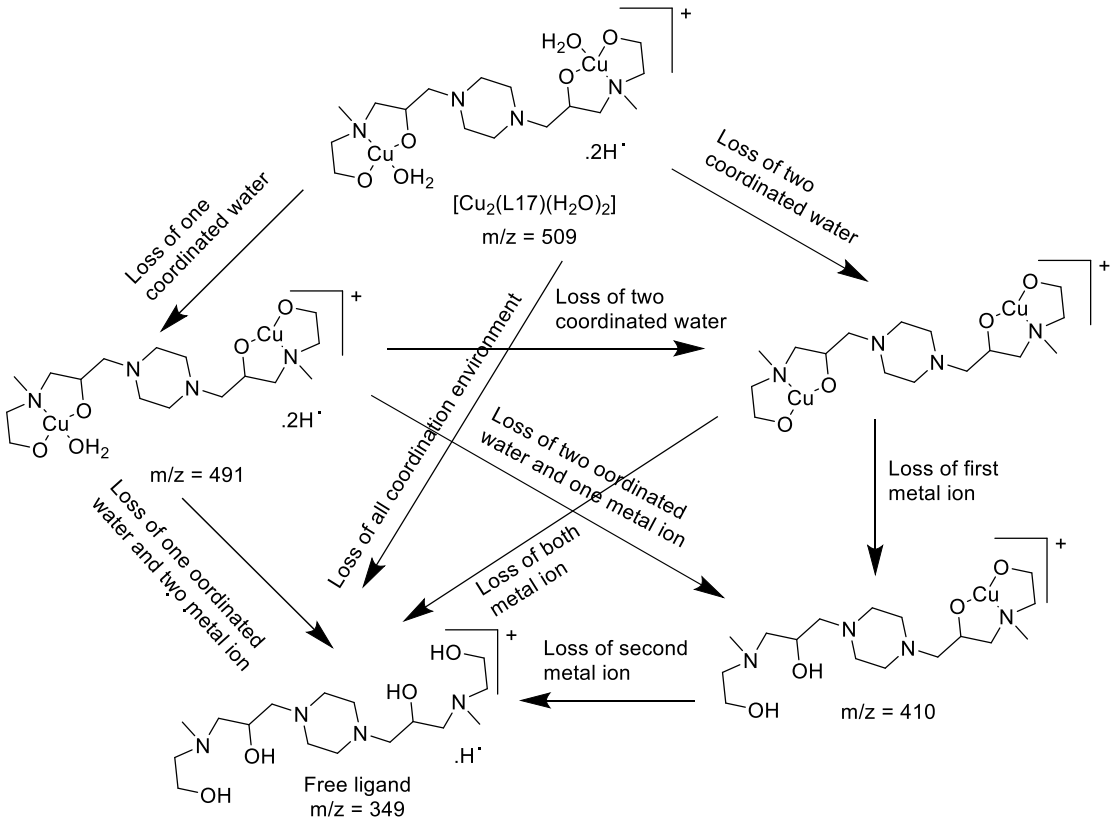

Figure 3.55: Mass spectra fragmentation of $[Cu_2L12(H_2O)_2]$

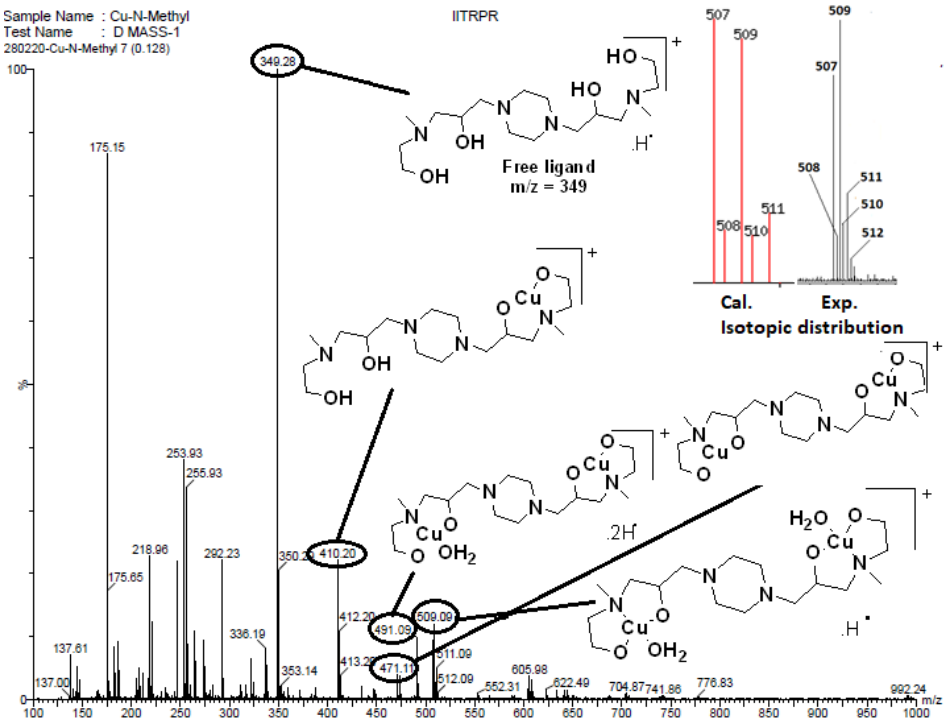

Figure 3.56: Mass spectra of $[Cu_2L12(H_2O)_2]$

In complex $[Cu_2L13(H_2O)_2]$ligand L13 binds with two metal centre in tetrahedral coordination mode with m/z peak at 537 corresponds to molecular formula of the complex. Further loss of one coordinated water molecules from one metal centre is not indicated at m/z corresponding to 517 while the subsequent loss of second coordinated water corresponds to m/z at 499. Loss of first metal ion from the m/z 499 gives the intermediate m/z at 438. From all species loss of complete coordination environment of ligands results in free ligands is observed at peak of 377.Thus, fragmentation pattern is in good agreement to the proposed structure of metal complex. This structure is also supported by mass fragmentation pattern and proposed structure of other two complexes of ligands H_4L12 and H_4L14 as they have similar coordination environment around the meal ions and binds with two copper ions in similar tetradentate coordination mode. Calculated and experimental isotopic distribution is also in agreement to the proposed molecular formula of complex (Figure 3.57 and 3.58).

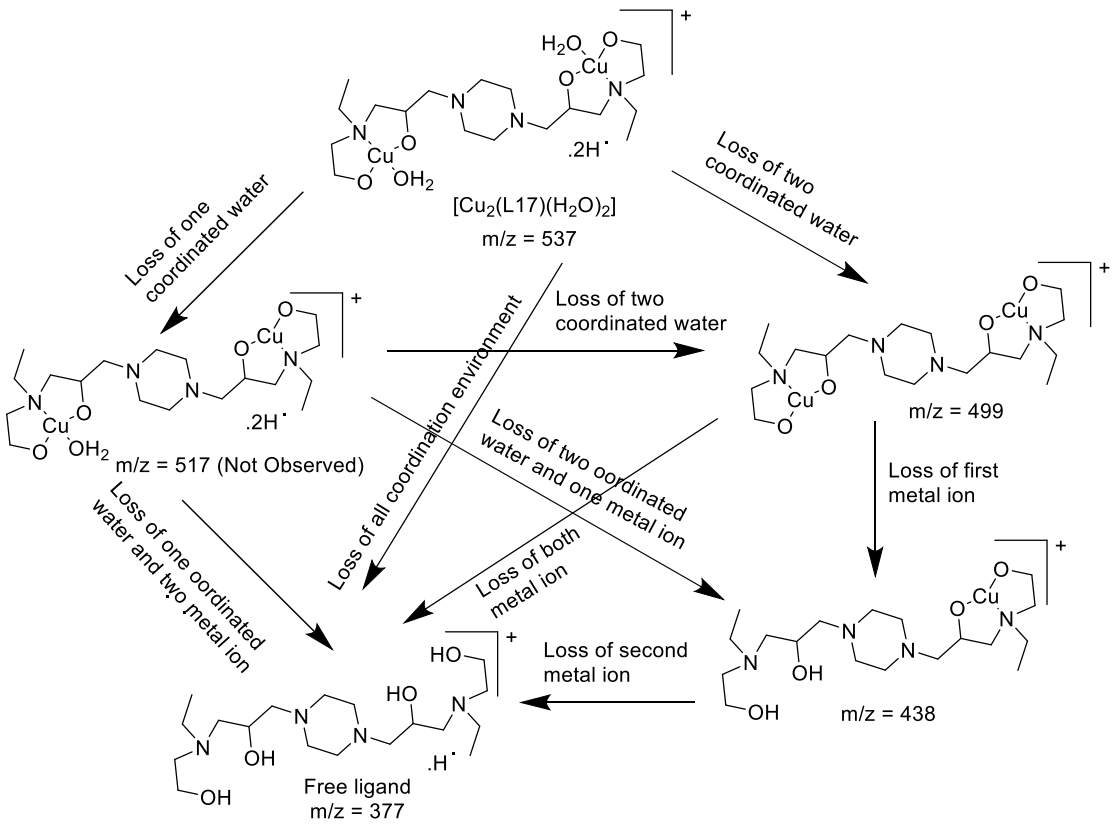

Figure 3.57: Mass spectra fragmentation of $[Cu_2L13(H_2O)_2]$

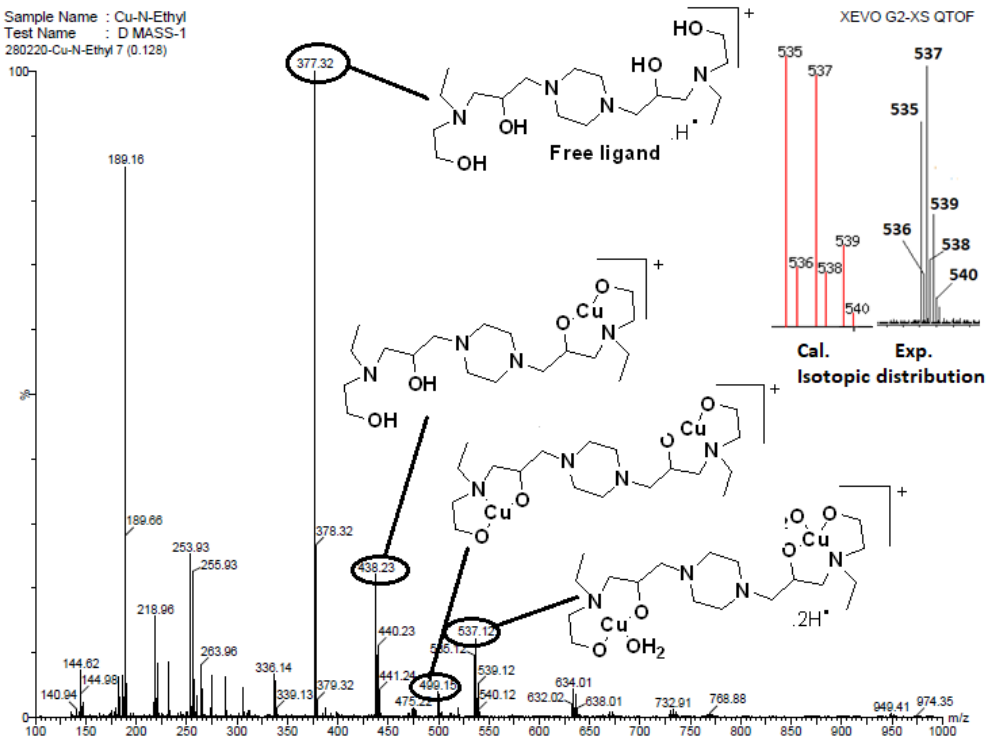

Figure 3.58: Mass spectraof $[Cu_2L13(H_2O)_2]$

In complex $[Cu_2L14(H_2O)_2]$ ligand L14 binds with two metal centre in tetrahedral coordination mode with m/z peak at 661 corresponds to molecular formula of the complex. Further loss of one coordinated water molecules from one metal centre is not indicated at m/z corresponding to 643 while the further loss of second coordinated water corresponds to m/z at 625. Loss of first metal ion from the m/z 625 gives the intermediate m/z at 562 and loss of water from 562 gives m/z 545. From all species (other than m/z at 545) loss of complete coordination environment of ligands results in free ligands is observed at peak of 377.Thus, fragmentation pattern is in good agreement to the proposed structure of metal complex. This structure is also supported by mass fragmentation pattern and proposed structure of other two complexes of ligands H_4L12 and H_4L13 as they have similar coordination environment around the meal ions and binds with two copper ions in similar tetradentate coordination mode. Calculated and experimental isotopic distribution is also in agreement to the proposed molecular formula of complex (Figure 3.59 and 3.60).

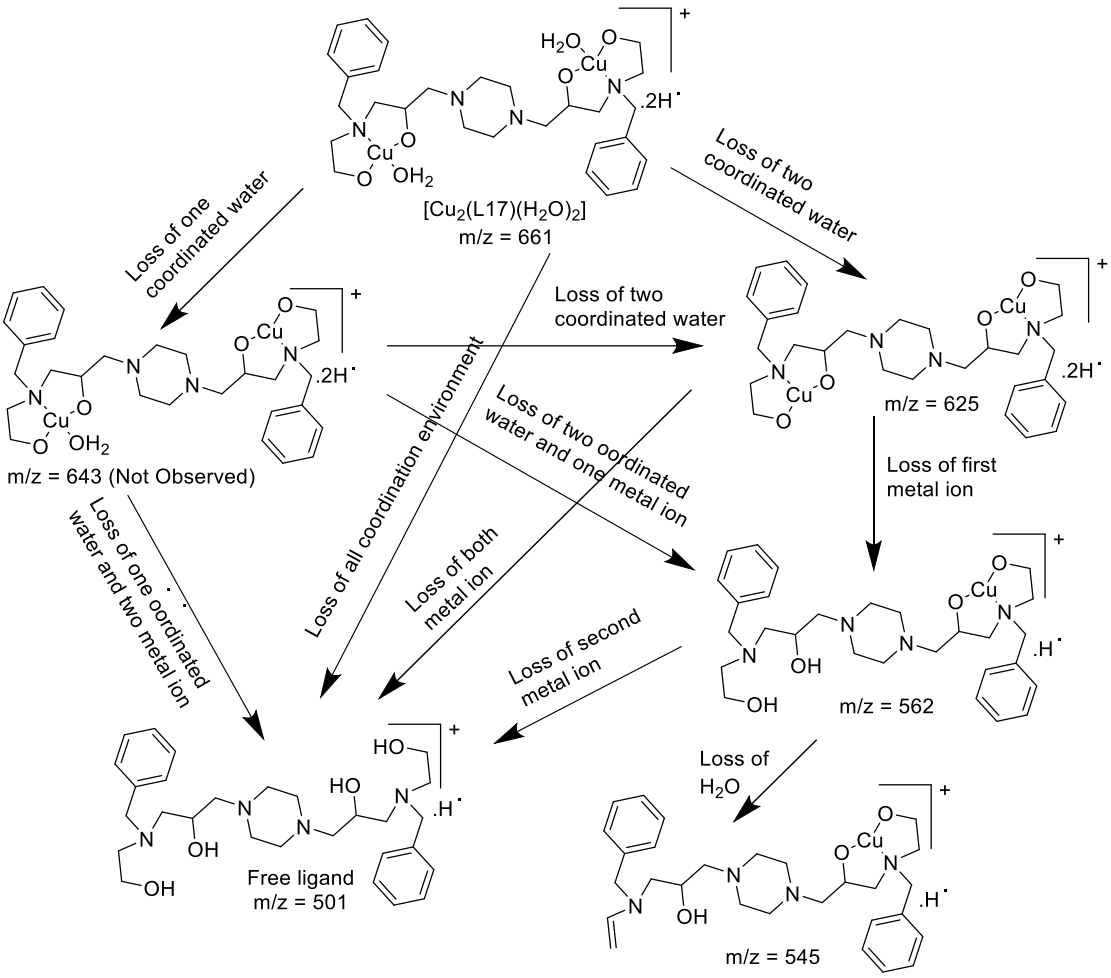

Figure 3.59: Mass spectra fragmentation of $[Cu_2L14(H_2O)_2]$

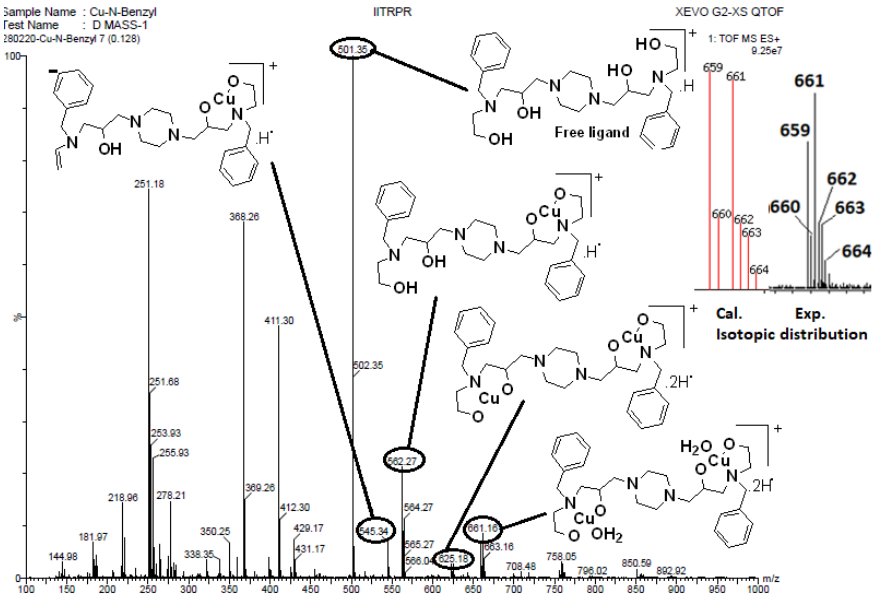

Figure 3.60: Mass spectraof $[Cu_2L14(H_2O)_2]$

3.3 Additional experimental studies to support proposed structure of metal complexes:

With so many attempts to obtain singe crystal with no fruitful results, structure of metal complexes have been proposed on the basis of IR and mass fragmentation pattern, we have performed additional studies to support the proposed structure of the complexes.

Electrochemical and Thermal Studies: To assist the proposed structure of complexes both electrochemical and thermal behaviour of metal complexes were recorded and analyzed. In electrochemical studies molar conductance values were recorded using calibrated conductivity meter where as in thermal studies TGA were used to analyzed decomposition behaviour with increase in temperature. The experimental studies so conducted supports the proposed structures of the complexes. The results are discussed below

3.3.1Molar conductance Measurements:

Molar conductance data of electrolytic nature of solutions have been matter of interest for scientists. Behaviour of metal complex in electrolytic solutions provide brief ideaabout their composition andnature.[5] Significant structural information can be idealized as conductance is directly related to current carrying capacity of an electrolyte which is directly related to number of ions present in the solution.[6,7] Evidently it can be established weather the nature of complex is ionic or non-ionic by using molar conductance data in different solvents (Table 3.3).[8] These studies further can be applied to analyzethe ligand-metal stoichiometry as well as geometries of complexes.[9,10]

Table 3.3: Electrolytes and nonelectrolytes molar conductance range for solvents[5]

Sr. No.	Solvent	Electrolytes molar conductance range ($Ohm^{-1}cm^2mol^{-1}$)	Nonelectrolytes molar conductance range ($Ohm^{-1}cm^2mol^{-1}$)
1	CH_3CN	>120	<120
2	CH_3COCH_3	>100	<95
3	CH_3OH	>80	<80
4	CH_3CH_2OH	>35	<30
5	DMSO	>50	<50
6	H_2O	>118	<80

Table 3.4: Experimental values of molar conductance for complexes

Code	Structural Formula	Molar Cond. in water(Ohm^{-1}cm^{2}mol^{-1})	Molar Cond. in DMSO(Ohm^{-1}cm^{2}mol^{-1})	Nature
CuL1	$[Cu(L1)_2(H_2O)_2]$	53.5	28.3	Nonionic
CuL3	$[Cu(L3)Cl(H_2O)(CH_3OH)_2]$	45.2	21.5	Nonionic
CuL4	$[CuL4(CH_3OH)(NO_3)(H_2O)_2]$	57.5	29.4	Nonionic
CuL5	$[Cu(L5)_2(H_2O)_2].2H_2O$	66.0	35.2	Nonionic
CuL6	$[Cu(L6)(H_2O)(Cl)(CH_3OH)_2].4H_2O$	70.7	37.6	Nonionic
CuL7	$[Cu(L7)(H_2O)(Cl)(CH_3OH)_2]$	74.1	38.6	Nonionic
CuL8	$[Cu(L8)(H_2O)_2(CH_3OH)(Cl)]$	54.0	29.1	Nonionic
CoL9	$[Co(L9)(H_2O)_2]$	60.2	31.5	Nonionic
Co_2L10	$[Co_2(L10)(CH_3OH)_4(Cl)_2(H_2O)_2]$	72.5	38.0	Nonionic
Cu_2L10	$[Cu_2(L10)(CH_3CN)Cl_2(H_2O)_5]$	56.2	28.2	Nonionic
Cu_3L11	$[Cu_3(L11)(H_2O)_3(CH_3OH)].CH_3OH$	80	41.3	Nonionic
Cu_2L12	$[Cu_2(L12)(H_2O)_2]$	112	46.0	Nonionic
Cu_2L13	$[Cu_2(L13)(H_2O)_2]$	75	39.7	Nonionic
Cu_2L14	$[Cu_2(L14)(H_2O)_2]$	110	47.7	Nonionic

Thus, the all complexes are non-ionic in nature as suggested by molar conductance data in both water and DMSO as solvents, which is in agreement with the proposed structures of metal complexes (Table 3.4). Essentially this data indicate that anion satisfy secondary valency behaving as ligands rather than primary valency as molar conductance is directly proportional to no of ions present in the solution. This data is further supported by thermogravimetric analysis.

3.3.2 Thermal Studies: Thermogravimetric analysis (TGA)

Thermal studies of compounds in the form of thermogram represents graphical representation of the % weightloss against temperature.[11,12]Thermal decomposition of individual compounds are important in term of their thermal stability, composition, life time, oxidative stability, kinetics and volatile or moisture content.[13,14] In general, following information can be obtained from a TG Curve:

Below 150°C, low weight solvent or physiosorbed water or any trapped gases starts evolving.Between 150°C-250°C, weight loss of coordinated water and other similar compounds occurs.Above 250°C, ligands and complexes decompositionstarts and

multiple variations in the temperature via different intermediates.[15,16] Thus TGA (Thermogravimetric analysis) data can predict the presence or absence of coordinated water and other molecules from a metal complexin the temperature range before theactual decomposition molecular backbone begins. The change in weight measured by TGA data has been important in interpreting the structure and thermal stability of metal complexes.[17-21]Complexes which were obtained in solid state and are non-hygroscopic in nature were analyzed by TGA and results thus obtained are discussed as.

In complex $[CuL4(CH_3OH)(NO_3)(H_2O)_2]$, initial loss of coordinated methanol is observed as indicated by the derivative peak in the range of 50-90°C, whereas loss of coordinated water ligands is observed in the temperature range 150-200°C and loss of nitrate occurs 200-250°C, further decomposition of ligands in the major peak occurs near 300-350°C. Another way to analyze is ash content % which indicate binding to one copper metal converting into the ash as CuO (Figure 3.61).

In complex $[Cu(L5)_2(H_2O)_2].2H_2O$, only initial loss of coordinated water is observed as indicated by the derivative peak in the range of 100-150°C, further decomposition of ligands in the major peak occurs near 250-350 ^{0}C. Ash content analysis corresponds to one copper metal converting into the ash as CuO (Figure 3.62).

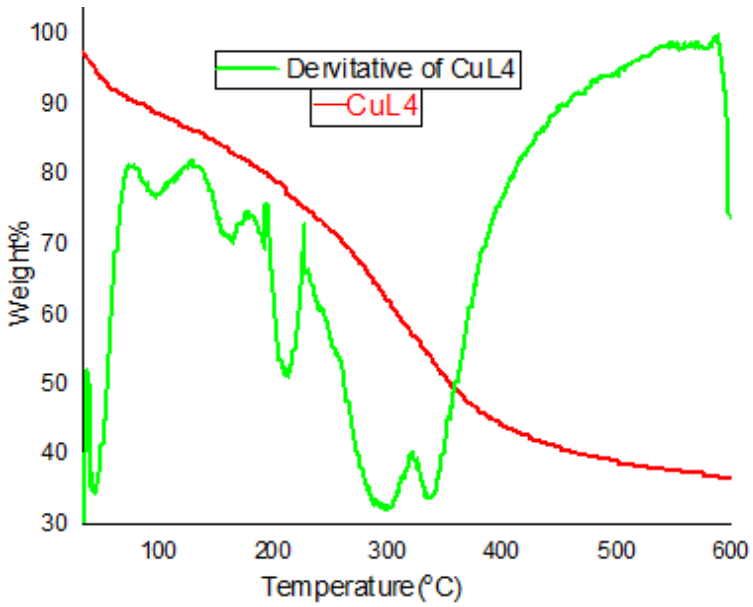

Figure 3.61: TGA and first derivative of CuL4

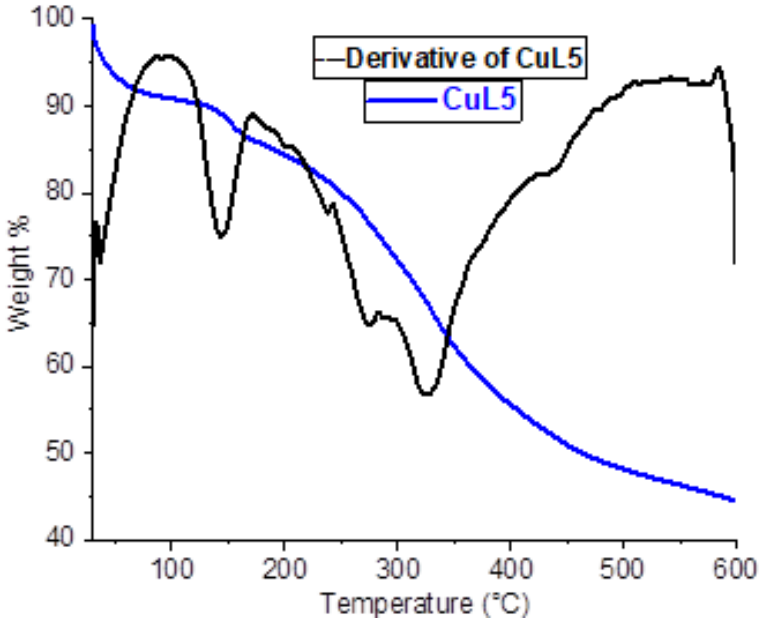

Figure 3.62 TGA and first derivative of CuL5

In the TGA of $[Cu(L6)(H_2O)(Cl)(CH_3OH)_2].4H_2O$, initial loss of non-coordinated water is observed as indicated by the derivative peak in the range of 50-90°C, whereas loss of coordinated water ligands is observed in the temperature range 100-140°Cand loss of chloride ligand is observed at 180-250°C, further decomposition of ligands in the major peak occurs near 300-350°C. Another way to analyze is ash content is % which indicate binding to one copper metal converting into the ash as CuO (Figure 3.63).

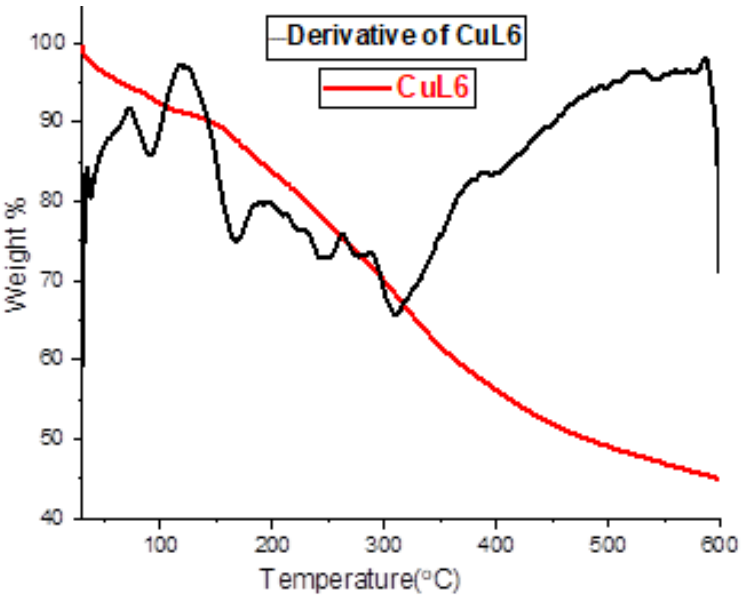

Figure 3.63 TGA and first derivative of CuL6

In the TGA of [Cu(L8)(H_2O)$_2$(CH_3OH)(Cl)], initial loss of coordinated methanol is observed as indicated by the derivative peak in the range of 50-90°C, whereas loss of coordinated water ligands is observed in the temperature range 100-150°C, further decomposition of ligands in the major peak occurs near 300-350°C. Another way to analyze is ash content % which indicate binding to one copper metal converting into the ash as CuO (Figure 3.64).

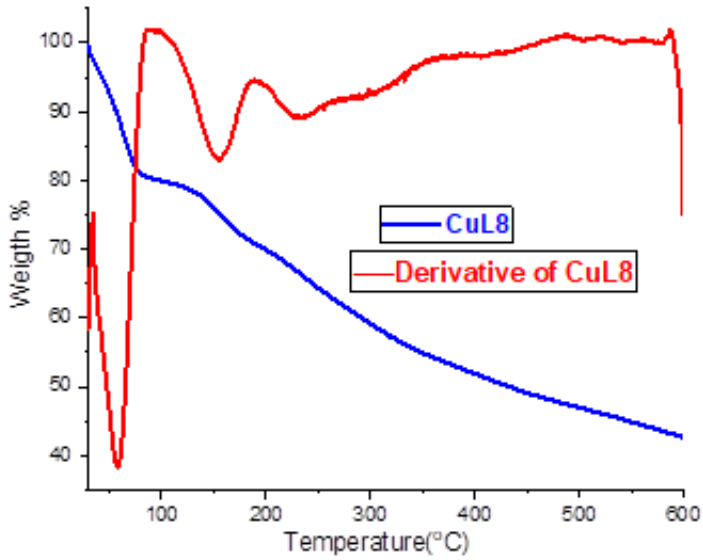

Figure 3.64 TGA and first derivative of CuL8

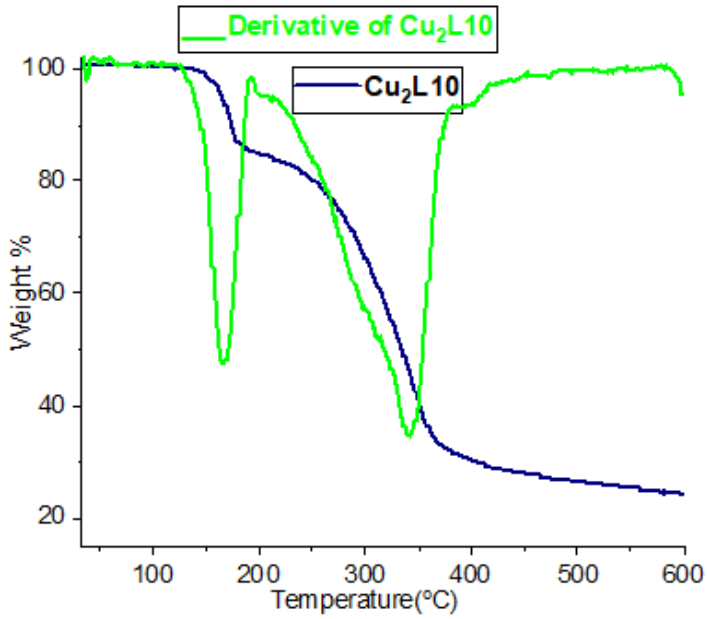

Figure 3.65 TGA and first derivative of Cu_2L10

In the TGA of $[Cu_2(L10)(CH_3CN)Cl_2(H_2O)_5]$, initial loss of coordinated acetonitrile/water is observed as indicated by the derivative peak in the range of 150-190°C, further decomposition of ligands in the major peak occurs near 300-350°C. Another way to analyze is ash content % which indicate binding to two copper metal converting into the ash as 2 CuO (Figure 3.65).

In the TGA of $[Zn_2(L10)(CH_3CN)_2Cl_2(H_2O)_4]$, initial loss of coordinated acetonitrile/water is observed as indicated by the derivative peak in the range of 150-190°C, further decomposition of ligands in the major peak occurs near 300-350°C. Another way to analyze is ash content % which indicate binding to two zinc metal converting into the ash as 2 ZnO (Figure 3.66).

In the TGA of $[Cu_2(L12)(H_2O)_2]$, initial loss of coordinated water is observed as indicated by the derivative peak in the range of 100-150°C, further decomposition of ligands in the major peak occurs near 300-350°C. Significantly no other than loss of water in the TGA derivative curve is obtained which confirm the only coordinated water as ligand. Another way to analyze is ash content is % which indicate binding to two copper metal converting into the ash as 2 CuO.

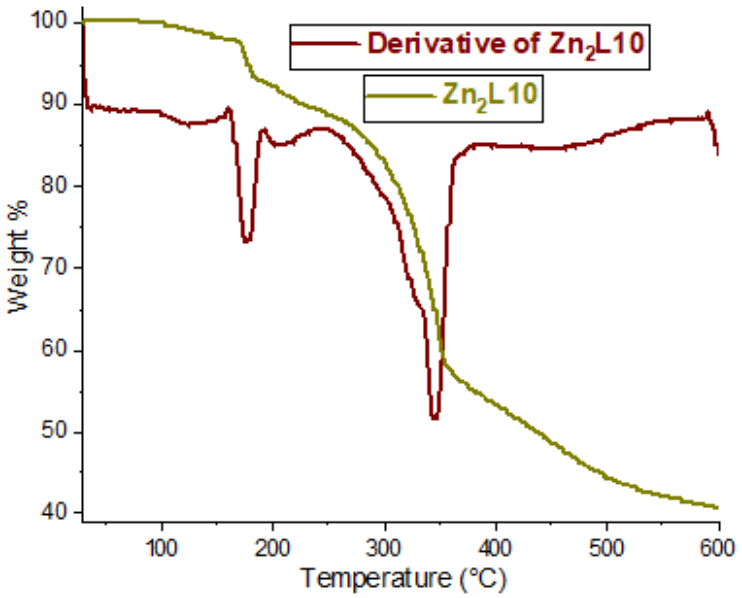

Figure 3.66 TGA and first derivative of Zn_2L10

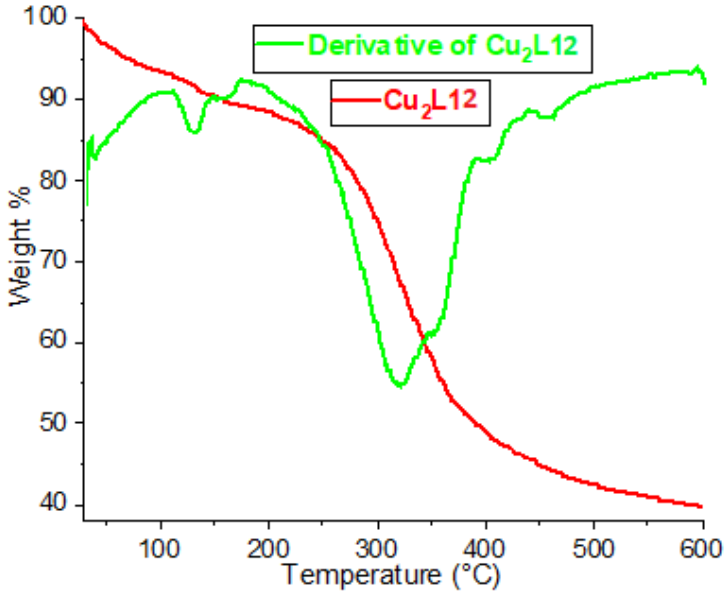

Figure 3.67 TGA and first derivative of Cu_2L12

In the TGA of $[Cu_2(L13)(H_2O)_2]$, initial loss of coordinated water is observed as indicated by the derivative peak in the range of 100-150°C, further decomposition of ligands in the major peak occurs near 300-350°C. Significantly no other than loss of water in the TGA derivative curve is obtained which confirm the only coordinated water as ligand. Another way to analyze is ash content is % which indicate binding to two copper metal converting into the ash as 2 CuO (Figure 3.67).

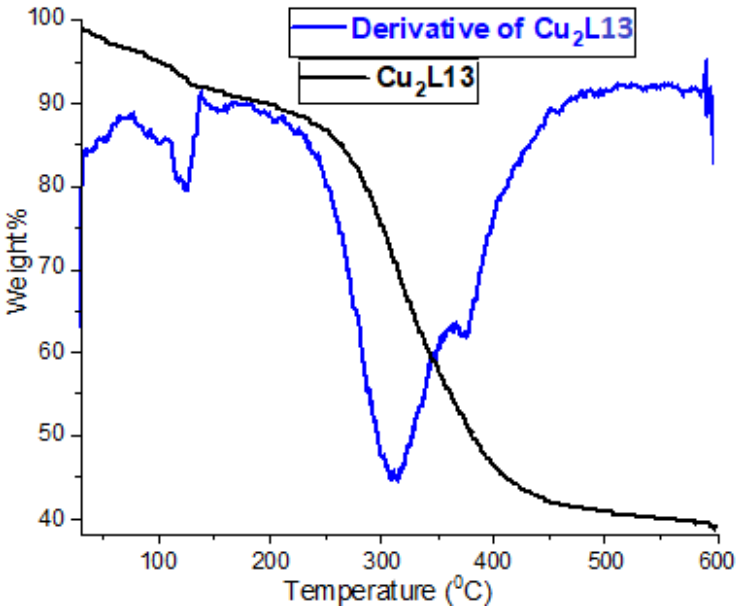

Figure 3.68 TGA and first derivative of Cu_2L13

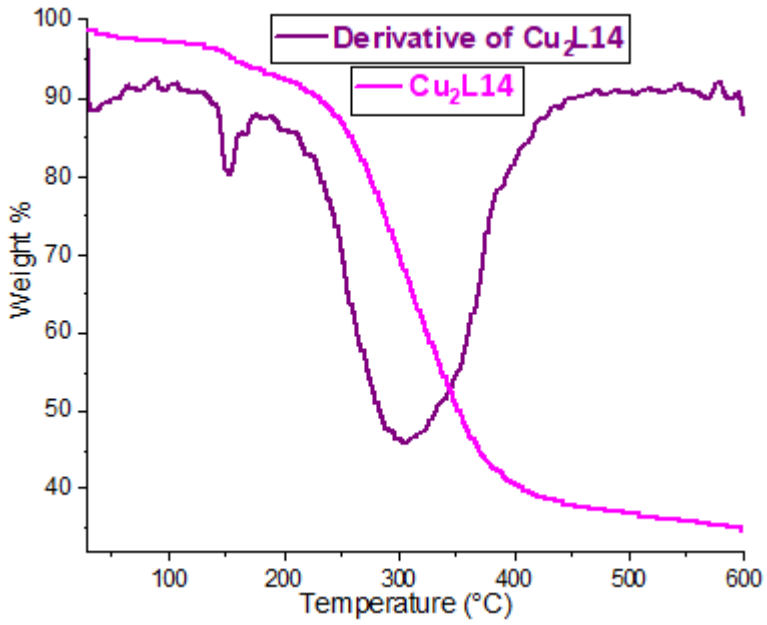

Figure 3.69 TGA and first derivative of Cu_2L14

In the TGA of $[Cu_2(L14)(H_2O)_2]$, initial loss of coordinated water is observed as indicated by the derivative peak in the range of 100-150ºC, further decomposition of ligands in the major peak occurs near 300-350ºC. Significantly no other than loss of water in the TGA derivative curve is obtained which confirm the only coordinated water as ligand. Another way to analyze is ash content is % which indicate binding to two copper metal converting into the ash as 2 CuO (Figure 3.68).

3.4 Conclusion:

In this chapter, we reported the copper and cobalt complexes of ligands and proposed the structures based on physical and spectroscopic measurements. In the UV-vis spectroscopy variation of maximum absorption as well as extinction coefficient correlated that, metal complexes are being formed which was further supported by FTIR spectroscopy. Along with the other vibrational frequencies, M–N and M–O peaks appeared in the range of 400-600 cm^{-1}, there by confirming the formation of metal complexes. Structure of complexes have been proposed based on mass fragmentation patterns. In general copper binds in octahedral coordination mode with the ligands bidentate and other sites occupied by solvent molecule and co-ions. Isotopic distribution pattern obtained for individual complex experimentally were compared with theocratical distribution and were in agreement to the proposed

formula and number of metal ion(s) present in the complexes. Proposed structure of these complexes were supported by additional studies which include molar conductance measurements and thermogravimetric analysis. Molar conductance data suggested the non-ionic nature of metal complexes which were in accordance with proposed formula of complexes. Also, in thermogravimetric analysis TGA curves indicated initial loss of solvent molecule than dissociation of ligand itself. Only one peak before the ligand dissociation was obtained where only water is coordinated to the metal complexes in the temperature range 100-150°C. While other complexes having different solvent like methanol along with water show two or more peaks in the derivative curves. Biological activities and computational studies of these complexes have been discussed in next chapters.

3.5 References:

(1) Alaghaz, A.N.M. and Ammar, R.A., New dimeric cyclodiphosph (V) azane complexes of Cr (III), Co (II), Ni (II), Cu (II), and Zn (II): Preparation, characterization and biological activity studies. *European journal of medicinal chemistry*, **2010**, *45* (4), 1314-1322.https://doi.org/10.1016/j.ejmech.2009.12.008

(2) Alaghaz, A.N.M., El-Sayed, B.A., El-Henawy, A.A. and Ammar, R.A., Synthesis, spectroscopic characterization, potentiometric studies, cytotoxic studies and molecular docking studies of DNA binding of transition metal complexes with 1, 1-diaminopropane–Schiff base. *Journal of Molecular Structure*, **2013**, *1035*, 83-93. https://doi.org/10.1016/j.molstruc.2012.09.032

(3) Chandra, S., Jain, D. and Sharma, A.K., EPR, mass, electronic, IR spectroscopic and thermal studies of bimetallic copper (II) complexes with tetradentate ligand, 1,4-diformylpiperazine bis(carbohydrazone). *Spectrochimica Acta Part A: Molecular and Biomolecular Spectroscopy*, **2009**, *71*(5), 1712-1719.https://doi.org/10.1016/j.saa.2008.06.028

(4) Mahmoud, W.H., Deghadi, R.G. and Mohamed, G.G., Preparation, geometric structure, molecular docking thermal and spectroscopic characterization of novel Schiff base ligand and its metal chelates. *Journal of Thermal Analysis*

and Calorimetry, **2017**, *127*(3), 2149-2171.https://doi.org/10.1007/s10973-016-5826-7

(5) Ali, I., Wani, W.A. and Saleem, K., Empirical formulae to molecular structures of metal complexes by molar conductance. *Synthesis and Reactivity in Inorganic, Metal-Organic, and Nano-Metal Chemistry*, **2013**, *43*(9), 1162-1170. https://doi.org/10.1080/15533174.2012.756898

(6) Tas, E., Kilic, A., Durgun, M., Küpecik, L., Yilmaz, I. and Arslan, S., Cu (II), Co (II), Ni (II), Mn (II), and Fe (II) metal complexes containing N, N′-(3, 4-diaminobenzophenon)-3, 5-But2-salicylaldimine ligand: synthesis, structural characterization, thermal properties, electrochemistry, and spectroelectrochemistry. *Spectrochimica Acta Part A: Molecular and Biomolecular Spectroscopy*, **2010**, *75*(2), 811-818. https://doi.org/10.1016/j.saa.2009.12.002

(7) Sway, M.I. and Samara, N., Molar conductance of the complexes of 18-crown-6 with alkaline earth metal ions in methanol+ water. *Journal of Chemical & Engineering Data*, **1999**, *44*(2), 343-348. https://doi.org/10.1021/je980160e

(8) Pasdar, H., Hedayati Saghavaz, B., Foroughifar, N. and Davallo, M., Synthesis, characterization and antibacterial activity of novel 1, 3-diethyl-1, 3-bis (4-nitrophenyl) urea and its metal (ii) complexes. *Molecules*, **2017**, *22*(12), p.2125. doi:10.3390/molecules22122125.

(9) Abd El-Wahed, M.G., Refat, M.S. and El-Megharbel, S.M., Synthesis, spectroscopic and thermal characterization of some transition metal complexes of folic acid. *Spectrochimica Acta Part A: Molecular and Biomolecular Spectroscopy*, **2008**, *70*(4), 916-922. https://doi.org/10.1016/j.saa.2007.10.008

(10) Refat, M.S., El-Deen, I.M., Zein, M.A., Adam, A.M.A. and Kobeasy, M.I., Spectroscopic, structural and electrical conductivity studies of Co (II), Ni (II) and Cu (II) complexes derived from 4-acetylpyridine with thiosemicarbazide. *International Journal of Electrochemical Science*, **2013**, *8*(7), 9894-9917. (11) Saadatkhah, N., Carillo Garcia, A., Ackermann, S., Leclerc, P., Latifi, M., Samih, S., Patience, G.S. and Chaouki, J., Experimental

methods in chemical engineering: thermogravimetric analysis—TGA. *The Canadian Journal of Chemical Engineering*, **2020**, *98*(1), 34-43.

(11) Tas, E., Aslanoglu, M., Kilic, A. and Kara, Z., Synthesis, spectroscopic and electrochemical studies of copper (II) and cobalt (II) complexes of three unsymmetrical vic-dioximes ligands. *Journal of Coordination Chemistry*, **2006**, *59*(8), 861-872. https://doi.org/10.1080/00958970500412206

(12) Toledo, M., **2001**, Interpreting TGA Curves. *Retrieved from Mettler Toledo:* https://www.mt.com/us/en/home/supportive_content/matchar_apps/MatChar_UC131. htm, 1.

(13) Thomas L.C., Schmidt S.J. (2017) Thermal Analysis. In: *Nielsen S. (eds) Food Analysis. Food Science Text Series*. Springer, Cham. https://doi.org/10.1007/978-3-319-45776-5_30

(14) Manjunath, M., Kulkarni, A.D., Bagihalli, G.B., Malladi, S. and Patil, S.A., Bio-important antipyrine derived Schiff bases and their transition metal complexes: synthesis, spectroscopic characterization, antimicrobial, anthelmintic and DNA cleavage investigation. *Journal of Molecular Structure*, **2017**, *1127*, 314-321. https://doi.org/10.1016/j.molstruc.2016.07.123

(15) Eğlence-Bakır, S., Şahin, M., Salt, B.Z., Tüzün, E., Kara, E.M., Atun, G., Çavuş, S. and Kızılcıklı, İ., Palladium (II) complexes with thione and thioalkylated thiosemicarbazones: Electrochemical, antimicrobial and thermogravimetric investigations. *Spectrochimica Acta Part A: Molecular and Biomolecular Spectroscopy*, **2020**, *237*, p.118358. https://doi.org/10.1016/j.saa.2020.118358

(16) Aggoun, D., Fernández-García, M., López, D., Bouzerafa, B., Ouennoughi, Y., Setifi, F. and Ourari, A., New nickel (II) and copper (II) bidentate Schiff base complexes, derived from dihalogenated salicylaldehyde and alkylamine: Synthesis, spectroscopic, thermogravimetry, crystallographic determination and electrochemical studies. *Polyhedron*, **2020**, *187*, p.114640. https://doi.org/10.1016/j.poly.2020.114640

(17) Bouzerafa, B., Ourari, A., Aggoun, D., Ruiz-Rosas, R., Ouennoughi, Y. and Morallon, E., Novel nickel (II) and manganese (III) complexes with bidentate

Schiff-base ligand: synthesis, spectral, thermogravimetry, electrochemical and electrocatalytical properties. *Research on Chemical Intermediates*, **2016**, *42*(5), 4839-4858. DOI 10.1007/s11164-015-2325-6

(18) Bouzerafa, B., Aggoun, D., Ouennoughi, Y., Ourari, A., Ruiz-Rosas, R., Morallon, E. and Mubarak, M.S., Synthesis, spectral characterization and study of thermal behavior kinetics by thermogravimetric analysis of metal complexes derived from salicylaldehyde and alkylamine. *Journal of Molecular Structure*, **2017**, *1142*, 48-57. https://doi.org/10.1016/j.molstruc.2017.04.029

(19) Kianfar, A.H., Ramazani, S., Fath, R.H. and Roushani, M., Synthesis, spectroscopy, electrochemistry and thermogravimetry of copper (II) tridentate Schiff base complexes, theoretical study of the structures of compounds and kinetic study of the tautomerism reactions by ab initio calculations. *Spectrochimica Acta Part A: Molecular and Biomolecular Spectroscopy*, **2013**, *105*, 374-382. https://doi.org/10.1016/j.saa.2012.12.010

(20) Rodembusch, F.S., Brand, F.R., Corrêa, D.S., Pocos, J.C., Martinelli, M. and Stefani, V., Transition metal complexes from 2-(2′-hydroxyphenyl) benzoxazole: A spectroscopic and thermogravimetric stability study. *Materials chemistry and physics*, **2005**, *92*(2-3), 389-393. https://doi.org/10.1016/j.matchemphys.2005.01.049

(21) Kavitha, N. and Lakshmi, P.A., Synthesis, characterization and thermogravimetric analysis of Co (II), Ni (II), Cu (II) and Zn (II) complexes supported by ONNO tetradentate Schiff base ligand derived from hydrazino benzoxazine. *Journal of Saudi Chemical Society*, **2017**, *21*, S457-S466. https://doi.org/10.1016/j.jscs.2015.01.003.

3.7 Annexure:

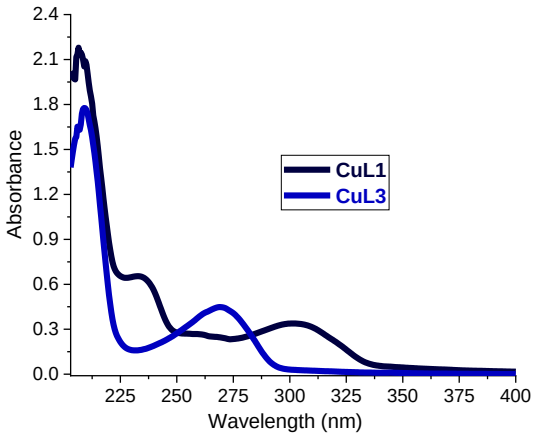

Annexure 3(a): UV-vis spectra CuL1/CuL3

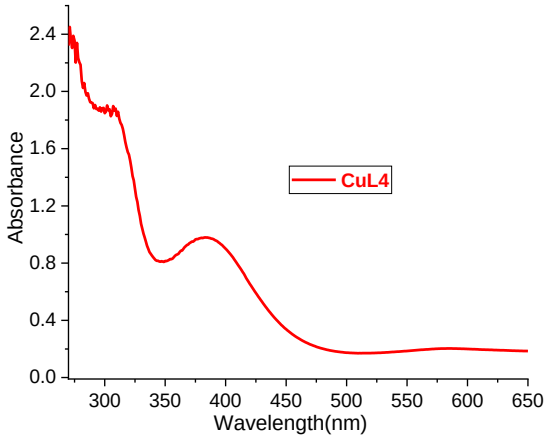

Annexure 3(b): UV-vis spectra CuL4

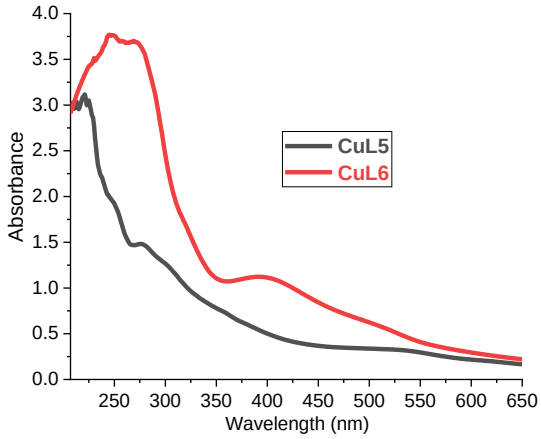

Annexure 3(c): UV-vis spectra CuL5/CuL6

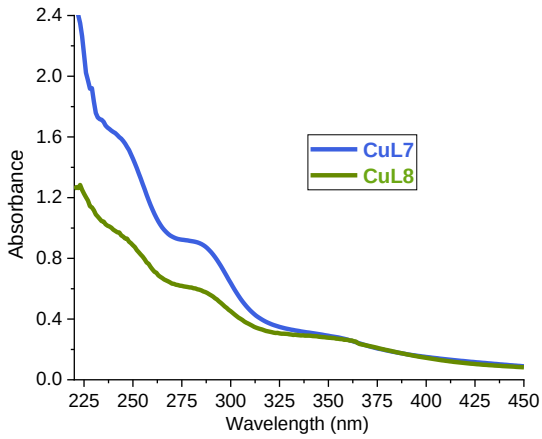

Annexure 3(d): UV-vis of CuL7/CuL8

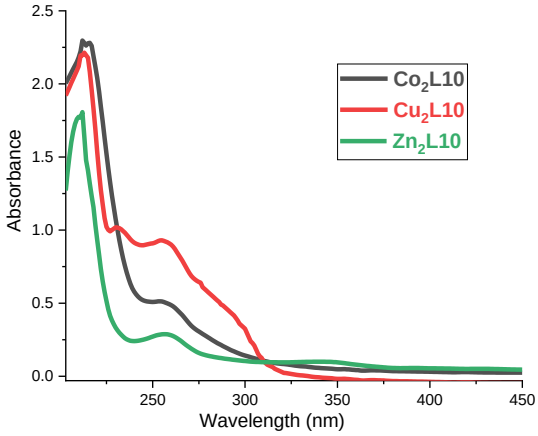

Annexure 3(e): UV-vis spectra M_2L10

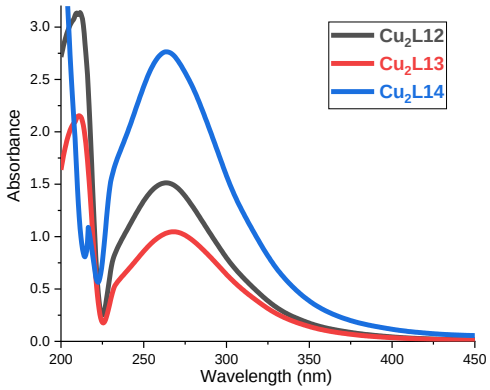

Annexure 3(f): UV-vis of Cu_2L12-14

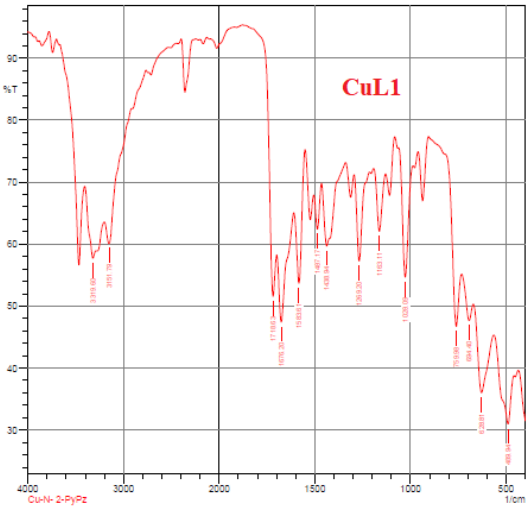

Annexure 3(g): IR spectra of CuL1

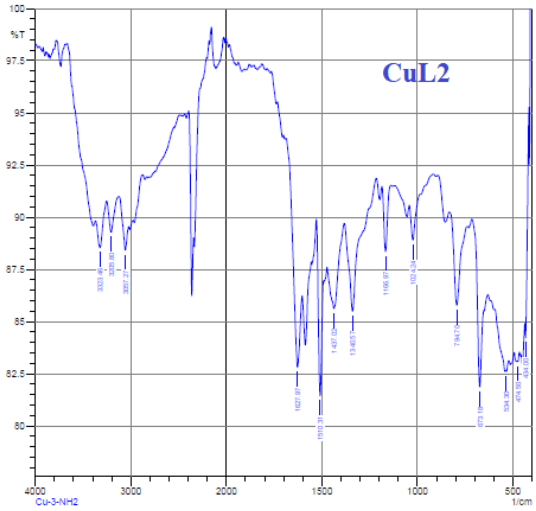

Annexure 3(h): IR spectra of CuL2

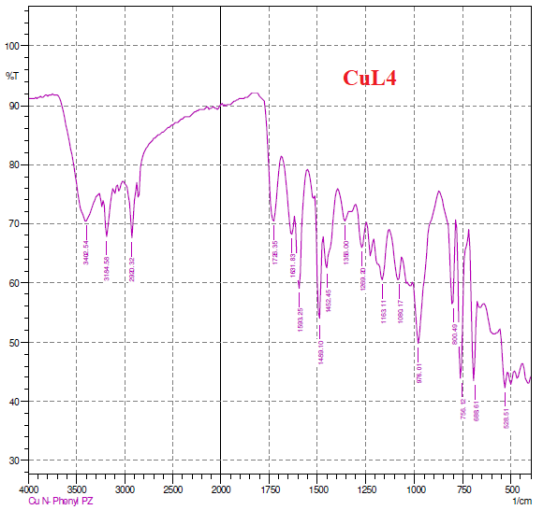

Annexure 3(i): IR spectra of CuL4

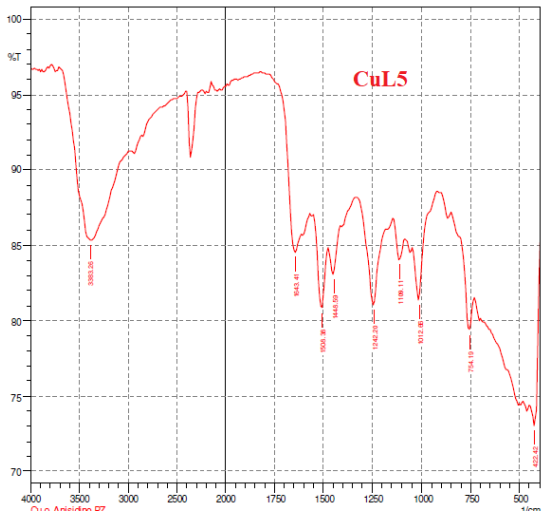

Annexure 3(j): IR spectra of CuL5

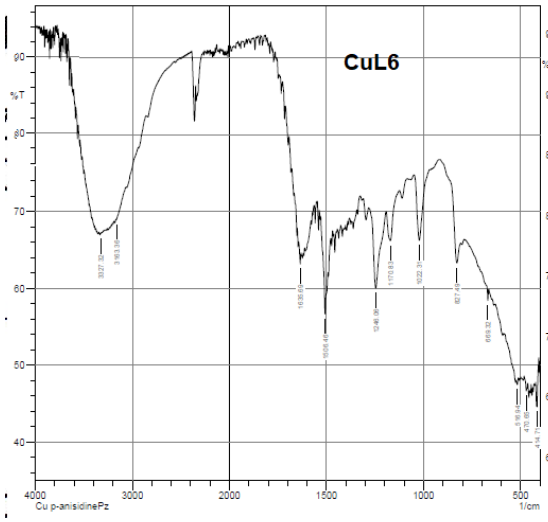

Annexure 3(k): IR spectra of CuL6

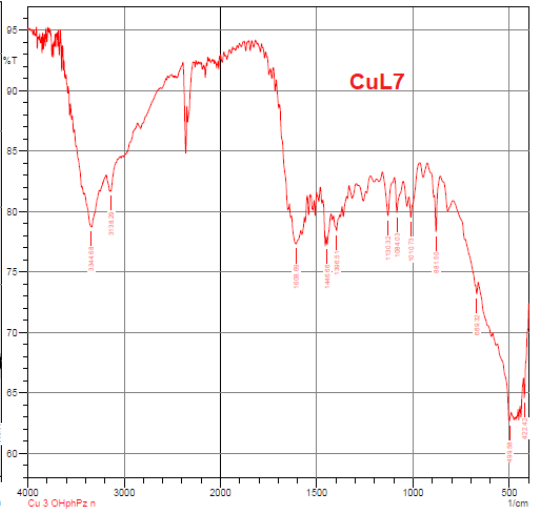

Annexure 3(l): IR spectra of CuL7

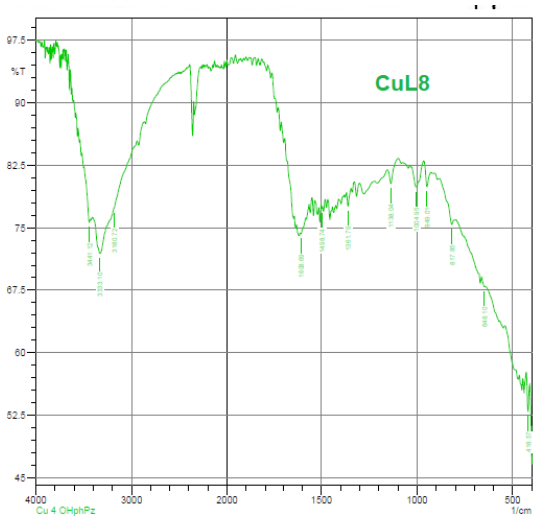

Annexure 3(m): IR spectra of CuL8

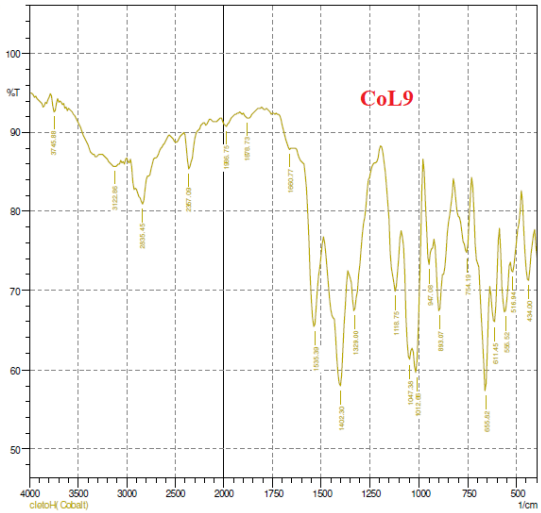

Annexure 3(n): IR spectra of CoL9

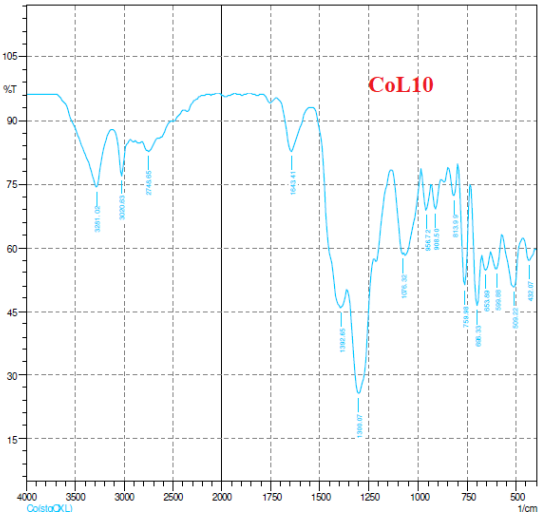

Annexure 3(m): IR spectra of Co_2L10

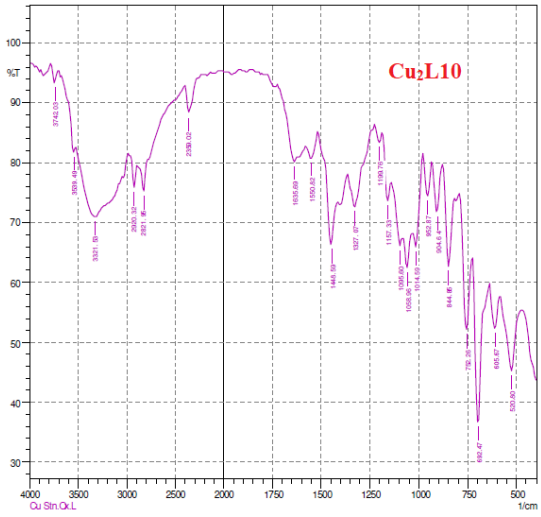

Annexure 3(n): IR spectra of Cu_2L10

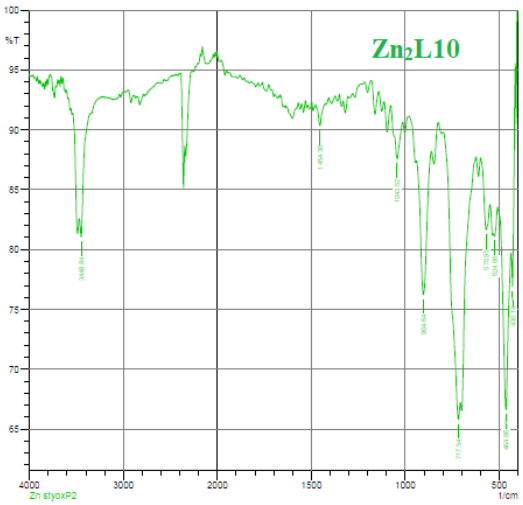

Annexure 3(o): IR spectra of Zn_2L10

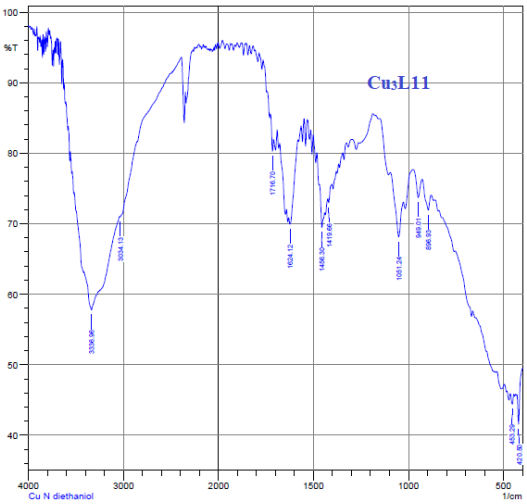

Annexure 3(p): IR spectra of Cu_3L11

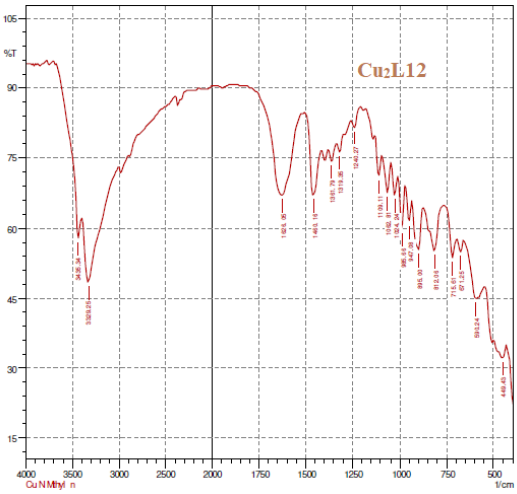

Annexure 3(q): IR spectra of Cu_2L12

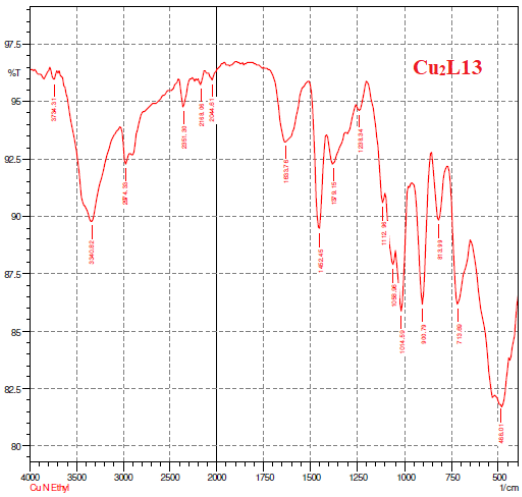

Annexure 3(r): IR spectra of Cu_2L13

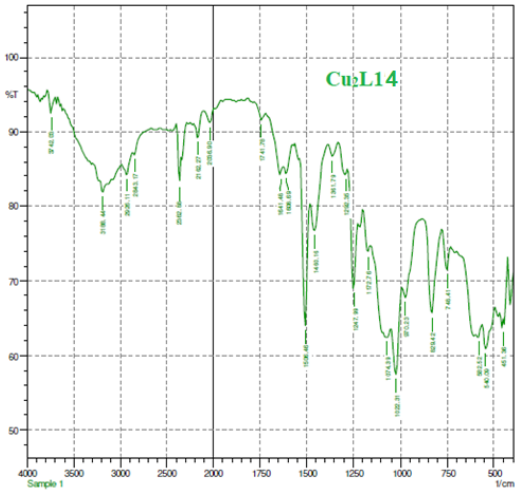

Annexure 3(s): IR spectra of Cu_2L14

CHAPTER 4

BIOLOGICAL ACTIVITIES OF SYNTHESIZED LIGANDS AND METAL COMPLEXES

4.1 Antibacterial Assays

Agar well diffusion assay has been used to evaluate the antibacterial action of synthesized ligands and their metal complexes. The concentrations of the samples were maintained by dissolving 5 mg in 1 ml of DMSO. The bacterial culture was homogeneously applied on Mueller Hinton agar (MHA)with sterile cotton swabs. For cutting of wells in agar plates sterilized cork borer of 9 mm diameter was used. Using micropipette 100 µL of each sample was loaded into the wells. The plates were incubated at 37°C for 24 h for bacterial strain. DMSO was used as negative control in well diffusion method. Agar disc diffusion method was used to evaluate antibacterial activity of standard antibiotic drug amikacin against test bacteria. Zone of inhibition was measured to determine the antibacterial activities surrounding each well/disc. Each experiment was performed three times in array to minimize the deviations (Table 1). Bacterial strain used in this study were *Escherichia coli* and *Staphylococcus aureus*.[1,2]

Table 4.1: Antibacterial activity of ligand and complexes

Zone of Inhibition (mm) ± Standard Deviation		
Code	***E. coli***	***S. aureus***
HL1	-	-
CuL1	15.16±0.58	11.26±0.58
HL2	-	-
CuL2	25.33±0.58	28.50±0.50
HL3	-	-
CuL3	23.66±0.58	21.30±0.58
HL4	10.33±0.58	7.45±0.58
CuL4	18.66±0.58	13.23±0.58
HL5	22.00±0.36	-
CuL5	14.00±0.50	21.28±0.36
HL6	-	-
CuL6	13.66±0.58	14.40±0.36
HL7	12.23±0.25	-
CuL7	16.80±0.25	8.45±0.36
HL8	-	-
CuL8	10.01±0.25	4.12±0.36
H_2L9	7.15±0.36	-
CoL9	7.15±0.36	5.12±0.36
H_2L10	6.55±0.58	4.11±0.25

Cu_2L10	27.22±0.58	24.55±0.25
Co_2L10	26.88±0.58	12.44±0.25
H_6L11	11.25±0.58	2.11±0.36
Cu_3L11	24.89±0.58	29.05±0.36
H_4L12	5.56±0.58	5.65±0.36
Cu_2L12	22.55±0.58	24.45±0.36
H_4L13	3.22±0.58	2.98±0.25
Cu_2L13	24.65±0.58	28.25±0.25
H_4L14	12.45±0.58	10.05±0.76
Cu_2L14	24.67±0.58	30.15±0.35
Amikacin	21.50±0.50	24.83±0.76
DMSO	Nil	Nil

Result of antibacterial studies (Figure 4.1-4.6) indicates ligands HL1-3, HL6, HL8 were not active against both the bacterial strain. Activities of all other ligands were very less or negligible. While the all the metal complexes were active against both the strain. Complexes CuL2, CuL3, Cu_2L10, Co_2L10, Cu_3L11, Cu_2L12, Cu_2L13, Cu_2L14 were more active than standard drug amikacin against *E. Coli*. Almost similar trend for these metal complexes were also observed against S. Aureus except Co_2L10 which was less active than standard. Structure based biocidal effect of activity of *E. Coli* has also been observed having the different substitution with similar basic skeleton. Asymmetric ligands with pyridyl group (HL1-3) did not show any activity. Ligand with phenyl ring (HL4) showed moderate activity and the activity was increased in ligands having ortho or meta-substitution (HL5, HL7) while decreased for ligands with para-substitution (HL6, HL8). The effect of substituent variations in multidentate ligands (H_6L11-H_4L14) were also observed where ligand H_6L11 showed moderate activity. Activity decreased in H_4L12 and H_4L13 with methyl and ethyl substitution and increased in benzyl substitution (H_4L14). Against *S. Aureus,* ligands were not active irrespective of structural variation. All the metal complexes were more active than their corresponding ligands which indicate binding of metal ion increases the activity. By increase in no of metal ion, activity was increased and become greater than standard drug. Thus, a range of variation can be seen in the antibacterial activities of ligands and their complexes and the major factor playing the role in the activity are hydrophilicity and hydrophobicity and their balance along with structural variations.

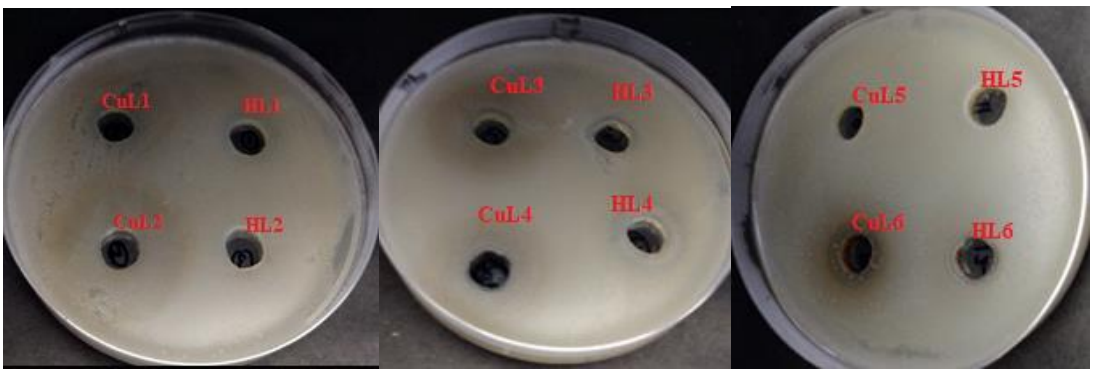

Figure 4.1: Antibacterial assay against E *Coli* of ligands (HL1-HL6) and their metal complexes (CuL1-CuL6)

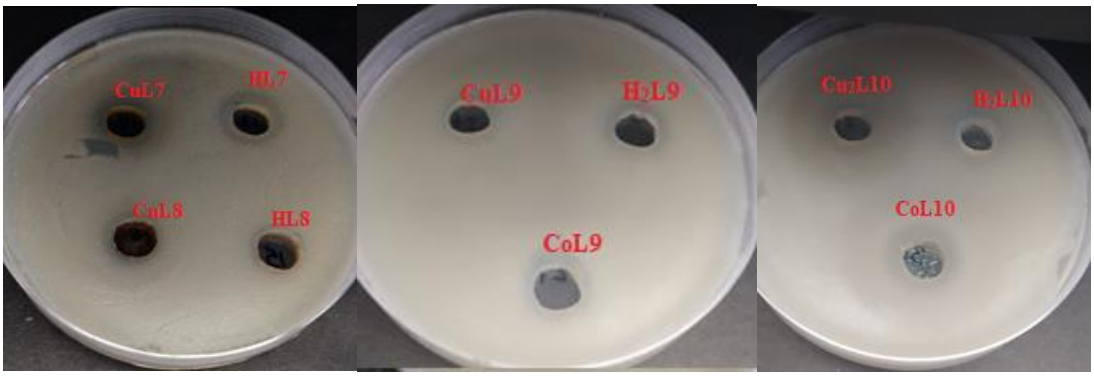

Figure 4.2: Antibacterial assay against E *Coli* of ligands (HL7-H_2L10) and their metal complexes (CuL7-Co_2L10)

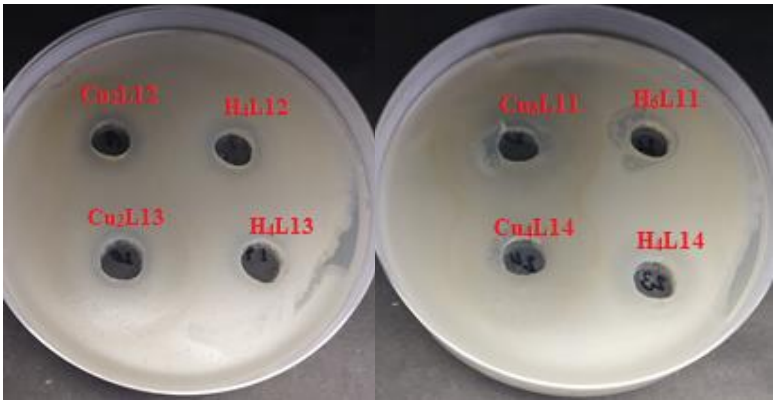

Figure 4.3: Antibacterial assay against E *Coli* of ligands(H_6L11-H_4L14) and their metal complexes (Cu_3L11-Cu_2L14)

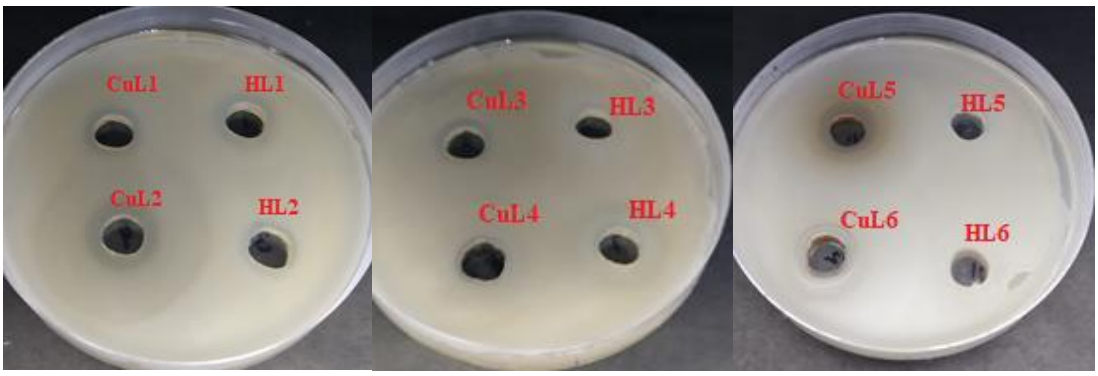

Figure 4.4: Antibacterial assay against S *Aureus* of ligands (HL1-HL6) and their metal complexes (CuL1-CuL6)

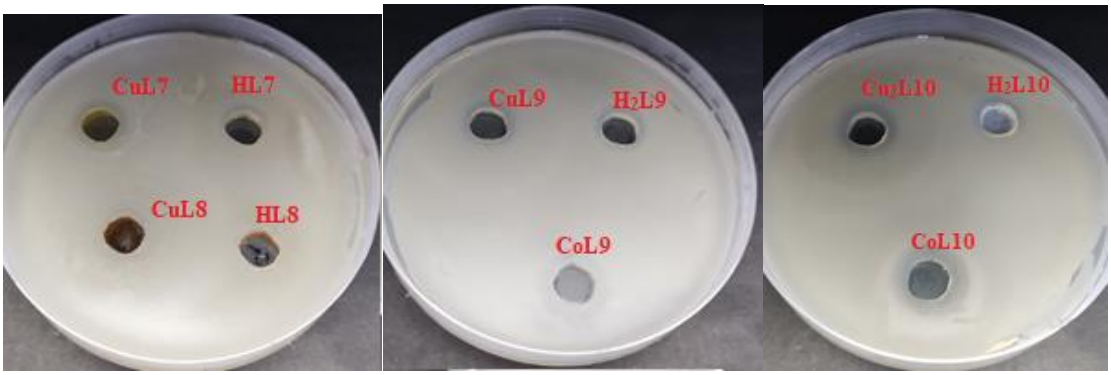

Figure 4.5: Antibacterial assay against S *Aureus* of ligands (HL7-H_2L10) and their metal complexes (CuL7-Co_2L10)

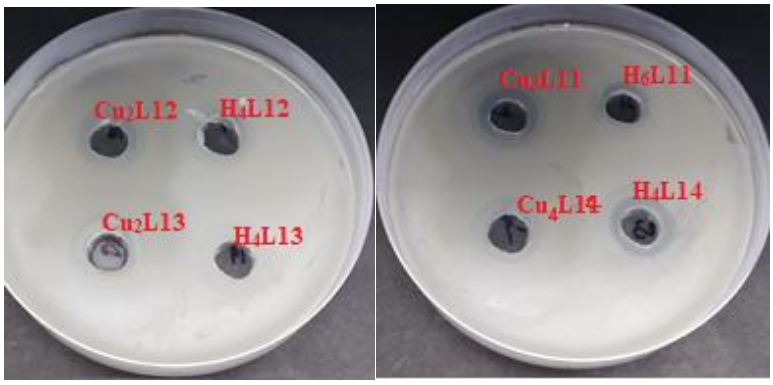

Figure 4.6: Antibacterial assay against S *Aureus* of ligands (H_6L11-H_4L14) and their metal complexes (Cu_3L11-Cu_2L14)

4.2 Antioxidant Activity: DPPH Method

Antioxidant compounds protects cells against free radicals and play role in cancer disease, heart and other diseases. Free radicals are produced in our body during metabolic activities or radiation. Compounds such as vitamin C (Ascorbic

acid), vitamin E and rosmarinic acid etc, are some common antioxidants used in foods and cosmetic industryto aids stability of products.[3-5]Antioxidants compounds are defined as reagents which limit of the oxidation of lipids, proteins, DNA or other molecules by blocking chain propagation stepin oxidative reactions.Primary antioxidants compounds prevent free radicals directly whereas, secondary antioxidant compounds indirectly scavenge free radicals' formation via Fenton's reaction.[6-10]

DPPH (Diphenylpicrylhydrazyl) act as stable free radical to analyze the antioxidant activityof metal complexes. The DPPH scavenging assay have advantages over the other methods owing to high sensitivity with minimum use of samples. DPPH accept an electron or hydrogen radical to become a stable diamagnetic molecule (Figure 4.7).[11-17]

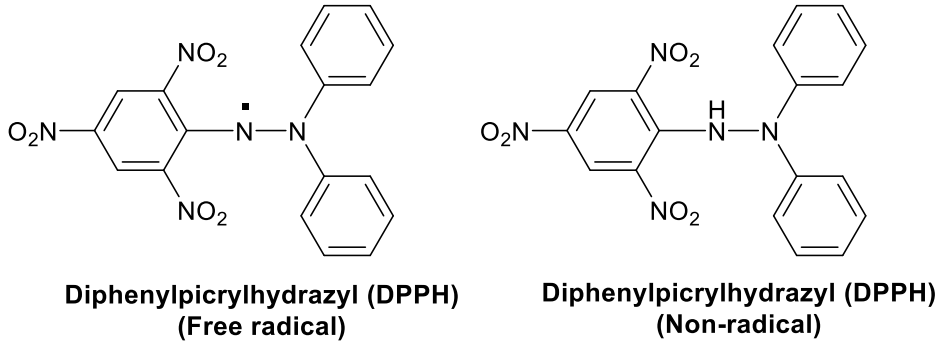

Figure 4.7**:** Structure of DPPH in radical and non-radical form

Systematic Procedure[18,19]

Preparation of stock solutions of compounds

In order to study the antioxidant behaviour of synthesized compounds, the studies were carried out preparing different concentration solutions of respective compound in methanol and which were subjected to mix up with standard DPPH solution and change in absorption spectrum under UV-Visible range was recorded.To prepare stock solutions and other concentrations the needed chemicals were methanol which acts as solvent, DPPH acts as stable free radical and different prepared complexes whose antioxidant activity have to detect.To prepare 1000µM stock solution, known amount of compound was poured in volumetric flask(100ml) and methanol was added to make up volume.Subsequent concentrations were prepared as below (Table 4.2).

Table 4.2: Preparation of different concentration of sample under study

Concentration (µM)	Stocksolution(ml)	Methanol(ml)	Make up to volume (ml)
10	0.1	9.9	10
50	0.5	9.5	10
100	1.0	9.0	10
200	2.0	8.0	10
400	4.0	6.0	10
600	6.0	4.0	10
800	8.0	2.0	10
1000	10.0	0.0	10

For the preparation of 100µM solution of DPPH, 3.94 mg of DPPH was dissolved in 100 ml of methanol in a volumetric flask and then solvent was added to make up volume (Table 4.3).

Table 4.3: Different concentration of complexes in solution and way of mixing with DPPH solution (50µM in overall solution)

Sr No	Concentration of complex in solution (µM)	Volume taken of complex (ml)	Volume of 100µM DPPH (ml)	Time of mixing (min)
1	5	2.0	2.0	30
2	25	2.0	2.0	30
3	50	2.0	2.0	30
4	100	2.0	2.0	30
5	200	2.0	2.0	30
6	300	2.0	2.0	30
7	400	2.0	2.0	30
8	500	2.0	2.0	30

Different solutions of prepared concentration of sample were taken in different test tubes as shown in the table 4.3. After mixing solutions with 100 µM DPPH, UV-vis spectrum and absorbance was recordedafter wait for 30 minutes incubation. Similar

above procedure was applied for measuring the absorbance of ascorbic acid which act as standard. Antioxidant activity was measured in term of % inhibition, calculated from the formula given below.[20-22]

$$\% \text{ Inhibition} = 1 - \frac{\mathbf{Abs}_{\boldsymbol{sample}} - \mathbf{Abs}_{\boldsymbol{blank}}}{\mathbf{Abs}_{\boldsymbol{control}} - \mathbf{Abs}_{\boldsymbol{blank}}} \times 100$$

Where

$\mathbf{Abs}_{\boldsymbol{sample}}$ = Absorbance of sample at 516nm

$\mathbf{Abs}_{\boldsymbol{control}}$ = Absorbance of Ascorbic acid at 516nm

$\mathbf{Abs}_{\boldsymbol{blank}}$ = Absorbance of blank at 516nm

Observed data and all calculation have been presented in the table 4.4. UV-vis graph of antioxidant activity of complexes along with their linear fit curve and visual colour changes are shown in the figures 4.8-4.13. The result of antioxidant activity performed for all complexes, but only few CuL4, Cu_2L10, Cu_3L11, Cu_2L12-14 complexes have showed greater % inhibition as compared to ascorbic acid. Exact mechanism of their inhibitory action still remains unexposed and can be explored in future.

Table 4.4: Antioxidant activity data for complexes along with their % inhibition

Sample Code	**Conc. (µM)**	**Abs** *sample*	**Abs** *blank*	**Abs** *control*	**% Inhibition**	**Sample Code**	**Conc. (µM)**	**Abs** *sample*	**Abs** *blank*	**Abs** *control*	**% Inhibition**
CuL4	5	0.457	0.659	0.48	-18.12	Cu_2L10	5	0.615	0.659	0.48	25.47
	25	0.198	0.659	0.26	-15.5		25	0.492	0.659	0.26	35.82
	50	0.114	0.659	0.057	9.46		50	0.46	0.659	0.057	42.72
	100	0.104	0.659	0.055	8.11		100	0.436	0.659	0.055	53.11
	200	0.148	0.659	0.032	18.50		200	0.365	0.659	0.032	63.07
	300	0.201	0.659	0.027	27.53		300	0.297	0.659	0.027	66.94
	400	0.243	0.659	0.025	34.38		400	0.252	0.659	0.025	70.34
	500	0.305	0.659	0.023	44.33		500	0.185	0.659	0.023	91.33
Cu_3L11	5	0.5684	0.659	0.48	11.71	Cu_2L12	5	0.615	0.659	0.48	74.26
	25	0.5054	0.659	0.26	31.01		25	0.649	0.659	0.26	97.49
	50	0.425	0.659	0.057	34.50		50	0.616	0.659	0.057	92.85
	100	0.3597	0.659	0.055	42.55		100	0.612	0.659	0.055	92.21

	200	0.2988	0.659	0.032	50.45		200	0.546	0.659	0.032	81.97
	300	0.22302	0.659	0.027	61.12		300	0.466	0.659	0.027	69.46
	400	0.1625	0.659	0.025	72.73		400	0.418	0.659	0.025	61.98
	500	0.0975	0.659	0.023	82.15		500	0.374	0.659	0.023	55.18
Cu_2L14	5	0.626	0.659	0.48	80.70						
	25	0.611	0.659	0.26	87.96						
	50	0.572	0.659	0.057	85.54						
	100	0.536	0.659	0.055	79.42						
	200	0.464	0.659	0.032	68.89						
	300	0.420	0.659	0.027	62.18						
	400	0.399	0.659	0.025	58.99						
	500	0.388	0.659	0.023	57.38						

Figure 4.8: Visual color change of DPPH by ascorbic acid after 30 min (acting as standard)

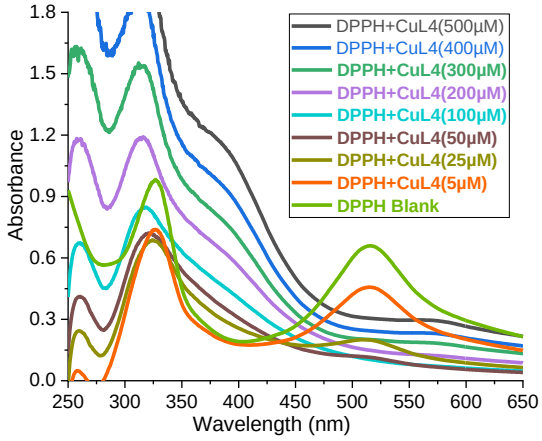

(a)

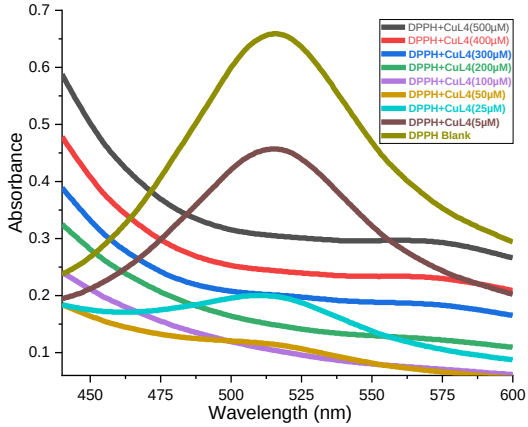

(b)

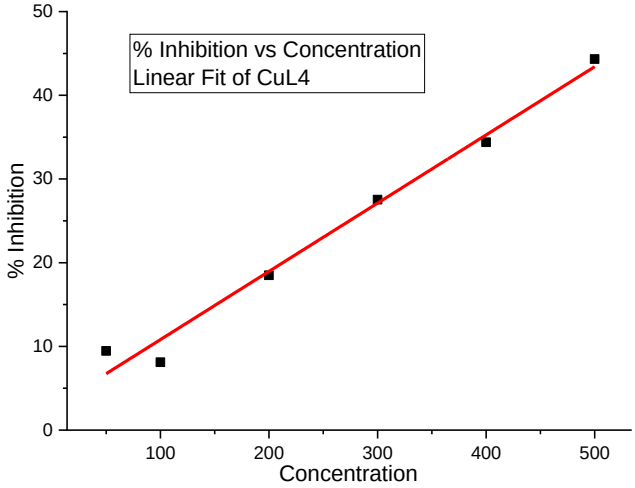

(c)

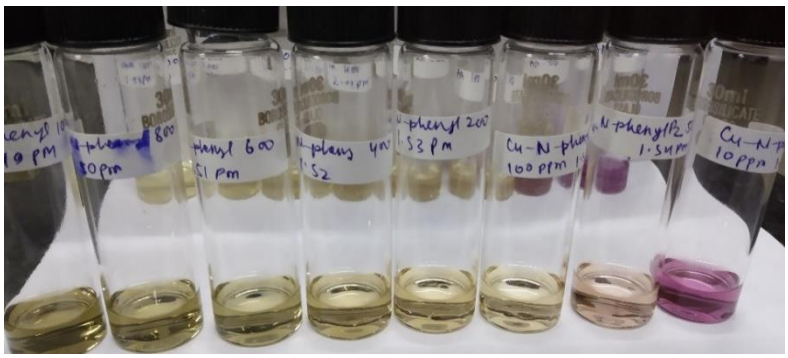

(d)

Figure 4.9: (a) UV-vis spectra of action of CuL4 with DPPH (b) UV Spectra(enlarged) showing absorbance changes at 516 nm (c) Linear fit of % inhibition vs concentration (d) Visual color change of DPPH by CuL4 after 30 min

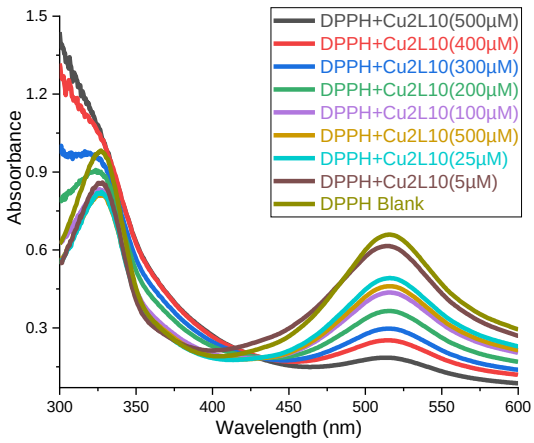

(a)

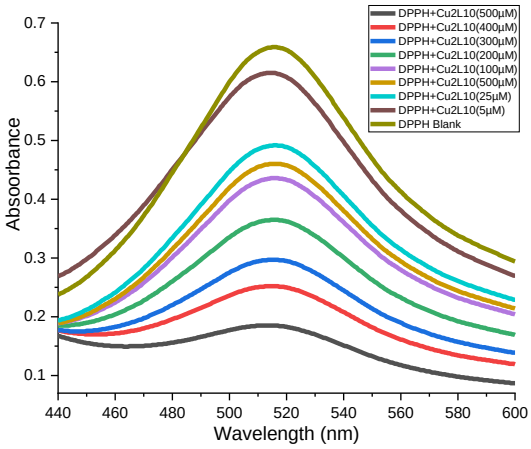

(b)

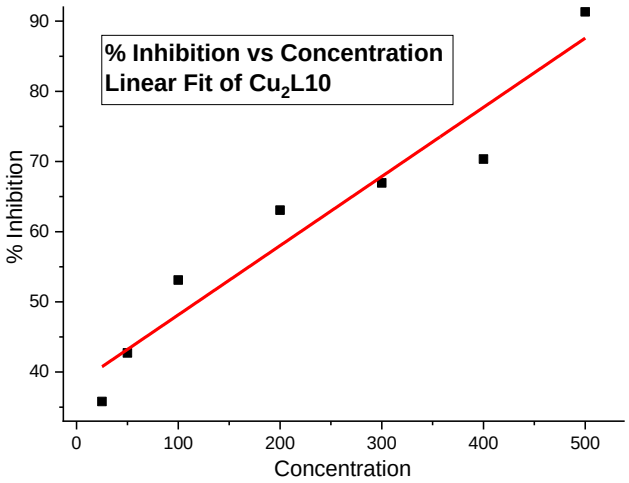

(c)

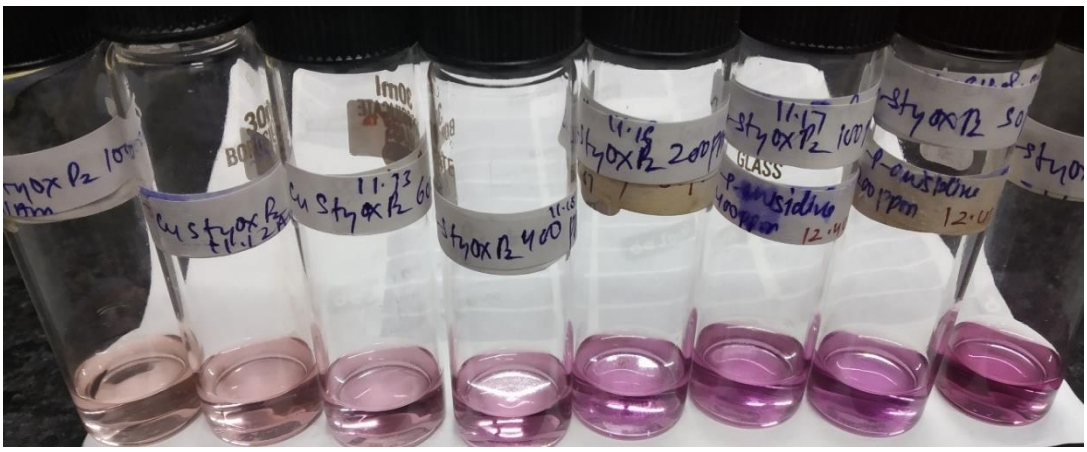

(d)

Figure 4.10: (a) UV-vis spectra of action of Cu_2L10 with DPPH (b) UV Spectra(enlarged) showing absorbance changes at 516 nm (c) Linear fit of % inhibition vs concentration (d) Visual color change of DPPH by Cu_2L10 after 30 min

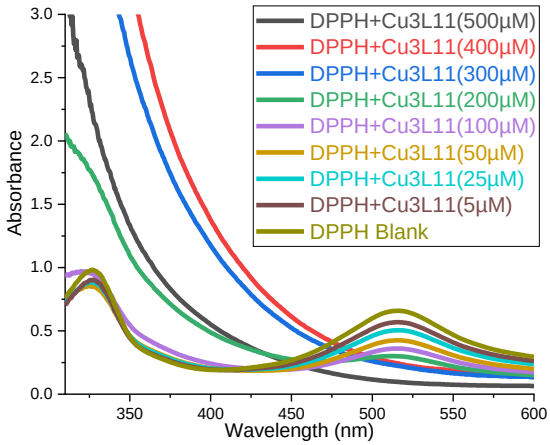

(a)

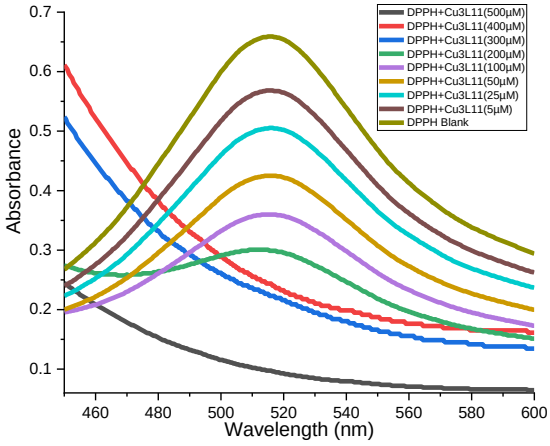

(b)

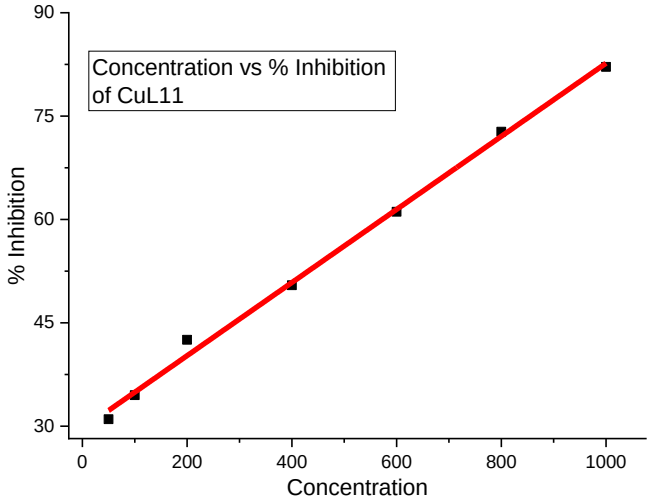

(c)

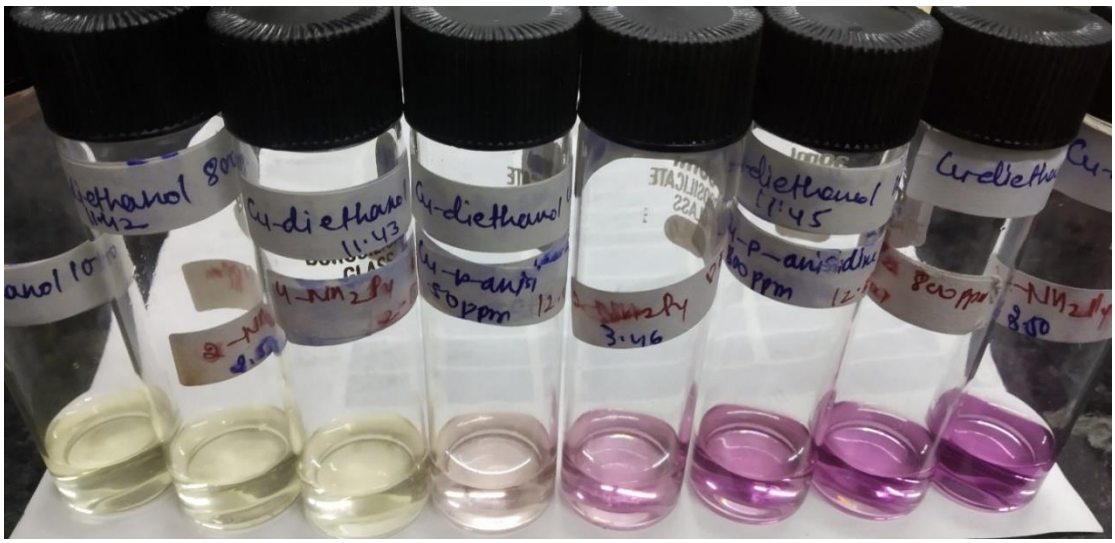

(d)

Figure 4.11: (a) UV-vis spectra of action of Cu_3L11 with DPPH (b) UV Spectra(enlarged) showing absorbance changes at 516 nm (c) Linear fit of % inhibition vs concentration (d) Visual color change of DPPH by Cu_3L11 after 30 min

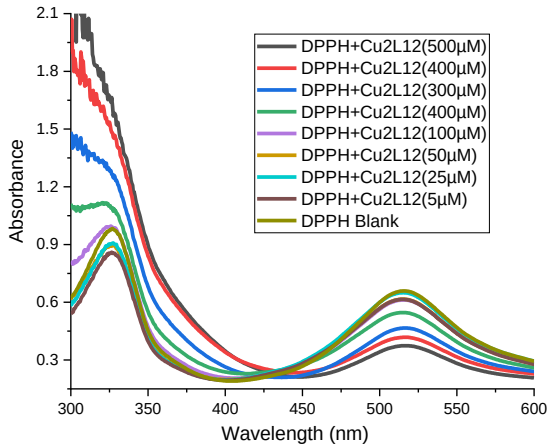

(a)

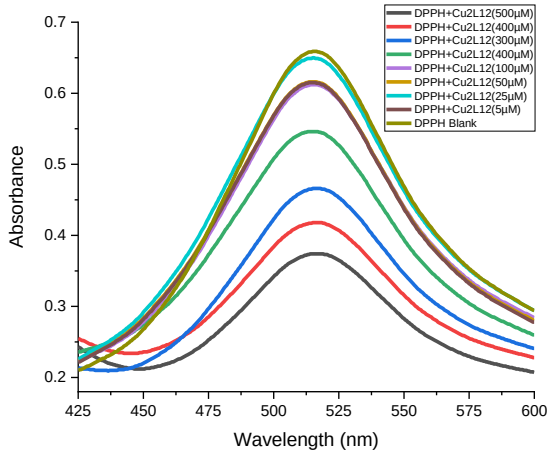

(b)

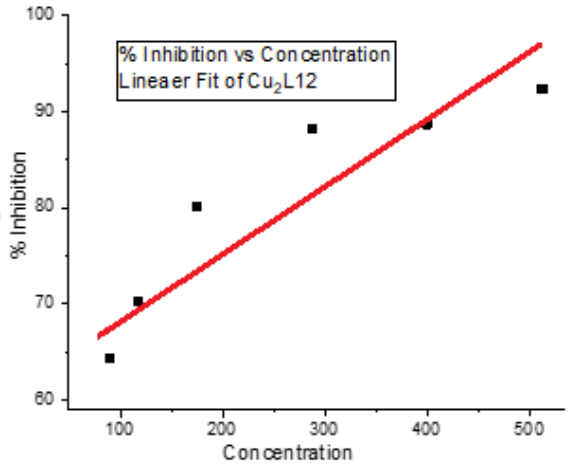

(c)

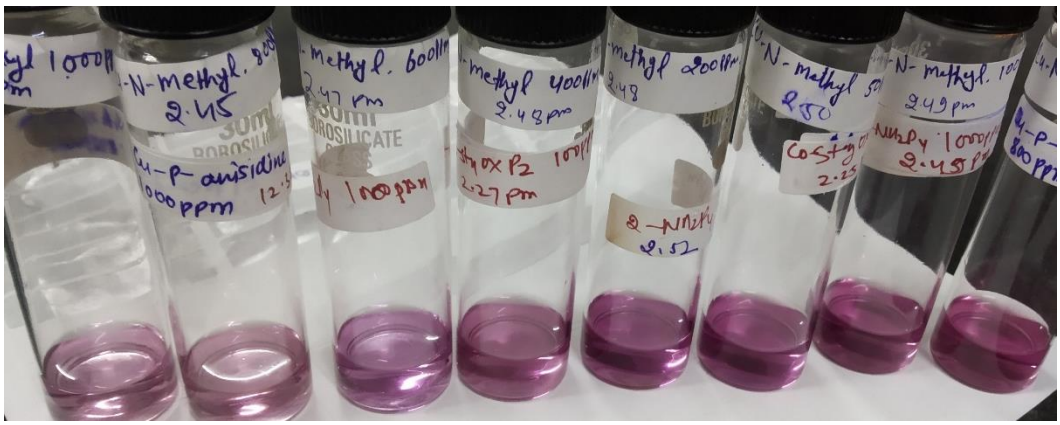

(d)

Figure 4.12: (a) UV-vis spectra of action of Cu_2L12 with DPPH (b) UV Spectra(enlarged) showing absorbance changes at 516 nm (c) Linear fit of % inhibition vs concentration (d) Visual color change of DPPH by Cu_2L12 after 30 min

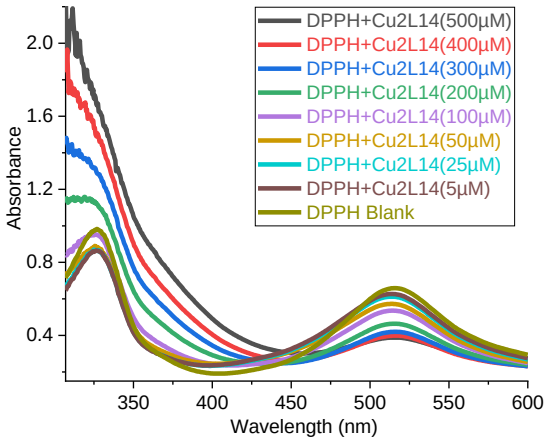

(a)

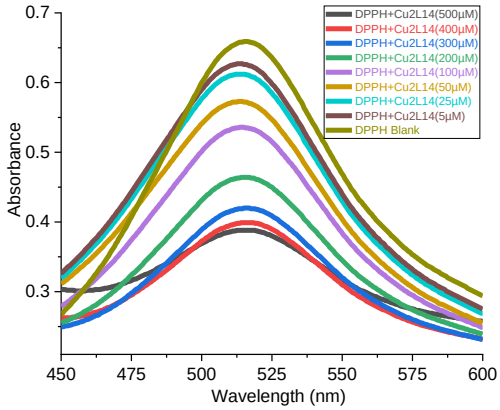

(b)

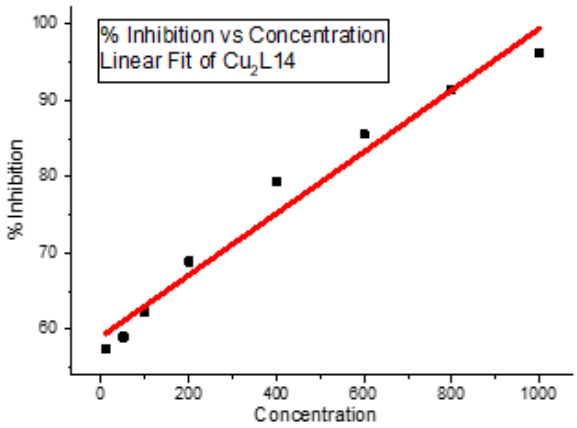

(c)

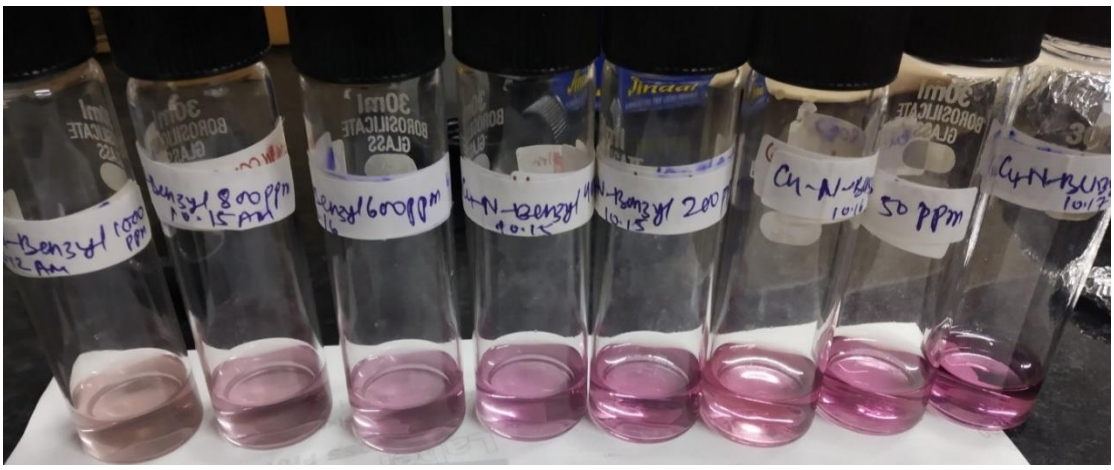

(d)

Figure 4.13:(a) UV-vis spectra of action of Cu_2L14 with DPPH (b) UV Spectra(enlarged) showing absorbance changes at 516 nm (c) Linear fit of % inhibition vs concentration (d) Visual color change of DPPH by Cu_2L14 after 30 min

4.3 Protein Binding studies:

Protein binding is considered clinically most significant studies for antimicrobial therapy, where a molecule with high protein bindingconstantis treated as a drug depot for the increased duration and maintaining the the drug concentration and adding to the antimicrobial efficacy.[23-24]

Many biomolecules are known to contain heterocyclic systems with or without any direct known interaction with the metal ions present in our body.[25,26]But the very fact that these heterocyclic systems themselves are good coordinators to metal ions forming various type of complexes, encourages many to put these heterocycles specially piperazine at the core of the ligand that binds to different metal ions showing a variety of applications.[27,28]In this regard protein binding studies of metal complexes derived from heterocyclic ligands are very much significant in behaving as potential drug molecule.[29-31]Drug protein interactionhaveeffect on both the pharmacodynamics(enzyme/receptor interaction) and pharmacokinetics (distribution, absorption and clearance) of a drug molecule. Among all the proteins, binding to plasma proteins suchas bovine serum albumin (BSA) or human serum albumin (HSA), havemore significance in drug protein binding interactions.[32,33]

UV-vis absorption studies of BSA

UV-vis absorption spectroscopy is a quite reliable and handy technique to analyze the binding interaction of metal complexes with serum proteins. 1000μMBSA solution and50 μM metal complexes were prepared using 0.1 M tris buffer as solvent. The UV spectra was recorded by taking stationary 50 μM metal complex vs increasing BSA concentrations in the order of 0-3 μM. There is a direct proportional relationship between the BSA concentration and the band intensity.Thus piperazine based copper and cobalt metal complexes were performed to test their protien binding activity with BSA using UV absorption spectroscopy and binding constant were calculated by following methodreported in literature.[34, 35]

Detailed experimental data used for calculating binding constant have been given in table 4.6. From the binding constant (Table 4.5) it is clear that complexes bind moderately with the value the range of 10^2 $M^{-1}$and is consistent with the BSA protein role as carrier for the parent drug delivery to targeted tissues.UV-vis graph of BSA activity of complexes along with their linear fit curve have been shown in the figures 4.14-4.25.

Table 4.5: Binding constant values of metal complexes (K_b M^{-1})

Complex	Structural formula of complex	K_b (M^{-1})
CuL1	$[Cu(L1)_2(H_2O)_2]$	-
CuL2	$[Cu(L2)Cl(H_2O)_2(CH_3OH)].2CH_3OH$	-
CuL3	$[Cu(L3)Cl(H_2O)(CH_3OH)_2].3H_2O$	-
CuL4	$[CuL4(CH_3OH)(NO_3)(H_2O)_2]$	0.22×10^2
CuL5	$[Cu(L5)_2(H_2O)_2].2H_2O$	0.54×10^2
CuL6	$[Cu(L6)(H_2O)(Cl)(CH_3OH)_2].4H_2O$	0.91×10^2
CuL7	$[Cu(L7)(H_2O)(Cl)(CH_3OH)_2]$	0.46×10^2
CuL8	$[Cu(L8)(H_2O)_2(CH_3OH)(Cl)]$	-
CoL9	$[CoL9(H_2O)_2]$	1.50×10^2
Co_2L10	$[Co_2(L10)(CH_3OH)_4(Cl)_2(H_2O)_2]$	0.86×10^2
Cu_2L10	$[Cu_2(L10)(CH_3CN)Cl_2(H_2O)_5]$	0.54×10^2

Zn_2L10	$[Zn_2(L10)(CH_3CN)_2Cl_2(H_2O)_4]$	-
Cu_3L11	$[Cu_3(L11)(H_2O)_3(CH_3OH)]CH_3OH$	0.32×10^2
Cu_2L12	$[Cu_2(L12)_2(H_2O)_2]$	2.95×10^2
Cu_2L13	$[Cu_2(L13)_2(H_2O)_2]$	6.64×10^2
Cu_2L14	$[Cu_2(L14)_2(H_2O)_2]$	2.91×10^2

Table 4.6: Descriptive analysis of absorbance and other terms required to calculate binding constant

Sample Code	**Vol. BSA(µL)**	**Abs** *sample*	**Abs** *blank*	**Abs** *sample-blank*	**1/Abs** *sample-blank*	**1/[BSA]**
CuL4	Blank	0.093	0.00052	0.0878	11.38	0
	0.1	0.111	0.00077	0.1102	9.07	30
	0.2	0.119	0.00262	01163	8.59	15
	0.3	0.125	0.00459	0.1204	8.30	10
	0.4	0.133	0.00629	0.1267	7.892	7.5
	0.5	0.140	0.00800	0.1320	7.575	6
	0.6	0.163	0.00972	0.1532	6.52	5
	0.7	0.176	0.01144	0.1646	6.07	4.28
	0.8	0.190	0.01294	0.1770	5.64	3.75
CuL5	Blank	0.558	0.00052	0.5528	1.80897	0
	0.1	0.583	0.00077	0.58222	1.71756	30
	0.2	0.608	0.00262	0.60538	1.65186	15
	0.3	0.636	0.00459	0.63141	1.58376	10
	0.4	0.668	0.00629	0.66171	1.51124	7.5
	0.5	0.683	0.00800	0.675	1.48148	6
	0.6	0.707	0.00972	0.69728	1.43414	5
	0.7	0.724	0.01144	0.71256	1.40339	4.28
	0.8	0.749	0.01294	0.73606	1.35858	3.75

CuL6	Blank	0.839	0.00052	0.8338	1.19933	0
	0.1	0.859	0.00077	0.85822	1.1652	30
	0.2	0.869	0.00262	0.86638	1.15423	15
	0.3	0.881	0.00459	0.87641	1.14102	10
	0.4	0.901	0.00629	0.89471	1.11768	7.5
	0.5	0.924	0.00800	0.916	1.0917	6
	0.6	0.947	0.00972	0.93728	1.06692	5
	0.7	0.994	0.01144	0.95956	1.04214	4.28
	0.8	0.999	0.01294	0.98106	1.01931	3.75
CuL7	Blank	0.548	0.00052	0.54280	1.84230	0
	0.1	0.591	0.00077	0.59022	1.69428	30
	0.2	0.654	0.00262	0.65138	1.53520	15
	0.3	0.664	0.00459	0.65941	1.51651	10
	0.4	0.674	0.00629	0.66771	1.49766	7.5
	0.5	0.747	0.00800	0.73900	1.35318	6
	0.6	0.766	0.00972	0.75628	1.32226	5
	0.7	0.786	0.01144	0.75628	1.28773	4.28
	0.8	0.808	0.01294	0.79506	1.25777	3.75
CuL8	Blank	0.822	0.00052	0.8168	1.22429	0
	0.1	0.8865	0.00077	0.88572	1.12902	30
	0.2	0.981	0.00262	0.97838	1.0221	15
	0.3	0.996	0.00459	0.99141	1.00866	10
	0.4	1.011	0.00629	1.00471	0.99531	7.5
	0.5	1.1205	0.00800	1.1125	0.89888	6
CoL9	Blank	0.1416	0.00052	0.14093	7.09572	0

	0.1	0.1671	0.00077	0.15346	6.51636	30
	0.2	0.1923	0.00262	0.16632	6.01251	15
	0.3	0.2125	0.00459	0.17753	5.63285	10
	0.4	0.2190	0.00629	0.17212	5.8099	7.5
	0.5	0.2370	0.00800	0.17591	5.68473	6
Cu_2L10	Blank	0.0999	0.00052	0.0947	10.55966	0
	0.1	0.1297	0.00077	0.12892	7.75675	30
	0.2	0.1527	0.00262	0.15009	6.66267	15
	0.3	0.1741	0.00459	0.16956	5.89762	10
	0.4	0.1882	0.00629	0.18191	5.49722	7.5
	0.5	0.2061	0.00800	0.19812	5.04745	6
Co_2L10	Blank	0.1381	0.00052	0.1376	7.26744	0
	0.1	0.1509	0.00077	0.15015	6.66001	30
	0.2	0.1631	0.00262	0.16235	6.15953	15
	0.3	0.1744	0.00459	0.1718	5.82072	10
	0.4	0.1883	0.00629	0.18373	5.44277	7.5
	0.5	0.2033	0.00800	0.19532	5.1198	6
Cu_3L11	Blank	0.1554	0.00052	0.1502	6.65779	0
	0.1	0.201	0.00077	0.20022	4.99451	30
	0.2	0.2449	0.00262	0.24236	4.12604	15
	0.3	0.2897	0.00459	0.2852	3.50633	10
	0.4	0.3388	0.00629	0.33255	3.00704	7.5
	0.5	0.3795	0.00800	0.3715	2.69176	6
Cu_2L12	Blank	0.6705	0.00052	0.66977	1.49305	0
	0.1	0.6943	0.00077	0.6807	1.46908	30

	0.2	0.7230	0.00262	0.69705	1.43462	15
	0.3	0.7495	0.00459	0.71455	1.39948	10
	0.4	0.7755	0.00629	0.72863	1.37244	7.5
	0.5	0.8015	0.00800	0.7404	1.35062	6
Cu_2L13	Blank	0.8485	0.00052	0.84782	0.92779	0
	0.1	0.8675	0.00077	0.85391	0.90735	30
	0.2	0.8875	0.00262	0.86156	0.89251	15
	0.3	0.9075	0.00459	0.85253	0.89489	10
	0.4	0.92755	0.00629	0.86061	0.88109	7.5
	0.5	0.9475	0.00800	0.86638	0.86750	6
Cu_2L14	Blank	0.7865	0.00052	0.78134	1.3151	0
	0.1	0.8121	0.00077	0.81137	1.27985	30
	0.2	0.8267	0.00262	0.82416	1.23248	15
	0.3	0.8336	0.00459	0.82903	1.21336	10
	0.4	0.8649	0.00629	0.85865	1.20623	7.5
	0.5	0.8908	0.00800	0.88289	1.16462	6

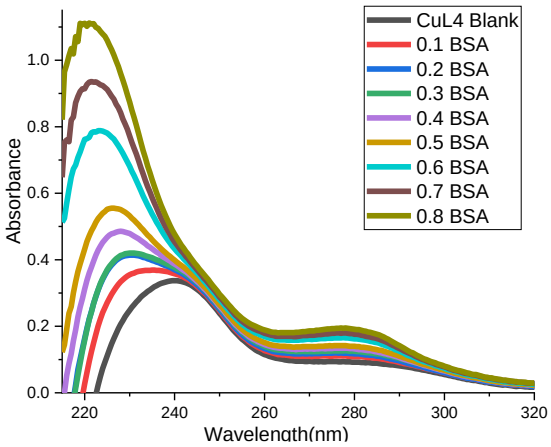

(a)

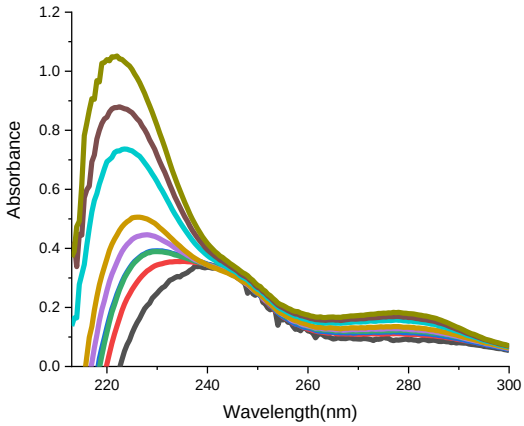

(b)

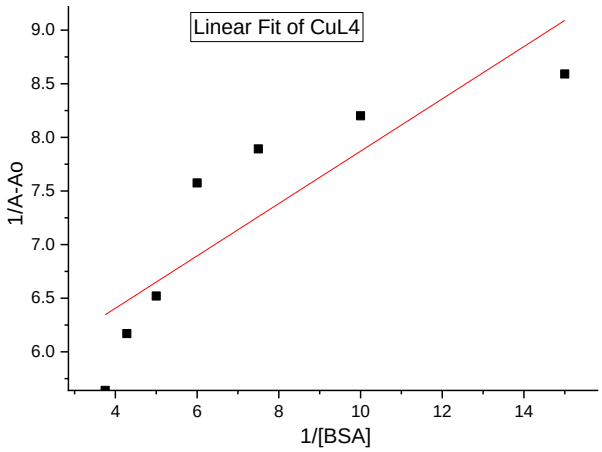

(c)

Figure 4.14: (a) UV-vis spectra of titration curves of complex CuL4 with increasing BSA concentration in the range 0-3 μM, (b) UV-vis spectra of titration curve after subtracting with blank absorption (c) Linear fit of $1/(A-A_0)$ vs 1/[BSA]

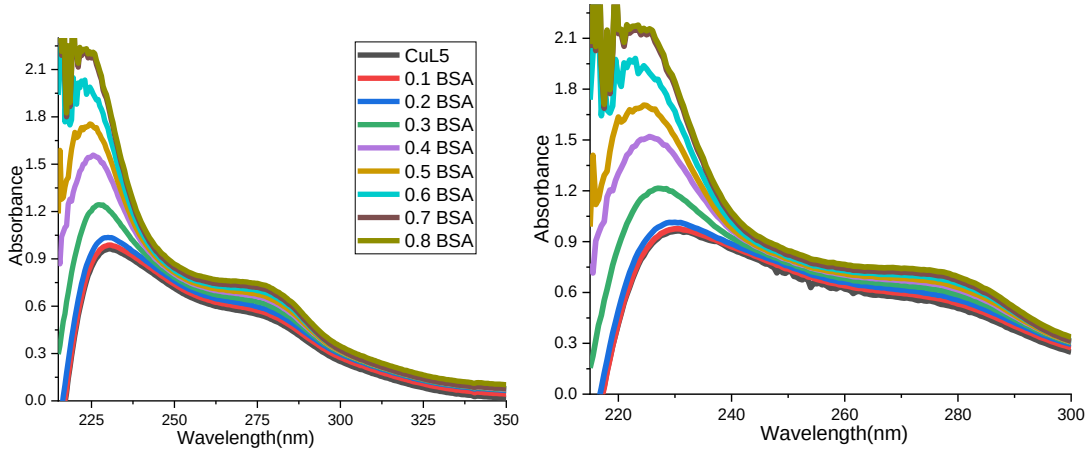

(a) (b)

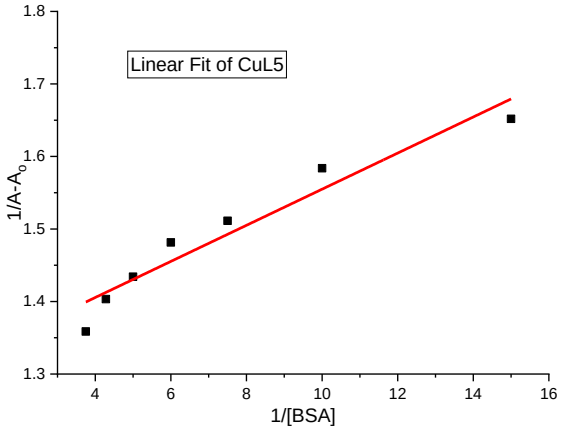

(c)

Figure 4.15: (a) UV-vis spectra of titration curves of complex CuL5 with increasing BSA concentration in the range 0-3 μM, (b) UV-vis spectra of titration curve after subtracting with blank absorption (c) Linear fit of $1/(A-A_0)$ vs 1/[BSA]

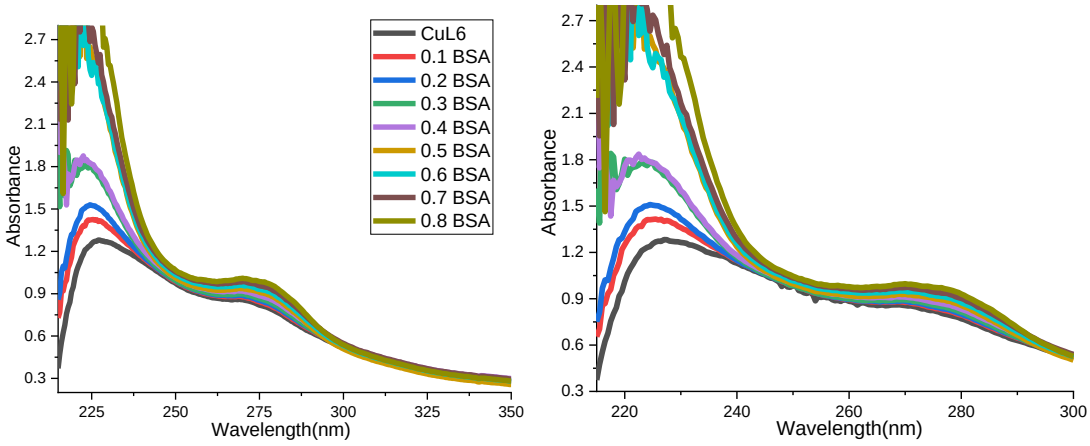

(a) (b)

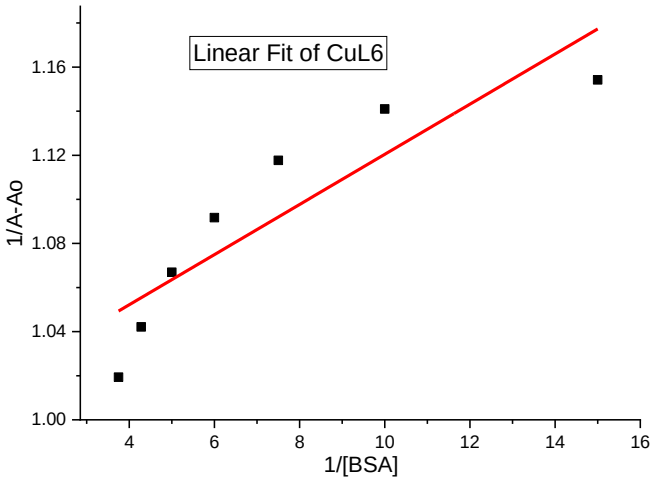

(c)

Figure 4.16: (a) UV-vis spectra of titration curves of complex CuL6 with increasing BSA concentration in the range 0-3 μM, (b) UV-vis spectra of titration curve after subtracting with blank absorption (c) Linear fit of $1/(A-A_0)$ vs 1/[BSA]

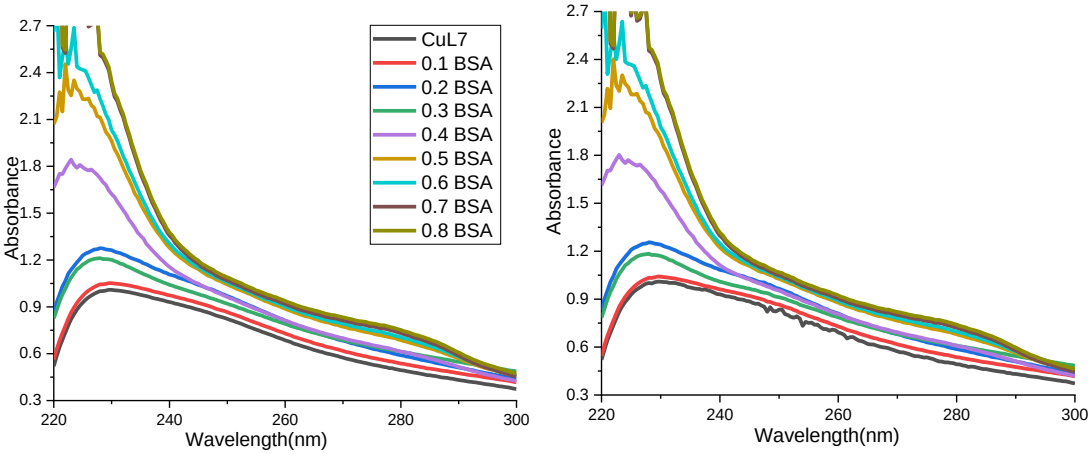

(a) (b)

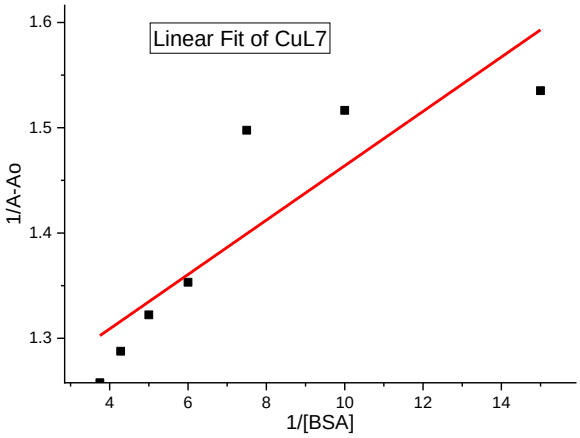

(c)

Figure 4.17:(a) UV-vis spectra of titration curves of complex CuL7 with increasing BSA concentration in the range 0-3 μM, (b) UV-vis spectra of titration curve after subtracting with blank absorption (c) Linear fit of $1/(A-A_0)$ vs 1/[BSA]

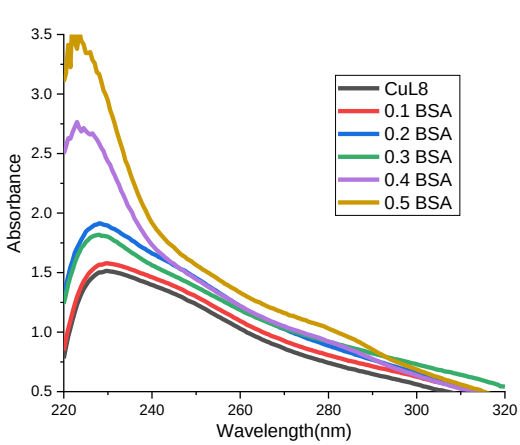

(a)

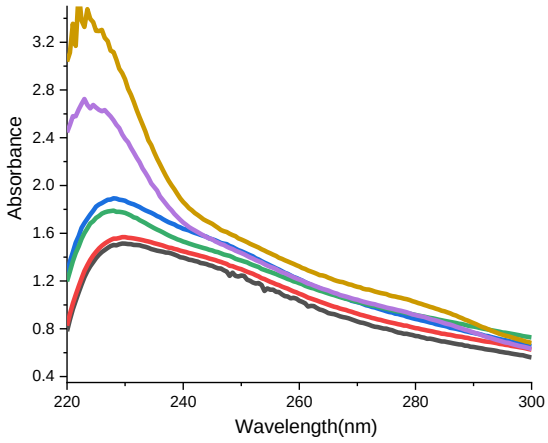

(b)

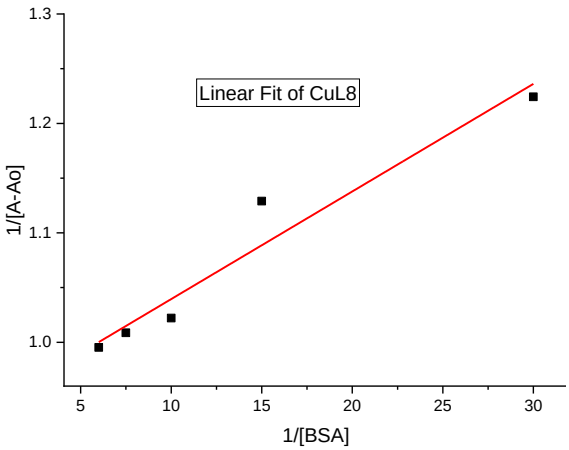

(c)

Figure 4.18:(a) UV-vis spectra of titration curves of complex CuL8 with increasing BSA concentration in the range 0-3 μM, (b) UV-vis spectra of titration curve after subtracting with blank absorption (c) Linear fit of $1/(A-A_0)$ vs 1/[BSA]

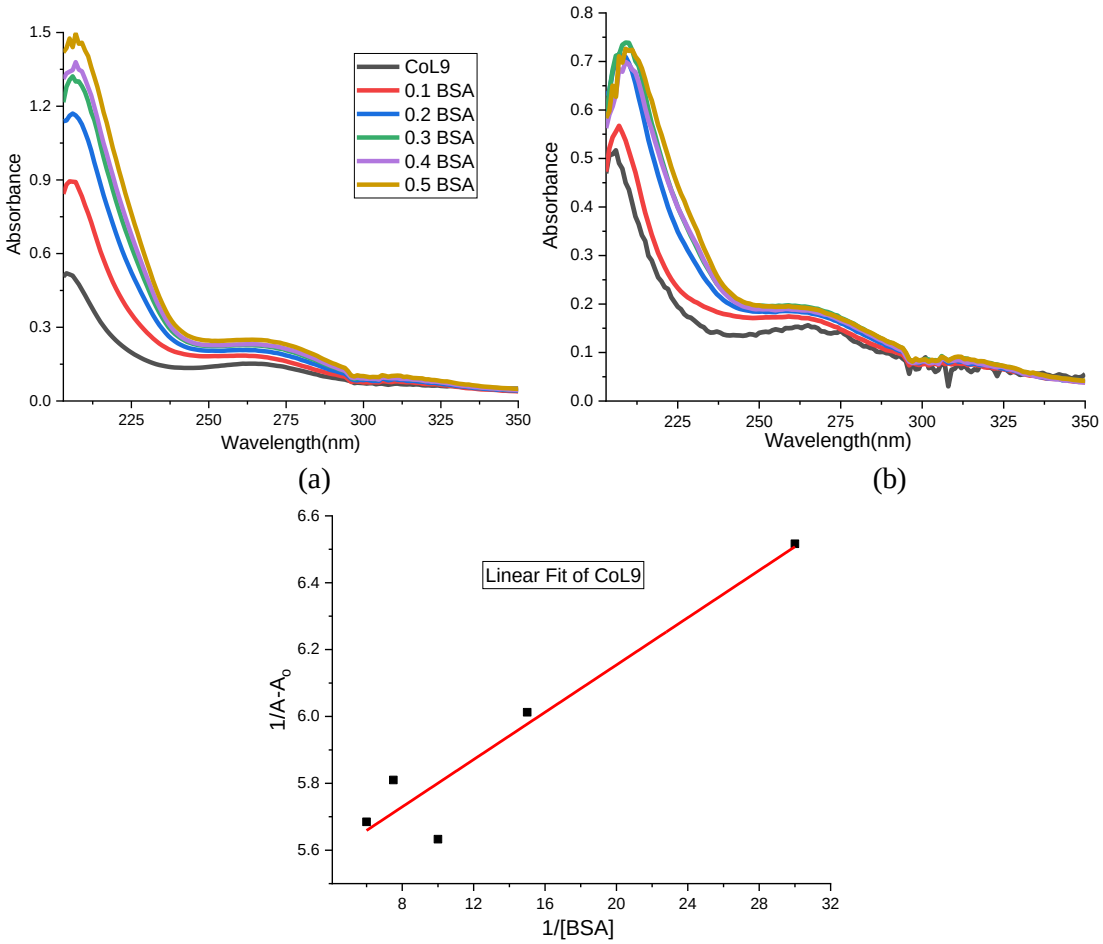

Figure 4.19: (a) UV-vis spectra of titration curves of complex CoL9 with increasing BSA concentration in the range 0-3 μM, (b) UV-vis spectra of titration curve after subtracting with blank absorption (c) Linear fit of $1/(A-A_0)$ vs 1/[BSA]

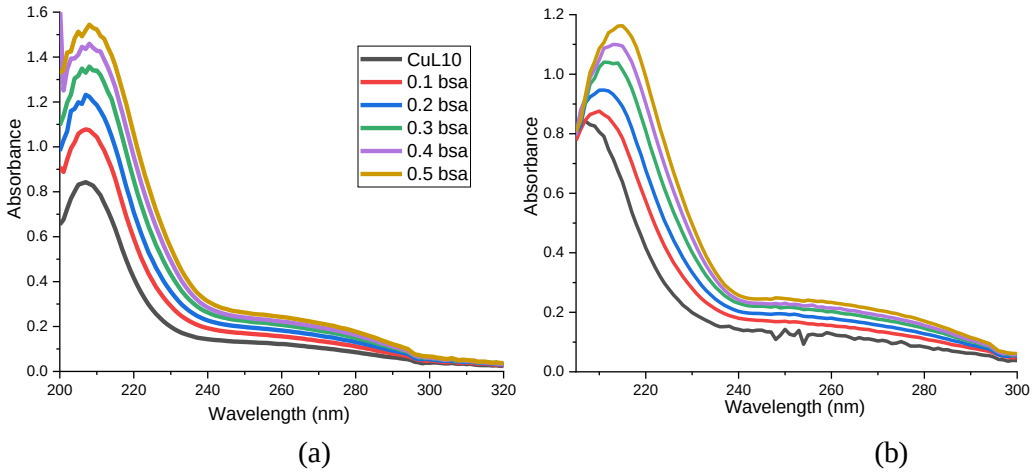

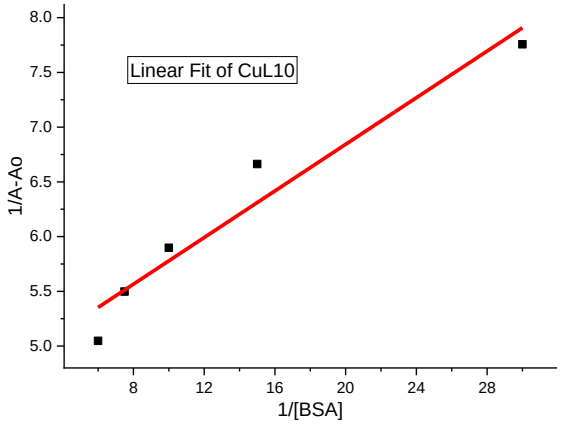

(c)

Figure 4.20:(a) UV-vis spectra of titration curves of complex Cu_2L10 with increasing BSA concentration in the range 0-3 μM, (b) UV-vis spectra of titration curve after subtracting with blank absorption (c) Linear fit of $1/(A-A_0)$ vs 1/[BSA]

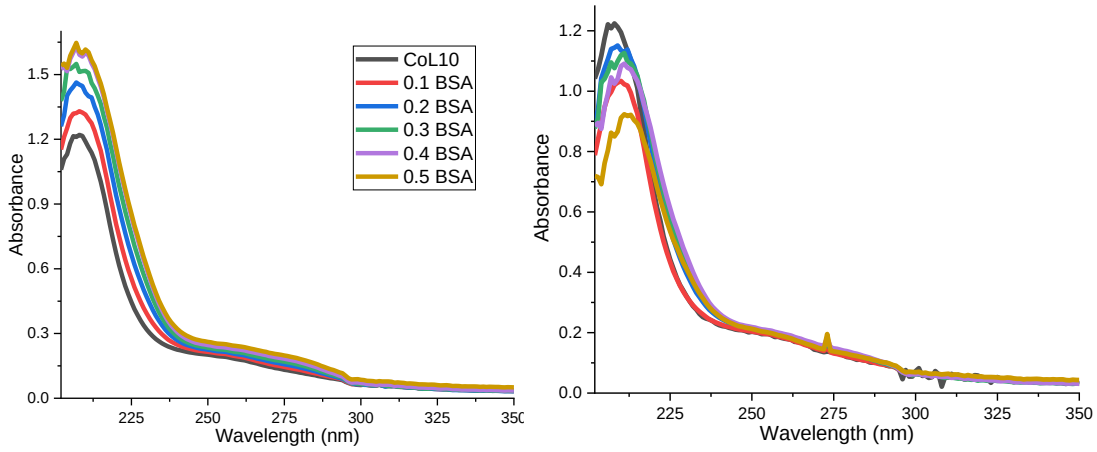

(a) (b)

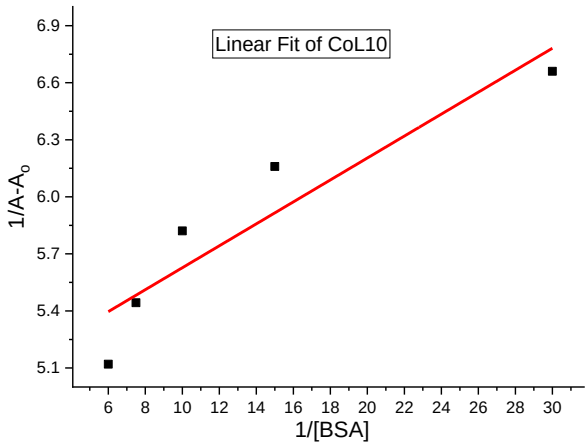

(c)

Figure 4.21:(a) UV-vis spectra of titration curves of complex Co_2L10 with increasing BSA concentration in the range 0-3 μM, (b) UV-vis spectra of titration curve after subtracting with blank absorption (c) Linear fit of $1/(A-A_0)$ vs 1/[BSA]

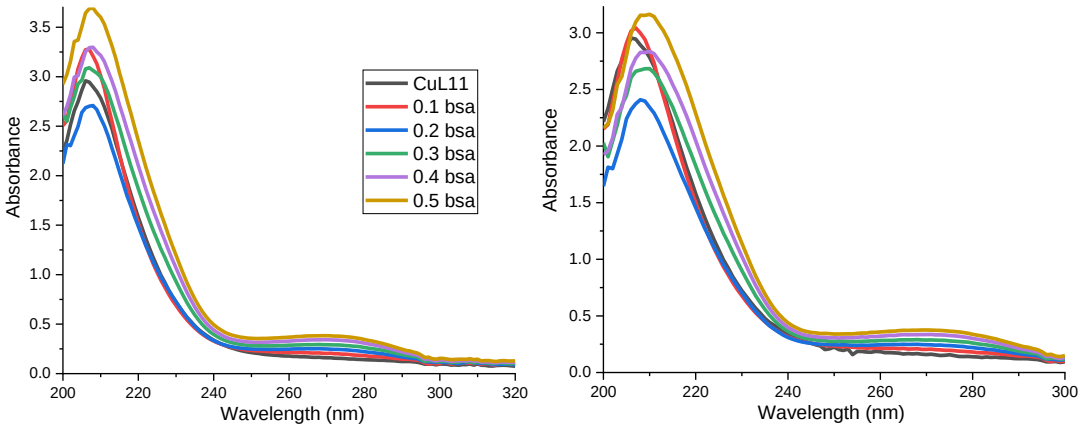

(a) (b)

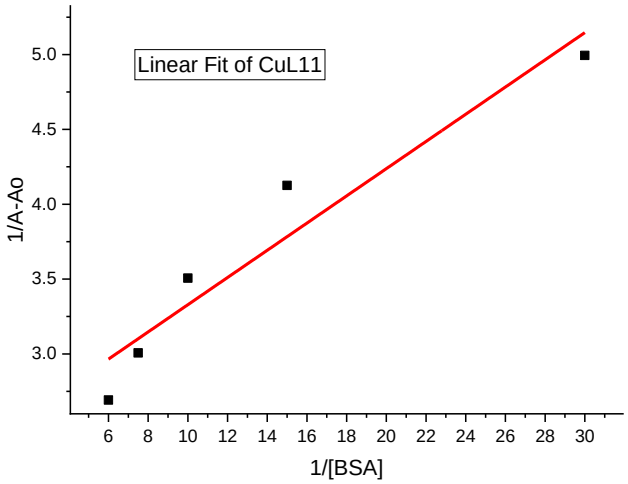

(c)

Figure 4.22:(a) UV-vis spectra of titration curves of complex Cu_3L11 with increasing BSA concentration in the range 0-3 μM, (b) UV-vis spectra of titration curve after subtracting with blank absorption (c) Linear fit of $1/(A-A_0)$ vs 1/[BSA]

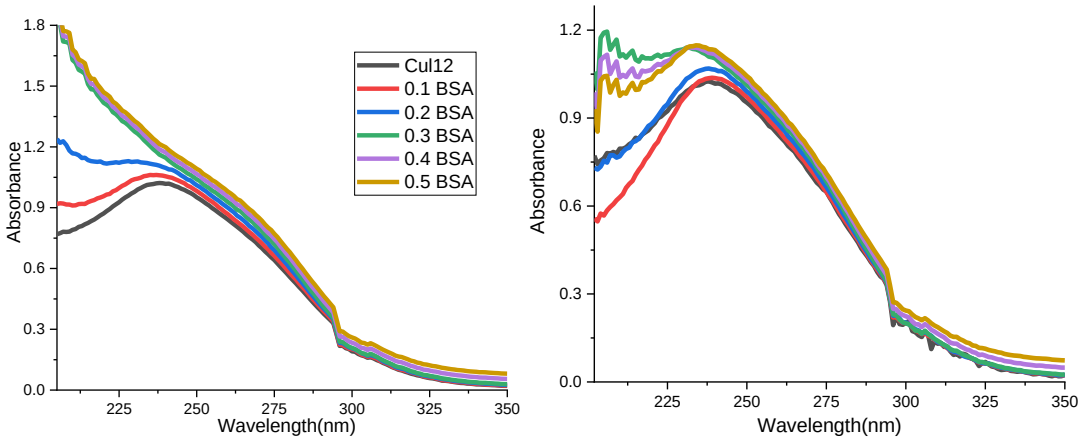

(a) (b)

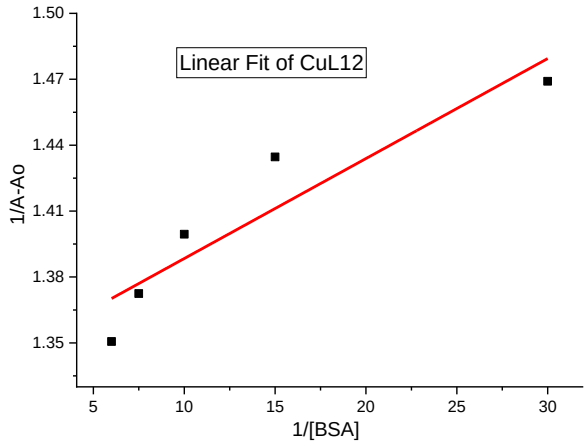

(c)

Figure 4.23:(a) UV-vis spectra of titration curves of complex Cu_2L12 with increasing BSA concentration in the range 0-3 μM, (b) UV-vis spectra of titration curve after subtracting with blank absorption (c) Linear fit of $1/(A-A_0)$ vs 1/[BSA]

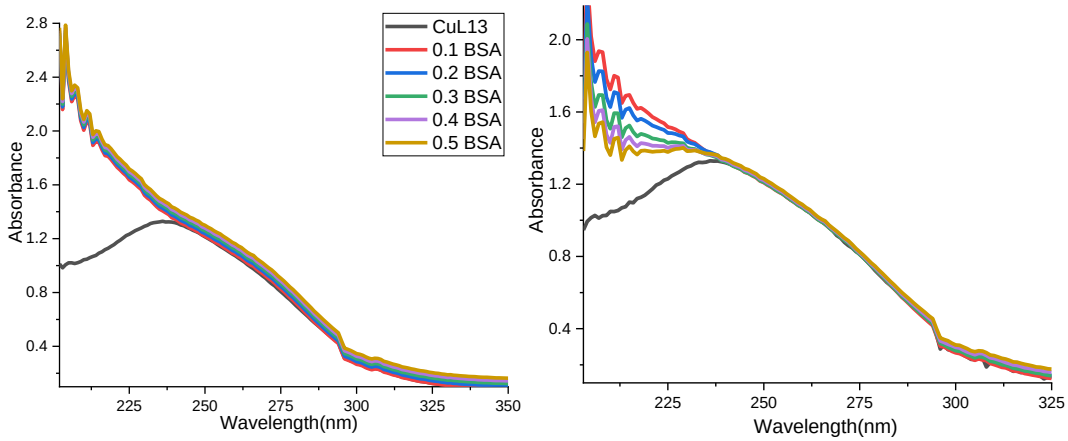

(a) (b)

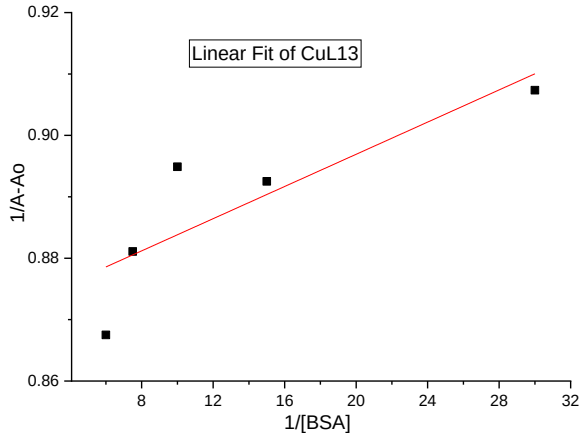

(c)

Figure 4.24:(a) UV-vis spectra of titration curves of complex Cu_2L13 with increasing BSA concentration in the range 0-3 μM, (b) UV-vis spectra of titration curve after subtracting with blank absorption (c) Linear fit of $1/(A-A_0)$ vs 1/[BSA]

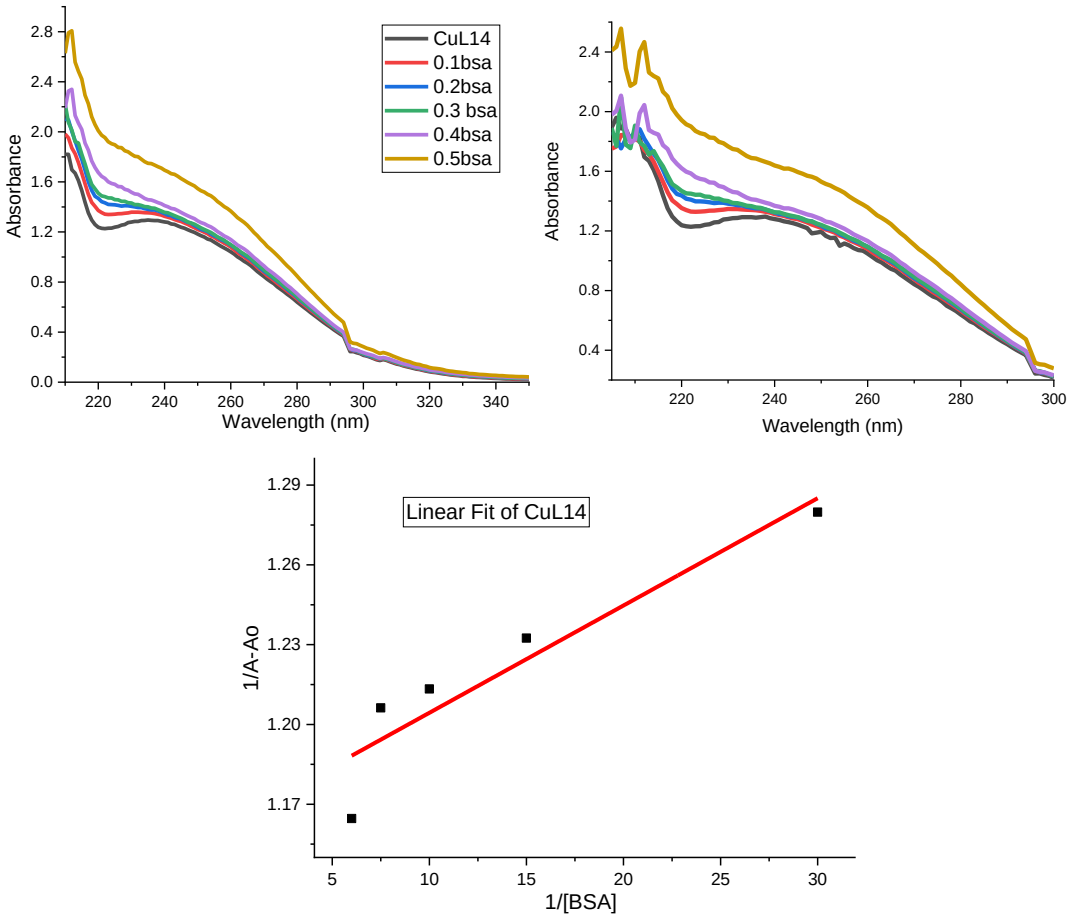

(c)

Figure 4.25: (a) UV-vis spectra of titration curves of complex Cu_2L14 with increasing BSA concentration in the range 0-3 μM, (b) UV-vis spectra of titration curve after subtracting with blank absorption (c) Linear fit of $1/(A-A_0)$ vs 1/[BSA]

4.4 Cytotoxic Studies:

Now a days, to test the potential of a samples (natural plant extracts or synthetic ones) cytotoxic studies are being performed for further screening ofthese molecules as potential anticancer drug for specific type of cell lines causing cancer as cancer is the world largest problem.[36-39]Cytotoxicity has become most reliable and important indicators for in vitro biological activities.[40-43]Different mechanisms like protein synthesis prevention, reversible or irreversible receptor binding are followed in these studies.[44-47]Cytotoxicity studies are being used to screen library of compounds in drug discovery.There are several methods available in literature to monitor this activity butcolorimetric MTT assay is much superior to the other available methods because

of its ease, reproducibility, handling and is widely employed in determining cell viability and toxicity tests.[48-50] Piperazine based complexes have also gained remarkable interest to evaluate anticancer potentials of these molecules in terms of cytotoxic activity.[51-59]

Cytotoxicity activity was carried by MTT assay. MTT assay is a colorimetric assay. It measures the reduction of 3-(4,5-dimethythiazol-2-yl)-2,5-diphenyl tetrazolium bromide (MTT) (yellow) by enzyme mitochondrial succinate dehydrogenase (Figure 4.26). When MTT enters the cells and passes into the mitochondria, it is reduced to an insolubleformazan dark purple product.By using DMSO solvent, cells are then solubilised and released. The solubilised formazan is then measured spectrophotometrically. As reductions of MTT only occur in metabolic active cells, the level of activity is a measure of the cell viability.[61,62]

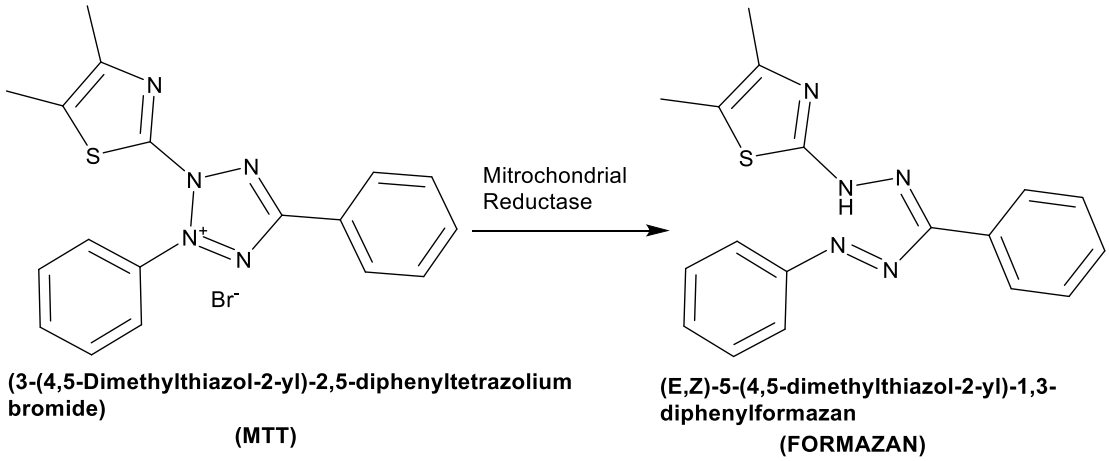

Figure 4.26: Mitochondrial reductase catalyzed conversion of MTT to formazan

Materials and Protocol:

MCF-7 (Breast cancer cell line), Fetal bovine serum (FBS), Dulbecco`s Modified Eagle Media (DMEM) with low glucose, Antibiotic(antimycotic).

The cells were seeded on a 96-well flat-bottom micro plate and maintained at 37ºC in environment(humidity 95% and $CO_2$5%) for overnight. Different concentration (200,100, 50, 25, 12.5, 6.25,µg/ml) of complexes were treated. The cells were incubated for another 48 hours. The wellswere washed twice with PBS and 20 µL of the MTT staining solution was added to each welland plate was incubated at 37ºC.After 4h, 100 µL of DMSO was added to each well todissolve the formazan

crystals, and absorbance was recorded with a 570 nm.[62] Results were calculated and expressed in terms of IC_{50} value. Formula used to calculate surviving cell percentage is following.

$$\textbf{Surviving cells (\%)} = \frac{\textbf{Mean OD of test compound}}{\textbf{Mean OD of Negative control}} \times 100$$

Table 4.7: IC_{50} value of complexes Cu_3L11, Cu_2L12-14 and standard cisplatin

Sample Code	IC_{50}
Cu_3L11	8.539
Cu_2L12	6.016
Cu_2L13	8.954
Cu_2L14	5.065
Cisplatin	2.201

Table 4.8: Cell viability data of complexes Cu_3L11, Cu_2L12-14 against MCF-7

Cell Viability of MCF-7								
Concentration µg/ml	Cu_3L11		Cu_2L12		Cu_2L13		Cu_2L14	
200.00	26.61	25.40	24.19	21.77	29.03	25.40	25.00	26.21
100.00	29.03	29.84	25.00	27.02	32.26	30.65	29.84	30.24
50.00	33.06	35.48	27.42	31.45	33.87	35.08	34.27	31.05
25.00	37.50	39.11	36.69	39.52	38.31	39.92	38.31	40.73
12.50	43.55	42.34	43.55	47.58	42.34	41.94	46.37	51.21
6.25	49.16	48.97	54.03	55.65	50.81	53.63	51.21	5524

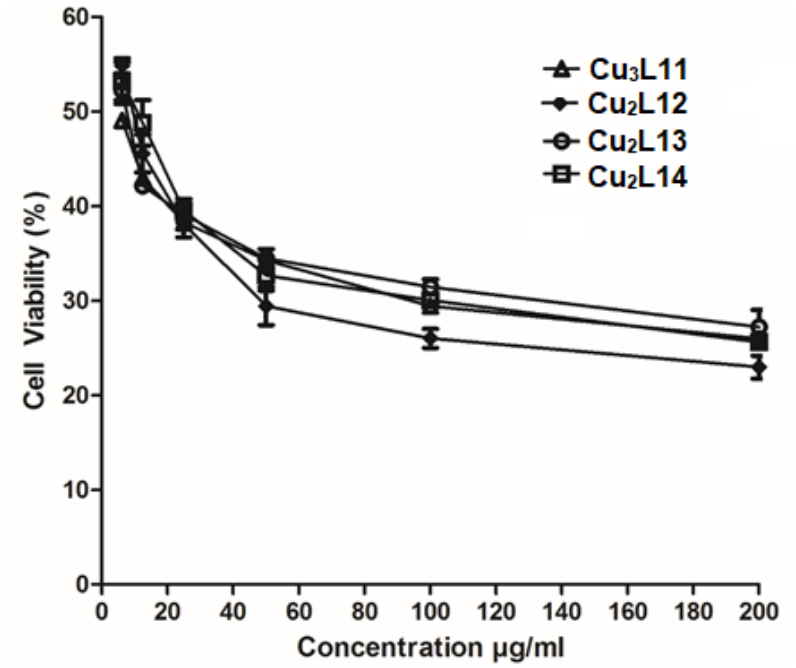

Figure 4.27: Graphical representation of cell viability vs concentrations

Cytotoxic activity of selected complexes measured in term of $IC_{50}$was in the range of 5-9 which is considered good and complexes possess cytotoxic potential. Cytotoxic activity of more complexes can be performed with other complexes in future using different cancer cell lines and promising results may be obtained. Table 4.7 and 4.8 describes IC_{50} value and cell viability data of complexes Cu_3L11, Cu_2L12-14 while figure 4.27 described graphical representation of cell viability of MCF-7.

4.5 DNA Binding Studies:

DNA is one among very crucial biological targets to check the covalent or noncovalent binding interactions with small molecules to know their anticancer potentials (Figure 4.28).[63-65]Depending on nature and active sites in DNA binding can occur in three ways via groove binding, intercalation and electrostatic interactions.[66,67]Thus, it becomes important to understand the binding properties of molecules with DNA by which replication of double stranded DNA is possibly blocked and we can develop the new anticancer potential drug.[68]With the discovery of cis-platin as anticancer to suppress cell division, transition metal complexes have shown promising potentials for metal-based drugs to cure cancer.[69]Many metal complexes have shown affinity for binding interaction to the targeted DNA via diffuse or site binding. In diffuse binding, long-range interaction occurs between metal ions

and nucleic acid. Whereas in site binding, ligands backbone or metal ion directly interact/bind the nucleic acid.[70-73] Piperazine ring-based transition metals complexes have also gained attention due to their DNA cleavage and binding properties.[74]

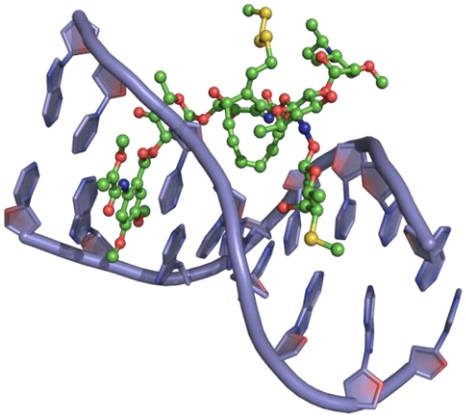

Figure 4.28: Model representation of DNA binding with molecules

DNA binding studies were performed using UV-vis absorption spectroscopy. Solution of CT-DNA (Calf Thymus DNA) was prepared in triss buffer (0.1 M, 7.4 pH) by dissolving 30 mg in 10 ml. Concertation of this solution was determined by recording the absorbance value at 260 nm and taking extinction coefficient of 6600 $Lmol^{-1}cm^{-1}$. Thisvarying concentration of prepared CT DNA solution was added to 25 µM solution of metal complexes and UV spectra was recorded. Binding constant was calculated by plotting the graph between 1/[DNA] and $1/[A-A_0]$.[70]

From the binding constant (Table 4.9) it is clear that complexes bind moderately with the value the range of 10^2 M^{-1}.Type of interaction of complexes have been further explained by supporting with theoretical studies. UV-vis graph of DNA binding activity of complexes along with their linear fit curve have been shown in the figures 4.29-4.34.

Table 4.9: DNA binding constants of selected complexes

Complex Code	Structure of complex	K_b (M^{-1})
Co_2L10	$[Co_2(L10)(CH_3OH)_4(Cl)_2(H_2O)_2]$	1.37×10^2
Cu_2L10	$[Cu_2(L10)(CH_3CN)Cl_2(H_2O)_5]$	1.01×10^2
Zn_2L10	$[Zn_2(L10)(CH_3CN)_2Cl_2(H_2O)_4]$	-
Cu_3L11	$[Cu_3(L11)(H_2O)_3(CH_3OH)]CH_3OH$	6.30×10^2
Cu_2L12	$[Cu_2(L12)_2(H_2O)_2]$	1.80×10^2

Cu_2L13	$[Cu_2(L13)_2(H_2O)_2]$	2.27×10^2
Cu_2L14	$[Cu_2(L14)_2(H_2O)_2]$	2.38×10^2

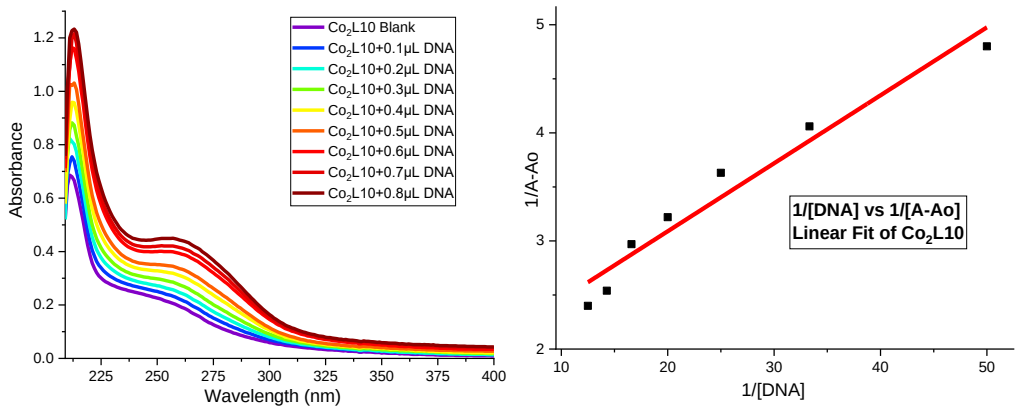

Figure 4.29: (a) UV-vis spectra of titration curves of complex Co_2L10 with increasing DNA concentration in the range of 0 0.08 μM, (b) Linear fit of $1/(A-A_0)$ vs 1/[DNA]

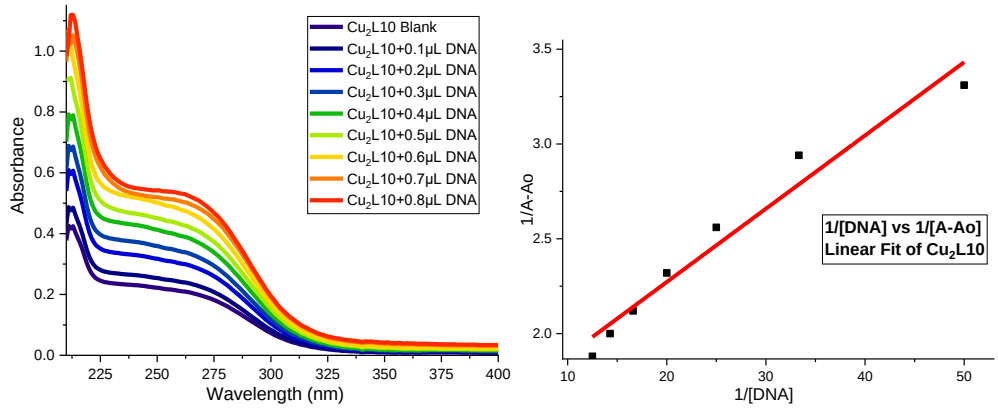

Figure 4.30: (a) UV-vis spectra of titration curves of complex Cu_2L10 with increasing DNA concentration in the range of 0–0.08 μM, (b) Linear fit of $1/(A-A_0)$ vs 1/[DNA]

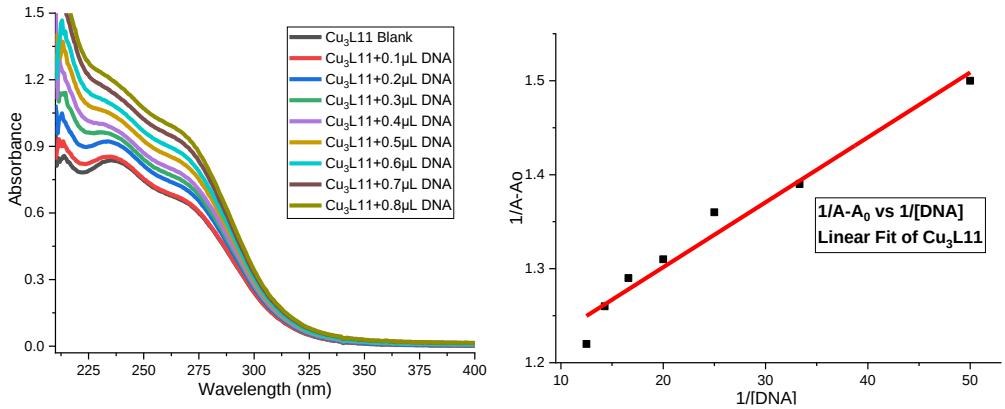

(a) (b)

Figure 4.31: (a) UV-vis spectra of titration curves of complex Cu_3L11 with increasing DNA concentration in the range of 0–0.08 μM, (b) Linear fit of $1/(A-A_0)$ vs 1/[DNA]

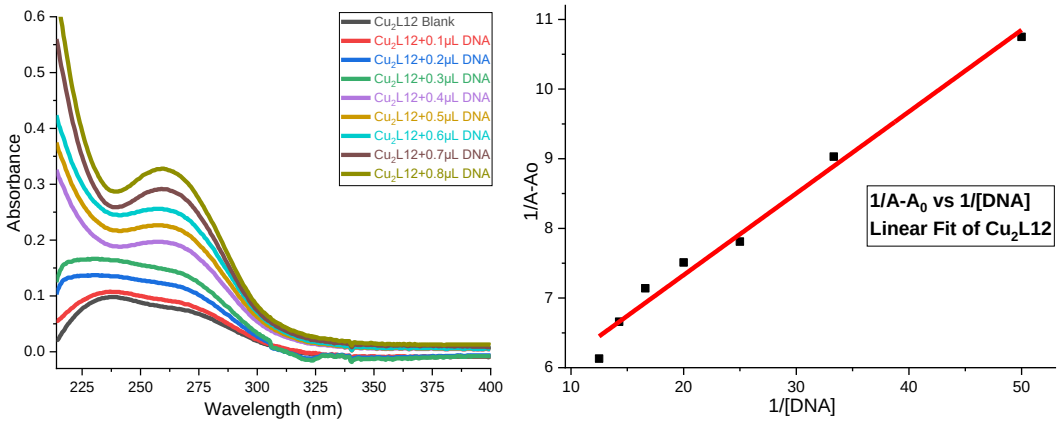

(a) (b)

Figure 4.32: (a) UV-vis spectra of titration curves of complex Cu_2L12 with increasing DNA concentration in the range of 0–0.08 μM, (b) Linear fit of $1/(A-A_0)$ vs 1/[DNA]

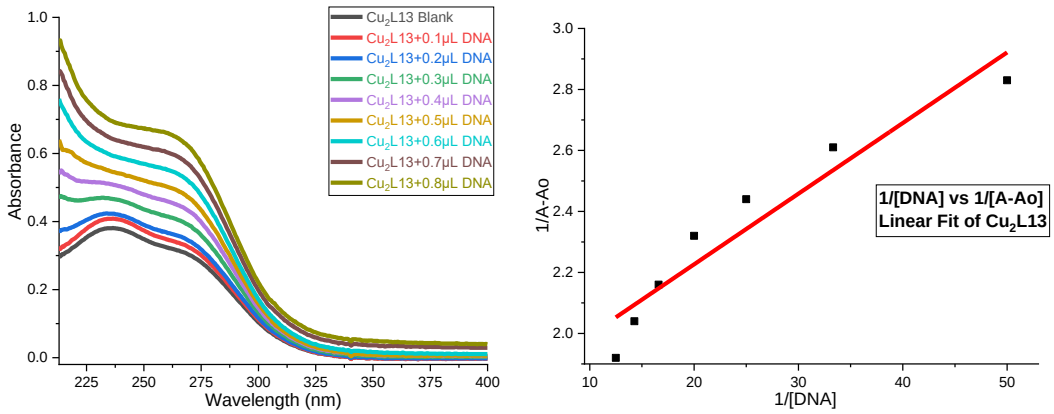

(a) (b)

Figure 4.33:(a) UV-vis spectra of titration curves of complex Cu_2L13 with increasing DNA concentration in the range of 0–0.08 μM, (b) Linear fit of $1/(A-A_0)$ vs 1/[DNA]

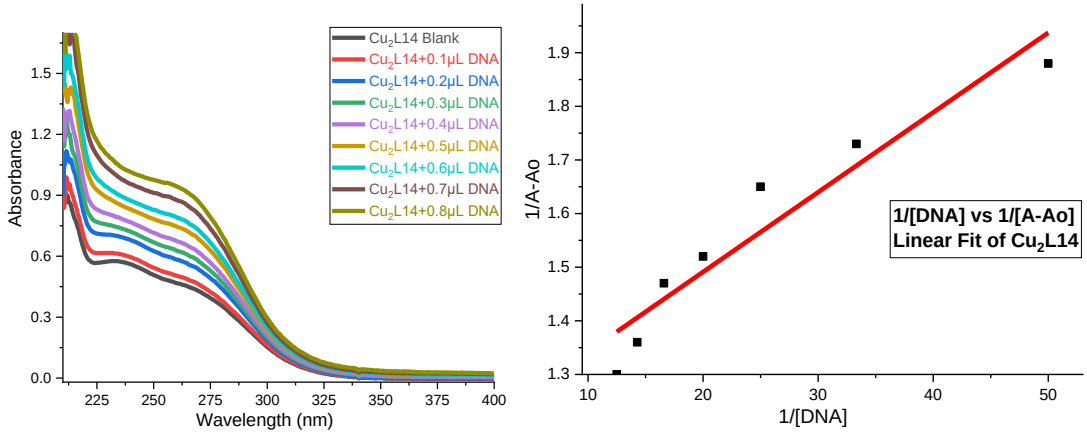

(a) (b)

Figure 4.34: (a) UV-vis spectra of titration curves of complex Cu_2L14 with increasing DNA concentration in the range of 0–0.08 μM, (b) Linear fit of $1/(A-A_0)$ vs 1/[DNA]

4.6 Conclusion:

This chapter focused on biological applications of synthesized ligand and complexes. In antimicrobial studies, antibacterial activity of synthesized ligands and their complexes has been tested with two strains *E.Coli* and *S. Aureus*. In all cases (except one) metal complexes were showing greater activity in comparison to the ligands. This indicated binding of metal to the ligands enhances the activity. Some of complexes were also found more active as compared to standard drug which explains their potential for drug delivery systems. Antioxidant activity tested of these complexes by DPPH scavenging assay indicated that complexes Cu_2L10 and Cu_3L11, Cu_2L12 and Cu_2L14 exhibit strong antioxidant behaviour in comparison to standard ascorbic acid. The exact mechanism of these complexes how they exhibit this activity still remained uncovered which can be further explored in future. Protein binding studies of complexes were also performed by UV-vis absorption spectroscopy and bind constant were calculated in order to know affinity of these complexes with BSA protein. Moderate value of binding constant of complexes indicated potential role of serum protein in drug delivery. Cytotoxic analysis has also been performed for few complexes with calorimetric MTT assay in MCF-7 (breast cancer cell line) to check the anticancer potential of these complexes. Calculated IC_{50}valuesindicated that complexes are showing good cytotoxic activity as the value range from 5-9 which was higher as compared to standard cis-platin (IC_{50} = 2.2) in the breast cancer cell lines which indicated complexes showed good cytotoxic potential. From the DNA binding constant, it was clear that complexes bind moderately with the value the range of 10^2 M^{-1}.Type of interaction of complexes have been further explained by supporting with theoretical studies in the next chapter. Thus, it is evident that all the complexes are actively showing biological activity. Exact mechanism of interaction can be further explored in future.

4.7 References:

(1) Aggarwal, N., *Synthesis Characterization and Biological Properties of Schiff Base and Mixed ligand Complexes of Copper and Zinc*,Submitted to Lovely Professional University, **2019**. http://hdl.handle.net/10603/308512

(2) Jayamani, A., Sengottuvelan, N., Kang, S.K. and Kim, Y.I., Studies on nucleic acid/protein interaction, molecular docking and antimicrobial properties of mononuclear nickel (II) complexes of piperazine based Schiff base. *Inorganic Chemistry Communications*,**2014**, *48*, 147-152.https://doi.org/10.1016/j.inoche.2014.08.029

(3) Pyrzynska, K., Pękal, A., Application of free radical diphenylpicrylhydrazyl (DPPH) to estimate the antioxidant capacity of food samples. *Analytics Methods*, **2013**, *5*(17), 4288-4295. https://doi.org/10.1039/C3AY40367J

(4) Ansari, A.Q., Ahmed, S.A., Waheed, M.A. and Juned, S., Extraction and determination of antioxidant activity of Withania somnifera Dunal. *Eur. J. Exp. Biol*, **2013**, *3*(5), 502-507.

(5) Shalaby, E.A. and Shanab, S.M., Antioxidant compounds, assays of determination and mode of action. *African journal of pharmacy and pharmacology*, **2013**, *7*(10), 528-539. https://doi.org/10.5897/AJPP2013. 3474

(6) Huang, D., Ou, B. and Prior, R.L., The chemistry behind antioxidant capacity assays. *Journal of agricultural and food chemistry*, **2005**, *53*(6), 1841-1856. https://doi.org/10.1021/jf030723c

(7) Moharram, H.A. and Youssef, M.M., Methods for determining the antioxidant activity: a review. *Alexandria Journal of Food Science and Technology*, **2014,** *11*(1), 31-42. https://doi.org/10.12816/0025348

(8) Bondet, V., Brand-Williams, W. and Berset, C.L.W.T., Kinetics and mechanisms of antioxidant activity using the DPPH. free radical method. *LWT-Food Science and Technology*, **1997**, *30*(6), 609-615. https://doi.org/10.1006/fstl.1997.0240

(9) Antolovich, M., Prenzler, P.D., Patsalides, E., McDonald, S. and Robards, K., Methods for testing antioxidant activity. *Analyst*, **2002**, *127*(1), 183-198. https://doi.org/10.1039/B009171P

(10) Athavale, A., Jirankalgikar, N., Nariya, P. and Des, S., Evaluation of in-vitro antioxidant activity of panchagavya: a traditional ayurvedic preparation. *Int J Pharm Sci Res*, **2012**, *3*(1), 2543-9.

(11) Leaves, L. and Leaves, L., Antioxidant activity by DPPH radical scavenging method of ageratum conyzoides. *American Journal of Ethnomedicine*, **2014**, *1*(4), 244-249. http://www.ajethno.com/

(12) Pisoschi, A.M. and Negulescu, G.P., Methods for total antioxidant activity determination: a review. *Biochem Anal Biochem*, **2011**,*1*(1), p.106. http://dx.doi.org/10.4172/2161-1009.1000106

(13) Hermund, D.B., *Extraction, characterization and application of antioxidants from the Nordic brown alga Fucus vesiculosus*. National Food Institute, Technical University of Denmark**2016**.

(14) Brand-Williams, W., Cuvelier, M.E. and Berset, C.L.W.T., Use of a free radical method to evaluate antioxidant activity. *LWT-Food science and Technology*, **1995**, *28*(1), 25-30. https://doi.org/10.1016/S0023-6438(95)80008-5.

(15) Garcia, E.J., Oldoni, T.L.C., Alencar, S.M.D., Reis, A., Loguercio, A.D. and Grande, R.H.M., Antioxidant activity by DPPH assay of potential solutions to be applied on bleached teeth. *Brazilian dental journal*, **2012**, *23*(1), 22-27. https://doi.org/10.1590/S0103-64402012000100004.

(16) Kostova, I. and Saso, L., Advances in research of Schiff-base metal complexes as potent antioxidants. *Current medicinal chemistry*, **2013**, *20*(36), 4609-4632.

(17) Kadhum, A.A.H., Mohamad, A.B., Al-Amiery, A.A. and Takriff, M.S., Antimicrobial and antioxidant activities of new metal complexes derived from 3-aminocoumarin. *Molecules*, **2011**, *16*(8), 6969-6984. https://doi.org/10.3390/molecules16086969.

(18) Marxen, K., Vanselow, K.H., Lippemeier, S., Hintze, R., Ruser, A. and Hansen, U.P., Determination of DPPH radical oxidation caused by methanolic extracts of some microalgal species by linear regression analysis of spectrophotometric measurements. *Sensors*, **2007**, *7*(10), 2080-2095. https://doi.org/10.3390/s7102080.

(19) Molyneux, P., The use of the stable free radical diphenylpicrylhydrazyl (DPPH) for estimating antioxidant activity. *Songklanakarin J. sci. technol*, **2004**, *26*(2), 211-219.

(20) Olalere, O.A., Abdurahman, H.N., Yunus, R.B.M., Alara, O.R., Ahmad, M.M., Zaki, Y.H. and Abdlrhman, H.S.M., Parameter study, antioxidant activities, morphological and functional characteristics in microwave extraction of medicinal oleoresins from black and white pepper. *Journal of Taibah University for Science*, **2018**, *12*(6), 730-737. https://doi.org/10.1080/16583655.2018.1515323.

(21) Shen, Q., Zhang, B., Xu, R., Wang, Y., Ding, X. and Li, P., Antioxidant activity in vitro of the selenium-contained protein from the Se-enriched Bifidobacterium animalis 01. *Anaerobe*, **2010**, *16*(4), 380-386. https://doi.org/10.1016/j.anaerobe.2010.06.006.

(22) Muñiz-Márquez, D.B., Wong-Paz, J.E., Contreras-Esquivel, J.C., Rodriguez-Herrera, R. and Aguilar, C.N., Extraction of phenolic compounds from Coriandrum sativum L. and Amaranthus hybridus L. by microwave technology. In *Polyphenols in plants*, **2019**, 185-190. https://doi.org/10.1016/B978-0-12-813768-0.00012-8.

(23) Reed, S.M., Bayly, W.M., Sellon, D.C., *Equine Internal Medicine-E-Book. Elsevier Health Sciences***2017**.

(24) Zeitlinger, M.A., Derendorf, H., Mouton, J.W., Cars, O., Craig, W.A., Andes, D. and Theuretzbacher, U., Protein binding: do we ever learn?. *Antimicrobial agents and chemotherapy*, **2011**, *55*(7), 3067-3074. https://doi.org/10.1128/AAC.01433-10.

(25) Vyas, K.M., Jadeja, R.N., Patel, D., Devkar, R.V. and Gupta, V.K., A new pyrazolone based ternary Cu (II) complex: Synthesis, characterization, crystal structure, DNA binding, protein binding and anti-cancer activity towards A549 human lung carcinoma cells with a minimum cytotoxicity to non-cancerous cells. *Polyhedron*, **2013**, *65*(1), 262-274. https://doi.org/10.1016/j.poly.2013.08.051

(26) Zhang, Y.P., Li, Y., Xu, G.C., Li, J.Y., Luo, H.Y., Li, J.Y., Zhang, L., and Jia, D.Z., Synthesis, crystal structure, DNA/bovine serum albumin binding and antitumor activity of two transition metal complexes with 4-acylpyrazolone derivative. *Applied Organometallic Chemistry*, **2019**, *33*(3), p.e4668. https://doi.org/10.1002/aoc.4668.

(27) Neelakantan, M.A., Balamurugan, K., Balakrishnan, C. and Subha, L., Interaction of amino acid Schiff base metal complexes with DNA/BSA protein and antibacterial activity: spectral studies, DFT calculations and molecular docking simulations. *Applied Organometallic Chemistry*, **2018**, *32*(4), p.e4259. https://doi.org/10.1002/aoc.4259.

(28) Damre, A.A. and Iyer, K.R., The significance and determination of plasma protein binding. *Encyclopedia of Drug Metabolism and Interactions*, **2011**, 1-18. https://doi.org/10.1002/9780470921920.edm032.

(29) Krishnamoorthy, P., Sathyadevi, P., Cowley, A.H., Butorac, R.R. and Dharmaraj, N., Evaluation of DNA binding, DNA cleavage, protein binding and in vitro cytotoxic activities of bivalent transition metal hydrazone complexes. *European journal of medicinal chemistry*, **2011**, *46*(8), pp.3376-3387. https://doi.org/10.1016/j.ejmech.2011.05.001.

(30) Mishra, M., Tiwari, K., Shukla, S., Mishra, R. and Singh, V.P., Synthesis, structural investigation, DNA and protein binding study of some 3d-metal complexes with N′-(phenyl-pyridin-2-yl-methylene)-thiophene-2-carboxylic acid hydrazide. *Spectrochimica Acta Part A: Molecular and Biomolecular Spectroscopy*, **2014**, *132*, 452-464. https://doi.org/10.1016/j.saa.2014.05.007.

(31) Rajendiran, V., Karthik, R., Palaniandavar, M., Stoeckli-Evans, H., Periasamy, V.S., Akbarsha, M.A., Srinag, B.S. and Krishnamurthy, H., Mixed-ligand copper (II)-phenolate complexes: effect of coligand on enhanced DNA and protein binding, DNA cleavage, and anticancer activity. *Inorganic chemistry*, **2007**, *46*(20), 8208-8221. https://doi.org/10.1021/ic700755p.

(32) Sakthi, M. and Ramu, A., Synthesis, structure, DNA/BSA binding and antibacterial studies of NNO tridentate Schiff base metal complexes. *Journal of Molecular Structure*, **2017**, *1149*, 727-735. https://doi.org/10.1016/j.molstruc.2017.08.040.

(33) Topală, T., Bodoki, A., Oprean, L. and Oprean, R., Bovine serum albumin interactions with metal complexes. *Clujul medical*, **2014**, *87*(4), p.215. https://dx.doi.org/10.15386%2Fcjmed-357.

(34) Aggarwal, N., Kant, R., Kumar, G., James, C. and Maji, S., Synthesis, characterization and biological evaluation studies of Cu (II) and Zn (II)

complexes with gly-o-andn or gly-p-andn as primary ligand and N, N'donors as secondary ligand. In *Journal of Physics: Conference Series* **2020**,1531(1), p. 012111). IOP Publishing. doi:10.1088/1742-6596/1531/1/012111.

(35) Aggarwal, N., Mehtab, S. and Maji, S., Synthesis of Salicylic Acid Based Mixed Ligand Complexes: Their Protein Binding Affinities and Antimicrobial Activities. *Asian Journal of Chemistry*, **2017**, *29*(9), 2069-2073.

(36) Mosaddegh, M., Gharanjik, B.M., Naghibi, F., Esmaeili, S., Pirani, A., Eslami Tehrani, B., Keramatian, B. and Hassanpour, A., A survey of cytotoxic effects of some marine algae in the Chabahar coast of Oman Sea. *Research Journal of Pharmacognosy*, **2014**, *1*(1), 27-31.

(37) Makhmalzade, B.S. and Chavoshy, F., Polymeric micelles as cutaneous drug delivery system in normal skin and dermatological disorders. *Journal of advanced pharmaceutical technology & research*, **2018**, *9*(1), p.2. https://dx.doi.org/10.4103%2Fjaptr.JAPTR_314_17.

(38) Brabec, V., Christofis, P., Slámová, M., Kostrhunová, H., Nováková, O., Najajreh, Y., Gibson, D. and Kašpárková, J., DNA interactions of new cytotoxic tetrafunctional dinuclear platinum complex trans, trans-[{PtCl2 (NH3)} 2 (piperazine)]. *Biochemical pharmacology*, **2007**, *73*(12), 1887-1900. https://doi.org/10.1016/j.bcp.2007.03.003.

(39) Daud, N.N.N.N.M., Septama, A.W., Simbak, N., Bakar, N.H.A. and Rahmi, E.P., Synergistic Effect of Flavonoids from Artocarpus heterophyllus Heartwoods on Anticancer Activity of Cisplatin Against H460 and MCF-7 Cell Lines. *Natural Product Sciences*, **2019**, *25*(4), 311-316. https://doi.org/10.20307/nps.2019.25.4.311.

(40) Oramas-Royo, S., Torrejon, C., Cuadrado, I., Hernandez-Molina, R., Hortelano, S., Estevez-Braun, A. and de Las Heras, B., Synthesis and cytotoxic activity of metallic complexes of lawsone. *Bioorganic & medicinal chemistry*, **2013**, *21*(9), 2471-2477. https://doi.org/10.1016/j.bmc.2013.03.002.

(41) Teixeira, L.J., Seabra, M., Reis, E., Girão da Cruz, M.T., Pedroso de Lima, M.C., Pereira, E., Miranda, M.A. and Marques, M.P.M., Cytotoxic activity of metal complexes of biogenic polyamines: polynuclear platinum (II)

chelates. *Journal of medicinal chemistry*, **2004**, *47*(11), 2917-2925. https://doi.org/10.1021/jm0311238.

(42) Varbanov, H., Valiahdi, S.M., Legin, A.A., Jakupec, M.A., Roller, A., Galanski, M. and Keppler, B.K., Synthesis and characterization of novel bis (carboxylato) dichloridobis (ethylamine) platinum (IV) complexes with higher cytotoxicity than cisplatin. *European journal of medicinal chemistry*, **2011**, *46*(11), 5456-5464. https://doi.org/10.1016/j.ejmech.2011.09.006.

(43) You, C., Yu, J., Sun, Y., Luo, Y., Zhang, X., Zhu, J. and Sun, B., Enhanced cytotoxicity by a benzothiazole-containing cisplatin derivative in breast cancer cells. *New Journal of Chemistry*, **2017**, *41*(2), 773-785. https://doi.org/10.1039/C6NJ02753A.

(44) Mirmalek, S.A., Azizi, M.A., Jangholi, E., Yadollah-Damavandi, S., Javidi, M.A., Parsa, Y., Parsa, T., Salimi-Tabatabaee, S.A. and Alizadeh-Navaei, R., Cytotoxic and apoptogenic effect of hypericin, the bioactive component of Hypericum perforatum on MCF-7 human breast cancer cell line. *Cancer cell international*, **2015**, *16*(1), 1-9. https://doi.org/10.1186/s12935-016-0279-4.

(45) Mirmalek, S.A., Jangholi, E., Jafari, M., Yadollah-Damavandi, S., Javidi, M.A., Parsa, Y., Parsa, T., Salimi-Tabatabaee, S.A., Kolagar, H.G., Jalil, S.K. and Alizadeh-Navaei, R., Comparison of in vitro cytotoxicity and apoptogenic activity of magnesium chloride and cisplatin as conventional chemotherapeutic agents in the MCF-7 cell line. *Asian Pacific Journal of Cancer Prevention*, **2016**, *17*(sup3), 131-134. https://doi.org/10.7314/APJCP.2016.17.S3.131.

(46) Aslantürk, Ö.S., *In vitro cytotoxicity and cell viability assays: principles, advantages, and disadvantages* **2018**, *2*(1), p. 64). InTech. https://doi.org/10.5772/intechopen.71923.

(47) Ferrari, M., Fornasiero, M.C. and Isetta, A.M., MTT colorimetric assay for testing macrophage cytotoxic activity in vitro. *Journal of immunological methods*, **1990**, *131*(2), 165-172. https://doi.org/10.1016/0022-1759(90)90187-Z.

(48) Ganot, N., Meker, S., Reytman, L., Tzubery, A. and Tshuva, E.Y., Anticancer metal complexes: synthesis and cytotoxicity evaluation by the MTT

assay. *Journal of visualized experiments: JoVE*, **2013**, (81). https://doi.org/10.3791/50767.

(49) Abd-El-Aziz, A.S., Abdelghani, A.A., El-Sadany, S.K., Overy, D.P. and Kerr, R.G., Antimicrobial and anticancer activities of organoiron melamine dendrimers capped with piperazine moieties. *European Polymer Journal*, **2016**, *82*(1), 307-323. https://doi.org/10.1016/j.eurpolymj.2016.04.002.

(50) Goswami, S., Maity, S., Maity, A.C., Das, A.K., Khanra, K., Mandal, T.K. and Bhattacharyya, N., A macrocyclic piperazine linked extremely Zn2+ selective fluorescent chemosensor with bio-imaging and for H2PO4− sensing. *Tetrahedron Letters*, **2014**, *55*(43), 5993-5997. https://doi.org/10.1016/j.tetlet.2014.09.014.

(51) Keypour, H., Rezaei, M.T., Jamshidi, M., Farida, S.H.M. and Karamian, R., Synthesis, cytotoxicity, and antioxidant activity by in vitro and molecular docking studies of an asymmetrical diamine containing piperazine moiety and related Zn (II), Cd (II) and Mn (II) macrocyclic schif base complexes. *Inorganic Chemistry Communications*, **2021**, *125*(1), p.108443. https://doi.org/10.1016/j.inoche.2021.108443.

(52) Prasad, H.N., Ananda, A.P., Najundaswamy, S., Nagashree, S., Mallesha, L., Dayananda, B.P., Jayanth, H.S. and Mallu, P., Design, synthesis and molecular docking studies of novel piperazine metal complexes as potential antibacterial candidate against MRSA. *Journal of Molecular Structure*, **2021**, *1232*(1), p.130047. https://doi.org/10.1016/j.molstruc.2021.130047.

(53) Pait, M., Kundu, B., Kundu, S.C. and Ray, D., Copper (II) complexes of piperazine based ligand: Synthesis, crystal structure, protein binding and evaluation of anti-cancerous therapeutic potential. *Inorganica Chimica Acta*, **2014**, *418*(1), 30-41. https://doi.org/10.1016/j.ica.2014.04.019.

(54) Bacher, F., Dömötör, O., Chugunova, A., Nagy, N.V., Filipović, L., Radulović, S., Enyedy, É.A. and Arion, V.B., Strong effect of copper (II) coordination on antiproliferative activity of thiosemicarbazone–piperazine and thiosemicarbazone–morpholine hybrids. *Dalton transactions*, **2015**, *44*(19), 9071-9090. https://doi.org/10.1039/c5dt01076d.

(55) Doniz Kettenmann, S., Nossol, Y., Louka, F.R., Legrande, J.R., Marine, E., Fischer, R.C., Mautner, F.A., Hergl, V., Kulak, N. and Massoud, S.S., Copper (II) Complexes with Tetradentate Piperazine-Based Ligands: DNA Cleavage and Cytotoxicity. *Inorganics*, **2021**, *9*(2), p.12.https://doi.org/10.3390/inorganics9020012.

(56) Kamal, A., Sreekanth, K., Shankaraiah, N., Sathish, M., Nekkanti, S. and Srinivasulu, V., Dithiocarbamate/piperazine bridged pyrrolobenzodiazepines as DNA-minor groove binders: Synthesis, DNA-binding affinity and cytotoxic activity. *Bioorganic chemistry*, **2015**, *59*(1), 23-30. https://doi.org/10.1016/j.bioorg.2015.01.002.

(57) Karthick, C.; Gurumoorthy, P.; Musthafa, M. A. I.; Lakra, R.; Korrapati, P. S.; Rahiman, A. K. Dinuclear Phenoxo-Bridged "End-off" Complexes Containing a Piperazine That Shows Chemical Nuclease and Cytotoxic Activities. J. Coord. Chem. **2014**, *67*(10), 1794–1808. https://doi.org/10.1080/00958972.2014.920501.

(58) Keypour, H.; Mahmoudabadi, M.; Shooshtari, A.; Hosseinzadeh, L.; Mohsenzadeh, F.; Gable, R. W. Synthesis of Mn(II) and Zn(II) Complexes with New Macrocyclic Schiff-Base Ligands Containing Piperazine Moiety: Spectroscopic, Structural, Cytotoxic and Antibacterial Properties. *Polyhedron*,**2017**, *127*(1), 345–354. https://doi.org/10.1016/j.poly.2017.02.008.

(59) Kovala-Demertzi, D., Alexandratos, A., Papageorgiou, A., Yadav, P.N., Dalezis, P. and Demertzis, M.A., Synthesis, characterization, crystal structures, in vitro and in vivo antitumor activity of palladium (II) and zinc (II) complexes with 2-formyl and 2-acetyl pyridine N (4)-1-(2-pyridyl)-piperazinyl thiosemicarbazone. *Polyhedron*, **2008**, *27*(13), 2731-2738. https://doi.org/10.1016/j.poly.2008.04.009.

(60) Sladowski, D., Steer SJ, Clothier RH, and Balls M. An improved MTT assay. *J Immunol Methods*, **1993**, *157*, 203-207. https://doi.org/10.1016/0022-1759(93)90088-O.

(61) Tolosa, L.; Donato, M. T.; Gómez-lechón, M. J. Chapter 26 General Cytotoxicity Assessment by Means of the MTT Assay. **2015**, *1250*, 333–348. https://doi.org/10.1007/978-1-4939-2074-7.

(62) Kumbar, V.M., Peram, M.R., Kugaji, M.S., Shah, T., Patil S.P., Muddapur, U.M., Bhat, K.G., Effect of curcumin on growth, biofilm formation and virulence factor gene expression of Porphyromonas gingivalis, *Odontology*, **2021**, *109*(1), 18-28. https://doi.org/10.1007/s10266-020-00514-y.

(63) Nair, M.S., Arish, D. and Johnson, J., Synthesis, characterization and biological studies on some metal complexes with Schiff base ligand containing pyrazolone moiety. *Journal of Saudi Chemical Society*, **2016**, *20*, S591-S598.https://doi.org/10.1016/j.jscs.2013.04.007

(64) Zhang, G.; Wang, L.; Zhou, X.; Li, Y.; Gong, D. Binding Characteristics of Sodium Saccharin with Calf Thymus DNA, *Journal of Agriculture and Food Chemistry*,**2014**, *62*(4) 991-1000.https://doi.org/10.1021/jf405085g.

(65) Zhang, H.; Liu, C.; Bu, X. Synthesis , Crystal Structure , Cytotoxic Activity and DNA-Binding Properties of the Copper (II) and Zinc (II) Complexes with 1- [3- (2-Pyridyl) Pyrazol-1-Ylmethyl] Naphthalene. **2005**, *99*, 1119–1125. https://doi.org/10.1016/j.jinorgbio.2005.02.005.

(66) Sunita, M.; Anupama, B.; Umesh, B.; Kumari, C. G. Synthesis , Characterization , DNA Binding And Cleavage Studies of Mixed-Ligand Copper(II) complexes of 2, 6-bis (benzimidazol-2-yl) pyridine. *Journal of Fluorescence*,**2012**, *22*(3), 1003-1012. https://doi.org/10.1016/j.arabjc.2014.01.017.

(67) Sarkar, D.; Das, P.; Basak, S.; Chattopadhyay, N. Binding Interaction of Cationic Phenazinium Dyes with Calf Thymus DNA: A Comparative Study. **2008**, *112*(30), 9243–9249.https://doi.org/10.1021/jp801659d.

(68) Kausar, N.; Siddiqa, A.; Yaqub, A.; Sabahat, S. Spectrochimica Acta Part A : Molecular and Biomolecular Spectroscopy Spectrophotometric Analysis of Flavonoid – DNA Binding Interactions at Physiological Conditions. **2009**, *74*, 1135–1137. https://doi.org/10.1016/j.saa.2009.09.022.

(69) Eshkourfu, R.; Vuj, M.; Turel, I.; Pevec, A.; Sep, K.; Zec, M.; Srdi, T.; Miti, D.; Andjelkovi, K. Synthesis , Characterization , Cytotoxic Activity and DNA

Binding Properties of the Novel Dinuclear Cobalt (III) Complex with the Condensation Product of 2-Acetylpyridine and Malonic Acid Dihydrazide. **2011**, *105*, 1196–1203. https://doi.org/10.1016/j.jinorgbio.2011.05.024.

(70) Hayat, F.; Faryad, R.; Bélanger-gariepy, F. Molecular , Supramolecular , DNA-Binding and Biological Studies of Piperazine and Piperidine Based Dithiocarbamates of Biocompatible Copper. Inorg. Chem. Commun. 2020, 121 (July), 108190. https://doi.org/10.1016/j.inoche.2020.108190.

(71) Chaires, J. B. A Thermodynamic Signature for Drug – DNA Binding Mode, **2006**, *453*, 26-31. https://doi.org/10.1016/j.abb.2006.03.027.

(72) Ghosh, S.; Kundu, P.; Paul, B. K.; Chattopadhyay, N.,Binding of an Anionic Fluorescent Probe with Calf Thymus DNA and Effect of Salt on the Probe–DNA Binding: A Spectroscopic and Molecular Docking Investigation, RSC Adv. **2014**, *4* (108), 63549-63558. https://doi.org/10.1039/C4RA14298E.

(73) Ricci, C. G.; Netz, P. A. Docking Studies on DNA-Ligand Interactions : Building and Application of a Protocol To Identify the Binding Mode. **2009**, 1925–1935.https://doi.org/10.1021/ci9001537.

(74) Bhat, I. ul H.; Tabassum, S. Synthesis of New Piperazine Derived Cu(II)/Zn(II) Metal Complexes, Their DNA Binding Studies, Electrochemistry and Anti-Microbial Activity: Validation for Specific Recognition of Zn(II) Complex to DNA Helix by Interaction with Thymine Base *Spectrochim. Acta - Part A Mol. Biomol. Spectrosc.***2009**, *72* (5), 1026–1033. https://doi.org/10.1016/j.saa.2008.12.037

CHAPTER 5

COMPUTATIONAL STUDIES OF SYNTHESIZED LIGANDS AND COMPLEXES

5.1 Introduction

Optimization of geometry has become one of the most fundamental components for modern computational chemists to study the structural reactivity of molecules. The optimized geometry is considered the geometry in which strain of a system is minimum. The main objective in geometry optimization process is to find out an atomic arrangement of molecules which makes the them most stable in the lowest energy state.[1,2]To optimize geometry of a molecule, different possibilities are tested to check the lowest energy by performing a series of iteration till the molecule is reached to minimum.[3,4]Minimization of energy becomes more essential forelucidating the correct molecular arrangement in 3D space as chemical structures drawn in 2D are notenergetically favourable sometimes. Molecular mechanics energy approximations search using conformational energy to find all possible energetically favoured conformations which are mathematically equivalent to locating energy minima and are considered most valid.[5] Before running any computational program, geometry of molecule must be understood in terms of bond angle, dihedral angle and bond distance etc, very carefully since molecular geometry is responsible for determining importantphysiochemical properties.[6] To explain the effect of different geometries on different energy levels PES (potential energy surface) is calculated which are characterized by following distinct parameters:LocalMinimawithlowest value of PES in a particular section or region. GlobalMinimawithlowest PES value in the entire region and/or Saddlepointwithmaximum PES value in one direction and a minimum in the other.[7-9]

5.2 Geometry Optimization of ligand:

Important additional insights are provided by computational chemistry which aid remarks to experimental studies by the information such as energy of ground state of a molecule which is not possible to generate experimentally (Table 5.1).[10] The optimized structures provide idea about the donor atoms orientation in the ligands available for bonding to the metals during complex formation.[11] All ligands (HL1-H_4L14) were optimized using Orca 4.0.1.2[12] to find the equilibrium structure. Hybrid functional method B3LYP was used for all the calculations using basis set 6-31G(2d,2p). Frequency calculations showed that optimized structures as global

minima as no negative frequencies were obtained in these structures. Figure 5.1-5.14 represents the optimized structure of ligands (HL1-H_4L14) and cartesian coordinates of all the optimized ligands have been given in the annexure file.

Table 5.1: Theoretical energy of optimized ligands

Ligand Code	Energy of optimized ground state (eV)	Ligand Code	Energy of optimized ground state (eV)
HL1	-514.507836073	HL8	-573.610486254
HL2	-513.885581690	H_2L9	-574.942998402
HL3	-514.532428171	H_2L10	-1036.38318747
HL4	-498.468224021	H_6L11	-1378.54139046
HL5	-612.892956347	H_4L12	-1150.49856030
HL6	-612.891879840	H_4L13	-1228.45024288
HL7	-573.611085193	H_4L14	-1611.42314074

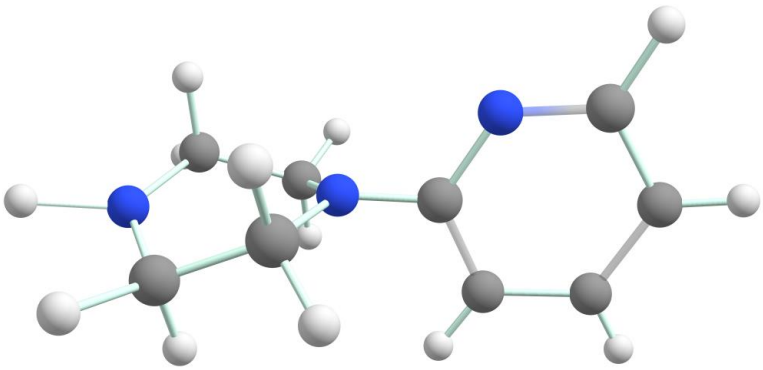

Figure 5.1: Geometrically optimized structure of HL1

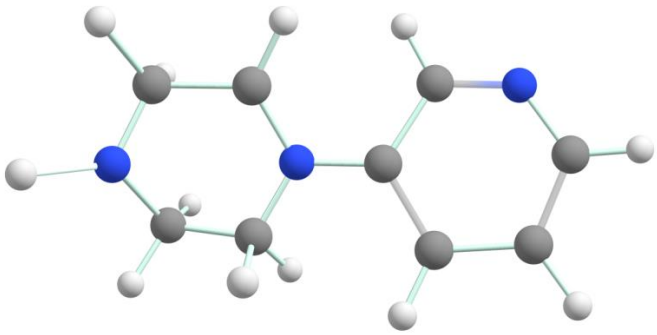

Figure 5.2: Geometrically optimized structure of HL2

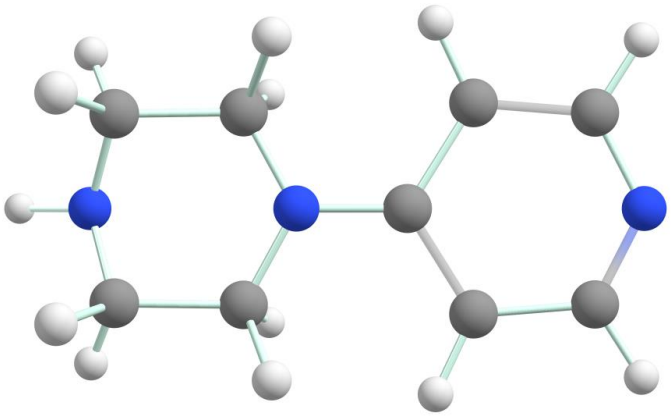

Figure 5.3: Geometrically optimized structure of HL3

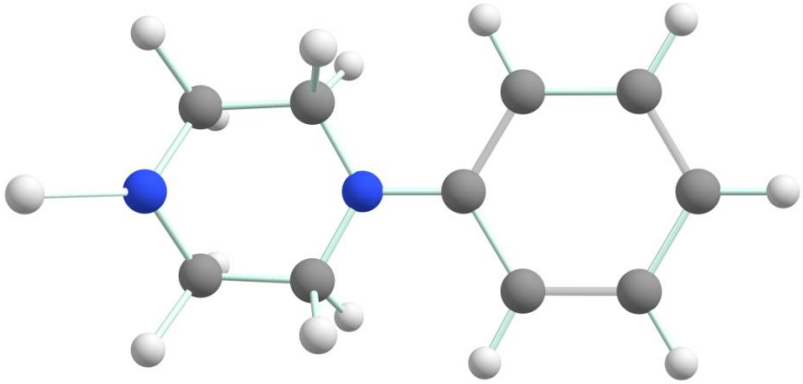

Figure 5.4:Geometrically optimized structure of HL4

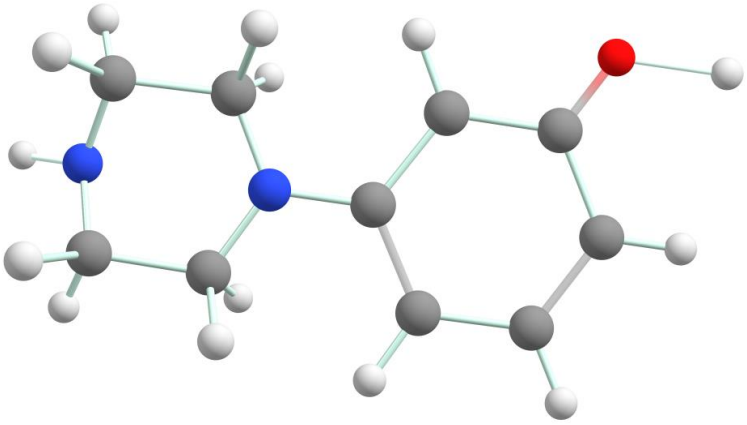

Figure 5.5: Geometrically optimized structure of HL5

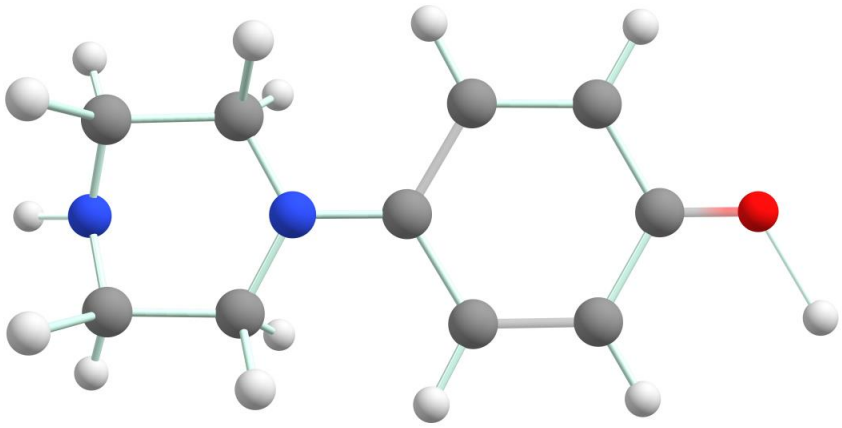

Figure 5.6: Geometrically optimized structure of HL6

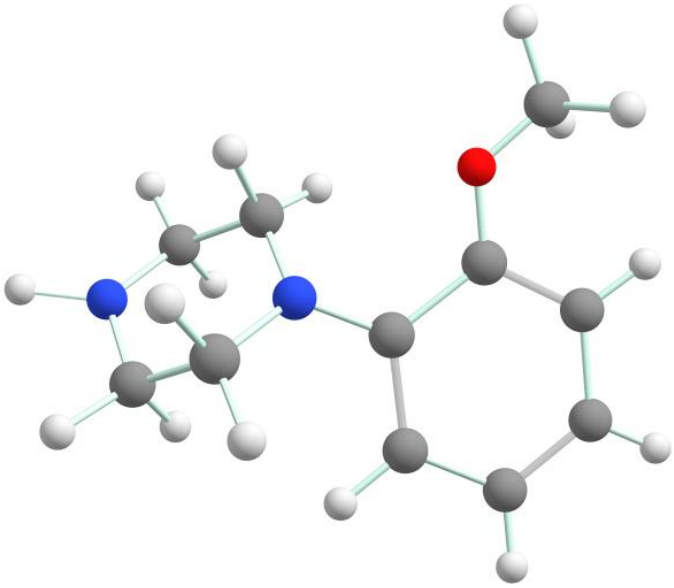

Figure 5.7: Geometrically optimized structure of HL7

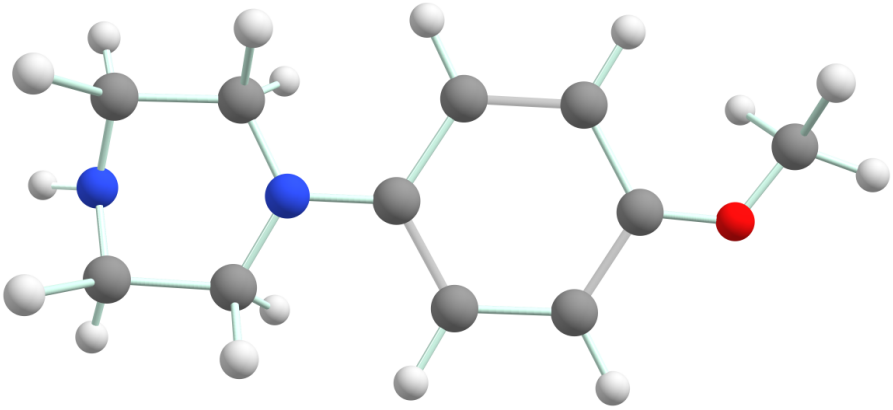

Figure 5.8:Geometrically optimized structure of HL8

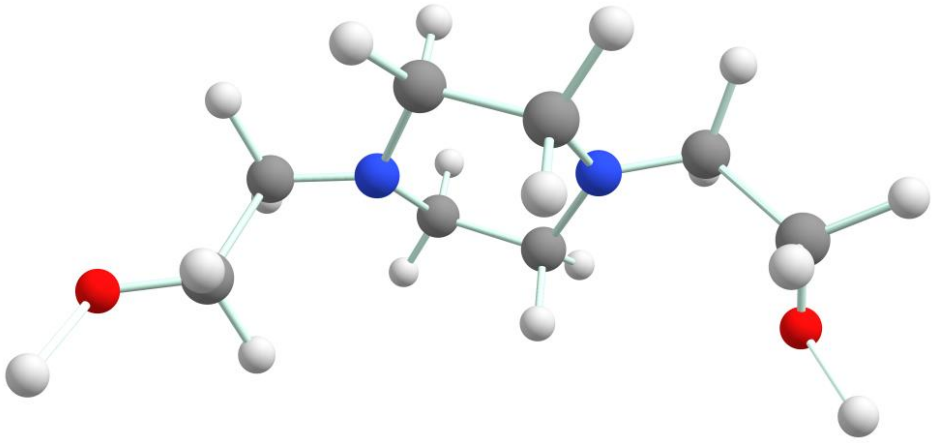

Figure 5.9:Geometrically optimized structure of H_2L9

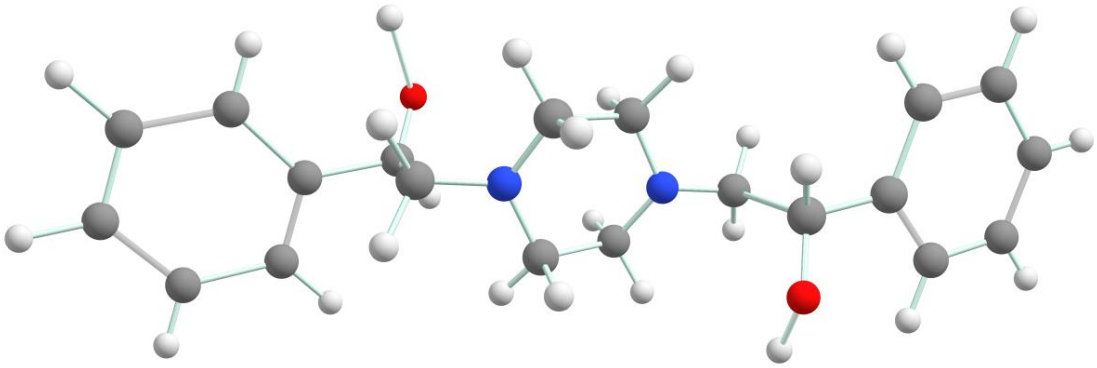

Figure 5.10:Geometrically optimized structure of H_2L10

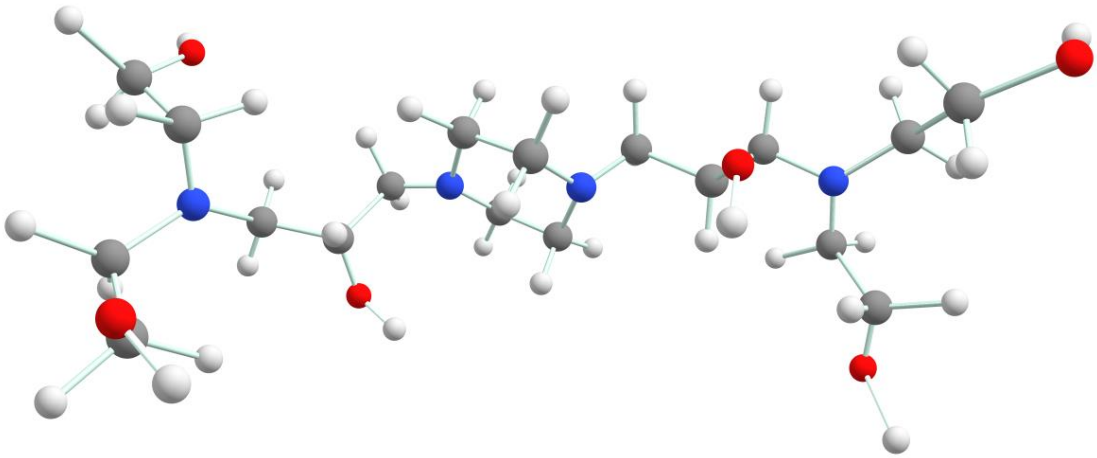

Figure 5.11:Geometrically optimized structure of ligand H_6L11

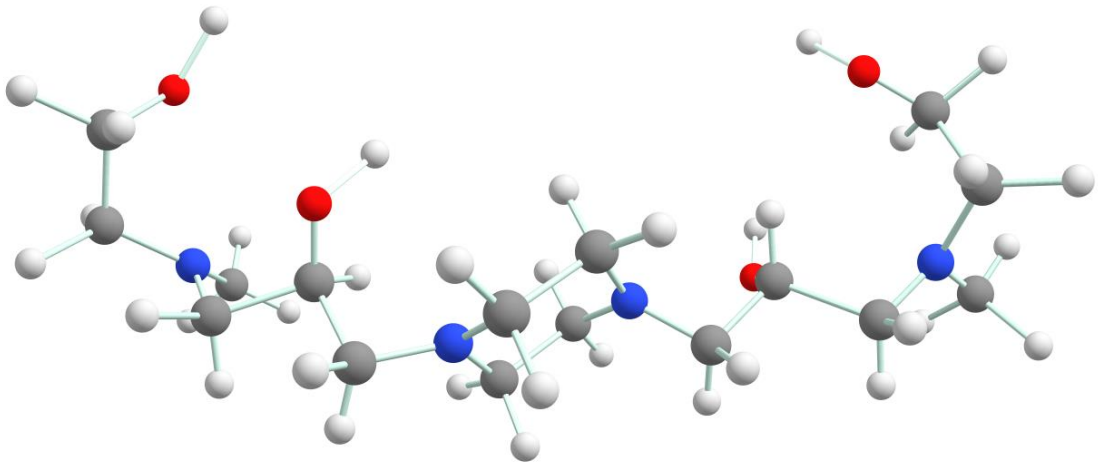

Figure 5.12: Geometrically optimized structure of H_2L12

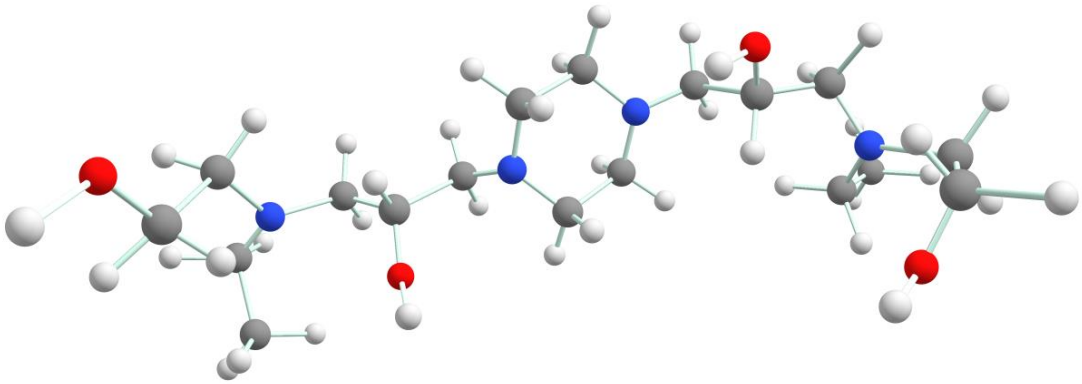

Figure 5.13: Geometrically optimized structure of H_2L13

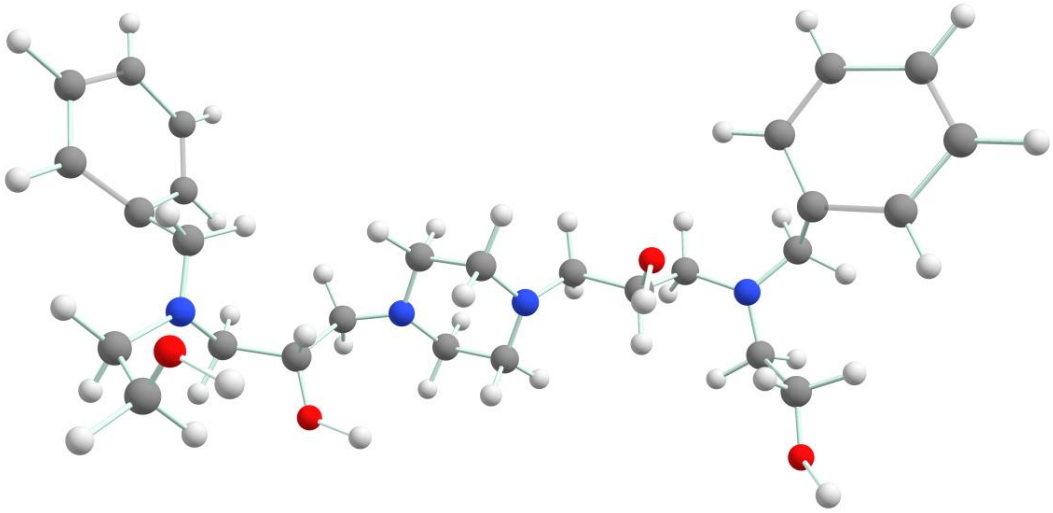

Figure 5.14: Geometrically optimized structure of H_2L14

5.3 TDDFT Calculation: Theoretical UV spectroscopic study

Geometry optimized ligands were analyzed by time dependent density functional theory (TDDFT) method.[13,14]UV-vis spectrum can be obtained and compared to the experimental observation by calculating energies of excited states,[15,16] oscillator strength (f_{osc}) and molecular orbitals contributioninvolved in the electronic transition.Thus, calculationswereperformed using the previously optimized geometry of ligandsin vacuumwith method hybrid functional-B3LYP and 6-31G(2d,2p) Pople style basis set using free computational software package ORCA 4.0.1.2[12,17]Different molecular orbitals (HOMO (highest occupied molecular orbital) and LUMO (lowest unoccupied molecular orbital) and FMO (frontier molecular orbital)) involved in most importantelectronic transitions are represented and visualized with software package Avogadro.[18] UV-vis graph have been sketched for both experimental performed data and theoretically obtained values. Experimental ligand's absorption maximum wavelength (λ_{max}) and their absorbance are corroborated with that of theoretically obtained values (Table 5.2).[19]Detailed analysis of seven different states along with orbital contributions and oscillator strength (f_{osc}), involved molecular orbitals transitionsand energies (in eV) are given in table (Table 5.3).

Table 5.2: Comparison of experimental and theoretical results

Code	**Experimental Observation**		**Theoretical Observation**	
	λ_{max}(nm)	**Abs.**	**λ_{max}(nm)**	**Abs.**
HL1	258	1.41	270	1.03
HL2	250	1.44	250	1.44
HL3	299	0.64	304	0.47
HL4	231, 290	2.45, 0.44	261, 298	2.33, 0.503
HL6	229, 281	3.05, 1.30	235, 283	3.02, 0.614
H_6L11	224	0.921	257	0.908
H_4L12	210	3.10	217	2.98
H_4L13	210	2.20	219	2.15
H_4L14	237	3.71	251	3.68

From the TDDFT calculation, compared UV-vis graphs for experimental and theoretical and the nearby molecular orbitals involved have been represented in figures 5.15-5.32. All the calculated graphs were in fair agreement to the experimental observations with slight shift in absorption maximum which is common in theoretical calculations.

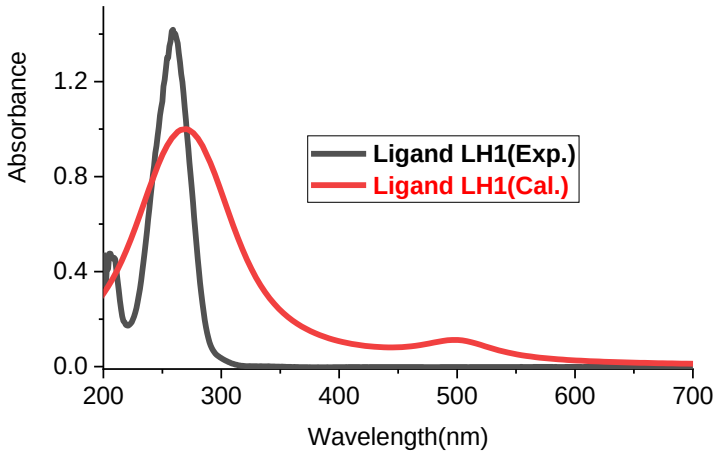

Figure 5.15:Compared experimental and theoretical UV graph of HL1

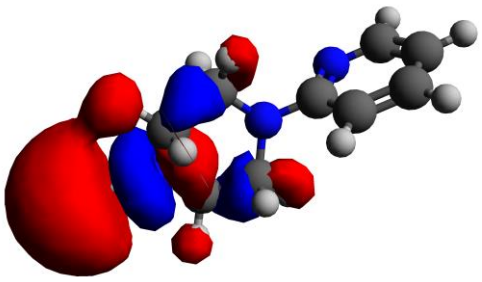

LUMO (45)

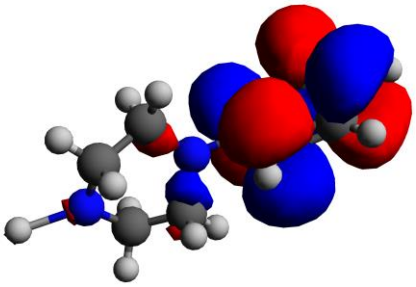

LUMO +1(46)

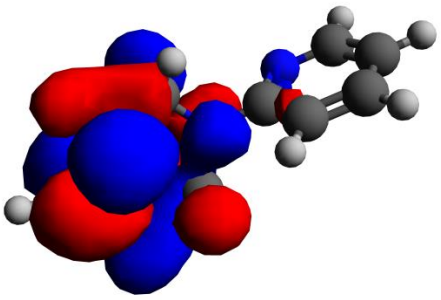

HOMO (44)

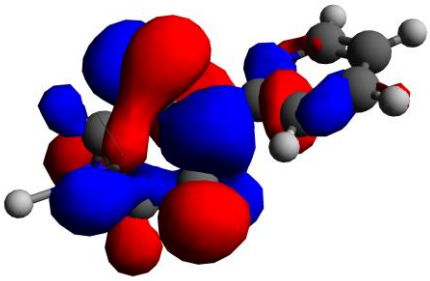

HOMO -1(43)

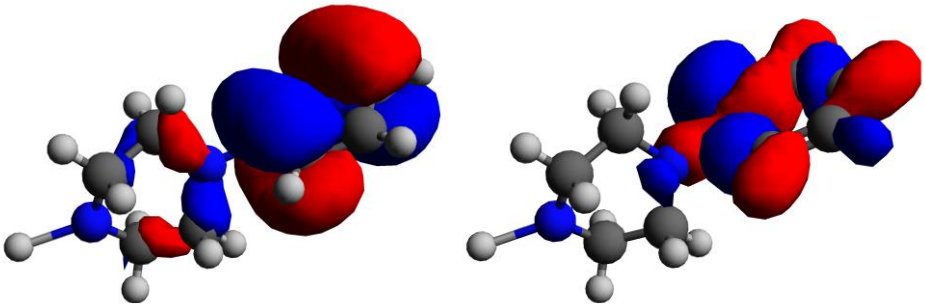

HOMO -2(44) **HOMO -3(43)**

Figure 5.16:Nearby molecular orbitals (isosurface value 0.02) involved in the electronic transition of HL1

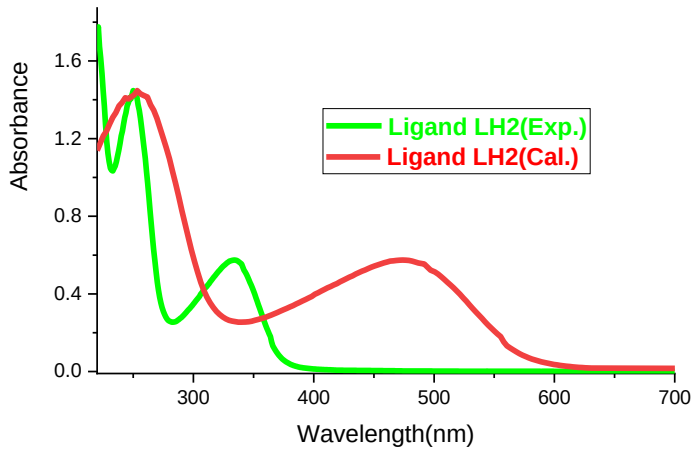

Figure 5.17:Compared experimental and theoretical UV graph of HL2

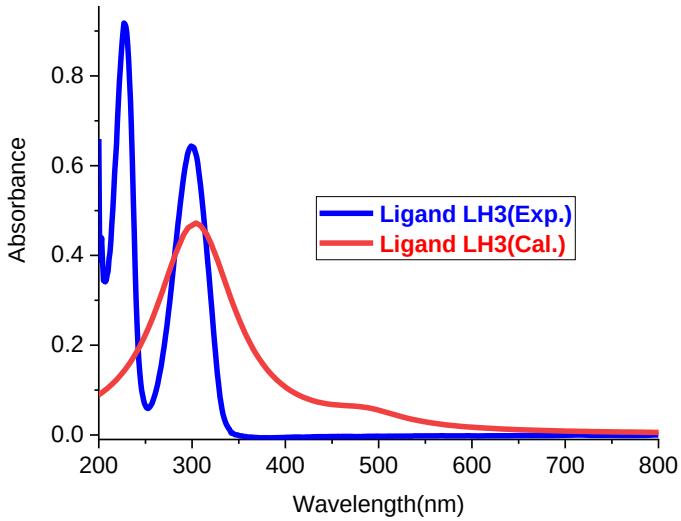

Figure 5.18:Compared experimental and theoretical UV graph of HL3

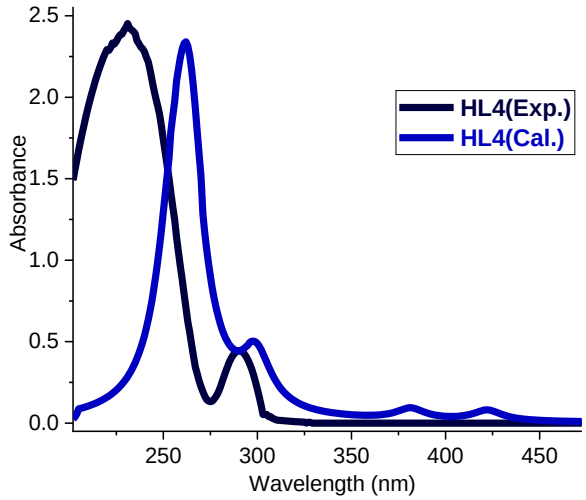

Figure 5.19:Compared experimental and theoretical UV graph of HL4

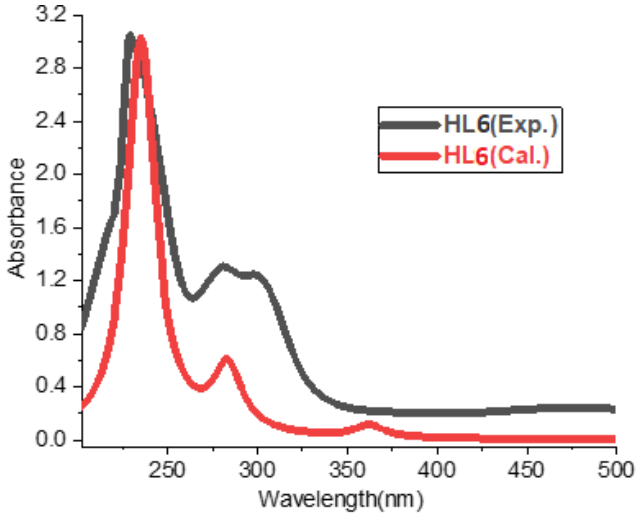

Figure 5.20:Compared experimental and theoretical UV graph of HL6

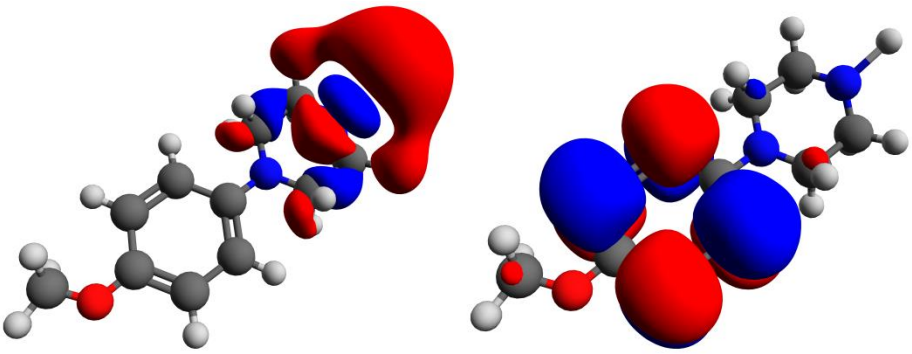

LUMO (53) **LUMO +1(54)**

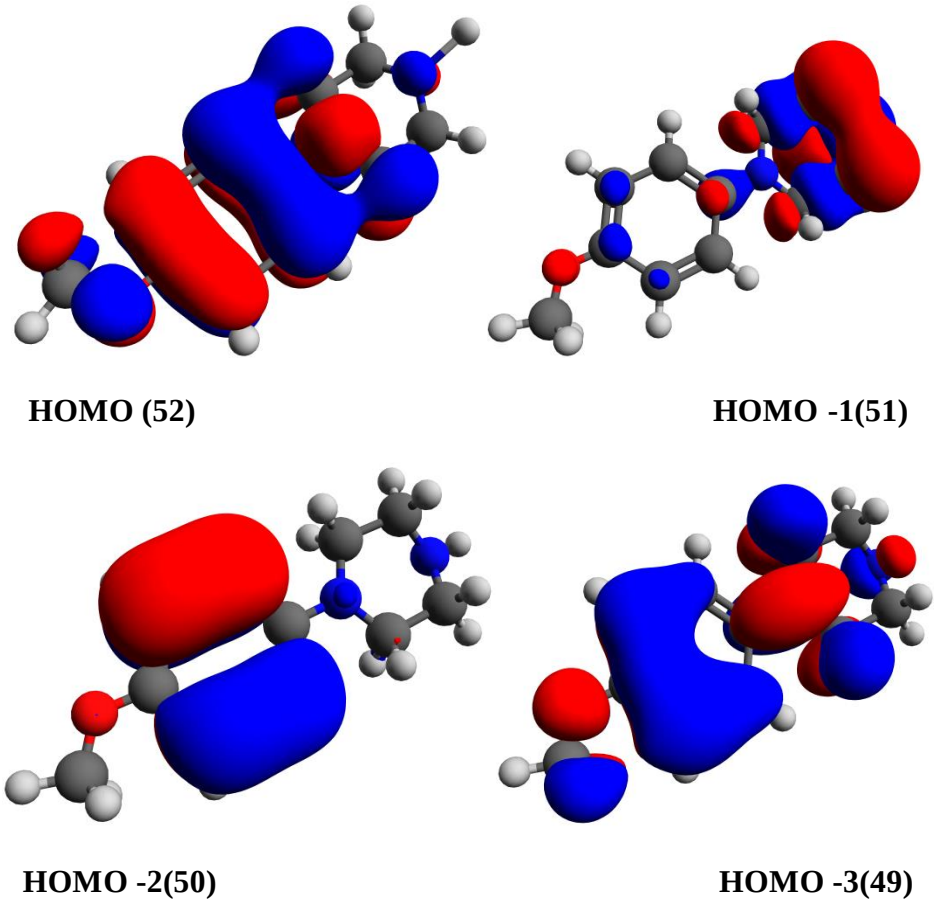

Figure 5.21:Nearby molecular orbitals (isosurface value 0.02) involved in the electronic transition of HL6

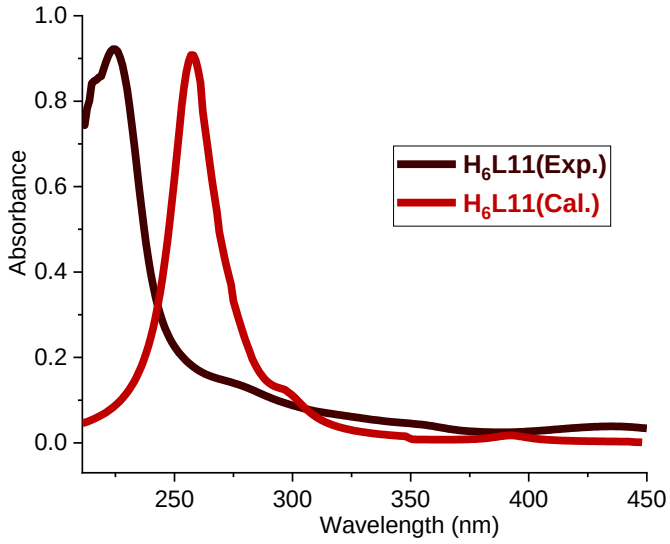

Figure 5.22:Compared experimental and theoretical UV graph of H_6L11

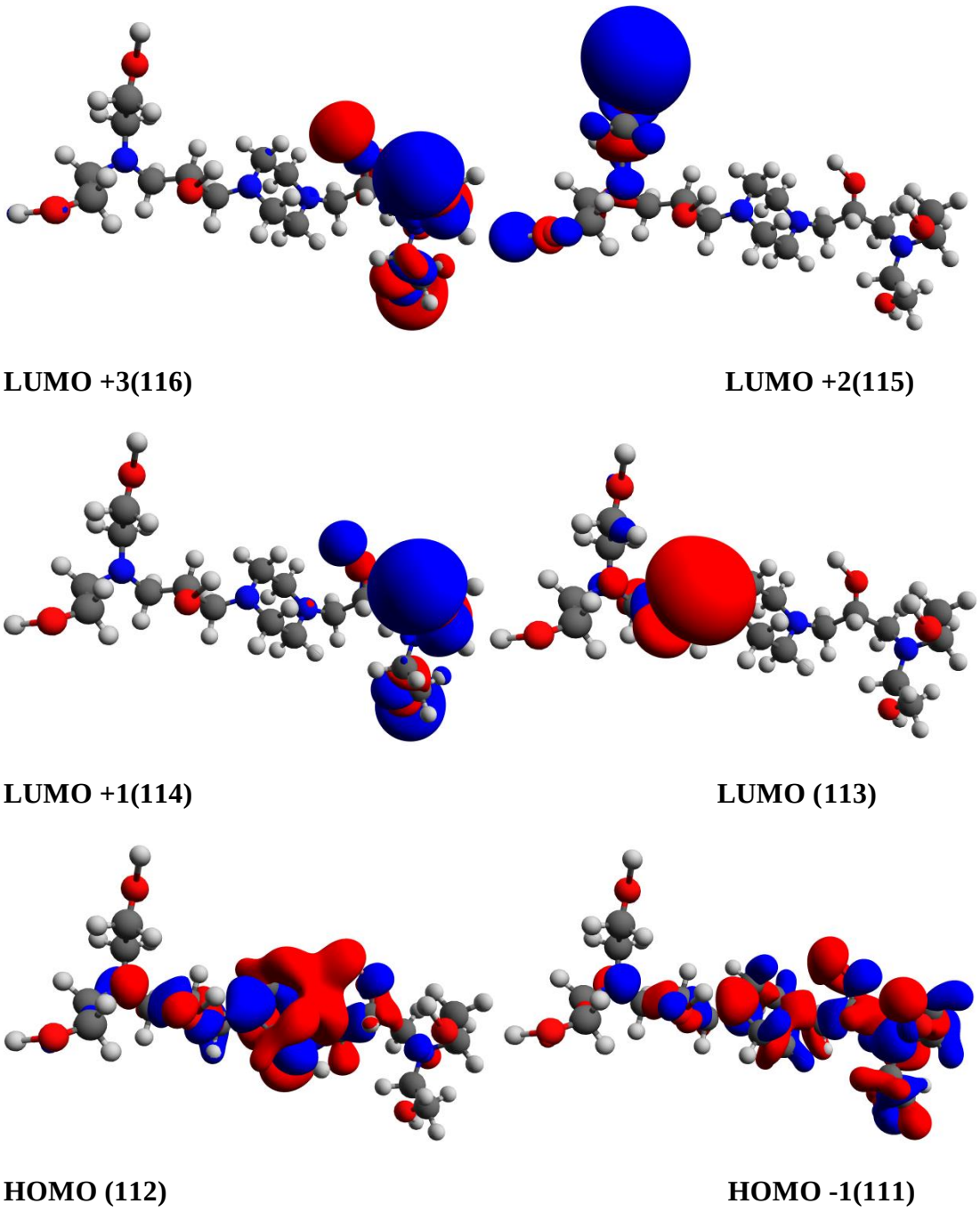

Figure 5.23:Nearby molecular orbitals (isosurface value 0.02) involved in the electronic transition of H_6L11

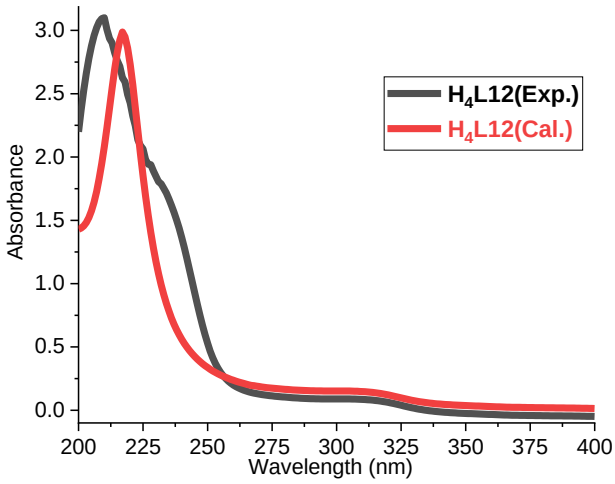

Figure 5.24:Compared experimental and theoretical UV graph of ligand H_4L12

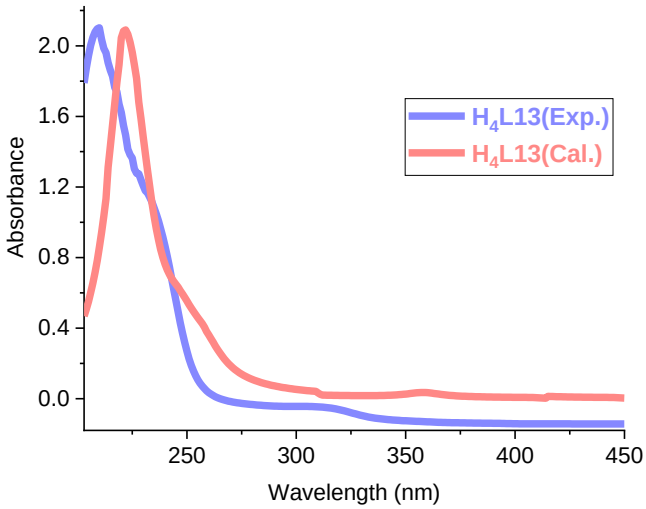

Figure 5.25:Compared experimental and theoretical UV graph of H_4L13

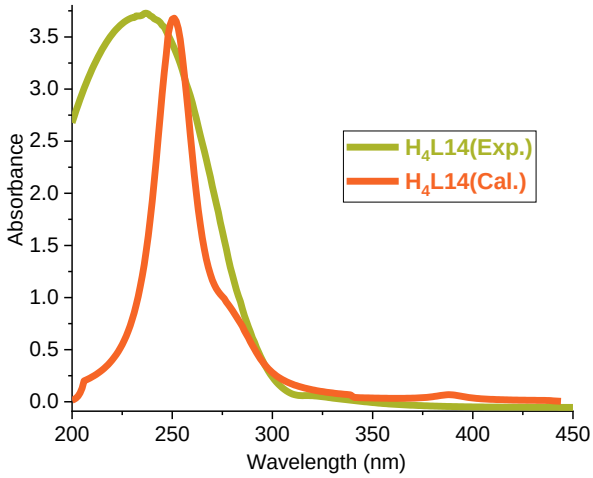

Figure 5.26:Compared experimental and theoretical UV graph of H_4L14

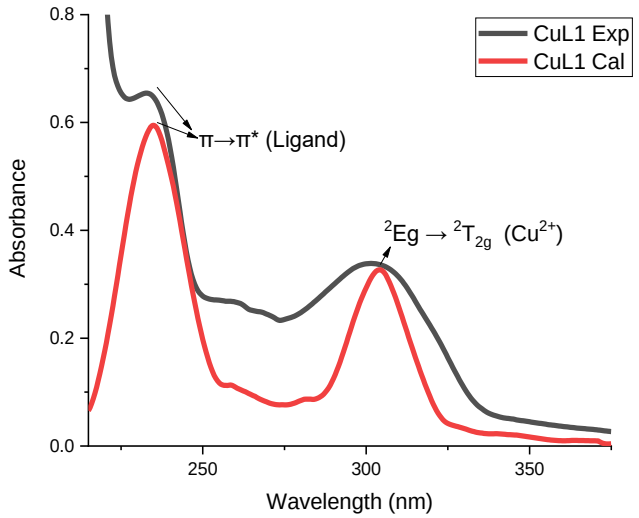

Figure 5.27:Compared experimental and theoretical UV graph of CuL1

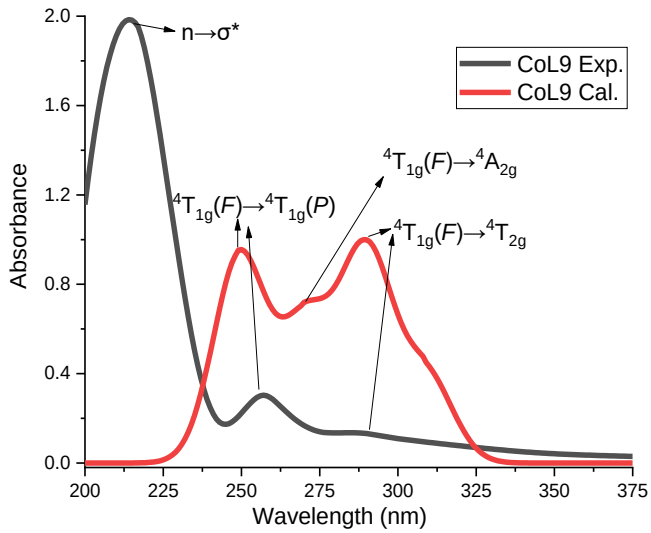

Figure 5.28:Compared experimental and theoretical UV graph of CoL9

Table 5.3: Transition state, orbital contributions, oscillator strength (f_{osc}), involved molecular orbitals and energies (in eV) theoretically calculated with B3LYP/TDDFT

Code	Transition states	Number of molecular orbital*	Oscillator strength (f_{osc})**	Type of Transition	Energy (eV)
HL1	State 1	44 → 45	0.982795	HOMO(0)→LUMO(0)	0.802
	State 2	43 → 45	0.985712	HOMO(-1) → LUMO(0)	2.064
	State 3	43 → 45	0.926135	HOMO(-1) → LUMO(0)	3.553
	State 4	42 → 45	0.997181	HOMO(-2) → LUMO(0)	3.648
	State 5	42 → 47	0.830541	HOMO(-2) → LUMO(+2)	3.922
	State 6	41 → 45	0.994964	HOMO(-3) → LUMO(0)	4.094

	State 7	43 → 46	0.835273	HOMO(-1) → LUMO(+1)	4.781
HL2	State 1	44 → 45	0.985601	HOMO(0) → LUMO(0)	1.102
	State 2	43 → 45	0.395800	HOMO(-1) → LUMO(0)	1.911
	State 3	44 → 45	0.887956	HOMO(0) → LUMO(0)	1.945
	State 4	44 → 47	0.532879	HOMO(0) → LUMO(+2)	2.681
	State 5	43 → 45 43→ 44	0.503156 0.421735	HOMO(-1) → LUMO(0) HOMO(-1) → HOMO(0)	2.786
	State 6	42 → 46 42 → 44 43 → 45	0.153408 0.202370 0.108468	HOMO(-2) →LUMO(+1) HOMO(-2) → HOMO(0) HOMO(-1) → LUMO(0)	3.654
	State 7	43 → 45	0.677848	HOMO(-1) → LUMO(0)	3.777
HL3	State 1	43 → 45 44 → 45	0.202422 0.787911	HOMO(-1) → LUMO(0) HOMO(0) → LUMO(0)	1.771
	State 2	43 → 45 44 → 45	0.787135 0.207074	HOMO(-1) → LUMO(0) HOMO(0) → LUMO(0)	2.589
	State 3	42 → 45	0.994640	HOMO(-2) → LUMO(0)	3.511
	State 4	41 → 45	0.997697	HOMO(-3) → LUMO(0)	3.843
	State 5	44 → 46	0.896518	HOMO(0) → LUMO(+1)	4.707
	State 6	42 → 46	0.879932	HOMO(-2) → LUMO(+1)	4.858
	State 7	43 → 47 44 → 47	0.178097 0.808423	HOMO(-1) → LUMO(+2) HOMO(0) → LUMO(+2)	5.062
HL4	State 1	42 → 44 43 → 44	0.439795 0.552492	HOMO(-1) → LUMO(0) HOMO(0) → LUMO(0)	2.436
	State 2	42 → 44 43 → 44	0.545968 0.443853	HOMO(-1) → LUMO(0) HOMO(0) → LUMO(0)	2.783
	State 3	41 → 46 43 → 45	0.156848 0.828137	HOMO(-2) → LUMO(+2) HOMO(0) → LUMO(+1)	3.889
	State 4	41 → 44	0.998741	HOMO(-2) → LUMO(0)	3.946
	State 5	41 → 46 42 → 45	0.033154 0.963010	HOMO(-2) → LUMO(+2) HOMO(-1) → LUMO(+1)	4.511
	State 6	41 → 45 42 → 46 43 → 46	0.055447 0.276492 0.642517	HOMO(-2) → LUMO(+1) HOMO(-1) → LUMO(+2) HOMO(0) → LUMO(+2)	4.744
	State 7	40 → 44	0.979556	HOMO(-3) → LUMO(0)	4.921
HL6	State 1	50 → 52 51 → 52	0.099687 0.896675	HOMO(-1) → LUMO(0) HOMO(0) → LUMO(0)	2.242
	State 2	50 → 52 51 → 52	0.886147 0.092636	HOMO(-1) → LUMO(0) HOMO(0) → LUMO(0)	2.615
	State 3	49 → 54 51 → 53	0.116656 0.858492	HOMO(-2) → LUMO(+2) HOMO(0) → LUMO(+1)	3.623
	State 4	49 → 52	0.994147	HOMO(-2) → LUMO(0)	4.006
	State 5	49 → 54 50 → 53	0.017989 0.980216	HOMO(-2) → LUMO(+2) HOMO(-1) → LUMO(+1)	4.382

	State 6	48 → 52	0.979785	HOMO(-3) → LUMO(0)	4.460
	State 7	49 → 53 51 → 54	0.102964 0.824221	HOMO(-2) → LUMO(+1) HOMO(0) → LUMO(+2)	4.779
H_2L9	State 1	44 → 48 47 → 48 47 → 49	0.153913 0.372205 0.447953	HOMO(-3) → LUMO(0) HOMO(0) → LUMO(0) HOMO(0) → LUMO(+1)	2.318
	State 2	44 → 48 47 → 48 47 → 49	0.210201 0.231367 0.508876	HOMO(-3) → LUMO(0) HOMO(0) → LUMO(0) HOMO(0) → LUMO(+1)	2.352
	State 3	45 → 49	0.985388	HOMO(-2) → LUMO(+1)	2.572
	State 4	44 → 48 46 → 48 47 → 48	0.180213 0.580478 0.227597	HOMO(-3) → LUMO(0) HOMO(-1) → LUMO(0) HOMO(0) → LUMO(0)	2.687
	State 5	44 → 48 46 → 48 46 → 49	0.310608 0.246932 0.318114	HOMO(-3) → LUMO(0) HOMO(-1) → LUMO(0) HOMO(-1) → LUMO(+1)	3.254
	State 6	44 → 48 46 → 48 46 → 49	0.116519 0.135048 0.594514	HOMO(-3) → LUMO(0) HOMO(-1) → LUMO(0) HOMO(-1) → LUMO(+1)	3.357
	State 7	45 → 48	0.990445	HOMO(-2) → LUMO(0)	3.763
H_2L10	State 1	86 → 88 87 → 88	0.099397 0.837850	HOMO(-1) → LUMO(0) HOMO(0) → LUMO(0)	1.821
	State 2	86 → 89 87 → 89	0.023573 0.942274	HOMO(-1) → LUMO(+1) HOMO(0) → LUMO(+1)	2.013
	State 3	84 → 89 86 → 89	0.213801 0.648408	HOMO(-3) → LUMO(+1) HOMO(-1) → LUMO(+1)	2.404
	State 4	84 → 89 86 → 88 86 → 89	0.481478 0.072180 0.198810	HOMO(-3) → LUMO(+1) HOMO(-1) → LUMO(0) HOMO(-1) → LUMO(+1)	2.205
	State 5	85 → 88 86 → 88 86 → 89	0.282455 0.492296 0.075893	HOMO(-2) → LUMO(0) HOMO(-1) → LUMO(0) HOMO(-1) → LUMO(+1)	2.091
	State 6	83 → 88 84 → 88 87 → 91	0.114768 0.253693 0.048672	HOMO(-4) → LUMO(0) HOMO(-3) → LUMO(0) HOMO(0) → LUMO(+2)	1.943
	State 7	85 → 88 86 → 88	0.191811 0.082969	HOMO(-2) → LUMO(0) HOMO(-1) → LUMO(0)	1.438
H_6L11	State 1	110 → 112 111 → 112	0.074268 0.898224	HOMO(-1) → LUMO(0) HOMO(0) → LUMO(0)	0.906
	State 2	111 → 113 111 → 115	0.962097 0.025755	HOMO(0) → LUMO(+1) HOMO(0) → LUMO(+3)	1.469
	State 3	110 → 112 111 → 112	0.874251 0.088809	HOMO(-1) → LUMO(0) HOMO(0) → LUMO(0)	1.591
	State 4	111 → 114	0.970304	HOMO(0) → LUMO(+2)	1.663

	State 5	111 → 113 111 → 115	0.023781 0.933755	HOMO(0) → LUMO(+1) HOMO(0) → LUMO(+3)	1.729
	State 6	111 → 116 111 → 117	0.937449 0.013107	HOMO(0) → LUMO(+4) HOMO(0) → LUMO(+5)	1.806
	State 7	110 → 113 111 → 117	0.871065 0.035898	HOMO(-1) → LUMO(+1) HOMO(0) → LUMO(+5)	1.871
H_4L12	State 1	95 → 96 95 → 98	0.550980 0.350600	HOMO(0) → LUMO(0) HOMO(0) → LUMO(+2)	5.435
	State 2	95 → 96 95 → 98	0.120506 0.170668	HOMO(0) → LUMO(0) HOMO(0) → LUMO(+2)	5.797
	State 3	95 → 96 95 → 97 95 → 98	0.268599 0.298363 0.317621	HOMO(0) → LUMO(0) HOMO(0) → LUMO(+1) HOMO(0) → LUMO(+2)	5.854
	State 4	95 → 99 95 → 100	0.531443 0.190683	HOMO(0) → LUMO(+3) HOMO(0) → LUMO(+4)	6.024
	State 5	93 → 96 94 → 96 94 → 97	0.119831 0.554912 0.119291	HOMO(-2) → LUMO(0) HOMO(-1) → LUMO(0) HOMO(-1) → LUMO(+1)	6.084
	State 6	93 → 96 93 → 97 95 → 100	0.192203 0.272078 0.133318	HOMO(-2) → LUMO(0) HOMO(-2) → LUMO(+1) HOMO(0) → LUMO(+4)	6.152
	State 7	93 → 97 94 → 97 95 → 100	0.139238 0.029389 0.301648	HOMO(-2) → LUMO(+1) HOMO(-1) → LUMO(+1) HOMO(0) → LUMO(+4)	6.203
H_4L13	State 1	102 → 104 103 → 104	0.077364 0.893210	HOMO(-1) → LUMO(0) HOMO(0) → LUMO(0)	0.968
	State 2	102 → 104 103 → 104	0.875431 0.090033	HOMO(-1) → LUMO(0) HOMO(0) → LUMO(0)	1.613
	State 3	103 → 105	0.964814	HOMO(0) → LUMO(+1)	1.623
	State 4	103 → 105 103 → 106	0.010598 0.010598	HOMO(0) → LUMO(+1) HOMO(0) → LUMO(+2)	1.720
	State 5	100 → 107 101 → 107 102 → 107	0.036074 0.036062 0.844284	HOMO(-3) → LUMO(+3) HOMO(-2) → LUMO(+3) HOMO(-1) → LUMO(+3)	1.915
	State 6	102 → 105 102 → 107 103 → 107	0.713785 0.171604 0.014139	HOMO(-1) → LUMO(+1) HOMO(-1) → LUMO(+3) HOMO(0) → LUMO(+3)	1.992
	State 7	102 → 105 103 → 107	0.181560 0.623377	HOMO(-1) → LUMO(+1) HOMO(0) → LUMO(+3)	2.023
H_4L14	State 1	134 → 136 135 → 136	0.094315 0.867475	HOMO(-1) → LUMO(0) HOMO(0) → LUMO(0)	1.013
	State 2	134 → 136 135 → 136	0.862761 0.111562	HOMO(-1) → LUMO(0) HOMO(0) → LUMO(0)	1.599
	State 3	135 → 137	0.04431	HOMO(-1) → LUMO(+1)	1.623

		135 → 138	0.933435	HOMO(-1) → LUMO(+2)	
	State 4	135 → 137 135 → 138	0.923911 0.041620	HOMO(-1) → LUMO(+1) HOMO(-1) → LUMO(+2)	1.699
	State 5	132 → 139 135 → 139	0.037140 0.836585	HOMO(-3) → LUMO(+3) HOMO(-1) → LUMO(+3)	1.940
	State 6	134 → 138 135 → 139	0.757094 0.144668	HOMO(-1) → LUMO(+2) HOMO(0) → LUMO(+3)	1.940
	State 7	134 → 137 134 → 139	0.226232 0.504752	HOMO(-1) → LUMO(+1) HOMO(-1) → LUMO(+3)	1.997

*(HOMO and LUMO transition are added to +1 value as ORCA counts molecular orbitals from zero)

5.4 Geometrical Optimization of Metal Complexes

Binding of metal ion with the ligands may impose change in the conformation of the ligand skelton. So, it becomes important to optimize these metal complexes to find the geometry of stable ground state with lowest energy. Since piperazine ring opt chair conformation in the free ligand, in boat conformation of ligands donor atoms are more exposed toward the metal centre which favours the metal complexing of ligands with one metal ion (monometallic complexes) whereas the chair configuration of ligands is retained when it binds with two metal centre (bimetallic complexes). All the proposed complexes were optimized using Gaussian software package. DFT calculation with Lan2DZ basis set were applied in the optimization. Selected optimized complexes have been represented in figure 5.33-5.42 and cartesian coordinates of standard orientation of complexes are given in the annexure file.[20-26]

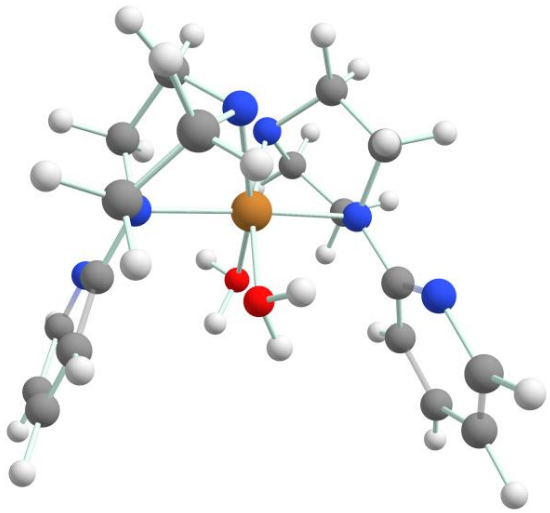

Figure 5.29: Optimized structure of CuL1

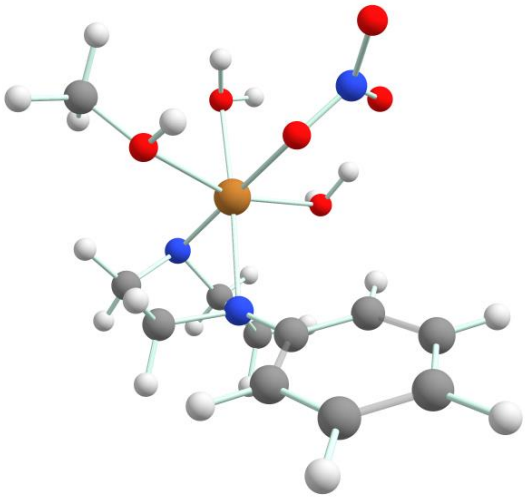

Figure 5.30: Optimized structure of CuL4

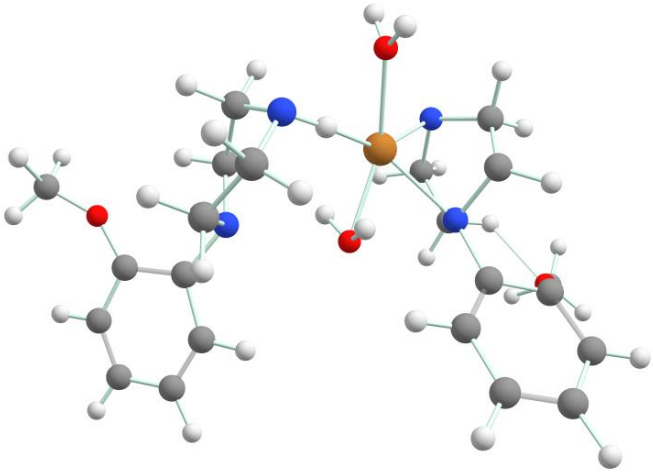

Figure 5.31: Optimized structure of CuL5

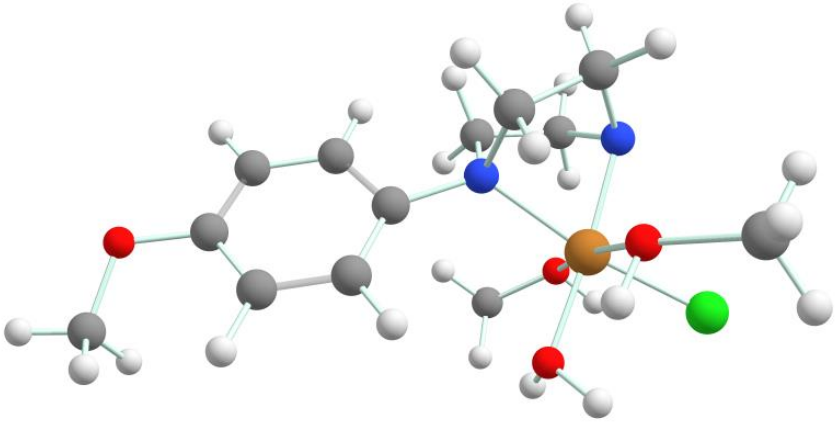

Figure 5.32: Optimized structure of CuL6

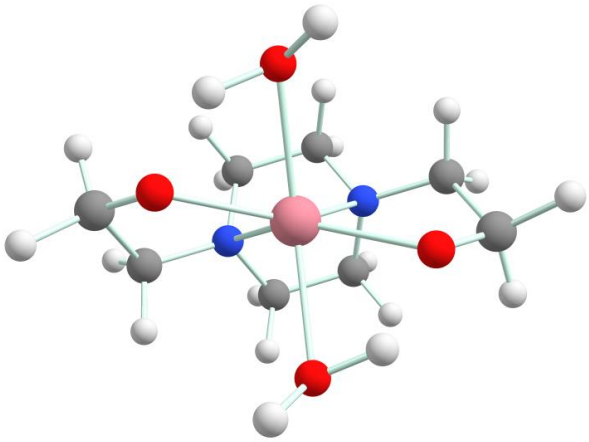

Figure 5.33: Optimized structure of CoL9

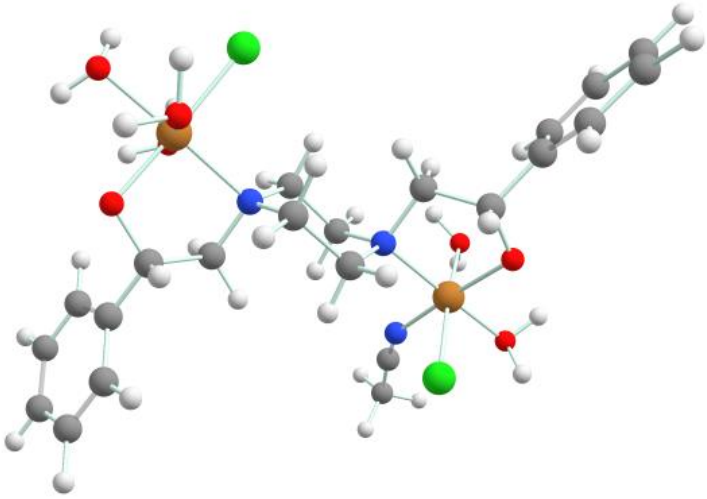

Figure 5.34: Optimized structure of Cu_2L10

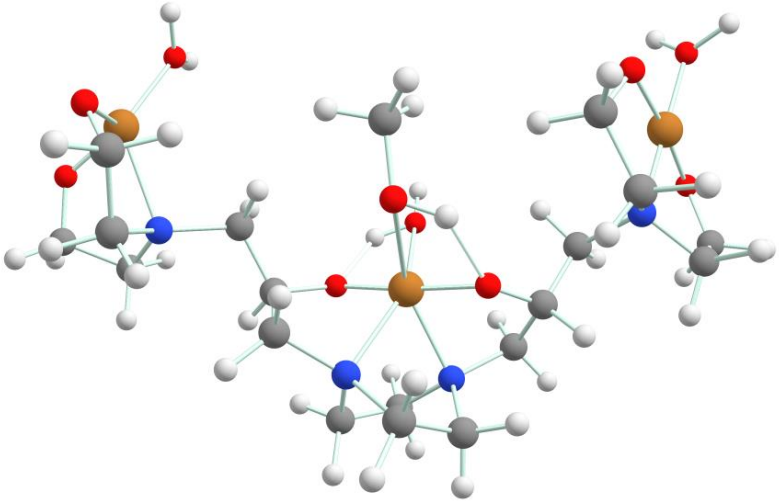

Figure 5.35: Optimized structure of Cu_3L11

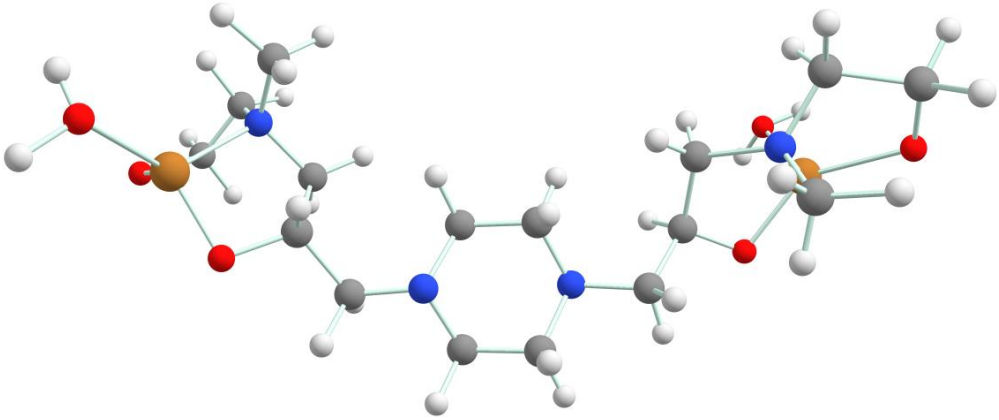

Figure 5.36: Optimized structure of Cu_2L12

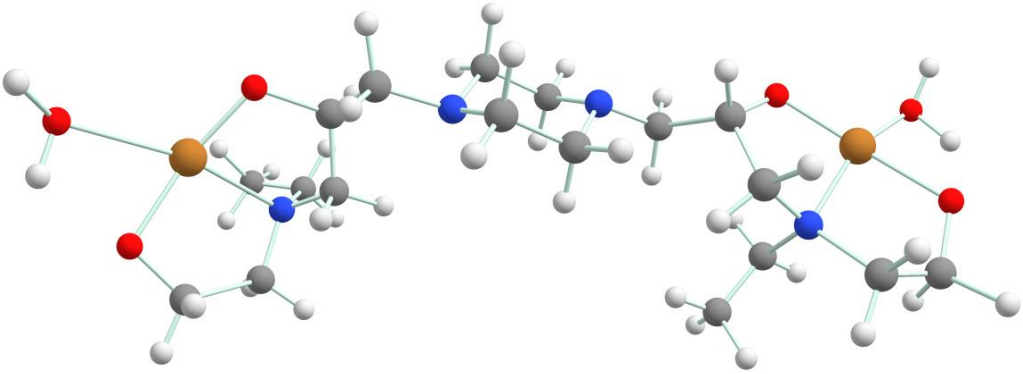

Figure 5.37: Optimized structure of Cu_2L13

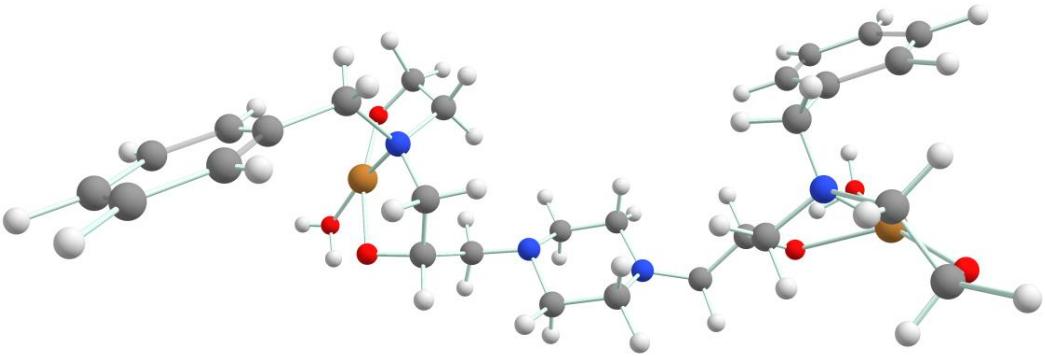

Figure 5.38: Optimized structure of Cu_2L14

5.5 Molecular Docking: Theoretical Studies of binding of complexes with BSA

Molecular docking studiesare now most frequently being usedmethodsby computational biologists and chemists in drug design on structural basis as these studies have potential to analyze the binding-conformation of ligand molecules to the appropriate targeted binding sites.[27,28,45]The concept of structural based drug design always promotes the in-silico methods formolecular docking before starting the actual lab screening process. In silico methods predicts the binding sites and predict the possible mechanism of ligand-protein interactions as well as targetbinding.[29,30] In docking studies we analyze how small molecules fit together with receptor molecules.[31,32]Thus, it is a molecular modelling technique used to interpret how a small molecule interacts with receptor proteins.[33]Binding affinity between the targeted protein and ligand (small molecule) have important influence in enhancing and suppressing the biological activity by finding correct binding pocket which depends on several factors such as search approach, rigidity, flexibility and algorithms.[34-42,46,47] Molecular docking of synthesized metal complexes has been performed to study the active binding site in the BSA protein chain which are available for binding interactions. Binding behaviour interpretation have played key role in deciding the potential to design a molecule as drug and explaining the possible mechanisms of biochemicalprocesses.[48,49]In order to find active binding sites in a targeted protein, the crystal structure is downloaded from protein data bank and bound ligand was extracted.[43,44]Thus, the targeted BSA protein crystal structure utilized was downloaded from the source protein data bank(PBD Code: 3v03)[50]and docking was performed by thefree software package Auto-dock Vina.[46,51,52]Initially, the protein structure was re-processed before using as receptor for docking. Necessary steps taken in pre-processing of protein were applied by adding hydrogen atom and assigning atomic charges. Unnecessary water molecules were deleted manually which were not in the protein chain. The Auto-dock tool package was used for grid generation with a size of 2700 Å (maximum) with 0.66 Å of grid box spacing. Pymol was used to visualize the result of docking studies.[53]

Table 5.4: Docking results of selected complexes along with binding affinity and binding interactions

Code	Binding affinity (kcal/mol)	Polar contacts through dipole-dipole and H-bond (distance in Å)	Nearby residue with polar and non-polar interaction (distance in Å)
CuL1	-7.1	ASP 258 (2.3)	ASP13(3.5), ASP236(4.7), TYR262(4.5)
CoL9	-5.0	LYS187 (3.2), SER191(3.4), TYR156(3.4)	ARG194 (4.3), GLU291(4.8) HIS287 (4.4)
Cu_2L10	-7.5	ASP36(2.4), LYS132(3.3)	PHE36(5.5), TYR134(3.9), ASP129(3.3)
Cu_3L11	-8.3	TYR451(2.7, 2.8, 3.2, 3.4) THR190(2.9, 3.4), ASP450(3.4),GLU186(2.2)	CYS447(2.8), ARG194(2.9), GLU291(3.7)
Cu_2L12	-7.1	ASP450(2.4, 3.4), ARG194(2.4), SER191(3.2,3.40	HIS287(5.4)
Cu_2L13	-7.4	PRO446(3.3,3.3), ARG435(3.5, 2.5), TYR451(3.3) THR434(2.9)	ASP450(4.5), GLN220(5.5)
Cu_2L14	-7.4	THR526(3.1), LYS523(3.3), GLU424(2.3)	HIS145(5.1), TYR134(5.0)

Complex CuL1 showed interaction with BSA protein chains with polar contacts via ASP258, 13 and 236 along with π–π stacking with TYR262 with aromatic ring in ligand. Complex CoL9 showed polar interaction with TYR156, LYS187 and SER191with nearby polar environment of ARG194, GLU291 and HIS287.

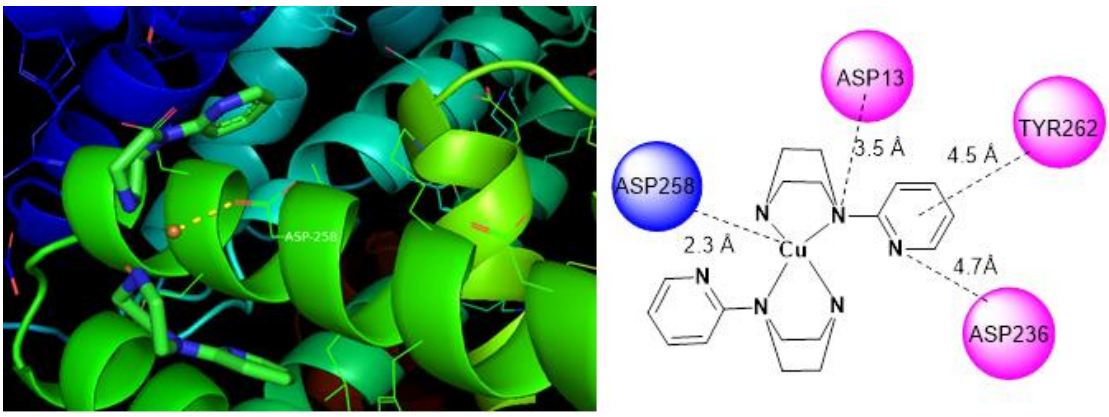

Figure 5.39:Binding mode of CuL1 with BSA protein and its 2D structural interpretation

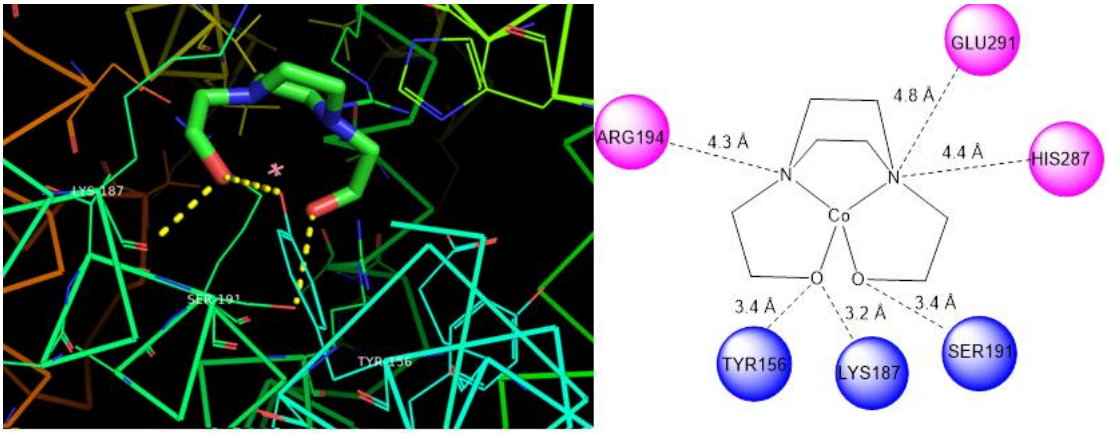

Figure 5.40: Binding mode of CoL9 with BSA protein and its 2D structural interpretation

Bimetallic copper complex Cu_2L10 showed polar contacts via ASP37, LYS132 and ASP 129 with π–π stacking with TYR134 and PHE36. Trimetallic copper complex Cu_3L11 showed multiple polar interaction with TYR451 and THR190 with other polar contacts GLU186, ASP450, CYS447, ARG194 and GLU 291.

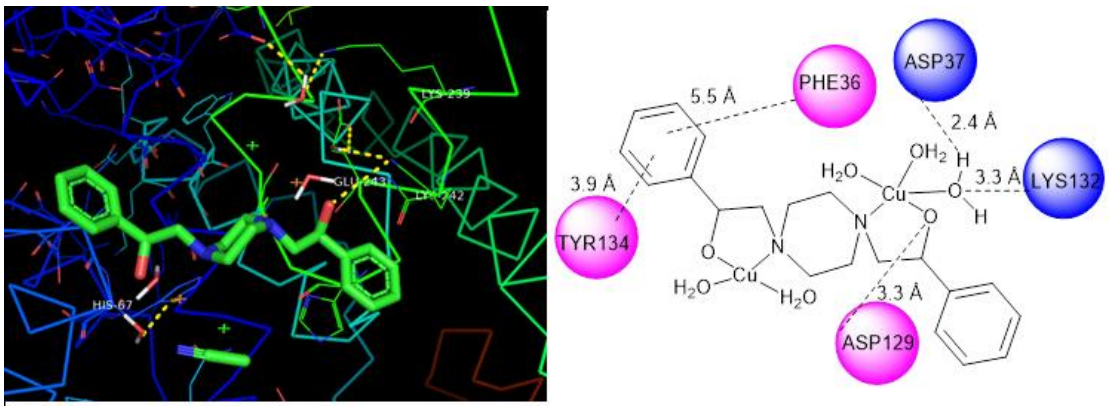

Figure 5.41:Binding mode of Cu_2L10 with BSA protein and its 2D structural interpretation

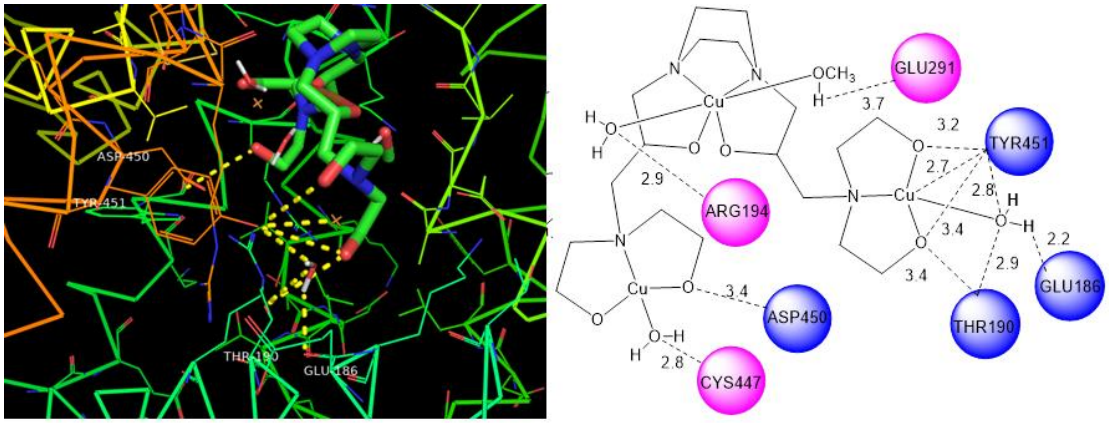

Figure 5.42:Binding mode of Cu_3L11 with BSA protein and its 2D structural interpretation

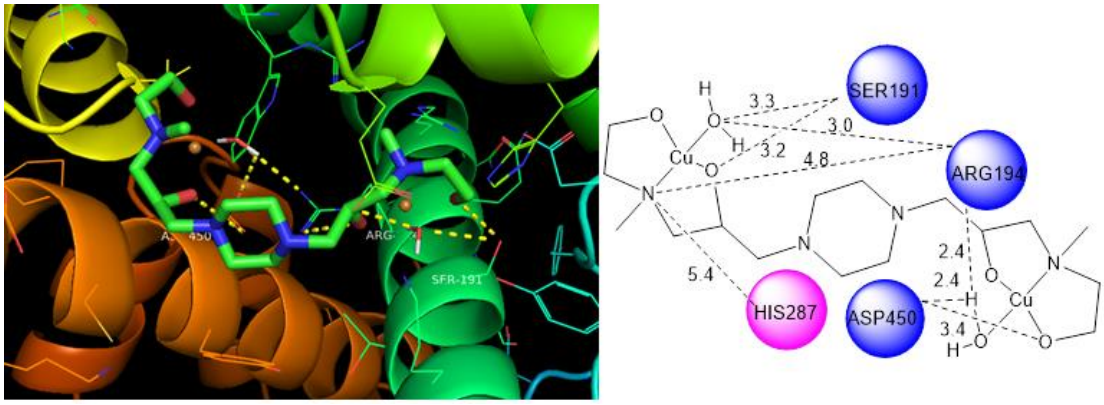

Figure 5.43:Binding mode of Cu_2L12 with BSA protein and its 2D structural interpretation

Complex Cu_2L12 showed multiple hydrogen bond interaction with ASP450, ARG194, SER191 with nearby polar environment of HIS287. While the complex Cu_2L13 show polar interaction with THR434, ARG435, TYR451, PRO446 and nearby polar environment of ASP450 and GLN220. In the complex Cu_2L14 showed polar interaction LYS523, THR526, GLU424 and π–π stacking with TYR134 and HIS 145.

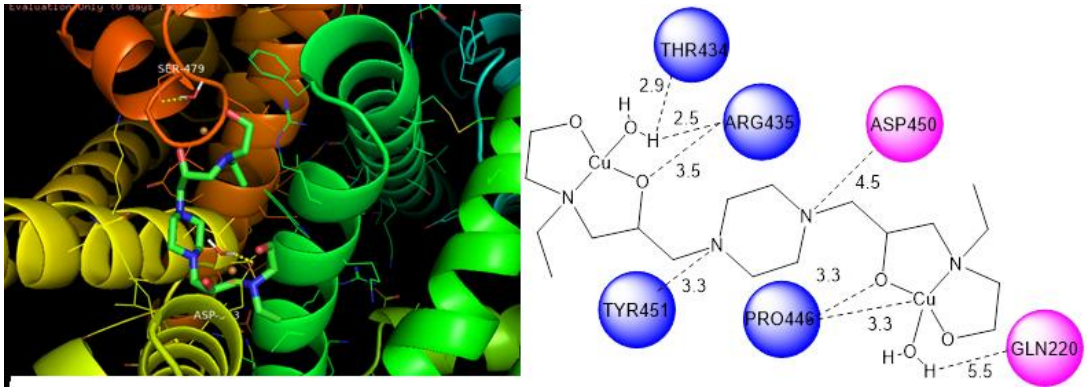

Figure 5.44:Binding mode of Cu_2L13 with BSA protein and its 2D structural interpretation

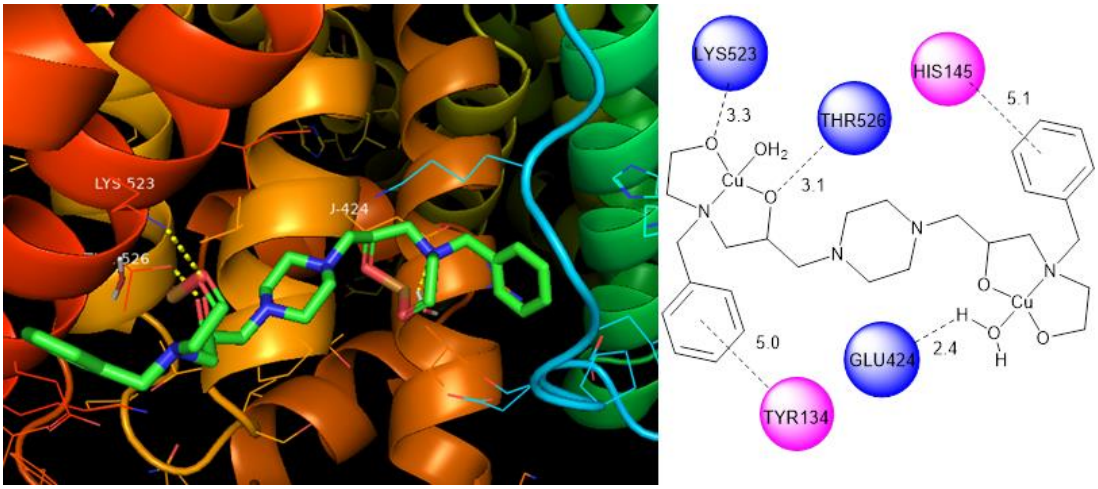

Figure 5.45:Binding mode of Cu_2L14 with BSA protein and its 2D structural interpretation

In order to visualize the binding mechanism with DNA these studies were further extended and binding interactions were also checked with B-DNA molecule. Sequence was downloaded from PDB source (Code: 1BNA) and before performing docking, complexes were made unsaturated by removing coordinate solvent

molecules. Docking result of CoL9 indicated that complex binds to only one strand ofDNA through Adenine (DA5) and Guanine (DG4) and this binding involve oxygen atoms of ligand and metal do not show direct interaction with the strand (Figure 26). Whereas in complex Cu_2L10 both the DNA strands are locked with metal ion interaction with Adenine DA5, DA17 and ligand oxygen atom interaction with Guanine DG4.

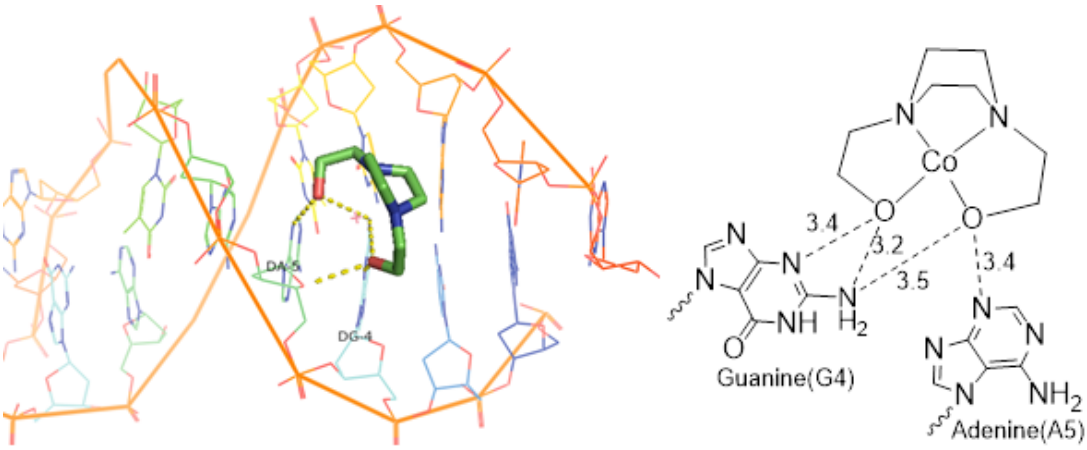

Figure 5.46:Theoretical binding pose of CoL9 with B-DNA and its 2D structural interpretation

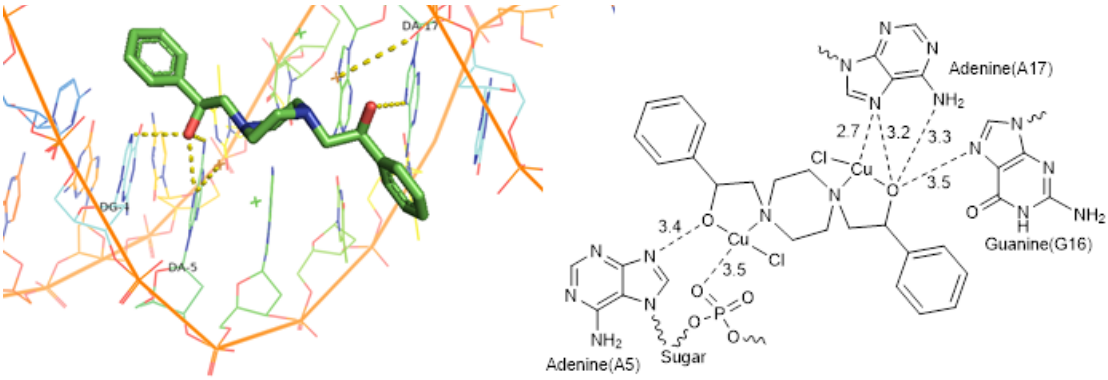

Figure 5.47:Theoretical binding pose of Cu_2L10 with B-DNAand its 2D structural interpretation

Complex Cu_2L12showed binding with DNA, where both the strands were locked with interaction with Guanine and Cytosine nitrogen base (DG4, DC3, DG22, DC21) and their corresponding phosphate and sugar. Similarity in binding is observed in the complex Cu_2L12 due to similar coordination environment and similar ligand skelton. Complex Cu_2L14 showed polar binding interaction with Guanine (DG4) along with

non-polar hydrophobic interaction with Guanine (DG24) owing to the aromatic bulk in the ligand skelton.

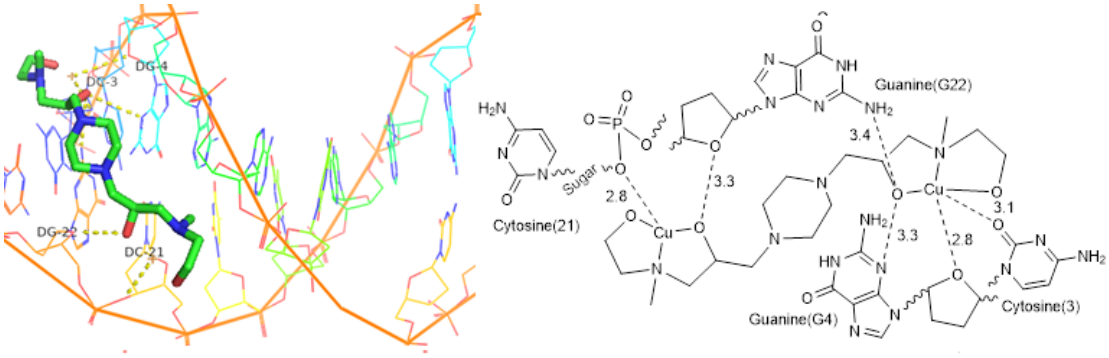

Figure 5.48:Theoretical binding pose of $Cu_2L12$with B-DNAand its 2D structural interpretation

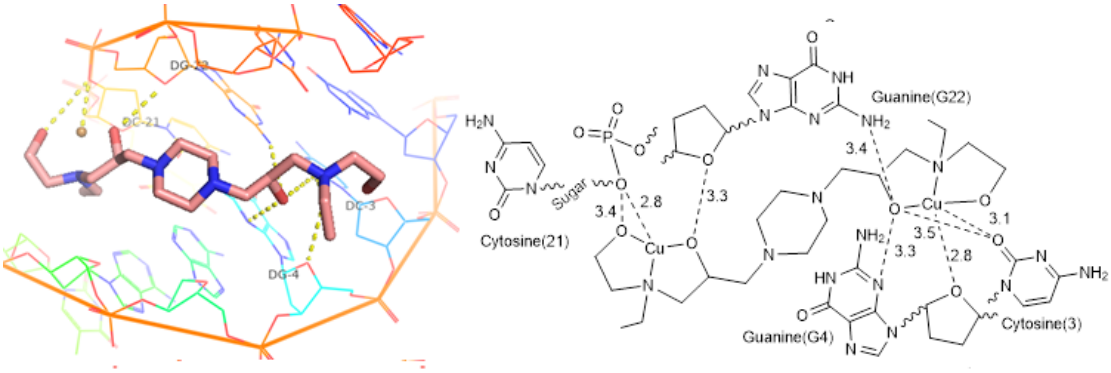

Figure 5.49:Theoretical binding pose of Cu_2L13 with B-DNAand its 2D structural interpretation

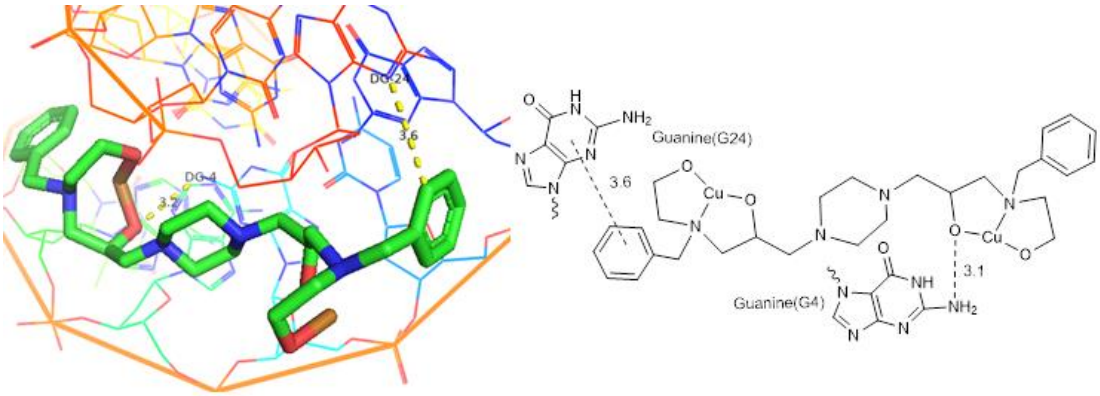

Figure 5.50:Theoretical binding pose of Cu_2L14 with B-DNAand its 2D structural interpretation

5.5 Conclusion:

This chapter mainly focused the computational properties of synthesized molecules. By geometry optimization, ligands were optimized to ground state having lowest value of energy. This provided the additional information about the position of donor atoms and most stable conformations of the ligands. Time dependent density functional theory (TDDFT) was performed in to corroborate the experimental UV spectra of the ligands with the theoretically obtained values. All the UV spectra compared were in strong agreement to the experimental results with the small difference in the observed and calculated value of wavelength aroused due to vacuum study of molecules. Molecular orbitals involved in nearby transition were sketched with the help of Avogadro which explains the type of molecular orbitals (HOMOs and LUMOs) and probability of electronic transitions. Metal complexes were also subjected to geometry optimization by using Gaussian Software by Lan2DZ basis set with DFT calculations. Molecular docking studies were also performed with BSA protein in order to evaluate experimental data to theoretical binding of complexes. All complexes have shown excellent binding interaction with protein chain which clearly indicate the potential of these complexes to behave as drug molecules. Hydrophilic interactions are dominant where complexes did not contain aromatic ring where as in the presence of aromatic ring additional π–π interactions are also shown in selected complexes. Theoretical DNA docking studies of selected complexes revealed that complexes are groove binder with variable capacity to interaction with both the strand of DNA through metal ion and ligand skelton.

5.6 References:

(1) Schlegel, H. B., Geometry optimization,*Wiley Interdisciplinary Reviews: Computational Molecular Science* **2011**, *1*(5), 790-809. https://doi.org/10.1002/wcms.34

(2) Schlegel, H. B., Optimization of Equilibrium Geometries and Transition Structures, *Journal of Computational Chemistry***1982**, *3*(2), 214-218. https://doi.org/10.1002/jcc.540030212

(3) Moharreri, E., Pardakhti, M., Srivastava, R., L. Suib, S. L., Energy−Geometry Dependency of Molecular Structures: A Multistep Machine Learning Approach, *ACS Comb. Sci.***2019**, *21* (9), 614-621. https://doi.org/10.1021/acscombsci.9b00028

(4) Roy, K., Kar, S. and Das, R.N., Understanding the Basics of QSAR for Applications in Pharmaceutical Sciences and Risk Assessment, In *AcademicPress*, **2015**. http://dx.doi.org/10.1016/B978-0-12-801505-6.00005-3

(5) https://www.intechopen.com/books/homology-molecular-modeling-perspectives-and-applications/energy-minimization

(6) https://www.shodor.org/chemviz/optimization/teachers/background.html.

(7) Schlegel, H. B., Exploring Potential Energy Surfaces for Chemical Reactions: An Overview of Some Practical Methods, *J Comput Chem***2003**, *24*(12), 1514–1527.https://doi.org/10.1002/jcc.10231

(8) Schlegel, H. Bernhard, Geometry Optimization on Potential Energy Surfaces, *Modern Electronic Structure Theory***1995**, 459-500.https://doi.org/10.1142/9789812832108_0008

(9) Vogiatzis,K. D., Polynski, M.V., Kirkland, J.K., Townsend, J., Hashemi, A., Liu, C., and Pidko, E.A., Computational Approach to Molecular Catalysis by 3d Transition Metals: Challenges and Opportunities Konstantinos, *Chemical Review* **2018**, *119*, 2453-2523. https://doi.org/10.1021/acs.chemrev.8b00361

(10) Ding C.C., Wu S.Y., Xu Y.Q., Wu L.N., Zhang L.J., DFT studies for three Cu (II) coordination polymers: Geometrical and electronic structures, g factors and UV–visible spectra. *Chemical Physics*,**2018**, *508*, 20-5. https://doi.org/10.1016/j.chemphys.2018.04.016

(11) Varsano, D., Di Felice, R., Marques, M.A. and Rubio, A., A TDDFT study of the excited states of DNA bases and their assemblies. *The Journal of Physical Chemistry B*, **2006**, *110* (14), 7129-7138. https://doi.org/10.1021/jp056120g

(12) Neese, F., Becker, U., ORCA: An ab Initio, DFT, and Semiempirical SCF-MO Package, version 3.0. Max Planck Institute for Bioinorganic Chemistry,**2012,** 45470.

(13) Üstün, E., Sönmez Çelebi, M. and Çol Ayvaz, M., Manganese (I) tricarbonyl complexes: UV-dependent antioxidant activity, electrochemistry, and

DFT/TDDFT calculation. *Journal of Coordination Chemistry*, **2018**, *71* (16-18), 2978-2992. https://doi.org/10.1080/00958972.2018.1506110

(14) Jacquemin, D., Perpète, E.A., Ciofini, I. and Adamo, C., Assessment of functionals for TD-DFT calculations of Singlet− Triplet transitions. *Journal of chemical theory and computation*,**2010**, *6*(5), 1532-1537.https://doi.org/10.1021/ct100005d

(15) Wang, F. and Ziegler, T., A simplified relativistic time-dependent density-functional theory formalism for the calculations of excitation energies including spin-orbit coupling effect. *The Journal of chemical physics*, **2005**, *123* (15), 154102. https://doi.org/10.1063/1.2061187

(16) Rabilloud, F., UV-visible absorption spectra of metallic clusters from TDDFT calculations. *The European Physical Journal D*, **2013**, *67* (1), 1-5. https://doi.org/10.1140/epjd/e2012-30448-x

(17) Neese, F.; The ORCA program system, *Wiley Interdiscip. Rev.: Comput. Mol. Sci.*, **2012**, 2, 73-78. https://doi.org/10.1002/wcms.81

(18) Hanwell, M.D., Curtis, D.E., Lonie, D.C., Vandermeersch, T., Zurek, E. and Hutchison, G.R., Avogadro: an advanced semantic chemical editor, visualization, and analysis platform. *Journal of cheminformatics*, **2012**, *4* (1), 1-17. https://doi.org/10.1186/1758-2946-4-17

(19) Kant, R., Kaur, T., Hilal, Z., Aggarwal, N., Maji, S. Synthesis and characterization of a series of phenyl piperazine based ligands. *Journal of Physics: Conference Series*, **2020**, *1531* (1), 012106. https://doi.org/10.1088/1742-6596/1531/012106

(20) Rad, A.S., Ardjmand, M., Esfahani, M.R. and Khodashenas, B., DFT calculations towards the geometry optimization, electronic structure, infrared spectroscopy and UV–vis analyses of Favipiravir adsorption on the first-row transition metals doped fullerenes; a new strategy for COVID-19therapy. *Spectrochimica Acta Part A: Molecular and Biomolecular Spectroscopy*, **2021**,*247*(1), 119082.https://doi.org/10.1016/j.saa.2020.119082

(21) Altaf, A.A., Kausar, S. and Badshah, A., Spectral Calculations with DFT. Density Functional Calculations–Recent Progresses of Theory and Application, **2018**, http://dx.doi.org/10.5772/intechopen.71080

(22) Gaussian 16, Revision 09W, Frisch, M. J.; *et al*, Gaussian, Inc., Wallingford CT, 2016.

(23) GaussView, Version 6, Dennington, Roy; Keith, Todd A.; Millam, John M. Semichem Inc., Shawnee Mission, KS, 2016.

(24) Pritchard, B.P.; Altarawy, D.; Didier, B.; Gibson, T.D.; Windus T.L. A New Basis Set Exchange: An Open, Up-to-date Resource for the Molecular Sciences Community. *J. Chem. Inf. Model.* **2019**, *59* (11), 4814-4820.https://doi.org/10.1021/acs.jcim.9b00725

(25) Waller, M.P., Braun, H., Hojdis, N., Bühl, M., Geometries of second-row transition-metal complexes from density-functional theory, *Journal of chemical theory and computation***2007**, *3* (6), 2234-42. https://doi.org/10.1021/ct700178y

(26) Chiodo, S., Russo, N., Sicilia, E., LANL2DZ basis sets recontracted in the framework of density functional theory,*The Journal of chemical physics***2006***125*(10), 104107. https://doi.org/10.1063/1.2345197

(27) Vlachakis, D. Introductory Chapter: Molecular Docking - Overview, Background, Application and What the Future Holds, **2018**, http://dx.doi.org/10.5772/intechopen.78266.

(28) Huang, B., MetaPocket: a meta approach to improve protein ligand binding site prediction. *OMICS A Journal of Integrative Biology*, **2009**, *13* (4), 325-330. https://doi.org/10.1089/omi.2009.0045

(29) Phillips, M.A., Stewart, M.A., Woodling, D.L. and Xie, Z.R., Has molecular docking ever brought us a medicine? *Molecular Docking. IntechOpen, London, UK*, 2018, 141-78.http://dx.doi.org/10.5772/intechopen.72898.

(30) Swietnicki, W. and Brzozowska, E., In silico analysis of bacteriophage tail tubular proteins suggests a putative sugar binding site and a catalytic mechanism. *Journal of Molecular Graphics and Modelling*, **2019**, *92* (1), 8-16.https://doi.org/10.1016/j.jmgm.2019.07.002

(31) Azam, S.S. and Abbasi, S.W., Molecular docking studies for the identification of novel melatoninergic inhibitors for acetylserotonin-O-methyltransferase using different docking routines. *Theoretical Biology and Medical Modelling*, **2013**, *10* (1), 1-16.https://doi.org/10.1186/1742-4682-10-63

(32) Jayamani, A., Sengottuvelan, N., Kang, S.K. and Kim, Y.I., Studies on nucleic acid/protein interaction, molecular docking and antimicrobial properties of mononuclear nickel (II) complexes of piperazine based Schiff base. *Inorganic Chemistry Communications*, **2014**, *48*(1), 147-152. https://doi.org/10.1016/j.inoche.2014.08.029

(33) Hussan, K.P.S., Thayyil, M.S., Ahamed, T.S. and Muraleedharan, K., Biological Evaluation and Molecular Docking Studies of Benzalkonium Ibuprofenate. In *Computational Biology and Chemistry*. IntechOpen.**2020**.

(34) Alaghaz, A.N.M., El-Sayed, B.A., El-Henawy, A.A. and Ammar, R.A., Synthesis, spectroscopic characterization, potentiometric studies, cytotoxic studies and molecular docking studies of DNA binding of transition metal complexes with 1,1-diaminopropane–Schiff base. *Journal of Molecular Structure*, **2013**, *1035* (1), 83-93.https://doi.org/10.1016/j.molstruc.2012.09.032

(35) Chen, W., Li, Y., Cui, Y., Zhang, X., Zhu, H.L. and Zeng, Q., Synthesis, molecular docking and biological evaluation of Schiff base transition metal complexes as potential urease inhibitors. *European journal of medicinal chemistry*, **2010**, *45* (10), 4473-4478.https://doi.org/10.1016/j.ejmech.2010.07.007

(36) Chen, Z.J., Chen, Y.N., Xu, C.N., Zhao, S.S., Cao, Q.Y., Qian, S.S., Qin, J. and Zhu, H.L., Synthesis, crystal structures, molecular docking, and in vitro biological activities evaluation of transition metal complexes with 4-(3, 4-dichlorophenyl) piperazine-1-carboxylic acid. *Journal of Molecular Structure*, **2016**, *1117* (1), 293-299.https://doi.org/10.1016/j.molstruc.2016.03.084

(37) Dhanaraj, C.J., Hassan, I.U., Johnson, J., Joseph, J. and Joseyphus, R.S., Synthesis, spectral characterization, DNA interaction, anticancer and molecular docking studies on some transition metal complexes with bidentate ligand. *Journal of Photochemistry and Photobiology B: Biology*, **2016,** *162* (1), 115-124.https://doi.org/10.1016/j.jphotobiol.2016.06.032

(38) Diab, M.A., Mohamed, G.G., Mahmoud, W.H., El-Sonbati, A.Z., Morgan, S.M. and Abbas, S.Y., Inner metal complexes of tetradentate Schiff base: Synthesis, characterization, biological activity and molecular docking

studies. *Applied Organometallic Chemistry*, **2019,** *33* (7), e4945. https://doi.org/10.1002/aoc.4945

(39) Fekri, R., Salehi, M., Asadi, A. and Kubicki, M., DNA/BSA interaction, bio-activity, molecular docking simulation study and electrochemical properties of hydrazone Schiff base derived Cu (II)/Ni (II) metal complexes: influence of the nuclearity and metal ions. *Polyhedron*, **2017**, *128* (1), 175-187.https://doi.org/10.1016/j.poly.2017.02.047

(40) Krawczyk, P., Jędrzejewska, B., Pietrzak, M. and Janek, T., Synthesis, spectroscopic, physicochemical properties and binding site analysis of 4-(1H-phenanthro [9, 10-d]-imidazol-2-yl)-benzaldehyde fluorescent probe for imaging in cell biology: experimental and theoretical study. *Journal of Photochemistry and Photobiology B: Biology*, **2016,** *164*(1), 112-122.https://doi.org/10.1016/j.jphotobiol.2016.07.044

(41) Mallela, R.; Konakanchi, R.; Guda, R.; Munirathinam, N.; Gandamalla, D.; Yellu, N.R.; Kotha, L.R. Zn (II), Cd (II) and Hg (II) metal complexes of 2-aminonicotinaldehyde: Synthesis, crystal structure, biological evaluation and molecular docking study. *Inorganica Chimica Acta*, **2018**, *469* (1), 66-75.https://doi.org/10.1016/j.ica.2017.08.042

(42) Sankarganesh, M.; Raja, J.D.; Sakthikumar, K.; Solomon, R.V.; Rajesh, J.; Athimoolam, S.; Vijayakumar, V. New bio-sensitive and biologically active single crystal of pyrimidine scaffold ligand and its gold and platinum complexes: DFT, antimicrobial, antioxidant, DNA interaction, molecular docking with DNA / BSA and anticancer studies, *Bioorganic Chemistry*, **2018**, *81* (1), 154-164.

(43) Rauf, M.A.; Zubair, S.; Azhar, A. Ligand docking and binding site analysis with pymol and autodock/vina, *International Journal of Basic and Applied Sciences*,**2015,***4* (2), 168-177.https://doi.org/10.14419/ijbas.v4i2.4123

(44) Yapati, H.; Devineni, S.R.; Chirumamilla, S.; Kallurua, S. Synthesis, characterization and studies on antioxidant and molecular docking of metal complexes of 1-(benzo[d)thiazol-2-yl)thiourea, *J. Chem. Sci.*, **2016**,*128* (1),43–51.https://doi.org/10.1007/s12039-015-0999-3

(45) Refaat, H.M.; El-Badway, H.A.; Morgan, S.M. Molecular docking, geometrical structure, potentiometric and thermodynamic studies of moxifloxacin and its metal complexes, *Journal of Molecular Liquids*, **2016**,*220* (1), 802–812.https://doi.org/10.1016/j.molliq.2016.04.124

(46) Di Muzio, E.; Toti, D.; Polticelli, F. DockingApp: a user friendly interface for facilitated docking simulations with AutoDock Vina, *J Comput Aided Mol Des*, **2017**, *31* (2), 213–218.https://doi.org/10.1007/s10822-016-0006-1

(47) Neelakantan, M.A.; Balamurugan, K.; Balakrishnan, C.; Subha, L. Interaction of Amino Acid Schiff Base Metal Complexes with DNA/BSA Protein and Antibacterial Activity: Spectral Studies, DFT Calculations and Molecular Docking Simulations, *Appl Organometal Chem.*,**2018,** *32* (4), e4259. https://doi.org/10.1002/aoc.4259.https://doi.org/10.1002/aoc.4259.

(48) Mudavath, R.; Ushaiah B.; Kishan Prasad, C.; Sudeepa K,; Ravindar P.; Sunitha S.N.T.; Sarala Devi C. Molecular Docking, QSAR Properties and DNA/BSA Binding, -proliferative Studies of 6-Methoxy Benzothiozole Imine Base and its Metal Complexes, *Journal of Biomolecular Structure and Dynamics*, **2019**, *38* (10), 2849-2864.https://doi.org/10.1080/07391102.2019.1647878

(49) Sakthi, M.; Ramu, A. Synthesis, structure, DNA/BSA binding and antibacterial studies of NNO tridentate Schiff base metal complexes, *Journal of Molecular Structure*, **2017**, *1149*, 727-735.https://doi.org/10.1016/j.molstruc.2017.08.040

(50) Majorek, K.A., Porebski, P.J., Chruszcz, M., Almo, S.C., Minor, W., New York Structural Genomics Research Consortium (NYSGRC), Crystal structure of Bovine Serum Albumin, **2012**, Protein Data Bank.

(51) Trott, O.; Olson, A. J. Autodock Vina: Improving the speed and accuracy of docking with a new scoring function, efficient optimization and multithreading, *Journal of computational Chemistry*, **2010**, *31* (2), 455-461.https://doi.org/10.1002/jcc.21334

(52) Seeliger, D.; Groot, B.L.; Ligand docking and binding site analysis with PyMOL and Autodock/Vina, *J Comput Aided Mol Des*,**2010**,*24* (5), 417–422. https://doi.org/10.1007/s10822-010-9352-6

(53) Lill, M.A.; Danielson, M.L. Computer-aided drug design platform using PyMOL. *J Comput Aided Mol Des*, **2011**,*25*(1),13–19.https://doi.org/10.1007/s10822-010-9395-8.

5.7 Annexure:

Annexure 5(a): Optimized geometry coordinates of ligand H_2L9

Atom	x	y	z
C	-0.68621	1.072155	0.435649
C	0.735928	1.379675	-0.10954
H	0.605883	2.029001	-0.97697
H	1.330431	1.918195	0.630279
H	-0.53739	0.544227	1.379065
H	-1.23967	1.991544	0.631917
N	1.360216	0.246148	-0.51968
C	0.684653	-0.57993	-1.35874
H	1.241869	-1.49834	-1.55054
H	0.548029	-0.06165	-2.30938
C	-0.73562	-0.89378	-0.81267
H	-0.58486	-1.52697	0.063248
H	-1.32699	-1.44388	-1.54597
N	-1.35319	0.245044	-0.40841
C	-2.68028	0.399962	-0.59917
H	-2.95648	1.455503	-0.56905
H	-2.98952	-0.06939	-1.5342
C	-3.42683	-0.31779	0.53861
H	-2.91278	-1.23093	0.841788
H	-4.40616	-0.61604	0.164127
O	-3.61001	0.380349	1.53526
H	-4.02265	-0.26512	2.853811
C	2.708007	0.228075	-0.54655
H	3.126938	1.232915	-0.46424
H	3.087283	-0.2849	-1.43254
C	3.155707	-0.56853	0.683695
H	2.777938	-0.09805	1.592509
H	2.739546	-1.57631	0.649279
O	4.377232	-0.66427	0.784036
H	4.988975	-1.42692	1.954379

Annexure 5(b): Optimized geometry coordinates of ligand H_2L10

Atom	x	y	z
C	0.307282	0.661938	-0.40498
C	1.729424	0.969462	-0.95016
H	1.599378	1.618791	-1.8176
H	2.323926	1.507979	-0.21034
H	0.456107	0.134006	0.538436
H	-0.24617	1.581326	-0.20871
N	2.353712	-0.16406	-1.36031
C	1.67815	-0.99014	-2.19937
H	2.235367	-1.90855	-2.39118
H	1.541526	-0.47186	-3.15001
C	0.257879	-1.30399	-1.6533
H	0.408633	-1.93718	-0.77739
H	-0.33349	-1.85409	-2.38661
N	-0.35969	-0.16517	-1.24904
C	-1.68678	-0.01025	-1.4398
H	-1.96298	1.045288	-1.40968
H	-1.99602	-0.4796	-2.37483
C	-2.43333	-0.728	-0.30202
H	-3.41266	-1.02626	-0.67651
O	-2.61652	-0.02988	0.694629
H	-3.02915	-0.67535	2.013178
C	3.701503	-0.18214	-1.38718
H	4.120434	0.822705	-1.30486
H	4.08078	-0.69511	-2.27318
C	4.149204	-0.97874	-0.15694
H	3.733043	-1.98652	-0.19136
O	5.370729	-1.07449	-0.0566
H	5.982472	-1.83714	1.113743
C	3.670132	-0.35945	1.163049
C	2.576288	-1.07705	1.956542
H	2.152754	-2.01343	1.593191
C	2.070082	-0.456	3.259655
H	1.287276	-0.95355	3.83197
C	2.661031	0.86663	3.758856
H	2.29755	1.306683	4.687387
C	3.759815	1.574232	2.958818
H	4.175108	2.515594	3.318361
C	4.271095	0.962278	1.653191
H	5.046738	1.46627	1.076481

C	-3.8922	-0.04074	-0.2752
C	-4.38071	1.01038	-1.32547
H	-3.73632	1.377657	-2.12059
C	-5.80815	1.561949	-1.2932
H	-6.11124	2.310006	-2.02567
C	-6.81974	1.063927	-0.26541
H	-7.83384	1.463356	-0.25982
C	-6.42396	-0.02752	0.722079
H	-7.15684	-0.40953	1.432647
C	-5.00634	-0.59639	0.709825
H	-4.75123	-1.38801	1.415221

Annexure 5(c): Optimized geometry coordinates of ligand H_6L11

Atom	x	y	z
N	0.098453	1.136882	-0.54366
C	-1.0118	0.471082	-0.95161
H	-1.67209	1.098637	-1.55203
H	-0.707	-0.41183	-1.5159
C	-1.78441	-0.06503	0.286904
H	-2.61924	-0.69957	-0.01504
H	-2.18782	0.80558	0.806887
N	-0.94515	-0.71504	1.134049
C	0.196507	-0.08069	1.506581
H	-0.07627	0.783261	2.114995
H	0.838475	-0.72964	2.104263
C	0.958134	0.466352	0.265402
H	1.330068	-0.41176	-0.26492
H	1.78775	1.095199	0.592828
C	0.089041	2.487429	-0.51516
H	0.488882	2.847729	0.434396
H	-0.91031	2.889123	-0.69357
C	1.019281	2.989644	-1.64111
H	1.929143	2.386277	-1.59898
O	0.530734	2.824719	-2.76057
H	0.597388	1.457103	-3.43232
C	1.319795	4.481372	-1.34897
H	0.816878	4.774197	-0.4258
H	0.957806	5.066876	-2.1967
N	2.657246	4.628755	-1.21662
C	3.419068	4.748221	-2.3269
H	4.410641	4.314275	-2.18989

H	2.916928	4.320757	-3.19691
C	3.602943	6.246498	-2.60064
H	4.27834	6.671533	-1.85822
H	2.654191	6.7776	-2.51184
O	4.072589	6.483602	-3.71174
H	4.188033	7.92383	-4.19957
C	3.236457	4.374596	-0.02169
H	4.267416	4.034117	-0.12889
H	2.643896	3.661506	0.55378
C	3.254688	5.686043	0.776284
H	2.31159	6.225524	0.679373
H	4.044718	6.317142	0.36945
O	3.494233	5.526796	1.972143
H	4.278371	4.308502	2.449808
C	-1.44649	-1.68221	1.931294
H	-2.52189	-1.54499	2.060131
H	-0.93511	-1.71514	2.89553
C	-1.22599	-3.03498	1.220683
H	-1.62492	-2.94371	0.208227
O	-0.03114	-3.32786	1.132297
H	0.7581	-2.94667	-0.11567
C	-2.02476	-4.07628	2.03594
H	-2.88736	-3.58301	2.486798
H	-1.35534	-4.47995	2.797874
N	-2.43012	-5.04445	1.182759
C	-1.65926	-6.13526	0.972567
H	-2.2787	-7.03297	0.945704
H	-0.86826	-6.22471	1.719546
C	-1.02193	-6.0216	-0.42429
H	-1.26853	-5.07769	-0.91317
H	-1.43098	-6.81606	-1.04888
O	0.201514	-6.14538	-0.41712
H	1.021226	-5.69263	-1.62068
C	-3.66929	-4.98472	0.64777
H	-3.72754	-5.55755	-0.27938
H	-3.97881	-3.94829	0.500835
C	-4.6506	-5.61836	1.644576
H	-4.6258	-5.08259	2.593993
H	-4.36268	-6.64916	1.853496
O	-5.8126	-5.62476	1.243365
H	-6.91834	-6.2062	2.117913

Annexure 5(d): Optimized geometry coordinates of ligand H_4L12

Atom	x	y	z
C	-0.31437	3.405079	0.790314
C	1.104217	2.924926	1.190663
C	1.477476	3.039615	-1.19791
C	-0.02303	2.814228	-1.53932
H	1.633062	3.780939	1.633691
H	1.068435	2.157623	1.966415
H	-0.27417	4.463102	0.508717
H	1.667914	4.113598	-1.10147
H	2.108268	2.6976	-2.02347
H	-0.1665	1.935146	-2.17278
H	-0.35796	3.674345	-2.13604
H	-0.99438	3.3493	1.644124
N	-0.87924	2.689772	-0.34696
N	1.89348	2.418246	0.054905
C	-1.34689	1.336022	-0.04735
H	-1.32338	1.17279	1.035498
H	-0.70189	0.567001	-0.50313
C	2.070477	0.967485	-0.0295
H	1.617916	0.478629	0.840519
H	1.581597	0.555322	-0.92288
C	3.552519	0.553082	-0.08882
H	3.98408	0.940393	-1.02513
C	-2.78433	1.077527	-0.53161
H	-2.7843	1.085111	-1.63433
C	3.643282	-0.97733	-0.12603
H	3.125975	-1.39179	0.755301
H	3.072372	-1.30528	-0.99911
C	-3.22256	-0.32786	-0.08525
H	-2.64829	-1.03124	-0.6975
H	-2.93184	-0.49541	0.966094
O	4.202381	1.135131	1.034564
H	5.150481	1.093082	0.879144
O	-3.61899	2.113202	-0.0368
H	-4.48058	2.001885	-0.45215
C	5.016466	-2.76245	-1.04687
H	6.061461	-3.06365	-1.17609
H	4.61955	-2.5376	-2.04289
C	4.213202	-3.95529	-0.50018
H	4.27096	-3.98975	0.595063

H	4.663419	-4.88237	-0.87383
C	5.729591	-1.65948	1.015592
H	5.031456	-1.71944	1.85984
H	6.299412	-2.59087	0.998993
C	-4.85909	-2.01041	-0.70321
H	-5.92341	-2.19747	-0.84195
H	-4.3969	-2.13461	-1.68895
C	-5.49592	-0.09246	0.780694
H	-4.95246	-0.0844	1.734956
H	-5.74322	0.953602	0.56582
C	-6.83005	-0.79076	1.001481
H	-7.47879	-0.08508	1.535949
H	-7.32265	-1.00627	0.043685
N	-4.64284	-0.61052	-0.31582
N	5.007844	-1.51796	-0.26554
O	2.833205	-3.86409	-0.86801
H	2.619593	-4.61968	-1.41959
O	-6.65042	-1.98966	1.754375
H	-7.42671	-2.11985	2.304574
H	6.396953	-0.80978	1.159158
H	-4.43302	-2.69537	0.029751

Annexure 5(e): Optimized geometry coordinates of ligand H_4L13

Atom	x	y	z
C	-0.36301	1.3597	-0.97949
C	0.154623	0.782478	0.368195
H	-0.69752	0.26934	0.816962
H	0.491706	1.596728	1.011386
H	0.44395	1.966805	-1.3934
H	-1.22892	2.00519	-0.8234
N	1.136415	-0.12359	0.128812
C	0.843373	-1.14624	-0.71436
H	0.019326	-1.72454	-0.29353
H	1.706645	-1.78838	-0.89645
C	0.315954	-0.58222	-2.0648
H	-0.04848	-1.3849	-2.70776
H	1.163648	-0.10729	-2.56164
N	-0.63845	0.361843	-1.8588
C	-1.55136	0.588103	-2.82678
H	-1.29268	0.071413	-3.75334
H	-1.66567	1.660173	-2.99656

C	-2.90521	0.034505	-2.32773
H	-3.01592	0.344909	-1.28601
O	-2.93721	-1.19731	-2.34309
H	-2.3486	-1.99296	-1.1828
C	-4.01105	0.654534	-3.21773
H	-3.53161	1.295813	-3.95872
H	-4.56166	-0.15329	-3.70388
N	-4.8211	1.395663	-2.42631
C	-4.47202	2.661863	-2.10732
H	-3.38861	2.774549	-2.06165
H	-4.94899	2.971563	-1.17614
C	-6.06806	0.959082	-2.13157
H	-6.72612	1.785026	-1.85529
H	-6.47637	0.383527	-2.96353
C	-5.98624	-0.00696	-0.9387
H	-5.31325	-0.83777	-1.1489
H	-6.98051	-0.42733	-0.78756
O	-5.65103	0.522745	0.120782
H	-5.0823	-0.32693	1.25216
C	2.427099	0.228592	0.316142
H	3.038159	-0.10542	-0.52448
H	2.532339	1.303899	0.473478
C	2.925528	-0.4951	1.58402
H	2.6216	-1.54172	1.526725
O	2.441882	-0.01124	2.610246
H	1.256475	-0.68957	3.288506
C	4.463949	-0.37085	1.535475
H	4.74573	0.679242	1.637076
H	4.782879	-0.75895	0.566288
N	5.001959	-1.13429	2.516405
C	5.05581	-2.4733	2.331207
H	6.084681	-2.83105	2.400379
H	4.608394	-2.77779	1.382928
C	4.28839	-3.13233	3.484903
H	3.324936	-2.64195	3.630325
H	4.845337	-3.01691	4.415316
O	4.080412	-4.33108	3.309527
H	3.293964	-5.12813	4.344783
C	5.903909	-0.56645	3.349573
H	6.484748	0.193654	2.824344
H	6.561124	-1.30422	3.81306
C	5.129322	0.165091	4.451577

H	4.650668	1.054536	4.040708
H	5.821617	0.460247	5.240032
H	4.367696	-0.49177	4.873854
C	-4.98507	3.595903	-3.21139
H	-4.53279	3.330392	-4.16733
H	-4.71436	4.6221	-2.9629
H	-6.07009	3.522636	-3.29185

Annexure 5(f): Optimized geometry coordinates of ligand H_4L14

Atom	x	y	z
C	-0.50443	0.652739	-1.23772
C	0.013204	0.075518	0.109962
H	-0.83894	-0.43762	0.558729
H	0.350287	0.889768	0.753153
H	0.302531	1.259844	-1.65163
H	-1.37034	1.29823	-1.08163
N	0.994995	-0.83055	-0.12942
C	0.701953	-1.8532	-0.97259
H	-0.12209	-2.4315	-0.55176
H	1.565225	-2.49534	-1.15468
C	0.174534	-1.28918	-2.32303
H	-0.1899	-2.09186	-2.966
H	1.022228	-0.81426	-2.81987
N	-0.77987	-0.34512	-2.11703
C	-1.69278	-0.11886	-3.08501
H	-1.4341	-0.63555	-4.01157
H	-1.80709	0.953212	-3.25479
C	-3.04663	-0.67246	-2.58596
H	-3.15734	-0.36205	-1.54425
O	-3.07862	-1.90427	-2.60133
H	-2.49002	-2.69992	-1.44104
C	-4.15247	-0.05243	-3.47596
H	-3.67303	0.588852	-4.21695
H	-4.70308	-0.86025	-3.96211
N	-4.96252	0.688703	-2.68454
C	-4.61344	1.954903	-2.36555
H	-3.53003	2.067588	-2.31988
H	-5.09041	2.264603	-1.43437
C	-6.20948	0.252122	-2.3898
H	-6.86754	1.078066	-2.11352
H	-6.61778	-0.32343	-3.22176

C	-6.12765	-0.71392	-1.19693
H	-5.45467	-1.54473	-1.40713
H	-7.12192	-1.13429	-1.04579
O	-5.79244	-0.18421	-0.13745
H	-5.22372	-1.03389	0.993928
C	2.28568	-0.47837	0.057909
H	2.896739	-0.81239	-0.78271
H	2.39092	0.596939	0.215244
C	2.784109	-1.20206	1.325787
H	2.48018	-2.24868	1.268492
O	2.300463	-0.7182	2.352013
H	1.115056	-1.39653	3.030273
C	4.32253	-1.07781	1.277242
H	4.604311	-0.02772	1.378843
H	4.641459	-1.46591	0.308055
N	4.86054	-1.84125	2.258172
C	4.91439	-3.18026	2.072974
H	5.943261	-3.53801	2.142146
H	4.466974	-3.48475	1.124696
C	4.14697	-3.83929	3.226671
H	3.183516	-3.34891	3.372093
H	4.703917	-3.72387	4.157084
O	3.938992	-5.03804	3.051295
H	3.152544	-5.83509	4.086551
C	5.76249	-1.27341	3.09134
H	6.343329	-0.51331	2.566111
H	6.419705	-2.01118	3.554827
C	4.987903	-0.54187	4.193344
C	-5.12649	2.888942	-3.46962
C	-6.19023	3.867898	-2.96071
H	-7.10336	3.483156	-2.50657
C	-5.92507	5.375277	-2.95858
H	-6.64865	6.056293	-2.51073
C	-4.66069	5.926716	-3.61665
H	-4.47205	7.00012	-3.62968
C	-3.99027	3.464864	-4.32257
H	-3.31573	2.79064	-4.85003
C	-3.70728	4.968907	-4.33036
H	-2.84145	5.358713	-4.86544
C	5.339434	-1.06493	5.589691
H	5.178369	-2.11609	5.828133
C	4.961893	0.979677	4.003438

H	4.51929	1.406307	3.103787
C	5.67225	1.898886	4.999846
H	5.734716	2.969693	4.80649
C	6.054868	-0.16444	6.599583
H	6.393698	-0.57279	7.551615
C	6.256811	1.318035	6.287094
H	6.751307	1.968785	7.00817

Annexure 5(f): Optimized geometry coordinates of complex CuL1

Atom	x	y	z
N	-1.11609	-1.59999	-0.96047
C	-1.82414	-2.45943	0.005706
C	-2.9931	-1.69827	0.702138
H	-2.21488	-3.37766	-0.47481
H	-1.10303	-2.76664	0.771115
N	-3.7452	-0.8827	-0.29543
H	-3.69205	-2.40429	1.184861
H	-2.58655	-1.04242	1.475403
C	-2.02825	-1.15969	-2.04683
C	-3.54582	-1.30081	-1.69765
H	-1.84293	-1.74216	-2.97245
H	-1.82239	-0.10554	-2.29669
H	-3.87181	-2.34217	-1.82462
H	-4.14688	-0.68007	-2.36891
C	-4.39086	0.289703	0.033619
C	-5.55209	0.741471	-0.67262
N	-3.89881	1.035244	1.078937
C	-6.20831	1.897472	-0.2523
C	-5.72844	2.618367	0.870022
C	-4.56984	2.144121	1.49128
N	1.115236	-1.59889	0.958209
C	2.023987	-1.15908	2.04742
C	3.542579	-1.29951	1.701934
H	1.817114	-0.10516	2.297443
H	1.836925	-1.74215	2.972389
N	3.744948	-0.88278	0.299757
H	4.141726	-0.67793	2.374087
H	3.868878	-2.34059	1.830461
C	1.825179	-2.46033	-0.00442
C	2.996913	-1.70114	-0.69858
H	1.106223	-2.76843	-0.77156

H	2.213906	-3.3783	0.478364
H	2.593424	-1.04726	-1.47504
H	3.697932	-2.40832	-1.17667
C	4.390661	0.289439	-0.02941
N	3.902437	1.0317	-1.07889
C	5.548321	0.744486	0.680719
C	4.573886	2.140417	-1.49094
C	6.204995	1.900155	0.260295
C	5.729155	2.617698	-0.86589
H	4.140949	2.665286	-2.34016
H	6.230396	3.508023	-1.23026
H	5.937623	0.158697	1.506369
H	7.09773	2.233539	0.784365
H	-5.94424	0.15294	-1.49499
H	-7.10374	2.228478	-0.77327
H	-6.22926	3.508934	1.234388
H	-4.13393	2.671484	2.33742
Cu	0.000411	-0.26328	-0.0018
O	1.273156	1.283746	-0.71634
O	-1.27233	1.284575	0.696596
H	0.845637	1.999011	-1.22062
H	-0.84505	2.019368	1.171963
H	2.252939	1.139665	-0.98004
H	-2.24986	1.143796	0.969781

Annexure 5(g): Optimized geometry coordinates of complex CuL3

Atom	x	y	z
C	0.488584	-1.09935	0.481576
C	1.333784	-0.85648	-0.84924
N	-0.10167	0.163139	0.91628
H	-0.29369	-1.8323	0.285009
H	1.188842	-1.46567	1.248191
C	0.93663	1.153881	1.176708
N	2.362452	0.145108	-0.59802
H	1.754809	-1.79857	-1.19928
H	0.625064	-0.49741	-1.60151
C	1.796366	1.413923	-0.14687
H	1.635678	0.772356	1.936771
H	0.486816	2.095781	1.492021
H	2.565397	2.148427	0.08864
H	1.111825	1.834706	-0.88938

C	3.686019	-0.2183	-0.27146
C	4.707017	0.763261	-0.14465
C	6.013304	0.364649	0.171408
C	4.076877	-1.57142	-0.07705
C	5.413961	-1.86442	0.235667
N	6.387011	-0.92767	0.367051
H	6.801614	1.107056	0.263652
H	4.511288	1.814422	-0.32335
H	3.373624	-2.39215	-0.1538
H	5.720916	-2.89534	0.392799
C	-4.36304	-3.86864	0.459249
O	-3.89644	-2.50865	0.681102
H	-3.52917	-4.58591	0.403474
H	-4.96599	-3.95373	-0.45838
H	-4.9895	-4.1276	1.317515
C	-4.88762	0.579497	0.218752
O	-3.62415	1.3035	0.466207
H	-5.11068	0.570673	-0.85382
H	-5.68687	1.07443	0.782439
H	-4.7388	-0.43911	0.580568
Cl	-1.32457	3.065963	-0.20227
Cl	-2.11635	-0.94595	-1.49314
Cu	-1.74345	0.746733	0.131275
H	-3.33091	-2.1934	-0.06535
H	-3.6556	2.265372	0.268578

Annexure 5(h): Optimized geometry coordinates of complex CuL5

Atom	x	y	z
N	0.521903	0.865643	-0.24092
C	1.274565	0.84708	-1.53243
C	2.458432	-0.13367	-1.51938
H	0.586331	0.584306	-2.34248
H	1.663708	1.85647	-1.76052
N	3.455111	0.307771	-0.51781
H	2.073791	-1.14779	-1.30494
H	2.933817	-0.16658	-2.50984
C	1.438556	0.64312	0.919924
C	2.894749	1.070435	0.634204
H	1.422527	-0.4146	1.220164
H	1.071023	1.22871	1.776377
H	3.501821	0.879231	1.521716

H	2.936208	2.151711	0.440738
C	4.6914	-0.35522	-0.44918
C	5.831226	0.219841	0.210927
C	7.05649	-0.46511	0.269091
C	7.214568	-1.71959	-0.36
C	4.891912	-1.60641	-1.09328
C	6.130276	-2.27739	-1.0547
H	7.904091	-0.01866	0.778978
H	-0.65031	-1.79387	0.981671
H	-1.4196	-2.93908	0.413364
H	-2.93522	-2.58951	0.223754
H	-0.97386	-3.21204	-0.55098
H	-1.33352	-3.81819	1.076672
H	-3.10636	-1.11657	0.480365
H	-3.26882	-2.80523	-0.7959
H	-3.55914	-3.17222	0.919647
H	-1.3418	-1.37422	2.235318
H	-2.7853	-0.82922	1.936723
H	-0.74941	-0.59518	2.728308
H	-1.41213	-2.22947	2.930194
H	-4.41443	-0.58501	0.115532
H	-5.55143	-1.41363	-0.00788
H	-4.59447	0.81191	-0.08628
C	-6.82334	-0.88086	-0.29324
C	-5.86499	1.353393	-0.34473
C	-6.98483	0.506437	-0.44446
H	-7.67734	-1.54671	-0.37984
H	-7.96389	0.930611	-0.6488
H	-5.98366	2.422593	-0.48494
Cu	-1.07269	-0.3037	-0.27546
O	-0.38908	3.247586	0.097184
O	-1.93535	0.579413	-2.00998
H	-0.0391	2.231925	-0.06139
H	-2.37454	0.052466	-2.70465
H	-2.58161	1.147147	-1.50394
H	0.355332	3.864325	0.24381
H	-2.83792	0.253793	2.078595
H	-3.54676	-1.30498	2.575365
H	6.233032	-3.23564	-1.55841
H	8.171325	-2.23247	-0.31168
H	-5.45629	-2.48413	0.132873
H	4.064726	-2.06901	-1.62058

O	-3.43116	1.606097	-0.08284
C	-3.53076	3.062314	0.161701
H	-4.04032	3.556295	-0.67389
H	-2.48756	3.387174	0.229858
H	-4.07441	3.239412	1.096181
O	5.658423	1.512752	0.738348
C	6.796127	2.161754	1.387204
H	7.132503	1.593208	2.26379
H	6.427915	3.13999	1.702549
H	7.632318	2.288893	0.687235

Annexure 5(i): Optimized geometry coordinates of complex CuL7

Atom	x	y	z
C	-7.40816	-0.21202	0.440063
C	-5.89127	-0.21202	0.440063
C	-6.22643	2.171264	1.145275
C	-7.56516	2.292193	0.441709
H	-5.52662	-0.77086	1.341535
H	-5.51303	-0.76211	-0.46131
H	-7.78205	-0.23207	1.497875
H	-6.38739	1.827019	2.200884
H	-5.73475	3.177285	1.194111
H	-7.52199	3.120483	-0.31321
H	-8.34756	2.575229	1.193735
H	-7.78398	-1.14046	-0.06324
C	-9.50537	0.912083	-0.31317
C	-10.1654	0.987222	-1.54005
C	-10.2368	0.749961	0.863391
C	-11.5565	0.900926	-1.59021
H	-9.58849	1.11581	-2.46737
C	-11.6283	0.662632	0.8133
C	-12.2882	0.738221	-0.41321
H	-12.0768	0.960773	-2.55715
H	-12.2047	0.534395	1.741089
N	-7.96935	1.008025	-0.25804
N	-5.31354	1.190627	0.440063
O	-13.7145	0.649697	-0.46496
H	-13.9766	-0.27222	-0.51961
Cu	-6.40691	1.526792	-1.19847
C	-7.45133	3.011507	-2.94248
H	-7.09467	2.002697	-2.94248

H	-7.09466	3.515905	-3.81614
H	-8.52133	3.01152	-2.94248
O	-6.97465	3.68561	-1.77489
H	-7.29299	4.591292	-1.77535
Cl	-6.9738	3.519385	0.344155

Annexure 5(j): Optimized geometry coordinates of complex CuL8

Atom	x	y	z
C	0.15319	2.007953	-1.04335
C	-1.29222	2.303598	-1.39598
C	-1.67276	1.534155	0.960468
C	-0.45353	0.631207	0.964684
H	-1.44539	3.414618	-1.40522
H	-1.51197	1.934147	-2.43201
H	0.545436	2.813318	-0.36756
H	-1.38555	2.553663	1.330384
H	-2.44375	1.128702	1.665731
H	-0.7662	-0.42514	1.174925
H	0.227777	0.943111	1.799152
H	0.777499	2.021557	-1.97426
C	1.790746	0.376648	-0.10179
C	2.362238	-0.79852	-0.59052
C	2.569937	1.286161	0.613191
C	3.712463	-1.06434	-0.3637
H	1.747487	-1.51572	-1.1535
C	3.920824	1.020869	0.839321
C	4.492134	-0.15422	0.351143
H	4.162841	-1.99089	-0.74835
H	4.535033	1.738358	1.402731
N	0.299692	0.669607	-0.35186
N	-2.26637	1.661444	-0.42653
O	5.876512	-0.42701	0.583477
H	6.403154	-0.02683	-0.1123
Cu	-1.37241	-0.07621	-0.8444
O	0.607716	-1.22235	-1.54854
H	-0.30704	-1.03525	-1.77172
H	0.639741	-1.77175	-0.76194
C	-0.87497	-2.50885	-0.43015
H	-0.91012	-1.89651	-1.30691
H	-1.39189	-3.42718	-0.61553
H	0.1446	-2.7174	-0.1814

C	-2.96372	-1.04167	-0.09399
H	-2.99887	-0.42933	-0.97075
H	-3.48065	-1.96	-0.27937
H	-1.94415	-1.25023	0.15476
O	-1.49977	-1.8212	0.656891
H	-1.47	-2.37095	1.443329
O	-3.58852	-0.35402	0.993049
H	-3.55722	-0.90307	1.77992
Cl	-1.39045	0.006127	1.73714

Annexure 5(k): Optimized geometry coordinates of complex CoL9

Atom	x	y	z
C	1.088098	-1.77008	0.950791
C	-0.41694	-1.76095	1.391815
H	-0.78883	-2.79078	1.536948
H	-0.5212	-1.20734	2.327386
H	1.694003	-1.2491	1.695754
H	1.468613	-2.80286	0.857457
N	-1.19425	-1.04789	0.34528
C	-1.0881	-1.77091	-0.9492
H	-1.69383	-1.2504	-1.69462
H	-1.46874	-2.80358	-0.85516
C	0.416968	-1.76228	-1.39013
H	0.521236	-1.20969	-2.32629
H	0.788888	-2.79227	-1.53405
N	1.194209	-1.04808	-0.34431
C	2.543108	-0.56782	-0.73236
H	3.306284	-1.36724	-0.69365
H	2.464568	-0.22132	-1.76943
C	2.956594	0.626197	0.172188
H	3.794409	1.151438	-0.31461
H	3.333656	0.246893	1.140368
O	1.848595	1.518926	0.382103
C	-2.54309	-0.56708	0.732916
H	-2.46441	-0.21948	1.769611
H	-3.30635	-1.36645	0.695114
C	-2.9565	0.626053	-0.17282
H	-3.79431	1.151818	0.313406
H	-3.33348	0.245872	-1.14068
O	-1.84844	1.518573	-0.38351
Cu	0.000004	0.794063	-0.00019

O	0.223726	1.25243	2.140897
O	-0.22394	1.248837	-2.1425
H	-0.32165	2.004238	2.442304
H	0.321166	2.000459	-2.44491
H	1.130486	1.542891	1.688157
H	-1.13064	1.54012	-1.68997

Annexure 5(l): Optimized geometry coordinates of complex Cu_2L10

Atom	x	y	z
C	-0.60493	-0.79908	1.396777
C	0.492511	0.306913	1.420383
H	0.023273	1.293912	1.483146
H	1.149722	0.18917	2.288334
H	-0.14364	-1.79	1.352282
H	-1.21876	-0.74846	2.300374
N	1.32298	0.258138	0.188989
C	0.483706	0.367251	-1.03001
H	1.109461	0.236198	-1.91747
H	0.073424	1.379858	-1.0847
C	-0.66653	-0.69513	-1.04714
H	-0.25474	-1.70381	-1.13671
H	-1.30575	-0.50415	-1.91581
N	-1.49242	-0.65516	0.198954
C	-2.40689	0.548009	0.273113
H	-2.67956	0.692143	1.323116
H	-1.89859	1.453447	-0.08666
C	-3.69967	0.255658	-0.52234
H	-3.44378	0.175268	-1.59681
O	-4.22238	-0.97921	-0.01531
C	2.308858	-0.88002	0.159665
H	2.471761	-1.20795	1.189428
H	1.919365	-1.72838	-0.41868
C	3.655138	-0.3708	-0.42099
H	3.512799	-0.11784	-1.48417
O	3.999427	0.832063	0.302222
C	4.767049	-1.4035	-0.3137
C	5.343033	-1.95729	-1.47556
H	4.998699	-1.62695	-2.45397
C	6.366408	-2.9192	-1.38126
H	6.802857	-3.33805	-2.28519
C	6.829328	-3.33306	-0.11753

H	7.6223	-4.07379	-0.04142
C	6.264409	-2.77723	1.048358
H	6.623483	-3.08969	2.026537
C	5.240228	-1.81953	0.952752
H	4.816794	-1.38511	1.85546
C	-4.71016	1.390468	-0.37104
C	-5.60547	1.394185	0.719122
H	-5.59869	0.551227	1.404191
C	-6.51624	2.453401	0.888175
H	-7.20763	2.443824	1.727932
C	-6.54267	3.52062	-0.03187
H	-7.25109	4.336145	0.095704
C	-5.65759	3.517156	-1.12843
H	-5.68454	4.329099	-1.85179
C	-4.7493	2.454853	-1.29718
H	-4.08073	2.447176	-2.15735
Cu	-2.82765	-2.31848	0.199182
Cu	2.608437	2.132216	0.091126
Cl	-1.07679	-4.01765	-0.03162
O	-2.84323	-3.10776	2.384713
H	-3.75504	-3.45992	2.413518
O	-4.4334	-3.53147	-0.31347
H	-4.15319	-4.06246	-1.12603
O	-3.18836	-4.74334	-2.14076
H	-3.28976	-5.43868	-2.81084
H	-2.21163	-3.82638	2.150333
H	-5.01617	-2.76501	-0.51569
H	-2.32497	-4.76428	-1.65845
Cl	2.629538	2.888979	-2.27588
O	4.050869	3.902749	0.161219
O	3.355086	0.61975	2.830208
H	4.50014	4.664455	0.56823
H	3.885079	1.097991	3.494883
H	3.732594	0.733654	1.896761
H	4.005959	3.93316	-0.82843
C	-0.23731	5.727445	0.621728
C	0.503403	4.465466	0.647904
H	0.42819	6.540977	0.312631
H	-0.64373	5.958473	1.612395
H	-1.06521	5.663584	-0.09291
N	1.115684	3.46534	0.634953

Annexure 5(m): Optimized geometry coordinates of complex Cu_3L11

Atom	x	y	z
H	1.267597	-2.10997	1.403824
H	-0.31879	-2.312	0.602269
H	-0.18076	-2.41929	2.389346
H	-0.90387	-0.15298	1.553462
H	0.505599	0.231669	-2.12953
H	-0.51525	-0.88734	-2.82142
H	4.865734	-3.91283	-2.32225
H	4.811245	-4.58425	-0.84352
H	-6.95513	-4.23595	-0.53749
H	-5.85011	-4.23145	-1.72719
H	-7.85447	0.493155	-0.7995
H	-6.50261	1.142339	-1.74133
H	-5.72843	1.750978	0.425236
H	-6.68797	0.473315	1.206684
H	-3.45207	-2.39833	2.81101
H	-2.60014	-1.87019	1.337348
H	-3.56274	0.170012	2.284498
H	-5.13721	-0.64017	2.556077
H	-3.07549	-0.34925	-0.86092
H	-4.40186	0.710371	-1.34866
H	-3.56665	2.098763	0.801946
H	7.72024	0.718182	-1.72775
H	7.652572	0.640712	0.044777
H	5.713286	1.962072	-0.70611
H	5.288673	0.728723	-1.93361
H	3.797535	-1.52794	2.283019
H	5.259874	-1.24429	3.260459
H	6.106662	0.412653	1.694851
H	4.428028	0.867052	2.108904
H	3.264504	-0.40713	-1.45199
H	2.7424	-0.7146	0.232834
H	3.214264	2.016935	-1.04287
H	-3.27577	3.379901	-1.1583
H	-2.29037	2.120283	-1.96253
H	3.132137	2.641553	1.230443
H	2.062744	1.272283	1.669429
H	0.140383	3.407179	-2.20944
H	-0.40584	4.987506	-1.54928
H	1.268084	4.954644	0.160021

H	2.082264	3.804629	-0.92633
H	-0.3088	2.63227	2.453551
H	0.401128	4.277692	2.332853
H	-1.25836	4.982157	0.765015
H	-2.19057	3.605502	1.407167
C	0.194442	-1.9104	1.488746
O	0.042682	-0.46714	1.598791
O	-0.43299	-0.10679	-2.24337
O	4.886861	-3.76019	-1.35976
O	-6.25203	-3.73683	-0.99123
Cu	-0.20106	1.277297	-0.18713
Cu	5.673913	-2.07124	-0.3708
Cu	-5.49584	-1.97372	-0.22075
O	-6.4567	-0.91617	-1.48585
C	-6.76965	0.375673	-0.98696
C	-6.04417	0.701738	0.345633
O	-4.40662	-2.90219	1.015003
C	-3.59619	-1.99242	1.795442
C	-4.25893	-0.58576	1.898802
O	7.108994	-1.09828	-0.96055
O	-1.75864	1.14597	0.682313
N	-4.75766	-0.2526	0.531384
C	-3.77769	0.413384	-0.5048
C	-2.93506	1.573926	0.055159
C	7.143215	0.307912	-0.8787
C	5.720093	0.883453	-0.93632
O	5.600832	-2.2204	1.466871
C	4.877266	-1.28035	2.224661
C	5.056426	0.113903	1.613414
N	4.764243	0.070953	0.039482
C	3.255286	-0.00874	-0.43031
O	1.317587	1.277057	-1.12088
C	2.547527	1.354685	-0.45637
C	-2.52265	2.593338	-0.99947
C	2.299632	2.009176	0.89242
C	-0.05278	3.976346	-1.29696
C	1.164952	3.997277	-0.37034
N	0.961784	2.846887	0.706384
C	-0.05218	3.446638	1.772136
C	-1.25215	3.896774	0.936507
N	-1.14255	3.171609	-0.48012

Annexure 5(n): Optimized geometry coordinates of complex Cu_2L12

Atom	x	y	z
C	-5.60522	2.309733	0.649831
N	-5.24474	0.853159	0.848199
C	-3.9232	0.452293	0.231476
C	-3.91367	-1.08225	-0.01532
C	-2.77281	-1.47876	-0.97938
C	2.721107	-0.9098	0.658234
N	1.416546	-1.30864	0.082608
N	-1.42711	-1.12543	-0.46505
C	-5.34509	0.430455	2.288325
C	3.916156	-1.01491	-0.33152
O	5.076516	-1.52089	0.372229
O	-5.16516	-1.50519	-0.59325
C	4.290662	0.297065	-1.10761
N	5.391608	1.063857	-0.41537
C	4.962757	1.805679	0.821657
C	6.286659	1.875286	-1.32083
C	7.715099	1.92977	-0.72318
C	-6.44274	2.489032	-0.64028
O	-7.4755	1.485119	-0.67021
O	8.134431	0.598813	-0.38141
Cu	-6.52587	-0.19406	-0.40731
Cu	6.633853	-0.48198	0.19166
O	-8.2273	-0.77718	-1.47007
O	8.30122	-1.32214	1.186775
C	0.409508	-1.5811	1.13297
C	-0.89975	-2.0969	0.520908
C	-0.42773	-0.89882	-1.53186
C	0.888953	-0.37795	-0.93499
H	2.9604	-1.61437	1.462121
H	2.659854	0.103864	1.111881
H	-2.87253	-2.5598	-1.19167
H	-2.94172	-0.94991	-1.92707
H	-3.75106	-1.59844	0.948995
H	-3.84534	0.967517	-0.73438
H	-3.08064	0.772384	0.861701
H	-6.22075	2.614219	1.501062
H	-4.69334	2.928613	0.642853
H	-4.83293	-0.53083	2.385877
H	-4.79644	1.160678	2.908302

H	3.607397	-1.75361	-1.09207
H	4.693843	0.010694	-2.08559
H	3.417291	0.941133	-1.28256
H	4.55742	1.066778	1.518534
H	5.868293	2.218552	1.280539
H	6.335911	1.349134	-2.28037
H	5.876435	2.881956	-1.49926
H	7.737692	2.602741	0.154738
H	8.395036	2.360747	-1.47729
H	-5.78414	2.429261	-1.52907
H	-6.89386	3.495579	-0.63632
H	-8.44456	0.183836	-1.60649
H	-8.2491	-1.32533	-2.2749
H	8.851545	-0.62335	0.734259
H	8.643884	-2.23116	1.116468
H	0.816658	-2.33708	1.816313
H	0.186342	-0.66849	1.726635
H	-0.71406	-3.08252	0.046619
H	-1.63831	-2.24246	1.318144
H	-0.82315	-0.15702	-2.23766
H	-0.21629	-1.8306	-2.09633
H	0.710897	0.633352	-0.50469
H	1.62071	-0.27729	-1.74533
H	-6.35183	0.32707	2.635716
H	4.25358	2.591117	0.66337

Annexure 5(o): Optimized geometry coordinates ofcomplex Cu_2L13

Atom	x	y	z
C	-5.60522	2.309733	0.649831
N	-5.24474	0.853159	0.848199
C	-3.9232	0.452293	0.231476
C	-3.91367	-1.08225	-0.01532
C	-2.77281	-1.47876	-0.97938
C	2.721107	-0.9098	0.658234
N	1.416546	-1.30864	0.082608
N	-1.42711	-1.12543	-0.46505
C	-5.34509	0.430455	2.288325
C	3.916156	-1.01491	-0.33152
O	5.076516	-1.52089	0.372229
O	-5.16516	-1.50519	-0.59325
N	4.290662	0.297065	-1.10761

N	5.391608	1.063857	-0.41537
C	4.962757	1.805679	0.821657
C	6.286659	1.875286	-1.32083
C	7.715099	1.92977	-0.72318
C	-6.44274	2.489032	-0.64028
O	-7.4755	1.485119	-0.67021
O	8.134431	0.598813	-0.38141
Cu	-6.52587	-0.19406	-0.40731
Cu	6.633853	-0.48198	0.19166
O	-8.2273	-0.77718	-1.47007
O	8.30122	-1.32214	1.186775
C	0.409508	-1.5811	1.13297
C	-0.89975	-2.0969	0.520908
C	-0.42773	-0.89882	-1.53186
C	0.888953	-0.37795	-0.93499
C	-6.79148	0.281922	2.787423
C	3.939508	2.938963	0.59327
H	2.9604	-1.61437	1.462121
H	2.659854	0.103864	1.111881
H	-2.87253	-2.5598	-1.19167
H	-2.94172	-0.94991	-1.92707
H	-3.75106	-1.59844	0.948995
H	-3.84534	0.967517	-0.73438
H	-3.08064	0.772384	0.861701
H	-6.22075	2.614219	1.501062
H	-4.69334	2.928613	0.642853
H	-4.83293	-0.53083	2.385877
H	-4.79644	1.160678	2.908302
H	3.607397	-1.75361	-1.09207
H	4.693843	0.010694	-2.08559
H	3.417291	0.941133	-1.28256
H	4.55742	1.066778	1.518534
H	5.868293	2.218552	1.280539
H	6.335911	1.349134	-2.28037
H	5.876435	2.881956	-1.49926
H	7.737692	2.602741	0.154738
H	8.395036	2.360747	-1.47729
H	-5.78414	2.429261	-1.52907
H	-6.89386	3.495579	-0.63632
H	-8.44456	0.183836	-1.60649
H	-8.2491	-1.32533	-2.2749
H	8.851545	-0.62335	0.734259

H	8.643884	-2.23116	1.116468
H	0.816658	-2.33708	1.816313
H	0.186342	-0.66849	1.726635
H	-0.71406	-3.08252	0.046619
H	-1.63831	-2.24246	1.318144
H	-0.82315	-0.15702	-2.23766
H	-0.21629	-1.8306	-2.09633
H	0.710897	0.633352	-0.50469
H	1.62071	-0.27729	-1.74533
H	-6.78551	-0.00021	3.848307
H	-7.368	1.2073	2.68259
H	-7.31484	-0.50342	2.228539
H	3.727573	3.426492	1.553636
H	4.318754	3.706876	-0.09134
H	2.989101	2.562156	0.198089

Future Scope

The present study helped us to identify the potential of piperazine ring towards metal binding. As an important fragment of large biomolecules as well synthetic organic compounds serving as drugs both in the medicinal form as well as the recreational forms, piperazine ring is omnipresent. The benzylpiperazine (BZP) or phenylpiperazines (PP) compounds with different substituents on the phenyl ring including the halides or methoxy groups are in high demand in the illegal market sold as ecstasy or many other different names. Once consumed piperazines are absorbed by the body from gastrointestinal tract. A portion of the drug molecules are metabolized mainly at the liver. Many therapeutic drugs also give piperazines as active metabolites.

Once in the body it causes depression and anxiety in addition to insomnia, headaches, and nausea. These molecules induce the increase of serotonin and dopamine in extracellular fluid as well as blocks the reuptake mechanism. Additionally, piperazine drugs have found many other potential applications are widely used as the backbone of many synthetic drug molecules. Although the pharmacological studies are being done to identify how they interact and gets transported in our body, it's still intriguing how these molecules not only affect proteins or enzymes, or small biomolecules at as potential donor site. The presence of piperazine in many other potential drugs are extensively used and already explained.

Thus, to identify the mechanism of action under different condition and circumstances it is important to synthesize a plethora of piperazine based molecules and study their interaction with different biomolecules and fragments. Interestingly the role of metal ions is important due to the basicity of the piperazine ring itself as a donor site. The configuration of these metal complexes can invoke different types of interaction and may stabilize a specific conformer of important biomolecules. The role of these metal ions in other type of reactions as catalyst must also be explored.

List of Publications

1. Recent advances in synthesis of piperazine based ligands, metal complexes and their applications - Dalton trans. 2021,50, 785-800 https://doi.org/10.1039/D0DT03569F

2. Synthesis and characterization of a series of phenyl piperazine based ligands – Journal of Physics: Conference Series 1531 (2020) 012111 DOI 10.1088/1742-6596/1531/1/012111

3. Synthesis, characterization and biological evaluation studies of Cu(II) and Zn(II) complexes with gly-o-andn or gly-p-andn as primary ligand and N, N' donors as secondary ligand – Journal of Physics: Conference Series 1531 (2020) 012106 DOI 10.1088/1742-6596/1531/1/012106 (Scopus)

4. Structural features of some Metal Organic Frameworks (MOFs) with Aromatic polycarboxylates and bis-(pyridylmethyl)-piperazine (bpmp) or bis-(pyridylformyl)-piperazine (bpfp) ligands – The Journal of Gujrat Research Society (ISSN: 0374-8588, Volume 21 Issue 8, November 2019)

5. Investigation on the role of Piperazine, a six membered heterocycle at the centre of many unique classes of drugs - Journal of Emerging Technologies and Innovative Research (ISSN: 2349-5162, Volume 5 Issue 10, October 2018)

6. Hydrogels, A New Class of Material with Huge Potential in Biomedical Applications - Journal of Emerging Technologies and Innovative Research (ISSN: 2349-5162, Volume 6 Issue 1, January 2019)